

UC Irvine

UC Irvine Electronic Theses and Dissertations

Title

Transition Metal Complexes of Modified Azaphosphatranes

Permalink

<https://escholarship.org/uc/item/09q6s2rf>

Author

Thammavongsy, Zachary

Publication Date

2019

Peer reviewed|Thesis/dissertation

UNIVERSITY OF CALIFORNIA,
IRVINE

Transition Metal Complexes of Modified Azaphosphatranes

DISSERTATION

submitted in partial satisfaction of the requirements
for the degree of

DOCTOR OF PHILOSOPHY

in Chemistry

by

Zachary Thammavongsy

Dissertation Committee:
Professor Jenny Y. Yang, Chair
Professor Andrew S. Borovik
Professor William J. Evans

2019

DEDICATION

For my mother, Kor, and my father, Vinai, who sacrificed their lives for me to live out mine.

TABLE OF CONTENTS

	Page
LIST OF FIGURES	vii
LIST OF TABLES	xv
LIST OF SCHEMES	xvi
LIST OF CHARTS	xvii
ACKNOWLEDGMENTS	xviii
CURRICULUM VITAE	xix
ABSTRACT OF THE DISSERTATION	xxv
INTRODUCTION	1
CHAPTER 1: The Electronic and Steric Tolman Parameters of Proazaphosphatranes: Synthesis, Characterization, and Measurements	12
1.1. Motivation and Specific Aims	13
1.2. Background	13
1.3. Results and Discussion	15
1.3.1. Synthesis and Structure of Ni(L ^R)(CO) ₃ Complexes (1-4)	15
1.3.2. Synthesis and Structure of Ni(L ^{Me}) ₂ (CO) ₂ Complex (5)	18
1.3.3. Tolman Electronic Parameters and Cone Angles of Ni(L ^R)(CO) ₃ Complexes (1-4)	21
1.4. Conclusion	23
1.5. Experimental Details	24
1.6. References	38
CHAPTER 2: Expanding the Denticity of Proazaphosphatranes: Ligand Synthesis	41
2.1. Motivation and Specific Aims	42
2.2. Background	43
2.3. Results and Discussion	43
2.3.1. Synthesis of Tri-Substituted Tris(2-aminoethyl)amines	43
2.3.2. Synthesis of Protonated Tri-Substituted Azaphosphatranes	44
2.3.3. Synthesis of Tri-Substituted Proazaphosphatranes	46
2.4. Conclusion	49
2.5. Experimental Details	49
2.6. References	70

CHAPTER 3: Tracking the Transannular Bond Interaction in Tris(2-pyridylmethyl)-azaphosphatrane (TPAP) with Various Transition Metal ions	75
3.1. Motivation and Specific Aims	76
3.2. Background	77
3.3. Results and Discussion	81
3.3.1. Synthesis and Structure of CoTPAP Complexes (1 & 2)	81
3.3.2. Attempted Synthesis and Characterization of Co(III)TPAP Complexes (2a-c)	84
3.3.3. Synthesis and Structure of NiTPAP (3 , 4 & 3a), PdTPAP (5) and PtTPAP (6) Complexes	87
3.3.4. Comparison of the Transannular Distance of Co(I)TPAP and Co(II)TPAP	91
3.3.5. Comparison of the Transannular Distance between Group 10 TPAP Complexes	92
3.3.6. Metal Ion Oxidation State Effects on TPAP	93
3.3.7. Quantum Mechanical Calculations	93
3.4. Conclusion	96
3.5. Experimental Details	97
3.6. References	116
CHAPTER 4: Small Molecule Activation with Transition Metal Tris(2-pyridylmethyl)azaphosphatrane Complexes	122
4.1. Motivation and Specific Aims	123
4.1.1. CO ₂ Reduction	123
4.1.2. O ₂ Reactivity	123
4.1.3. Hydrogenation (H ₂)	124
4.2. Background	124
4.2.1. Ni-CO ₂ Complexes	124
4.2.2. Cu ₂ O ₂ Complexes	125
4.2.3. Ir-H ₂ Complexes	126
4.3. Results and Discussion	127
4.3.1. Reaction of Ni(TPAP)(COD) with CO ₂	127
4.3.2. Synthesis and Structure of CuTPAP Complex	129
4.3.3. Reaction of CuTPAP with O ₂	131
4.3.4. Synthesis of IrH(TPAP)Cl	133
4.3.5. Synthesis of IrH ₂ (TPAP)	134
4.3.6. Reaction of IrH(TPAP)Cl with H ₂	135
4.4. Conclusion	136
4.4.1. Ni(TPAP)(COD) + CO ₂	136
4.4.2. Cu(TPAP) + O ₂	137
4.4.3. IrH(TPAP)Cl + H ₂	137
4.5. Experimental Details	137
4.6. References	146

APPENDIX A: Crystal Structure of NiFe(CO)₅(Tris(2-pyridylmethyl)azaphosphatrane); A Synthetic Mimic of the NiFe Hydrogenase Active Site Incorporating a Pendant Pyridine Base	148
A.1. Motivation and Specific Aims	149
A.2. Background	150
A.3. Results and Discussion	151
A.3.1. Structural Commentary	151
A.3.2. Database Survey	153
A.4. Conclusion	154
A.5. Experimental Details	154
A.6. References	158
APPENDIX B: Attempted Protonation and p<i>K</i>_a Measurement of Tris(2-pyridylmethyl)azaphosphatraneoxide	160
B.1. Motivation and Specific Aims	161
B.2. Background	161
B.3. Results and Discussion	162
B.3.1. Synthesis and Characterization of Tris(2-pyridylmethyl)azaphosphatrane- oxide (TPAPO)	162
B.3.2. Protonation study of Tris(2-pyridylmethyl)azaphosphatraneoxide (TPAPO)	163
B.3.3. Protonation study of Tris(benzyl)azaphosphatraneoxide (TBAPO)	166
B.4. Conclusion	168
B.5. Experimental Details	169
B.6. References	173
APPENDIX C: Coordination Complexes of Phosphine Ligands without Transannular Interactions	174
C.1. Motivation and Specific Aims	175
C.2. Background	175
C.3. Results and Discussion	176
C.3.1. Synthesis of Co(II)(Tris(2-pyridylmethyl)aminophosphine) Complex	176
C.3.2. Synthesis of Tris(2-pyridylethyl)aminophosphine (TPEAP)	177
C.3.3. Synthesis of Co(II)TPEAP Complex	178
C.4. Conclusion	180
C.5. Experimental Details	180
C.6. References	184
APPENDIX D: Attempted Synthesis of an Fe-Sulfur-Carbide Cluster	185
D.1. Motivation and Specific Aims	186
D.2. Background	186
D.3. Results and Discussion	187
D.4. Conclusion	190
D.5. Experimental Details	191
D.6. References	202

APPENDIX E: CH₄ Activation Study with Fe(depe)₂ Derivatives	203
E.1. Motivation and Specific Aims	204
E.2. Background	204
E.2.1. Oxidative Addition	205
E.2.2. Sigma-Bond Metathesis	206
E.2.3. 1,2-Addition	206
E.2.4. Metalloradicals	206
E.2.5. Electrophilic Activation	207
E.2.6. Base Assisted Activation for C-H Activation	207
E.3. Results and Discussion	207
E.3.1. Synthesis of [FeCl(CO)(depe) ₂]Cl	207
E.3.2. Reactivity with CH ₄	208
E.3.3. Reactivity with CH ₄ and DBU	209
E.4. Conclusion	210
E.5. Experimental Details	210
E.6. References	215

LIST OF FIGURES

		Page
Figure 0.1.	Chemical Structures of the work done by (left) Stephan's group, (middle) Krempner's group and (right) Martinez's group on expanding the use of azaphosphatranes.	2
Figure 0.2.	Chemical Structures of transition metal complexes of isobutyl-azaphosphatrane by (left) Martinez's group and (right) Johnson's group.	4
Figure 1.1.	Chemdraw depicting the Tolman Electronic (TEP) and Steric Parameter (cone angle Θ) of a generic Ni(phosphine)(CO) ₃ .	14
Figure 1.2.	IR spectra of (purple) Ni(L ^{Me})(CO) ₃ (1), (green) Ni(L ^{iPr})(CO) ₃ (2), (red) Ni(L ^{iBu})(CO) ₃ (3) and (brown) Ni(L ^{Bz})(CO) ₃ (4) in CH ₂ Cl ₂ .	16
Figure 1.3.	Crystal structure of Ni(L ^{iPr})(CO) ₃ (2), Ni(L ^{iBu})(CO) ₃ (3), Ni(L ^{Bz})(CO) ₃ (4) and Ni(L ^{Me}) ₂ (CO) ₂ (5). Thermal ellipsoids are drawn at 80% probability; hydrogen atoms are omitted for clarity. Carbon atoms from the minor part of a disorder in 3 are also omitted.	19
Figure 1.4.	Comparison of Tolman electronic parameter (TEP) and cone angles. Red dots (●) represent proazaphosphatranes measured herein and black dots (●) represent phosphines measured by Tolman.	21
Figure 1.5.	Proposed electronic properties of generic tri(dialkylamino)phosphine and the metrical parameters observed from crystal structures.	23
Figure 1.6.	¹ H NMR spectrum of Ni(L ^{Me})(CO) ₃ (1) in C ₆ D ₆ .	27
Figure 1.7.	¹³ C NMR spectrum of Ni(L ^{Me})(CO) ₃ (1) in C ₆ D ₆ .	28
Figure 1.8.	³¹ P NMR spectrum of Ni(L ^{Me})(CO) ₃ (1) in C ₆ D ₆ .	28
Figure 1.9.	¹ H NMR spectrum of Ni(L ^{iPr})(CO) ₃ (2) in C ₆ D ₆ .	29
Figure 1.10.	¹³ C NMR spectrum of Ni(L ^{iPr})(CO) ₃ (2) in C ₆ D ₆ .	30
Figure 1.11.	³¹ P NMR spectrum of Ni(L ^{iPr})(CO) ₃ (2) in C ₆ D ₆ .	30
Figure 1.12.	¹ H NMR spectrum of Ni(L ^{iBu})(CO) ₃ (3) in C ₆ D ₆ .	31
Figure 1.13.	¹³ C NMR spectrum of Ni(L ^{iBu})(CO) ₃ (3) in C ₆ D ₆ .	32

Figure 1.14.	^{31}P NMR spectrum of $\text{Ni}(\text{L}^{i\text{Bu}})(\text{CO})_3$ (3) in C_6D_6 . Resonances around 20 ppm are due to oxidized $\text{L}^{i\text{Bu}}$.	32
Figure 1.15.	^1H NMR spectrum of $\text{Ni}(\text{L}^{\text{Bz}})(\text{CO})_3$ (4) in C_6D_6 .	33
Figure 1.16.	^{13}C NMR spectrum of $\text{Ni}(\text{L}^{\text{Bz}})(\text{CO})_3$ (4) in C_6D_6 .	34
Figure 1.17.	^{31}P NMR spectrum of $\text{Ni}(\text{L}^{\text{Bz}})(\text{CO})_3$ (4) in C_6D_6 .	34
Figure 1.18.	^1H NMR spectrum of $\text{Ni}(\text{L}^{\text{Me}})_2(\text{CO})_2$ (5) in C_6D_6 .	36
Figure 1.19.	^{13}C NMR spectrum of $\text{Ni}(\text{L}^{\text{Me}})_2(\text{CO})_2$ (5) in C_6D_6 .	36
Figure 1.20.	^{31}P NMR spectrum of $\text{Ni}(\text{L}^{\text{Me}})_2(\text{CO})_2$ (5) in C_6D_6 .	37
Figure 1.21.	IR spectrum $\text{Ni}(\text{L}^{\text{Me}})_2(\text{CO})_2$ (5) in CH_2Cl_2 .	37
Figure 2.1.	Crystal structure of $[\text{HP}((2\text{-PyrCH}_2)\text{-NCH}_2\text{CH}_2)_3\text{N}][\text{Cl}]$ (1b). Thermal ellipsoids are drawn at 50% probability; hydrogen atoms except for H1, which is located in the difference map and refined freely, and Cl^- anion were omitted for clarity.	46
Figure 2.2.	Crystal structure of $[\text{P}((3\text{-PyrCH}_2)\text{-NCH}_2\text{CH}_2)_3\text{N}]$ (2c). Thermal ellipsoids are drawn at 50% probability; hydrogen atoms were omitted for clarity.	49
Figure 2.3.	^1H NMR spectrum of tris[[4-(2-pyridyl)benzyl]amino]ethyl]amine (4a) in CDCl_3 .	53
Figure 2.4.	$^{13}\text{C}\{^1\text{H}\}$ NMR spectrum of tris[[4-(2-pyridyl)benzyl]amino]ethyl]amine (4a) in CDCl_3 .	53
Figure 2.5.	^1H NMR spectrum of $[\text{HP}((2\text{-PyrCH}_2)\text{-NCH}_2\text{CH}_2)_3\text{N}][\text{Cl}]$ (1b) in CD_3CN .	55
Figure 2.6.	$^{31}\text{P}\{^1\text{H}\}$ NMR spectrum of $[\text{HP}((2\text{-PyrCH}_2)\text{-NCH}_2\text{CH}_2)_3\text{N}][\text{Cl}]$ (1b) in CD_3CN .	55
Figure 2.7.	^{31}P NMR spectrum of $[\text{HP}((2\text{-PyrCH}_2)\text{-NCH}_2\text{CH}_2)_3\text{N}][\text{Cl}]$ (1b) in CD_3CN .	56
Figure 2.8.	$^{13}\text{C}\{^1\text{H}\}$ NMR spectrum of $[\text{HP}((2\text{-PyrCH}_2)\text{-NCH}_2\text{CH}_2)_3\text{N}][\text{Cl}]$ (1b) in CD_3CN .	56
Figure 2.9.	^1H NMR spectrum of $[\text{P}((2\text{-PyrCH}_2)\text{-NCH}_2\text{CH}_2)_3\text{N}]$ (1c) in CD_3CN .	58

Figure 2.10.	^{31}P NMR spectrum of $[\text{P}((2\text{-PyrCH}_2)\text{-NCH}_2\text{CH}_2)_3\text{N}]$ (1c) in CD_3CN .	59
Figure 2.11.	$^{31}\text{P}\{^1\text{H}\}$ NMR spectrum of $[\text{P}((2\text{-PyrCH}_2)\text{-NCH}_2\text{CH}_2)_3\text{N}]$ (1c) in C_6D_6 .	59
Figure 2.12.	$^{13}\text{C}\{^1\text{H}\}$ NMR spectrum of $[\text{P}((2\text{-PyrCH}_2)\text{-NCH}_2\text{CH}_2)_3\text{N}]$ (1c) in CD_3CN .	60
Figure 2.13.	^1H NMR spectrum of $[\text{P}((3\text{-PyrCH}_2)\text{-NCH}_2\text{CH}_2)_3\text{N}]$ (2c) in CD_3CN .	62
Figure 2.14.	$^{31}\text{P}\{^1\text{H}\}$ NMR spectrum of $[\text{P}((3\text{-PyrCH}_2)\text{-NCH}_2\text{CH}_2)_3\text{N}]$ (2c) in C_6D_6 .	62
Figure 2.15.	$^{13}\text{C}\{^1\text{H}\}$ NMR spectrum of $[\text{P}((3\text{-PyrCH}_2)\text{-NCH}_2\text{CH}_2)_3\text{N}]$ (2c) in CD_3CN .	63
Figure 2.16.	^1H NMR spectrum of $[\text{P}((\text{Furan-CH}_2)\text{-NCH}_2\text{CH}_2)_3\text{N}]$ (3c) in CD_3CN .	64
Figure 2.17.	$^{31}\text{P}\{^1\text{H}\}$ NMR spectrum of $[\text{P}((\text{Furan-CH}_2)\text{-NCH}_2\text{CH}_2)_3\text{N}]$ (3c) in C_6D_6 .	65
Figure 2.18.	$^{13}\text{C}\{^1\text{H}\}$ NMR spectrum of $[\text{P}((\text{Furan-CH}_2)\text{-NCH}_2\text{CH}_2)_3\text{N}]$ (3c) in CD_3CN .	65
Figure 2.19.	^1H NMR spectrum of $[\text{P}((2\text{-Pyr-Ph-CH}_2)\text{-NCH}_2\text{CH}_2)_3\text{N}]$ (4c) in CD_3CN .	66
Figure 2.20.	$^{13}\text{C}\{^1\text{H}\}$ NMR spectrum of $[\text{P}((2\text{-Pyr-Ph-CH}_2)\text{-NCH}_2\text{CH}_2)_3\text{N}]$ (4c) in CD_3CN .	67
Figure 2.21.	$^{31}\text{P}\{^1\text{H}\}$ NMR spectrum of $[\text{P}((2\text{-Pyr-Ph-CH}_2)\text{-NCH}_2\text{CH}_2)_3\text{N}]$ (4c) in C_6D_6 .	67
Figure 2.22.	^1H NMR spectrum of $[\text{P}((2\text{-CH}_3\text{-Thiophene-CH}_2)\text{-NCH}_2\text{CH}_2)_3\text{N}]$ (5c) in CD_3CN .	68
Figure 2.23.	$^{31}\text{P}\{^1\text{H}\}$ NMR spectrum of $[\text{P}((2\text{-CH}_3\text{-Thiophene-CH}_2)\text{-NCH}_2\text{CH}_2)_3\text{N}]$ (5c) in C_6D_6 .	69
Figure 2.24.	$^{13}\text{C}\{^1\text{H}\}$ NMR spectrum of $[\text{P}((2\text{-CH}_3\text{-Thiophene-CH}_2)\text{-NCH}_2\text{CH}_2)_3\text{N}]$ (5c) in CD_3CN .	69
Figure 3.1.	Chemdraw structures of azaphosphatrane in three different forms based on the transannular distance of P-N_{ax} .	76
Figure 3.2.	Chemdraw structures of (a) Peters', (b) Parkin's, (c) Lu's and (d) Agapie's transition metal complexes, featuring an adaptable ligand platform.	78

- Figure 3.3. (Left) Plot of the transannular distance versus the θ puckering of the axial nitrogen above the plane of the three adjacent carbon atoms for Verkade's Superbase with various main groups (denoted in black circles ●) and TPAP with various transition metals (denoted in red diamonds ◆). (Right) Depiction of the angle, θ , as the degree of puckering of the axial nitrogen (N_{ax}) out of the $C_1-C_3-C_5$ plane. Values used in this figure are from structural data. 79
- Figure 3.4. Crystal structure of CoTPAP(Cl) (**1**). Thermal ellipsoids are drawn at 50% probability. Hydrogen atoms and counteranions are omitted for clarity. 82
- Figure 3.5. Crystal structure of [Co(TPAP)(CH₃CN)][BF₄]₂ (**2**). Thermal ellipsoids are drawn at 50% probability. Hydrogen atoms and counteranions are omitted for clarity. 83
- Figure 3.6. Crystal structure of [Co(II)(acac)][TPAPH] (**2a**). Thermal ellipsoids are drawn at 50% probability. Hydrogen atoms are omitted for clarity. 84
- Figure 3.7. Crystal structure of [TPAP][BF₄]₂ (**2b**). Thermal ellipsoids are drawn at 50% probability. Hydrogen atoms and BF₄ counteranions are omitted for clarity. 86
- Figure 3.8. Crystal structure of [CoCl₃(TPAPH)] (**2c**). Thermal ellipsoids are drawn at 50% probability. Hydrogen atoms are omitted for clarity. 87
- Figure 3.9. Crystal structure of NiTPAP(COD) (**3**). Thermal ellipsoids are drawn at 50% probability. Hydrogen atoms are omitted for clarity. 88
- Figure 3.10. Crystal structure of NiTPAP(CO₂) (**3a**). Thermal ellipsoids are drawn at 80% probability. Hydrogen atoms and counteranions are omitted for clarity. 89
- Figure 3.11. Crystal structure of (a) [NiTPAP(CH₃CN)][BF₄]₂ (**4**), (b) [PdTPAP(CH₃CN)][BF₄]₂ (**5**) and (c) [PtTPAP(Cl)][PF₆] (**6**). Structures **5** and **6** display one of two molecules in the asymmetric unit. Thermal ellipsoids drawn are at 50% probability. Hydrogen atoms and counteranions are omitted for clarity. Electron density from the minor disorder of the Pt atom in **6** is also omitted. 90
- Figure 3.12. (Left) HOMOs of Ni(0)TPAP(CO)₂ (**3a**) and (Right) [Ni(II)TPAP(CH₃CN)]²⁺ (**4**). All surfaces are at an isovalue of 0.035. 95

Figure 3.13.	Crystal structure of CoTPAP(Cl) (1b) Thermal ellipsoids are drawn at 50% probability. Hydrogen atoms are omitted for clarity. Grown from a pentane diffusion into a concentrated THF solution by Reed J. Eisenhart from the University of Minnesota.	101
Figure 3.14.	EPR spectrum of [CoTPAP(CH ₃ CN)][BF ₄] ₂ (2) in a frozen solution of acetonitrile at 77 K.	102
Figure 3.15.	UV-vis spectrum of [CoTPAP(CH ₃ CN)][BF ₄] ₂ (2) in acetonitrile at 22° C. An inset display a close up of the bands between 500 and 1000 nm.	103
Figure 3.16.	Variable scan rate cyclic voltammograms of [CoTPAP(CH ₃ CN)][BF ₄] ₂ (2) with 1.0 mM analyte in acetonitrile with 0.02 M Bu ₄ NPF ₆ .	103
Figure 3.17.	Solution magnetic susceptibility. ¹ H NMR spectra of [CoTPAP(CH ₃ CN)][BF ₄] ₂ (2) at 237, 268 and 298 K in in CD ₃ CN.	104
Figure 3.18.	¹ H NMR spectrum of NiTPAP(COD) (3) in C ₆ D ₆ .	106
Figure 3.19.	³¹ P { ¹ H} spectrum of NiTPAP(COD) (3) in C ₆ D ₆ .	106
Figure 3.20.	IR spectrum of NiTPAP(CO) ₂ (3a) in CH ₂ Cl ₂ .	108
Figure 3.21.	¹ H NMR spectrum of NiTPAP(CO) ₂ (3a) in C ₆ D ₆ .	108
Figure 3.22.	¹³ C NMR spectrum of NiTPAP(CO) ₂ (3a) in C ₆ D ₆ .	109
Figure 3.23.	³¹ P { ¹ H} NMR spectrum of NiTPAP(CO) ₂ (3a) in C ₆ D ₆ .	109
Figure 3.24.	¹ H NMR of spectrum of [NiTPAP(CH ₃ CN)][BF ₄] ₂ (4) in CD ₃ CN.	111
Figure 3.25.	¹ H NMR spectrum of [PdTPAP(CH ₃ CN)][BF ₄] ₂ (5) in CD ₃ CN.	113
Figure 3.26.	³¹ P { ¹ H} NMR spectrum of [PdTPAP(CH ₃ CN)][BF ₄] ₂ (5) in CD ₃ CN.	113
Figure 3.27.	¹ H NMR spectrum of [PtTPAPCl][PF ₆] ₂ (6) in CD ₃ CN.	115
Figure 3.28.	³¹ P { ¹ H} NMR spectrum of [PtTPAPCl][PF ₆] ₂ (6) in CD ₃ CN.	115
Figure 4.1.	Structurally characterized Ni-CO ₂ mononuclear complexes.	125
Figure 4.2.	Structurally characterized Cu ₂ O ₂ complexes with di- and tri-dentate N ligands.	126
Figure 4.3.	Ir(III) complexes bearing strong sigma donor ligands.	127

Figure 4.4.	IR spectrum of brown solid from the reactivity of Ni(TPAP)(COD) with CO ₂ .	128
Figure 4.5.	IR spectra of (blue) NiTPAP(CO) ₂ and (red) Ni(TPAP)(COD) + CO ₂ after 3 days of sitting at room temperature.	129
Figure 4.6.	Crystal structure of [Cu(TPAP)] ₂ [BF ₄] ₂ . Thermal ellipsoids are drawn at 50% probability; hydrogen atoms and counter anions omitted for clarity.	131
Figure 4.7.	UV-vis spectra of (red) CuTPAP and (green) CuTPAP + O ₂ in CH ₃ CN.	132
Figure 4.8.	EPR spectrum of green product from the reaction of CuTPAP with O ₂ in CH ₃ CN at 77K.	132
Figure 4.9.	Crystal structure of IrH(TPAP)Cl. Solvents molecules (dichloromethane and diethyl ether) and hydrogens are omitted for clarity except for H1, which was located in the difference map and refined freely.	134
Figure 4.10.	Crystal structure of IrH ₂ (TPAP). Solvents molecule (tetrahydrofuran), LiCl, and hydrogens are omitted for clarity except for H1 and H2, which were located in the difference map and refined freely.	135
Figure 4.11.	¹ H NMR spectrum of IrH(TPAP)Cl + AgBF ₄ + H ₂ in CD ₂ Cl ₂ . Inset displays a close up view of the hydride region.	136
Figure 4.12.	¹ H NMR spectrum of Cu(TPAP) complex in CD ₃ CN.	140
Figure 4.13.	³¹ P { ¹ H} NMR spectrum of Cu(TPAP) complex in CD ₃ CN.	140
Figure 4.14.	¹ H NMR spectrum of IrH(TPAP)Cl in CD ₂ Cl ₂ . Inset displays a close up view of the hydride region.	142
Figure 4.15.	³¹ P { ¹ H} NMR spectrum of IrH(TPAP)Cl in CD ₂ Cl ₂ . Inset displays a close up view of the resonance.	142
Figure 4.16.	¹ H NMR spectrum of IrH ₂ (TPAP) in CD ₂ Cl ₂ .	143
Figure 4.17.	³¹ P { ¹ H} NMR spectrum of IrH ₂ (TPAP) in CD ₂ Cl ₂ .	144
Figure 4.18.	³¹ P { ¹ H} NMR spectrum of [IrH(TPAP)Cl] + AgBF ₄ + H ₂ in CD ₂ Cl ₂ .	145

Figure A.1.	The molecular structure of complex NiFe(TPAP)(CO) ₅ . The displacement ellipsoids are drawn at the 50% probability level. For clarity, the hydrogen atoms have been omitted.	152
Figure A.2.	¹ H NMR spectrum of NiFe(TPAP)(CO) ₅ in C ₆ D ₆ .	157
Figure A.3.	³¹ P{ ¹ H} NMR spectrum of NiFe(TPAP)(CO) ₅ in C ₆ D ₆ .	157
Figure B.1.	³¹ P{ ¹ H} NMR spectrum of tris(2-pyridylmethyl)azaphosphatranexoxide (TPAPO) + HBF ₄ in CD ₃ CN.	164
Figure B.2.	³¹ P{ ¹ H} NMR spectrum of tris(2-pyridylmethyl)azaphosphatranexoxide (TPAPO) + TsOH in CD ₃ CN.	165
Figure B.3.	³¹ P{ ¹ H} NMR spectrum of tris(benzy)azaphosphatranexoxide (TBAPO) + HBF ₄ in CD ₃ CN.	167
Figure B.4.	³¹ P{ ¹ H} NMR spectrum of tris(benzy)azaphosphatranexoxide (TBAPO) + TsOH in CD ₃ CN.	168
Figure B.5.	¹ H NMR spectrum of tris(2-pyridylmethyl)azaphosphatranexoxide (TPAPO) in CD ₃ CN.	170
Figure B.6.	³¹ P{ ¹ H} NMR spectrum of tris(2-pyridylmethyl)azaphosphatranexoxide (TPAPO) in CD ₃ CN.	171
Figure C.1.	Crystal structure of [Co(TPMAP) ₂][BF ₄] ₂ . Thermal ellipsoids are drawn at 50% probability. Hydrogen atoms and counter anions are omitted for clarity.	177
Figure C.2.	Crystal structure of [Co(TPEAP)(CH ₃ CN)][BF ₄] ₂ . Thermal ellipsoids are drawn at 50% probability. Hydrogen atoms and counter anions are omitted for clarity.	179
Figure C.3.	¹ H NMR spectrum of tris(2-pyridylethyl)aminophosphine (TPEAP) in CD ₃ CN.	183
Figure C.4.	³¹ P{ ¹ H}NMR spectrum of tris(2-pyridylethyl)aminophosphine (TPEAP) in CD ₃ CN.	183
Figure D.1.	Structurally characterized Fe complexes containing either sulfur or carbide-like components as partial FeMoco synthetic mimics.	187
Figure D.2.	Crystal structure of Fe ₅ (CO) ₁₅ C. Thermal ellipsoids are drawn at 50% probability.	190

Figure D.3.	IR spectra of (red, top) $[\text{Me}_4\text{N}]_2[\text{Fe}_6(\text{CO})_{16}\text{C}^{2-}]$ and the product of (blue, bottom) $[\text{Me}_4\text{N}]_2[\text{Fe}_6(\text{CO})_{16}\text{C}^{2-}] + \text{S}_8$.	192
Figure D.4.	IR spectra of (red, top) $[\text{Me}_4\text{N}]_2[\text{Fe}_6(\text{CO})_{16}\text{C}^{2-}]$ and the product of (blue, bottom) $[\text{Me}_4\text{N}]_2[\text{Fe}_6(\text{CO})_{16}\text{C}^{2-}] + \text{S}_8$ under UV light.	193
Figure D.5.	IR spectra of (red, top) $[\text{Me}_4\text{N}]_2[\text{Fe}_6(\text{CO})_{16}\text{C}^{2-}]$ and the product of (blue, bottom) $[\text{Me}_4\text{N}]_2[\text{Fe}_6(\text{CO})_{16}\text{C}^{2-}] + \text{PhCH}_2\text{SH}$.	194
Figure D.6.	IR spectra of (red, top) $[\text{Me}_4\text{N}]_2[\text{Fe}_6(\text{CO})_{16}\text{C}^{2-}]$ and the product of (blue, bottom) $[\text{Me}_4\text{N}]_2[\text{Fe}_6(\text{CO})_{16}\text{C}^{2-}] + \text{PhCH}_2\text{SH}$ under UV light.	195
Figure D.7.	IR spectra of (red, top) $[\text{Me}_4\text{N}]_2[\text{Fe}_6(\text{CO})_{16}\text{C}^{2-}]$ and the product of (blue, bottom) $[\text{Me}_4\text{N}]_2[\text{Fe}_6(\text{CO})_{16}\text{C}^{2-}] + {}^i\text{PrSH}$.	196
Figure D.8.	IR spectra of (red, top) $[\text{Me}_4\text{N}]_2[\text{Fe}_6(\text{CO})_{16}\text{C}^{2-}]$ and the product of (blue, bottom) $[\text{Me}_4\text{N}]_2[\text{Fe}_6(\text{CO})_{16}\text{C}^{2-}] + {}^i\text{PrSH}$ under UV light.	197
Figure D.9.	IR spectra of (red, top) $[\text{Me}_4\text{N}]_2[\text{Fe}_6(\text{CO})_{16}\text{C}^{2-}]$ and the product of (blue, bottom) $[\text{Me}_4\text{N}]_2[\text{Fe}_6(\text{CO})_{16}\text{C}^{2-}] + p\text{-FC}_6\text{H}_4\text{SH}$.	198
Figure D.10.	IR spectra of (red, top) $[\text{Me}_4\text{N}]_2[\text{Fe}_6(\text{CO})_{16}\text{C}^{2-}]$ and the product of (blue, bottom) $[\text{Me}_4\text{N}]_2[\text{Fe}_6(\text{CO})_{16}\text{C}^{2-}] + p\text{-FC}_6\text{H}_4\text{SH}$ under UV light.	199
Figure D.11.	IR spectra of (red, top) $[\text{Me}_4\text{N}]_2[\text{Fe}_6(\text{CO})_{16}\text{C}^{2-}]$ and the product of (blue, bottom) $[\text{Me}_4\text{N}]_2[\text{Fe}_6(\text{CO})_{16}\text{C}^{2-}] + \text{Me}_2\text{S}_2$.	200
Figure D.12.	IR spectra of (red, top) $[\text{Me}_4\text{N}]_2[\text{Fe}_6(\text{CO})_{16}\text{C}^{2-}]$ and the product of (blue, bottom) $[\text{Me}_4\text{N}]_2[\text{Fe}_6(\text{CO})_{16}\text{C}^{2-}] + \text{Me}_2\text{S}_2$ under UV light.	201
Figure E.1.	${}^1\text{H}$ NMR spectrum of $[\text{Fe}(\text{CO})(\text{depe})_2]\text{Cl} + \text{AgSbF}_6 + \text{CH}_4$ in CD_2Cl_2 .	212
Figure E.2.	${}^{31}\text{P}\{^1\text{H}\}$ NMR spectrum of $[\text{Fe}(\text{CO})(\text{depe})_2]\text{Cl} + \text{AgSbF}_6 + \text{CH}_4$ in CD_2Cl_2 .	212
Figure E.3.	${}^1\text{H}$ NMR spectrum of $[\text{Fe}(\text{CO})(\text{depe})_2]\text{Cl} + \text{AgSbF}_6 + \text{CH}_4 + \text{DBU}$ in CD_2Cl_2 .	213
Figure E.4.	${}^{31}\text{P}\{^1\text{H}\}$ NMR spectrum of $[\text{Fe}(\text{CO})(\text{depe})_2]\text{Cl} + \text{AgSbF}_6 + \text{CH}_4 + \text{DBU}$ in CD_2Cl_2 .	214

LIST OF TABLES

	Page
Table 1.1. CO vibrational frequencies (in CH ₂ Cl ₂) and cone angle of complexes 1-4 and selected Ni(CO) ₃ (PR ₃) complexes.	17
Table 1.2. Crystallographic data and refinement parameters for complexes 2-5 .	20
Table 1.3. Selected distances and angles of 2-5 .	20
Table 2.1. ³¹ P NMR values of 1c-5c and various alkyl- and benzyl-substituted proazaphosphatranes in C ₆ D ₆ reported by Verkade <i>et al.</i> Grey out rows represents asymmetric proazaphosphatranes.	48
Table 3.1. Bond lengths and angles of complexes 1-6 . Metrics 5 and 6 were taken from one of two molecules in the asymmetric unit. Metal ion is denoted as M. Non-italicized values are from the X-ray structural analysis and italicized values are from the geometry optimized structures calculated using quantum mechanical methods.	91
Table 3.2. Results of NBO analysis of donor-acceptor interactions in compound adducts, estimated by second-order perturbation theory, E ⁽²⁾ _{i→j} (kcal mol ⁻¹).	94
Table 3.3. Calculated geometrical parameters for selected mono-Cationic and di-cationic comparison.	96
Table A.1. Selected geometric parameters of NiFe(TPAP)(CO) ₅ (Å, °).	153
Table D.1. Attempted substitution of carbonyl with sulfur reagents in [Me ₄ N] ₂ [Fe ₆ (CO) ₁₆ C ²⁻].	188

LIST OF SCHEMES

	Page
Scheme 2.1. Synthesis of tri-substituted tris(2-aminoethyl)amine.	44
Scheme 2.2. Synthesis of protonated tri-substituted azaphosphatranes	45
Scheme 2.3. Synthesis of tri-substituted proazaphosphatranes	47
Scheme 4.1. Proposed reactivity of CO ₂ with NiTPAP(COD).	128
Scheme 4.2. Synthesis of [Cu(TPAP)] ₂ [BF ₄] ₂ complex.	130
Scheme 4.3. Synthesis of [IrH(TPAP)Cl] and [IrH ₂ (TPAP)].	133
Scheme A.1. Synthesis of NiFe(TPAP)(CO) ₅ .	151
Scheme B.1. Proposed Reduction-Coupled Oxo Activation (ROA) mechanism in VPO system.	161
Scheme B.2. Synthesis of tris(2-pyridylmethyl)azaphosphatraneoxide (TPAPO).	162
Scheme B.3. Proposed reactivity of tris(2-pyridylmethyl)azaphosphatraneoxide (TPAPO) with HBF ₄ .	163
Scheme B.4. Proposed reactivity of tris(2-pyridylmethyl)azaphosphatraneoxide (TPAPO) with TsOH.	165
Scheme B.5. Reactivity of tris(benzyl)azaphosphatraneoxide (TBAPO) with HBF ₄ or TsOH.	166
Scheme C.1. Coordination of TPMPAP with [Co(CH ₃ CN) ₆][BF ₄] ₂ .	176
Scheme C.2. Synthesis of tris(2-pyridylethyl)aminophosphine (TPEAP).	178
Scheme C.3. Coordination of TPEAP with [Co(CH ₃ CN) ₆][BF ₄] ₂ .	178
Scheme E.1. Categories of C-H activation of methane. a) oxidative addition, b) σ-bond metathesis, c) electrophilic activation, d) 1,2 addition and e) metalloradical.	205
Scheme E.2. Synthesis of FeCl ₂ (depe) ₂ and [FeCl(CO)(depe) ₂]Cl.	208
Scheme E.3. Reactivity of [FeCl(CO)(depe) ₂]Cl with CH ₄ .	209
Scheme E.4. Reactivity of [FeCl(CO)(depe) ₂]Cl with CH ₄ and DBU.	210

LIST OF CHARTS

	Page
Chart 0.1. Protonation of proazaphosphatranes (Verkade's Superbases) with a generic proton. The pK_a values of the conjugate acid shown in the table to the right, with various R groups.	1
Chart 1.1. Series of $Ni(CO)_x$ ($x = 2$ or 3) complexes of Verkade's Superbases.	15
Chart 2.1. Series of Proazaphosphatrane Compounds with Various Functional Groups.	42
Chart 3.1. Transition Metal Complexes of TPAP.	81
Chart C.1. Ligand with Bicyclic Caged Framed (TPAP) and without (TPMAP & TPEAP).	175

ACKNOWLEDGMENTS

I want to thank my professor for encouraging me every step of the way.
(*Professor Jenny Y. Yang*)

I want to thank my committee members for pushing me to become the best chemist I can be.
(*Professor A.S. Borovik & Professor Bill Evans*)

I want to thank everyone in the Yang lab for making my time in graduate school feel like home.
(*Brian, Bianca, Juliet, Charlene, Annie, Steve, Jake, Alex, Caitlin, Jeff, Drew, Ivy, Wyeth, Rebecca, Sam, Nehal, Natty, Kevin, Hazel, Reyna, Jessica and Andrew*)

I want to thank every graduate student at UCI that shared a meal with me.
(*Austin, Dan, Casey, Rommy, Miles, Mike x2, Sarah, Luke, Stan, Kevin, Kellen, Lin, Raph, Yilin, Kate, Gerald, Tyler, Claudia, Chad, David, Dalen, Millie, and Adam*)

I want to thank my family and friends who came to visit me.
(*Som, Sarah, Eric, Pranee, Ular, Lincy, Nalong, Thongsai, Aunt Phet, Ali, Russ, Andrea, Ryan, Andrew x2, Dennis, Will, Tien, Randy, Val, Daniel and Eddie*)

I want to thank the Irvine friends that made Southern California feel like home.
(*Frank, Shauna, John, Jina, Khang, Lawrence, Robert, Pranee and Sensei*)

I want to thank my parents for inspiring me to work hard.
(*Kor and Vinai*)

I want to thank my grandparents for their love and care.
(*Mong and Thongdam*)

I want to thank my wife for everything. I love her with every atom in my body. I would not have made it through graduate school without her. I am happy to have completed this journey with her and I look forward to the rest of our journey together on this planet.
(*Kim V. Le*)

CURRICULUM VITAE

Zachary Thammavongsy

Education

University of California, Irvine , Irvine, CA Ph.D. in Chemistry: Spring 2019	2013 - 2019
Western Washington University , Bellingham, WA M.S. in Chemistry: June 2013 B.S. in Chemistry: June 2011 Minor in German	2006 - 2013

Research Experience

University of California, Irvine , <i>Graduate Research</i> , Irvine, CA Advisor: Professor Jenny Y. Yang Research Project Title: "Transition Metal Complexes of Modified Azaphosphatranes"	2013 - 2019
Western Washington University , <i>Graduate Research</i> , Bellingham, WA Advisor: Professor John D. Gilbertson Research Project Title: "Ligand Based Reduction of Carbon Dioxide and Release of Carbon Monoxide on Iron (II)"	2011 - 2013
Western Washington University , <i>Undergraduate Research</i> , Bellingham, WA Advisor: Professor John D. Gilbertson Research Project Title: "Metalloenzyme Mimics with Hydrogen Bond Directors Located in the Secondary Coordination Sphere"	2010 - 2011

Peer-Reviewed Research Publications **corresponding author*

1. Sutthirat, N.; Ziller, J. W.; Yang, J. Y.; **Thammavongsy, Z.*** "Crystal Structure of NiFe(CO)₂[tris(pyridylmethyl)-azaphosphatranes]: A Synthetic Mimic of the NiFe Hydrogenase Active Site Incorporating a Pendant Pyridine Base." *Acta Cryst.* **2019**, E75, 438-442
2. **Thammavongsy, Z.**; Cunningham, D. W.; Sutthirat, N.; Eisenhart, R. J.; Ziller, J. W.; Yang, J. Y.* "Adaptable Ligand Donor Strength: Tracking Transannular Bond Interactions in Tris(2-pyridylmethyl)-azaphosphatranes (TPAP)." *Dalton Trans.* **2018**, 47, 14101-14110
3. **Thammavongsy, Z.**; Kha, I. M.; Ziller, J. W.; Yang, J. Y.* "Electronic and Steric Tolman Parameters for Proazaphosphatranes, the Superbase Core of the Tri(pyridylmethyl)azaphosphatranes (TPAP) Ligand." *Dalton Trans.* **2016**, 45, 9853-9859
4. **Thammavongsy, Z.**; Khosrowabadi Kotyk, J. F.; Tsay, C.; Yang, J. Y.* "Flexibility is Key: Synthesis of a Tripyridylamine (TPA) Congener with a Phosphorus Apical Donor and Coordination to Cobalt(II)." *Inorg. Chem.* **2015**, 54, 11505-11510
5. **Thammavongsy, Z.**; LeDoux, M. E.; Breuhaus-Alvarez, A. G.; Seda, T.; Zakharov, L. N.; Gilbertson, J. D.* "Pyridinediimine Iron Dicarbonyl Complexes with Pendant Lewis Bases and Lewis Acids Located in the Secondary Coordination Sphere." *Eur. J. Inorg. Chem.* **2013**, 22-23, 4008-4015
6. **Thammavongsy, Z.**; Seda, T.; Zakharov, L. N.; Kaminsky, W.; Gilbertson, J. D.* "Ligand Based Reduction of Carbon Dioxide and Release of Carbon Monoxide on Iron (II)." *Inorg. Chem.* **2012**, 51, 9168-9170

Presentations (Oral and Poster – Primary Presenter Only)

1. Oral Presentation: “Playing a cooperative ^1H NMR board game during office hour: Lessons Learned.” ACS Biennial Conference on Chemical Education 2018, South Bend, IN, July 29th – August 2nd, 2018
2. Poster Presentation: “Utilizing Proazaphosphatrane Ligands in Metal Complexes.” UC Chemical Symposium 2018, Los Angeles, CA, March 26th–28th, 2018
3. Oral Presentation: “Synthesis of Proazaphosphatrane Complexes.” UC-Irvine Inorganic Seminar, Irvine, CA. June 1st, 2017
4. Poster Presentation: “Incorporating a proazaphosphatrane donor into a tripodal ligand.” SoCal Organometallic Winter 2017 Meeting, Los Angeles, CA, December 4th, 2016
5. Poster Presentation: “Incorporating a proazaphosphatrane donor into a tripodal ligand.” SoCal Organometallic Spring 2016 Meeting, Irvine, CA. April 23rd, 2016
6. Oral Presentation: “Incorporating a proazaphosphatrane donor into a tripodal ligand.” 251th ACS National Meeting, San Diego, CA. March 13th–17th, 2016
7. Oral Presentation: “Ligand Design Incorporating Proazaphosphatrane, a Strong Electron Donating Group.” SoCal Organometallic Fall 2015 Meeting, Riverside, CA. December 5th, 2015
8. Oral Presentation: “Incorporation of Lewis acidic or Lewis basic group in the secondary coordination sphere of metal complexes for the modulation of C-H bond formation and cleavage.” 249th ACS National Meeting, Denver, CO. March 22th–26th, 2015
9. Poster Presentation: “Breakdown of CO_2 on Pyridinediimine Iron(II) Complexes.” 2nd Western Washington University’s Graduate Research Conference hosted by STEMGRO, June 1st, 2013
10. Poster Presentation: “Breakdown of CO_2 on Pyridinediimine Iron(II) Complexes.” Western Washington University’s Scholars Week, Bellingham, WA. May 13-17th, 2013
11. Oral Presentation: “Synthesis and Activity of Pyridinediimine Iron Complexes” Thesis Defense, Bellingham, WA. May 10th, 2013
12. Poster Presentation: “Production of CO Gas from CO_2 on Redox-Active Iron(II) Complexes.” 245rd ACS National Meeting, New Orleans, LA. April 7th–11th, 2013
13. Oral Presentation: “Metalloenzyme Mimics with Hydrogen Bond Directors Located in the Secondary Coordination Sphere.” Thesis Proposal, Bellingham, WA. April 27th, 2012
14. Poster Presentation: “Small Molecule Activation by Pyridinediimine Iron Complexes.” Western Washington University’s Scholars Week, Bellingham, WA. May 13th-17th, 2012
15. Poster Presentation: “Small Molecule Activation by Pyridinediimine Iron Complexes.” 243rd ACS National Meeting, San Diego, CA. March 25th–29th, 2012
16. Poster Presentation: “Hydrogen Bonding in the Secondary Coordination Sphere of Zinc and Iron Enzyme Mimics.” Western Washington University’s Scholars Week, Bellingham, WA. May 15th-19th, 2011
17. Poster Presentation: “Hydrogen Bonding in the Secondary Coordination Sphere of Zinc and Iron Enzyme Mimics.” 2011 ACS Puget Sound Section: Undergraduate Research Symposium, Seattle, WA. April 30th, 2011

Teaching Experience

- University of California, Irvine, Graduate Teaching Assistant, Irvine, CA* 2013 - 2019
Lecture Course Teaching Assistant, Inorganic Chemistry I, Chem 107 Fall 2017
Discussion enrollment: 90 students (3 sections)
- Integrated active learning activities such as Kahoot to address prior knowledge
 - Prepared weekly problem sets and mini lectures
 - Led weekly discussions on inorganic topics
 - Set up iClicker quizzes for instructor
 - Worked with a diverse population of students including international and EAL students
- Lecture Course Teaching Assistant, Inorganic Chemistry I, Chem 127** Winter 2014
Discussion enrollment: ~29 students (3 sections)
- Prepared weekly problem sets and mini lectures
 - Assisted in the preparation of exams and homework
 - Encouraged a friendly learning environment by learning names
 - Held reviews for students and graded exams to provide students with helpful feedback
- Lecture Course Teaching Assistant, Organic Chemistry I, II & III, Chem 51A, B & C** Spring 2019
Discussion enrollment: ~179 students (5 sections) Summer 2018
- Led discussions on organic chemistry worksheets via think-pair-share Winter 2018
 - Assisted in the preparation of teaching materials such as problem sets and exams Spring 2017
 - Held review sessions and graded exams to provide students with helpful feedback Fall 2016
 - Worked with a diverse population of students including international and EAL students
- Laboratory Course Teaching Assistant, Inorganic Chemistry, Chem 107** Winter 2016
Laboratory enrollment: 11
- Supervised and instructed students in inorganic chemistry lab techniques
 - Graded and provided feedback on student's lab report
 - Began each lab section with an overview of laboratory technique and set-up, objectives, and safety
- Laboratory Course Teaching Assistant, Organic Chemistry, Chem 51LB & 51LC** Winter 2019
Laboratory enrollment: 40 (2 sections) Winter 2017
- Supervised and instructed students in organic chemistry lab techniques Fall 2013
 - Graded and provided feedback on student's electronic laboratory notebook and lab reports
 - Began each lab section with an overview of laboratory technique and set-up, objectives, and safety
- Laboratory Course Teaching Assistant, General Chemistry, Chem 1LC** Summer 2016
Laboratory enrollment: 50 (2 sections) Spring 2016
- Supervised and instructed students in general chemistry lab techniques Spring 2015
 - Taught students to keep complete and accurate scientific records Spring 2014
 - Graded and provided feedback on student's electronic laboratory notebook and post labs
- Western Washington University, Graduate Teaching Assistant, Bellingham, WA* 2011-2013
- Laboratory Course Teaching Assistant, General Chemistry, Chem 121 - 123** Winter 2013
Laboratory enrollment: 40 (2 sections) Spring 2013
- Supervised and instructed students in general chemistry lab techniques Fall 2013
 - Taught students to keep complete and accurate scientific records Winter 2012
 - Graded and provided feedback on student's post lab Spring 2012
 - Began each lab section with a demo of laboratory techniques and safety Fall 2011
- Western Washington University, Undergraduate Teaching Assistant, Bellingham, WA* 2010-2011

Laboratory Course Teaching Assistant, General Chemistry, Chem 123	Spring 2011
<ul style="list-style-type: none"> • Helped supervise students in general chemistry lab techniques • Stocked chemicals and make solutions • Collected post lab and entered in grades • Assisted in students understanding of the experiment through the Socratic method 	Spring 2010

Professional Development

<i>University of California, Irvine, Division of Teaching Excellence & Innovation (DTEI)</i>	2017 - 2018
University Studies 395, Teaching as Research	Winter 2018
<ul style="list-style-type: none"> • Be familiarized with the primary aspects of doing educational research (IRB) • Planned and carry out a small study to measure the effectiveness of teaching 	
University Studies 390A, Advanced Pedagogy and Academic Job Preparation	Winter 2017
<ul style="list-style-type: none"> • Introduced to principles of course design and instructional development • This course covers topics on active learning, inclusive learning, and educational research 	
University Studies 390B, Advanced Pedagogy and Academic Job Preparation	Spring 2017
<ul style="list-style-type: none"> • Application of US 390A material in the design and implementation of the Teaching Assistant Professional Development Program (TAPDP) • Design a workshop meant to model best teaching practices as well as introduce new TAs to their roles and responsibilities 	
University Studies 390C, Advanced Pedagogy and Academic Job Preparation	Fall 2017
<ul style="list-style-type: none"> • Recruit and interviewed potential pedagogical fellows • Designed a course to assist pedagogical fellows to develop long-term teaching plans and prepared for the academic job market 	
Center for Integration of Research, Teaching and Learning (CIRTL) Associate	Winter 2017
<ul style="list-style-type: none"> • Designed a potential research project around teaching with definable goals and outcomes • This program teaches graduate students and faculty to effectively implement research-based practices in different learning environments 	
<i>University of California, Irvine Graduate Resource Center Workshop</i>	2018 - 2019
Public Speaking: Activate to Captivate	Winter 2018
<ul style="list-style-type: none"> • Learned techniques to turn passive presentations into active ones • Practice our research presentation in front of a general audience 	
Improv for Teaching	Spring 2018
<ul style="list-style-type: none"> • Learned to think on our feet and engaged in active listening techniques • Expanding our imagination to lead a dynamic classroom 	
<i>Southern California PKAL Regional Network Annual Meeting</i>	2017 - 2019
Building More Transparent Assignments and Evaluation in STEM Courses	Winter 2019
<ul style="list-style-type: none"> • Apply the principles of a transparent design, evaluation, and assessment to our own class work • Look at common assignments in STEM classrooms in light of transparent pedagogy 	
Inclusive Pedagogy: Finding the Right Approach for You and Your Context	Winter 2018
<ul style="list-style-type: none"> • Shared inclusive practices between professors and graduate students in their respective field • Listed inclusive activities that could be effortlessly implemented in chemistry and physics 	

Active Learning in Chemistry: Using Toys, Simulations, and Data Analysis to Enhance Learning Winter 2018

- A workshop aimed to introduce cheap and effective science demonstration to enhance student's chemistry concepts.

Discipline-Based Education Research 101 Spring 2017

- Designed a study to conduct at an institution
- A workshop that introduced educators on effective educational research studies in their college science classroom

A Conversation Forum Between Two and Four-Year Faculty about Transfer Students Spring 2017

- Listened to the discussion between instructors in two and four year institutions about the challenges and success stories of transfer students
- A workshop aimed towards sharing ideas between instructors on how to improve the transition of transfer students to four year institutions

Mentorship (Undergraduate Researcher)

Jessica Mendoza

Current Location: Undergraduate at UC Berkeley Summer 2018
Summer Undergraduate Researcher from UC Berkeley

Natwara Sutthirat

Current Location: Undergraduate Researcher at UCI 2017 - 2018
DAAD RISE Germany Summer Internship (\$3,000)
Undergraduate Research Opportunities Program (UROP) Grant (\$1,500)
Poster Presentation at 255th ACS National Meeting, New Orleans, LA

Ivy Kha

Current Location: Western University – Optometry Program 2015 - 2017
Undergraduate Research Opportunities Program (UROP) Grant (\$2,000)
Poster Presentation at 251th ACS National Meeting, San Diego, CA

Hannah Bui

Current Location: George Washington University – Master in Public Health 2015 - 2017
Poster Presentation at 251th ACS National Meeting, San Diego, CA

Service

University of California Chemical Symposium, Social Media Manager 2018 - 2019

University of California

- Advertise the UC Chemical Symposium to UC graduate and postdoctoral members
- Engage with the scientific community on the scientific breakthroughs from UC schools
- Manage UC Chemical Symposium social media accounts (Twitter and Instagram)

Teaching Assistant Professional Development Program, Workshop Instructor Fall 2018

University of California, Irvine, Irvine, CA Fall 2017

- Led a day and a half long workshop for incoming graduate student TAs on their roles and responsibilities
- Introduced TA duties such as grading, holding office hours and teaching via active learning
- Provided feedback to new TAs on their microteaching lessons

Chemistry Outreach, Volunteer 2017 - 2019
University of California, Irvine, Irvine, CA

- Travel to elementary and middle schools to perform chemistry demonstrations
- Engaged with elementary and middle school students on the topic of chemistry once every month
- Expose students to the world of chemistry and explain the life of a chemist

Laboratory Experiments and Activities in Physical Sciences (LEAPS), Volunteer 2014 - 2019
University of California, Irvine, Irvine, CA

- Students and teachers take a tour around the Yang Lab
- Engaged with middle and high school students on the topic of chemistry once every quarter
- Demonstrate chemistry experiments and explain their applicability in the world around them

Research Saturday, Volunteer 2014 - 2019
University of California, Irvine, Irvine, CA

- Tour undergraduate students around the chemistry laboratory
- Advise undergraduate students in picking research groups
- Assist undergraduate students in drafting admission emails to research professors

SoCal Undergraduate Research Symposium, Poster Judge Summer 2018
University of California, Irvine, Irvine, CA Summer 2016

- Judge posters presented by undergraduate researchers
- Ask scientific questions on undergraduate research projects
- Encourage undergraduate researchers to keep pursuing their scientific goals

Awards

UCI Dissertation Fellowship	2018
UCI Chemistry Most Promising Future Chemistry Teacher	2018
UCI Most Promising Future Faculty Member Award	2018
UC Chemical Symposium Social Media Award	2018
UCI Chemistry Outstanding Contributions to the Department Award	2017
CIRTL Certification, Associate Level	2017
UCI Pedagogical Fellow Award	2017
UCI Chemistry Gebel Award	2016
UCI Graduate Student Travel Grant	2015

Affiliations

American Chemical Society, Member	2011 - 2019
UC Chemical Symposium Organizing Member	2018 - 2019
Association of American Colleges & University, Member	2017 - 2019

Related Affiliations

Founder and Designer of *d*-Orbital Games – Science Table Top Game Company 2017 - 2019

Game Titles Produced:

1. Selenium Argon Carbon Hydrogen [SeArCH] – Periodic Table Game
2. Slap Count – *d*-Electron Count Game
3. Sym Slam – Point Group Game
4. LINK – Amino Acid Game
5. ¹H NMR Spectrum – Proton NMR Game
6. 18 Electron Rule
7. Rare Earth Elements

Website: www.dorbitalgames.org

ABSTRACT OF THE DISSERTATION

Transition Metal Complexes of Modified Azaphosphatranes

by

Zachary Thammavongsy

Doctor of Philosophy in Chemistry

University of California, Irvine, 2019

Professor Jenny Y. Yang, Chair

The non-ionic, super-basic phosphorus of proazaphosphatranes has been extensively studied as organic catalysts and stoichiometric bases. They are commercially available and have been used as ligands for palladium cross-coupling reactions. Despite this utility, a fundamental understanding of proazaphosphatranes as ligands in coordination chemistry and transition metal catalysis has not been thoroughly investigated. Herein, modification of proazaphosphatrane compounds with pyridine, thiophene, and furan groups expand its chelating ability beyond its monodentate frame. The coordination chemistry of modified and unmodified proazaphosphatranes with various transition metal ions is explored, specifically investigating their electron donating properties and transannular interactions. Additionally, the reactivity of these transition metal azaphosphatrane complexes with small molecules (CO_2 , H_2 , and O_2) is examined. A multidisciplinary approach is employed to study these transition metal azaphosphatrane complexes, founded on the design and synthesis of organic ligands and the development of metal complexes. Reactivity studies and inorganic, organic, and analytical characterization methods are carried out.

Chapter 1 describes the electronic and steric parameters of azaphosphatranes using the Tolman electronic parameters and cone angle.

Chapter 2 describes the modification of azaphosphatranes incorporating pyridine, thiophene and furan substituents.

Chapter 3 describes the experimental and computational investigation of the varying degree of transannular interaction in tris(2-pyridylmethyl)azaphosphatrane (TPAP) when coordinated to transition metals ions in different oxidation states.

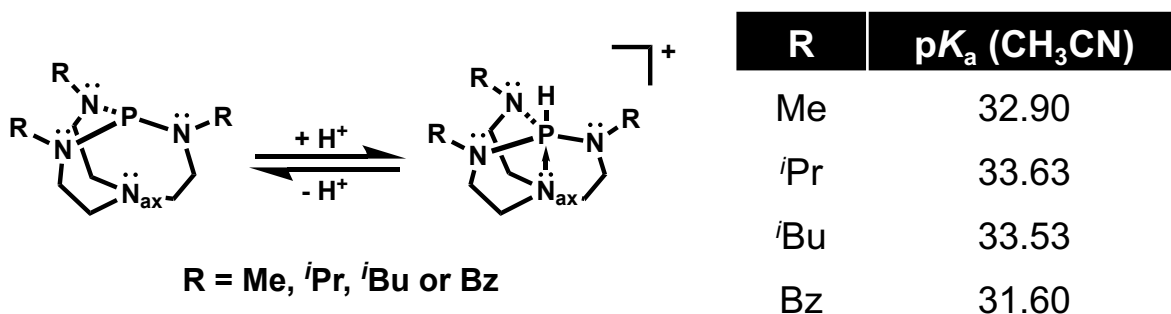
Chapter 4 describes the attempted reactivity of transition metal complexes of TPAP with small molecules such as H₂, O₂, and CO₂.

INTRODUCTION

0.1. Proazaphosphatranes (Verkade's Superbases)

Proazaphosphatranes are powerful non-ionic organic bases. Proazaphosphatranes have demonstrated great utility and versatility in synthetic chemistry, and have been used as stoichiometric bases,¹⁻¹⁷ organic catalysts¹⁸⁻⁴⁶ and ligands in organometallic reactions.⁴⁷⁻⁶⁰ Pioneered by the late John G. Verkade, the “molecular football” shaped compound is commonly known as Verkade's Superbase.⁶¹⁻⁶³ The term “Superbase” is given to organic compounds whose basicity is greater than that of 1,8-bis(dimethylamino)naphthalene (proton sponge), which have a pK_a of 18.6 (conjugate acid form) in acetonitrile.⁶⁴ The pK_a of the protonated form of proazaphosphatranes ranges from 31.6 to 33.6 in acetonitrile depending on the substituents attached to the equatorial nitrogen atoms (R) (Chart 0.1). The most basic site on proazaphosphatrane is the phosphorus center,⁶⁵ which owes its extreme basicity to the electron donation from its three neighboring equatorial nitrogen atoms, and the potential formation of a stable three-centered four-electron transannular interaction between P and N_{ax} .^{66, 67}

Chart 0.1. Protonation of proazaphosphatranes (Verkade's Superbases) with a generic proton. The pK_a values of the conjugate acid shown in the table to the right, with various R groups.



0.2. Expanding the Use of Proazaphosphatranes

Outside of Verkade's work on proazaphosphatranes in the 1990s and early 2000s, most groups have been using proazaphosphatranes as stoichiometric bases, particularly in inorganic chemistry.^{8, 9, 12, 13} The recent development of proazaphosphatranes outside of their use as stoichiometric bases started in the 2010s, with effort from Martinez and coworkers. The design of a molecular cage,⁶⁸⁻⁷¹ that incorporated the azaphosphatrane system is established (Figure 0.1) for the catalytic conversion of CO₂ into cyclic carbonates.⁷² The "Cage Effect" found by Martinez and coworkers described an increase in stability of the organocatalyst by protecting the azaphosphatrane framework from potential deactivation pathways.⁷² In addition, Martinez and coworkers expanded the use of their azaphosphatrane caged systems to encapsulate anions from water.⁷¹

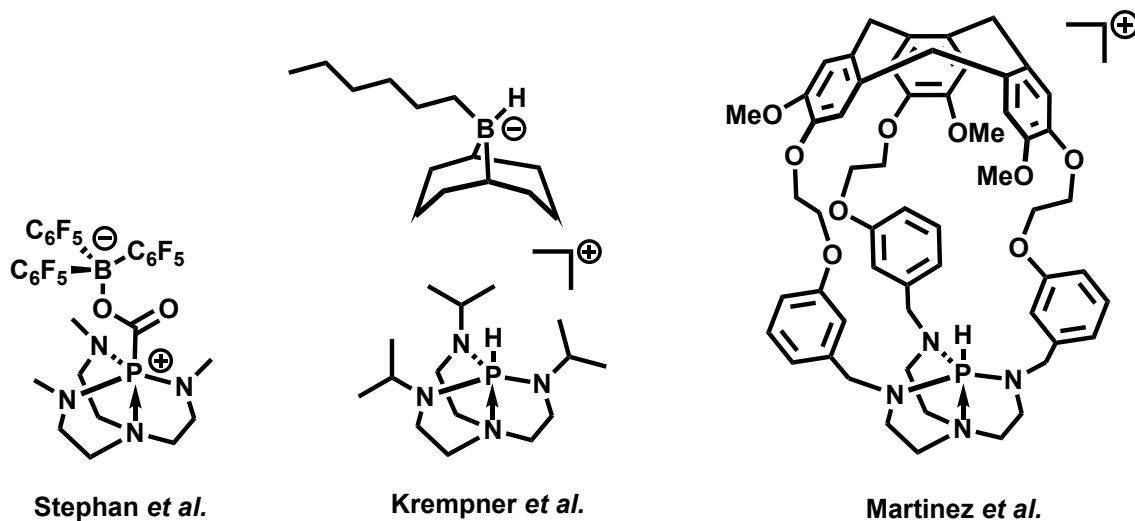


Figure 0.1. Chemical structures of the work done by (left) Stephan's group, (middle) Krempner's group and (right) Martinez's group on expanding the use of azaphosphatranes.

Krempner *et al.*, along with work by Stephan *et al.* have been investigating proazaphosphatranes as strong Lewis bases in frustrated Lewis acid-base pair systems. They noted the ability of proazaphosphatranes to activate Si-H and Si-C bonds in Verkade's previous work,^{18, 73} and subsequently examined the activation of H-H bond of H₂ and C=O bond of CO₂ (Figure 0.1). Krempner *et al.* demonstrated the frustrated Lewis acid-base pair, with isopropyl-proazaphosphatrane as the Lewis base and 9-hexyl-borobicyclo[3.3.1]nonane as the Lewis acid could not only activate H₂, but could also catalyze the hydrogenation of imines.⁷⁴ Stephan *et al.* demonstrated the smaller sterically constrained methyl-proazaphosphatrane cooperatively activated CO₂ with B(C₆F₅)₃.⁷⁵ Furthermore, the classical Lewis adduct of the methyl-proazaphosphatrane/B(C₆F₅)₃ activated other small molecules in the same way as fully frustrated Lewis acid-base pair systems.

More recently, the successful use of proazaphosphatranes as ligands in organometallic cross-coupling reactions have prompted the laboratory of Martinez and Johnson to explore the coordination chemistry of proazaphosphatranes (Figure 0.2).^{76, 77} Martinez's group structurally characterized a gold-azaphosphatrane complex by applying a synthetic approach similar to that for gold-N-heterocyclic carbene (NHC) complexes. Martinez concluded by stating that proazaphosphatrane should make interesting alternatives to NHC, due to their shared properties, such as high basicity, efficiency as organic catalysts, strong electron donating ability and the similarities between the azaphosphatrane salts and imidazolium salts as pre-ligands (precursors). Johnson's group structurally characterized several palladium-azaphosphatrane complexes, and investigated the effects of the transannular interaction in azaphosphatranes during palladium

catalyzed cross-coupling reactions.⁷⁷ From these two studies, proazaphosphatranes are found to display unique properties as ligands. Yet, complexation studies with various transition metals have been lacking. In addition, the ligand design of proazaphosphatranes have been limited to alkyl substituents, thereby restricting its growth as ligands in organometallic catalysis. A modular synthetic pathway can help expand the proazaphosphatrane beyond its mono-dentate framework and increase its stability as a ligand through the chelate effect.

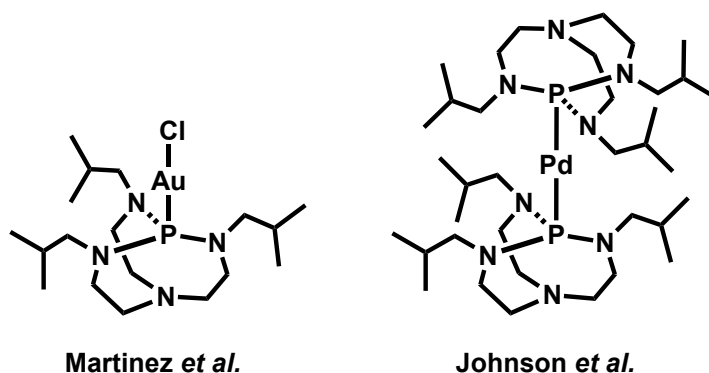


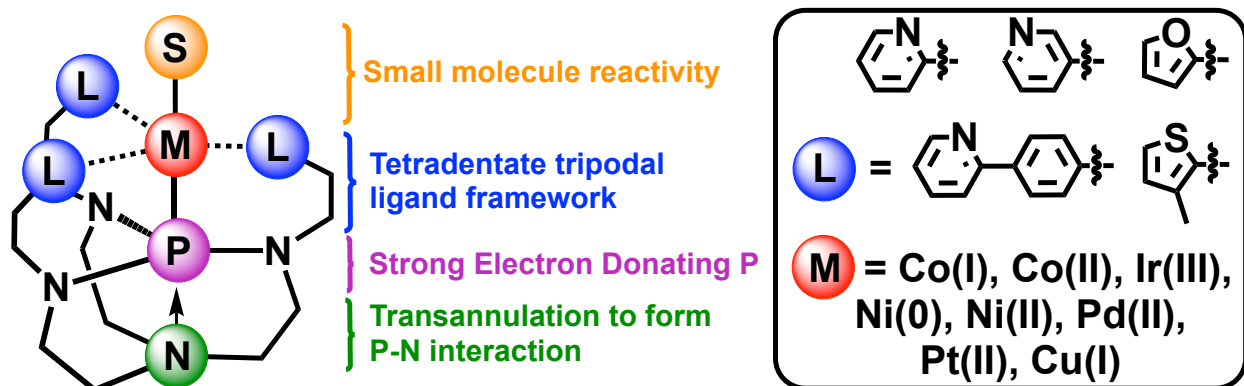
Figure 0.2. Chemical structures of transition metal complexes of isobutyl-azaphosphatrane by (left) Martinez's group and (right) Johnson's group.

0.3. Research Goals

The research presented in this dissertation is a synthetic inorganic approach to advancing the design of proazaphosphatranes as ligands in inorganic and organometallic chemistry. The facile modification of proazaphosphatranes will be utilized to increase the denticity and flexibility of the framework. Structural characterization of inorganic complexes with modified proazaphosphatranes will reveal the unique coordination environment and properties of the proazaphosphatrane ligands. Small molecule activation, such as CO₂, H₂ and O₂ will be explored, along with attempted stabilization of high valent transition metal ions.

The chapters of this dissertation follows the schematic outline in Chart 0.2, where Chapter 1 reveals the strong donor-ability of proazaphosphatranes (outlined in purple in Chart 0.2), Chapter 2 presents the facile modification of proazaphosphatrane incorporating pyridine and other functional donors (outlined in blue in Chart 0.2), Chapter 3 displays the coordination mode and unique transannular interaction of the modified azaphosphatrane (outlined in red and green in Chart 0.2), Chapter 4 demonstrates the reactivity of transition metal azaphosphatrane complexes with small molecules (outlined in orange in Chart 0.2).

Chart 0.2. Proazaphosphatrane Framework with Various Donor Groups and Transition Metal Ions Employed in this Research.



Data found in this dissertation were collected using nuclear magnetic resonance (NMR), ultraviolet-visible (UV-vis), infrared (IR) and electron paramagnetic resonance (EPR) spectroscopies, mass spectrometry, elemental analysis, X-ray crystallography and cyclic voltammetry.

0.4. References

1. Wang, Z.; Verkade, J. G., P(MeNCH₂CH₂)₃N: An efficient nonionic superbase for Wittig and Wittig-Horner reactions. *Heteroatom Chemistry* **1998**, *9* (7), 687-689.
2. Arumugam, S.; Verkade, J. G., P(CH₃NCH₂CH₂)₃N: A Nonionic Superbase for Efficient Dehydrohalogenation. *The Journal of Organic Chemistry* **1997**, *62* (14), 4827-4828.
3. Arumugam, S.; McLeod, D.; Verkade, J. G., Use of the Nonionic Superbase P(MeNCH₂CH₂)₃N in the Selective Monoalkylation of Active-Methylene Compounds. *The Journal of Organic Chemistry* **1998**, *63* (11), 3677-3679.
4. Tang, J.; Verkade, J. G., Nonionic Superbase-Promoted Synthesis of Oxazoles and Pyrroles: Facile Synthesis of Porphyrins and alpha-C-Acyl Amino Acid Esters. *The Journal of Organic Chemistry* **1994**, *59* (25), 7793-7802.
5. Wróblewski, A. E.; Verkade, J. G., P(CH₃NCH₂CH₂)₃N as a Dehydrobromination Reagent: Synthesis of Vitamin A Derivatives Revisited. *The Journal of Organic Chemistry* **2002**, *67* (2), 420-425.
6. Kingston, J. V.; Verkade, J. G., P[N(iBu)CH₂CH₂]₃N: A versatile non-ionic base for the synthesis of higher coordinate silicates. *Inorganic Chemistry Communications* **2005**, *8* (7), 643-646.
7. Gianotti, M.; Corti, C.; Fratte, S. D.; Di Fabio, R.; Leslie, C. P.; Pavone, F.; Piccoli, L.; Stasi, L.; Wigglesworth, M. J., Novel imidazobenzazepine derivatives as dual H1/5-HT2A antagonists for the treatment of sleep disorders. *Bioorganic & Medicinal Chemistry Letters* **2010**, *20* (17), 5069-5073.
8. Roberts, J. A. S.; Appel, A. M.; DuBois, D. L.; Bullock, R. M., Comprehensive Thermochemistry of W-H Bonding in the Metal Hydrides CpW(CO)₂(IMes)H, [CpW(CO)₂(IMes)H]⁺, and [CpW(CO)₂(IMes)(H)₂]⁺. Influence of an N-Heterocyclic Carbene Ligand on Metal Hydride Bond Energies. *Journal of the American Chemical Society* **2011**, *133* (37), 14604-14613.
9. Mock, M. T.; Potter, R. G.; O'Hagan, M. J.; Camaioni, D. M.; Dougherty, W. G.; Kassel, W. S.; DuBois, D. L., Synthesis and Hydride Transfer Reactions of Cobalt and Nickel Hydride Complexes to BX₃ Compounds. *Inorganic Chemistry* **2011**, *50* (23), 11914-11928.
10. Hong, S. Y.; Nandurdikar, R. S.; Keefer, L. K.; Saavedra, J. E.; Chakrapani, H., An improved synthesis of V-PROLI/NO, a cytochrome P450-activated nitric oxide prodrug. *Tetrahedron Letters* **2009**, *50* (31), 4545-4548.
11. Murashima, T.; Tamai, R.; Fujita, K.-i.; Uno, H.; Ono, N., Ambident reactivity of nitro heteroaromatic anions. *Tetrahedron Letters* **1996**, *37* (46), 8391-8394.
12. Cammarota, R. C.; Vollmer, M. V.; Xie, J.; Ye, J.; Linehan, J. C.; Burgess, S. A.; Appel, A. M.; Gagliardi, L.; Lu, C. C., A Bimetallic Nickel-Gallium Complex Catalyzes CO₂ Hydrogenation via the Intermediacy of an Anionic d¹⁰ Nickel Hydride. *Journal of the American Chemical Society* **2017**, *139* (40), 14244-14250.
13. Moore, C. M.; Bark, B.; Szymczak, N. K., Simple Ligand Modifications with Pendent OH Groups Dramatically Impact the Activity and Selectivity of Ruthenium Catalysts for Transfer Hydrogenation: The Importance of Alkali Metals. *ACS Catalysis* **2016**, *6* (3), 1981-1990.

14. Jeletic, M. S.; Helm, M. L.; Hulley, E. B.; Mock, M. T.; Appel, A. M.; Linehan, J. C., A Cobalt Hydride Catalyst for the Hydrogenation of CO₂: Pathways for Catalysis and Deactivation. *ACS Catalysis* **2014**, *4* (10), 3755-3762.
15. Bays, J. T.; Priyadarshani, N.; Jeletic, M. S.; Hulley, E. B.; Miller, D. L.; Linehan, J. C.; Shaw, W. J., The Influence of the Second and Outer Coordination Spheres on Rh(diphosphine)₂ CO₂ Hydrogenation Catalysts. *ACS Catalysis* **2014**, *4* (10), 3663-3670.
16. Ewing, W. C.; Marchione, A.; Himmelberger, D. W.; Carroll, P. J.; Sneddon, L. G., Syntheses and Structural Characterizations of Anionic Borane-Capped Ammonia Borane Oligomers: Evidence for Ammonia Borane H₂ Release via a Base-Promoted Anionic Dehydropolymerization Mechanism. *Journal of the American Chemical Society* **2011**, *133* (42), 17093-17099.
17. Owarzany, R.; Fijalkowski, K. J.; Jaroń, T.; Leszczyński, P. J.; Dobrzycki, Ł.; Cyrański, M. K.; Grochala, W., Complete Series of Alkali-Metal M(BH₃NH₂BH₂NH₂BH₃) Hydrogen-Storage Salts Accessed via Metathesis in Organic Solvents. *Inorganic Chemistry* **2016**, *55* (1), 37-45.
18. Wang, Z.; Kisanga, P.; Verkade, J. G., P(i-PrNCH₂CH₂)₃N: An Effective Lewis Base Promoter for the Allylation of Aromatic Aldehydes with Allyltrimethylsilane. *The Journal of Organic Chemistry* **1999**, *64* (17), 6459-6461.
19. Wang, Z.; Wroblewski, A. E.; Verkade, J. G., P(MeNCH₂CH₂)₃N: An Efficient Promoter for the Reduction of Aldehydes and Ketones with Poly(methylhydrosiloxane). *The Journal of Organic Chemistry* **1999**, *64* (21), 8021-8023.
20. Kisanga, P. B.; Verkade, J. G., P(RNCH₂CH₂)₃N: An Efficient Promoter for the Nitroaldol (Henry) Reaction. *The Journal of Organic Chemistry* **1999**, *64* (12), 4298-4303.
21. Ilankumaran, P.; Verkade, J. G., P(RNCH₂CH₂)₃N: Efficient Catalysts for Transesterifications, Acylations, and Deacylations. *The Journal of Organic Chemistry* **1999**, *64* (9), 3086-3089.
22. D'Sa, B. A.; Kisanga, P.; Verkade, J. G., Direct Synthesis of α,β-Unsaturated Nitriles Catalyzed by Nonionic Superbases. *The Journal of Organic Chemistry* **1998**, *63* (12), 3961-3967.
23. Fei, X.-S.; Verkade, J. G., P(RNCH₂CH₂)₃N: A versatile and efficient catalyst for the conversion of aldoximes to nitriles. *Heteroatom Chemistry* **1999**, *10* (7), 541-543.
24. D'Sa, B. A.; McLeod, D.; Verkade, J. G., Nonionic Superbase-Catalyzed Silylation of Alcohols. *The Journal of Organic Chemistry* **1997**, *62* (15), 5057-5061.
25. D'Sa, B. A.; Verkade, J. G., P(MeNCH₂CH₂)₃N: An Efficient Silylation Catalyst. *Journal of the American Chemical Society* **1996**, *118* (50), 12832-12833.
26. Liu, X.; Verkade, J. G., Free and Polymer-Bound Tricyclic Azaphosphatranes HP(RNCH₂CH₂)₃N⁺: Precatalysts in Dehydrohalogenations and Debrominations with NaH. *The Journal of Organic Chemistry* **1999**, *64* (13), 4840-4843.
27. Yu, Z.; Verkade, J. G., P(MeNCH₂CH₂)₃N: An Efficient Catalyst for the Desilylation of tert-Butyldimethylsilyl Ethers. *The Journal of Organic Chemistry* **2000**, *65* (7), 2065-2068.
28. Kisanga, P. B.; Ilankumaran, P.; Fetterly, B. M.; Verkade, J. G., P(RNCH₂CH₂)₃N: Efficient 1,4-Addition Catalysts. *The Journal of Organic Chemistry* **2002**, *67* (11), 3555-3560.

29. Kisanga, P. B.; Verkade, J. G., P(RNCH₂CH₂)₃N-Catalyzed 1,2-Addition Reactions of Activated Allylic Synthons. *The Journal of Organic Chemistry* **2002**, *67* (2), 426-430.
30. Su, W.; McLeod, D.; Verkade, J. G., P(RNCH₂CH₂)₃N: Catalysts for the Head-to-Tail Dimerization of Methyl Acrylate. *The Journal of Organic Chemistry* **2003**, *68* (24), 9499-9501.
31. Yu, Z.; Verkade, J. G., Catalytic Dimerization of Allyl Phenyl Sulfone in the Presence of a Proazaphosphatrane Catalyst. *Advanced Synthesis & Catalysis* **2004**, *346* (5), 539-541.
32. Uргаonkar, S.; Verkade, J. G., P(i-BuNCH₂CH₂)₃N: An Efficient Promoter for the Nucleophilic Aromatic Substitution Reaction of Aryl Fluorides with Aryl TBDMS (or TMS) Ethers. *Organic Letters* **2005**, *7* (15), 3319-3322.
33. Raders, S. M.; Verkade, J. G., P(i-BuNCH₂CH₂)₃N: an efficient promoter for the microwave synthesis of diaryl ethers. *Tetrahedron Letters* **2008**, *49* (21), 3507-3511.
34. Wadhwa, K.; Chintareddy, V. R.; Verkade, J. G., P(PhCH₂NCH₂CH₂)₃N: An Efficient Lewis Base Catalyst for the Synthesis of Propargylic Alcohols and Morita–Baylis–Hillman Adducts via Aldehyde Alkynylation. *The Journal of Organic Chemistry* **2009**, *74* (17), 6681-6690.
35. Chintareddy, V. R.; Wadhwa, K.; Verkade, J. G., P(PhCH₂NCH₂CH₂)₃N Catalysis of Mukaiyama Aldol Reactions of Aliphatic, Aromatic, and Heterocyclic Aldehydes and Trifluoromethyl Phenyl Ketone. *The Journal of Organic Chemistry* **2009**, *74* (21), 8118-8132.
36. Wadhwa, K.; Verkade, J. G., P(i-PrNCH₂CH₂)₃N: Efficient Catalyst for Synthesizing β-Hydroxyesters and α,β-Unsaturated Esters using α-Trimethylsilylethylacetate (TMSEA). *The Journal of Organic Chemistry* **2009**, *74* (11), 4368-4371.
37. Wadhwa, K.; Verkade, J. G., P(i-PrNCH₂CH₂)₃N: an efficient catalyst for TMS-1,3-dithiane addition to aldehydes. *Tetrahedron Letters* **2009**, *50* (30), 4307-4309.
38. Wadhwa, K.; Verkade, J. G., P(i-PrNCH₂CH₂)₃N as a Lewis Base Catalyst for the Synthesis of β-Hydroxynitriles Using TMSAN. *The Journal of Organic Chemistry* **2009**, *74* (15), 5683-5686.
39. Chintareddy, V. R.; Ellern, A.; Verkade, J. G., P[N(i-Bu)CH₂CH₂]₃N: Nonionic Lewis Base for Promoting the Room-Temperature Synthesis of α,β-Unsaturated Esters, Fluorides, Ketones, and Nitriles Using Wadsworth–Emmons Phosphonates. *The Journal of Organic Chemistry* **2010**, *75* (21), 7166-7174.
40. Yu, Z.; Yan, S.; Zhang, G.; He, W.; Wang, L.; Li, Y.; Zeng, F., Proazaphosphatrane P(RNCH₂CH₂)₃N (R=Me, i-Pr)-Catalyzed Isomerization of Allylaromatics, Allyl Phenyl Sulfide, Allyl Phenyl Sulfone, and bis-Allylmethylene Double Bond-Containing Compounds. *Advanced Synthesis & Catalysis* **2006**, *348* (1-2), 111-117.
41. Kakuchi, T.; Chen, Y.; Kitakado, J.; Mori, K.; Fuchise, K.; Satoh, T., Organic Superbase as an Efficient Catalyst for Group Transfer Polymerization of Methyl Methacrylate. *Macromolecules* **2011**, *44* (12), 4641-4647.
42. Williams, D. B. G.; Sibiya, M. S.; van Heerden, P. S.; Kirk, M.; Harris, R., Verkade super base-catalysed transesterification of propylene carbonate with methanol to co-produce dimethyl carbonate and propylene glycol. *Journal of Molecular Catalysis A: Chemical* **2009**, *304* (1), 147-152.
43. Nakano, J.; Masuda, K.; Yamashita, Y.; Kobayashi, S., Highly Efficient Organosuperbase-Catalyzed Mannich-type Reactions of Sulfonylimidates with Imines: Successful

Use of Aliphatic Imines as Substrates and a Unique Reaction Mechanism. *Angewandte Chemie International Edition* **2012**, 51 (38), 9525-9529.

44. Honey, M. A.; Yamashita, Y.; Kobayashi, S., A cooperative water effect in proazaphosphatane-catalysed heterocycle synthesis. *Chemical Communications* **2014**, 50 (25), 3288-3291.
45. Masuda, K.; Nakano, J.; Yamashita, Y.; Kobayashi, S., Organosuperbase-catalyzed Direct-type Michael Addition Reactions of Sulfonylimidates as Ester Surrogates. *Asian Journal of Organic Chemistry* **2013**, 2 (4), 303-306.
46. Blondiaux, E.; Pouessel, J.; Cantat, T., Carbon Dioxide Reduction to Methylamines under Metal-Free Conditions. *Angewandte Chemie International Edition* **2014**, 53 (45), 12186-12190.
47. You, J.; Verkade, J. G., P(i-BuNCH₂CH₂)₃N: An Efficient Ligand for the Direct α -Arylation of Nitriles with Aryl Bromides. *The Journal of Organic Chemistry* **2003**, 68 (21), 8003-8007.
48. Urgaonkar, S.; Nagarajan, M.; Verkade, J. G., P[N(i-Bu)CH₂CH₂]₃N: A Versatile Ligand for the Pd-Catalyzed Amination of Aryl Chlorides. *Organic Letters* **2003**, 5 (6), 815-818.
49. You, J.; Verkade, J. G., A General Method for the Direct α -Arylation of Nitriles with Aryl Chlorides. *Angewandte Chemie International Edition* **2003**, 42 (41), 5051-5053.
50. Urgaonkar, S.; Verkade, J. G., Synthesis of N-aryl-aza-crown ethers via Pd-catalyzed amination reactions of aryl chlorides with aza-crown ethers. *Tetrahedron* **2004**, 60 (51), 11837-11842.
51. Urgaonkar, S.; Verkade, J. G., Scope and Limitations of Pd₂(dba)₃/P(i-BuNCH₂CH₂)₃N-Catalyzed Buchwald–Hartwig Amination Reactions of Aryl Chlorides. *The Journal of Organic Chemistry* **2004**, 69 (26), 9135-9142.
52. Su, W.; Urgaonkar, S.; Verkade, J. G., Pd₂(dba)₃/P(i-BuNCH₂CH₂)₃N-Catalyzed Stille Cross-Coupling of Aryl Chlorides. *Organic Letters* **2004**, 6 (9), 1421-1424.
53. Urgaonkar, S.; Verkade, J. G., Palladium/Proazaphosphatane-Catalyzed Amination of Aryl Halides Possessing a Phenol, Alcohol, Acetanilide, Amide or an Enolizable Ketone Functional Group: Efficacy of Lithium Bis(trimethylsilyl)amide as the Base. *Advanced Synthesis & Catalysis* **2004**, 346 (6), 611-616.
54. Urgaonkar, S.; Nagarajan, M.; Verkade, J. G., P(i-BuNCH₂CH₂)₃N: An Effective Ligand in the Palladium-Catalyzed Amination of Aryl Bromides and Iodides. *The Journal of Organic Chemistry* **2003**, 68 (2), 452-459.
55. Su, W.; Urgaonkar, S.; McLaughlin, P. A.; Verkade, J. G., Highly Active Palladium Catalysts Supported by Bulky Proazaphosphatane Ligands for Stille Cross-Coupling: Coupling of Aryl and Vinyl Chlorides, Room Temperature Coupling of Aryl Bromides, Coupling of Aryl Triflates, and Synthesis of Sterically Hindered Biaryls. *Journal of the American Chemical Society* **2004**, 126 (50), 16433-16439.
56. Aneetha, H.; Wu, W.; Verkade, J. G., Stereo- and Regioselective Pt(DVDS)/P(iBuNCH₂CH₂)₃N-Catalyzed Hydrosilylation of Terminal Alkynes. *Organometallics* **2005**, 24 (11), 2590-2596.

57. Nandakumar, M. V.; Verkade, J. G., Pd₂dba₃/P(i-BuNCH₂CH₂)₃N: a highly efficient catalyst for the one-pot synthesis of trans-4-*N,N*-diarylamino stilbenes and *N,N*-diarylamino styrenes. *Tetrahedron* **2005**, *61* (41), 9775-9782.
58. Venkat Reddy, C. R.; Uргаonkar, S.; Verkade, J. G., A Highly Effective Catalyst System for the Pd-Catalyzed Amination of Vinyl Bromides and Chlorides. *Organic Letters* **2005**, *7* (20), 4427-4430.
59. Han Kim, S.; Jang, W.; Kim, M.; Verkade, J. G.; Kim, Y., Synergistic Effect of a Bis(proazaphosphatrane) in Mild Palladium-Catalyzed Direct α -Arylations of Nitriles with Aryl Chlorides. *European Journal of Organic Chemistry* **2014**, *2014* (27), 6025-6029.
60. Kim, S. H.; Kim, M.; Verkade, J. G.; Kim, Y., A Tuned Bicyclic Proazaphosphatrane for Catalytically Enhanced N-Arylation Reactions with Aryl Chlorides. *European Journal of Organic Chemistry* **2015**, *2015* (9), 1954-1960.
61. Lensink, C.; Xi, S. K.; Daniels, L. M.; Verkade, J. G., The unusually robust phosphorus-hydrogen bond in the novel cation [cyclic] HP(NMeCH₂CH₂)₃N⁺. *Journal of the American Chemical Society* **1989**, *111* (9), 3478-3479.
62. Schmidt, H.; Lensink, C.; Xi, S. K.; Verkade, J. G., New Prophosphatranes: Novel intermediates to five-coordinate phosphatranes. *Zeitschrift für anorganische und allgemeine Chemie* **1989**, *578* (1), 75-80.
63. Gudat, D.; Lensink, C.; Schmidt, H.; Xi, S. K.; Verkade, J. G., Novel Properties of New Phosphatranes and Silatranes. *Phosphorus, Sulfur, and Silicon and the Related Elements* **1989**, *41* (1-2), 21-29.
64. Kaljurand, I.; Kütt, A.; Sooväli, L.; Rodima, T.; Mäemets, V.; Leito, I.; Koppel, I. A., Extension of the Self-Consistent Spectrophotometric Basicity Scale in Acetonitrile to a Full Span of 28 pK_a Units: Unification of Different Basicity Scales. *The Journal of Organic Chemistry* **2005**, *70* (3), 1019-1028.
65. Ullah, S. S.; Rohman, S. S.; Kashyap, C.; Guha, A. K., Protonation of Verkade bases: a theoretical study. *New Journal of Chemistry* **2019**, *43* (6), 2575-2582.
66. Windus, T. L.; Schmidt, M. W.; Gordon, M. S., Theoretical Investigation of Azaphosphatrane Bases. *Journal of the American Chemical Society* **1994**, *116* (25), 11449-11455.
67. Galasso, V., Theoretical Study of the Structure and Bonding in Phosphatrane Molecules. *The Journal of Physical Chemistry A* **2004**, *108* (20), 4497-4504.
68. Raytchev, P. D.; Martinez, A.; Gornitzka, H.; Dutasta, J.-P., Encaging the Verkade's Superbases: Thermodynamic and Kinetic Consequences. *Journal of the American Chemical Society* **2011**, *133* (7), 2157-2159.
69. Chatelet, B.; Gornitzka, H.; Dufaud, V.; Jeanneau, E.; Dutasta, J.-P.; Martinez, A., Superbases in Confined Space: Control of the Basicity and Reactivity of the Proton Transfer. *Journal of the American Chemical Society* **2013**, *135* (49), 18659-18664.
70. Chatelet, B.; Dufaud, V.; Dutasta, J.-P.; Martinez, A., Catalytic Activity of an Encaged Verkade's Superbase in a Base-Catalyzed Diels-Alder Reaction. *The Journal of Organic Chemistry* **2014**, *79* (18), 8684-8688.

71. Zhang, D.; Ronson, T. K.; Mosquera, J.; Martinez, A.; Guy, L.; Nitschke, J. R., Anion Binding in Water Drives Structural Adaptation in an Azaphosphatrane-Functionalized Fe^{II}L₄ Tetrahedron. *Journal of the American Chemical Society* **2017**, *139* (19), 6574-6577.
72. Chatelet, B.; Joucla, L.; Dutasta, J.-P.; Martinez, A.; Dufaud, V., Azaphosphatrane Organocatalysts in Confined Space: Cage Effect in CO₂ Conversion. *Chemistry – A European Journal* **2014**, *20* (28), 8571-8574.
73. Fetterly, B. M.; Verkade, J. G., P(RNCH₂CH₂)N: efficient catalysts for the cyanosilylation of aldehydes and ketones. *Tetrahedron Letters* **2005**, *46* (46), 8061-8066.
74. Mummadi, S.; Unruh, D. K.; Zhao, J.; Li, S.; Krempner, C., “Inverse” Frustrated Lewis Pairs – Activation of Dihydrogen with Organosuperbases and Moderate to Weak Lewis Acids. *Journal of the American Chemical Society* **2016**, *138* (10), 3286-3289.
75. Johnstone, T. C.; Wee, G. N. J. H.; Stephan, D. W., Accessing Frustrated Lewis Pair Chemistry from a Spectroscopically Stable and Classical Lewis Acid-Base Adduct. *Angewandte Chemie International Edition* **2018**, *57* (20), 5881-5884.
76. Chatelet, B.; Nava, P.; Clavier, H.; Martinez, A., Synthesis of Gold(I) Complexes Bearing Verkade's Superbases. *European Journal of Inorganic Chemistry* **2017**, *2017* (37), 4311-4316.
77. Matthews, A. D.; Gravalis, G. M.; Schley, N. D.; Johnson, M. W., Synthesis, Structure, and Reactivity of Palladium Proazaphosphatrane Complexes Invoked in C–N Cross-Coupling. *Organometallics* **2018**, *37* (18), 3073-3078.

CHAPTER 1

The Electronic and Steric Tolman Parameters of Proazaphosphatrane: Synthesis, Characterization, and Measurements

Portions of this chapter have been published:

Thammavongsy, Z.; Kha, I. M.; Ziller, J. W.; Yang, J. Y. *Dalton Trans.* **2016**, 45, 9853-9859

1.1. Motivation and Specific Aims

Proazaphosphatranes are widely utilized as ligands in organometallic catalysis, but a fundamental understanding of why these proazaphosphatranes are good ligands is lacking. Insights into the properties of the proazaphosphatranes can be obtained by measuring their steric and electron parameters. Key elemental steps in organometallic catalysis, such as oxidative addition and reductive elimination are highly dependent on the electronic and steric parameters of the ligand. This chapter describes the experimental determination of the Tolman electronic parameters (TEP) and cone angles for a series of substituted proazaphosphatranes ligands. Tolman parameters of phosphine ligands are classically determined by the synthesis of their respective $\text{Ni}(\text{L}^{\text{R}})(\text{CO})_3$ complexes and evaluating their steric parameters and CO vibrational frequencies. The complexes $\text{Ni}(\text{L}^{\text{Me}})(\text{CO})_3$ (**1**), $\text{Ni}(\text{L}^{\text{iPr}})(\text{CO})_3$ (**2**), $\text{Ni}(\text{L}^{\text{iBu}})(\text{CO})_3$ (**3**) and $\text{Ni}(\text{L}^{\text{Bz}})(\text{CO})_3$ (**4**) are synthesized and their properties are compared to previously described $\text{Ni}(\text{phosphine})(\text{CO})_3$ complexes.

1.2. Background

Phosphines are ubiquitous ligands in transition metal synthesis¹ and catalysis,^{2, 3} as their steric and electronic properties can be easily tuned *via* substituent modification.⁴ The relative stereoelectronic effects between phosphine ligands are most commonly evaluated by the Tolman electronic parameter (TEP) and cone angle (Figure 1.1).⁵

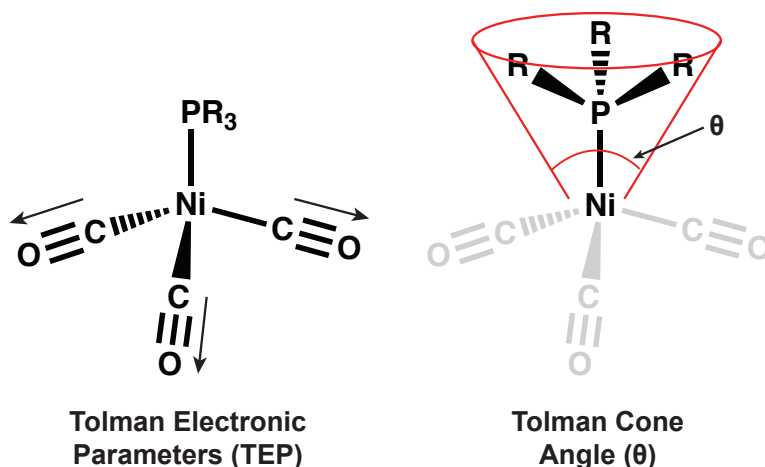
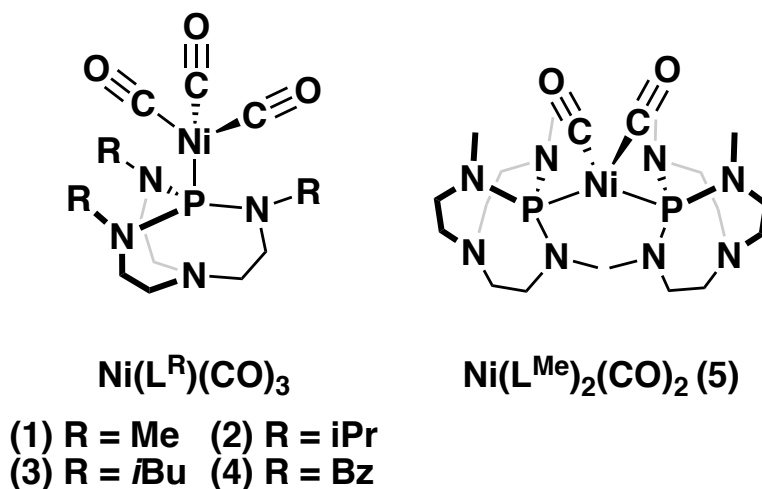


Figure 1.1. Chemdraw depicting the Tolman Electronic (TEP) and Steric Parameter (cone angle Θ) of a generic Ni(phosphine)(CO)₃.⁵

Proazaphosphatranes are monodentate phosphines that serve as ligands in organometallic catalysis. Recently, mechanistic insights were provided with Pd catalyzed C-C cross-coupling reactions utilizing the isobutyl version of proazaphosphatrane.⁷ Although prior studies suggested that proazaphosphatranes (colloquially known as Verkade's Superbases) are strong electron donor ligands,⁸⁻¹⁰ the Tolman parameters had never been measured. In this chapter, experimental measurements of the TEP and cone angle for a series of proazaphosphatranes (L) with various functionalities (L^R , R = Me, *i*Pr, *i*Bu, and Bz) are presented. The corresponding Ni(L^R)(CO)₃ complexes were synthesized, shown in Chart 1.1 as complexes **1-4**. The TEP was evaluated by the infrared vibrational stretching frequencies of the CO bonds,¹¹ and the cone angle was measured using X-ray crystallographic analysis of complexes **2-5**.¹² The Tolman electronic parameters for the proazaphosphatranes place them among the most electron donating phosphine ligands. The TEPs are comparable to P(*t*Bu)₃, the most donating phosphine measured by Tolman, and only recently exceeded by a series of imidazolin-2-ylidaminophosphines.¹³ The cone angles are also

larger compared to the equivalently substituted trialkyl phosphines. The combined electron donor strength and large steric size of proazaphosphatranes is likely an important factor in their successful use as ligands in Pd and Pt catalyzed C–C,¹⁴⁻¹⁷ C–N,^{9, 18-23} and C–Si²⁴ bond coupling reactions.

Chart 1.1. Series of Ni(CO)_x (x = 2 or 3) complexes of Verkade’s Superbases. Reproduced by permission of The Royal Society of Chemistry.



1.3. Results and Discussion

1.3.1. Synthesis and Structure of Ni(L^R)(CO)₃ Complexes (1-4)

Bis(1,5-cyclooctadiene)nickel(0) was added to a solution of L^R (L = P(RNCH₂CH₂)₃N, R = Me, *i*Bu, *i*Pr and Bz) in THF. After stirring for 1 hour, CO gas (1 atm) was added and the respective products were isolated by recrystallization to furnish Ni(L^{Me})(CO)₃ (**1**), Ni(L^{*i*Pr})(CO)₃ (**2**), Ni(L^{*i*Bu})(CO)₃ (**3**), and Ni(L^{Bz})(CO)₃ (**4**) in 84, 87, 74 and 93% yield, respectively. Complexes **1-4** were analyzed by ¹H, ¹³C, and ³¹P NMR spectroscopies (shown in Experimental Details), and their purity was confirmed by elemental analysis.

Solution infrared spectra of **1-4** in CH₂Cl₂ displayed two CO vibrational stretches assigned to the A₁ and E vibrational modes (Figure 1.2). The A₁ resonances for **1-4** are at 2057.0, 2054.6, 2054.9, and 2059.1 cm⁻¹, and the E resonances are at 1977.7, 1974.7, 1975.3, and 1981.1 cm⁻¹, respectively. The values are also listed in Table 1.1.

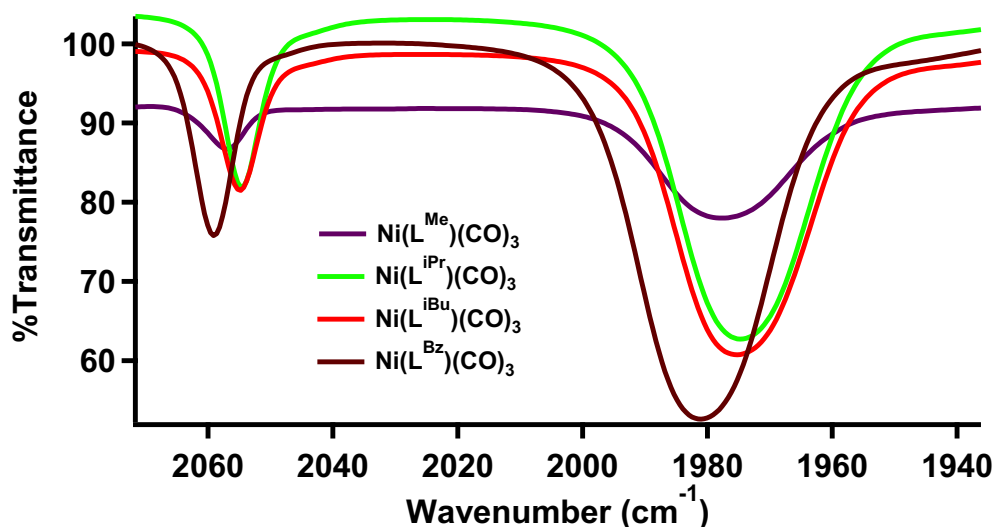


Figure 1.2. IR spectra of (purple) Ni(L^{Me})(CO)₃ (**1**), (green) Ni(L^{iPr})(CO)₃ (**2**), (red) Ni(L^{iBu})(CO)₃ (**3**) and (brown) Ni(L^{Bz})(CO)₃ (**4**) in CH₂Cl₂. Reproduced by permission of The Royal Society of Chemistry.

Single crystals suitable for X-ray analysis were grown from slow evaporation of pentane solutions of **2-4**. Crystallographic data and selected bond distances and angles are given in Tables 1.2 and 1.3, respectively. The structures are shown in Figure 1.3 and are used to determine the cone angles for L^R.

Table 1.1. CO vibrational frequencies (in CH₂Cl₂) and cone angle of complexes **1-4** and selected Ni(CO)₃(PR₃) complexes. Reproduced by permission of The Royal Society of Chemistry.

Complex	$\tilde{\nu}_{\text{co}}$	$\tilde{\nu}_{\text{co}}$	Cone Angle (°)
	A ₁ (cm ⁻¹)	E (cm ⁻¹)	
Ni(CO) ₃ (L ^{Me}) (1)	2057.0	1977.7	152 ^a
Ni(CO) ₃ (L ^{iPr}) (2)	2054.6	1974.7	179
Ni(CO) ₃ (L ^{iBu}) (3)	2054.9	1975.3	200
Ni(CO) ₃ (L ^{Bz}) (4)	2059.1	1981.1	207
Ni(CO) ₃ (P(<i>t</i> Bu) ₃) ^b	2056.1	1971	182
Ni(CO) ₃ (P(Me) ₃) ^b	2064.1	1982	118
Ni(CO) ₃ (P(<i>i</i> Pr) ₃) ^b	2059.2	1977	160
Ni(CO) ₃ (P(<i>i</i> Bu) ₃) ^b	2059.7	-----	143
Ni(CO) ₃ (P(Bz) ₃) ^b	2066.2	1986	165

a. Cone angle is measured from crystal structure of **5**.

b. TEP values taken from Tolman *et al.*⁵

Most Ni(phosphine)(CO)₃ complexes prepared by Tolman were not structurally characterized. Instead, cone angles were determined by a space-filling CPK (Corey–Pauling–Koltun) model based on a tetrahedral coordination geometry and a P–Ni bond length of 2.28 Å.²⁵ Consistent with this model, the structures of **2-4** display near ideal tetrahedral geometries with τ_4 values of 0.977, 0.955, and 0.968, respectively, where $\tau_4 = 1$ represents a tetrahedral geometry and $\tau_4 = 0$ represents a square planar geometry.²⁶ The P–Ni distances of **2-4** are 2.2680(5), 2.2519(3) and 2.2424(5) Å, respectively. Although the P–Ni distances are slightly shorter, Tolman remarked that variations of up to 0.1 Å “seldom change the cone angle by more than 3 or 4°”.⁵ Therefore, the structurally determined cone angles are consistent with the parameters originally reported by Tolman using the CPK model. The values for the P–Ni bond lengths in **2-4** display an inverse relationship with Tolman’s cone angle parameters. Additionally, more electronegative substituents on the proazaphosphatranes (R = Bz > *i*Bu > *i*Pr)²⁷ results in shorter P–Ni bond lengths. The

observed trend is consistent with Tolman's observation that more electronegative substituents increase the phosphorus s orbital character, which shortens the bond.⁵

1.3.2. Synthesis and Structure of Ni(L^{Me})₂(CO)₂ Complex (**5**)

Complex **5** was synthesized and crystallized in a similar fashion as complexes **2-4**, in order to experimentally measure the cone angle of L^{Me}. Ni(L^{Me})₂(CO)₂ (**5**) was synthesized from a 2:1 ratio of L^{Me} and bis(1,5-cyclooctadiene)nickel(0) in THF under an atmosphere of CO gas. Upon exposure to CO the color changed from dark orange to colorless. The crude product was recrystallized from CH₂Cl₂ to give the product in 62% yield. Complex **5** was characterized by ¹H, ¹³C, and ³¹P NMR and IR spectroscopies (shown in Experimental Details), and the purity was confirmed by elemental analysis. Single crystals suitable for X-ray analysis were grown from slow evaporation of a diethyl ether solution. The structure of **5** shown in Figure 1.3, displays a tetrahedral geometry around Ni with τ_4 values of 0.971.²⁶ Crystallographic data and selected bond distances and angles are given in Tables 1.2 and 1.3, respectively.

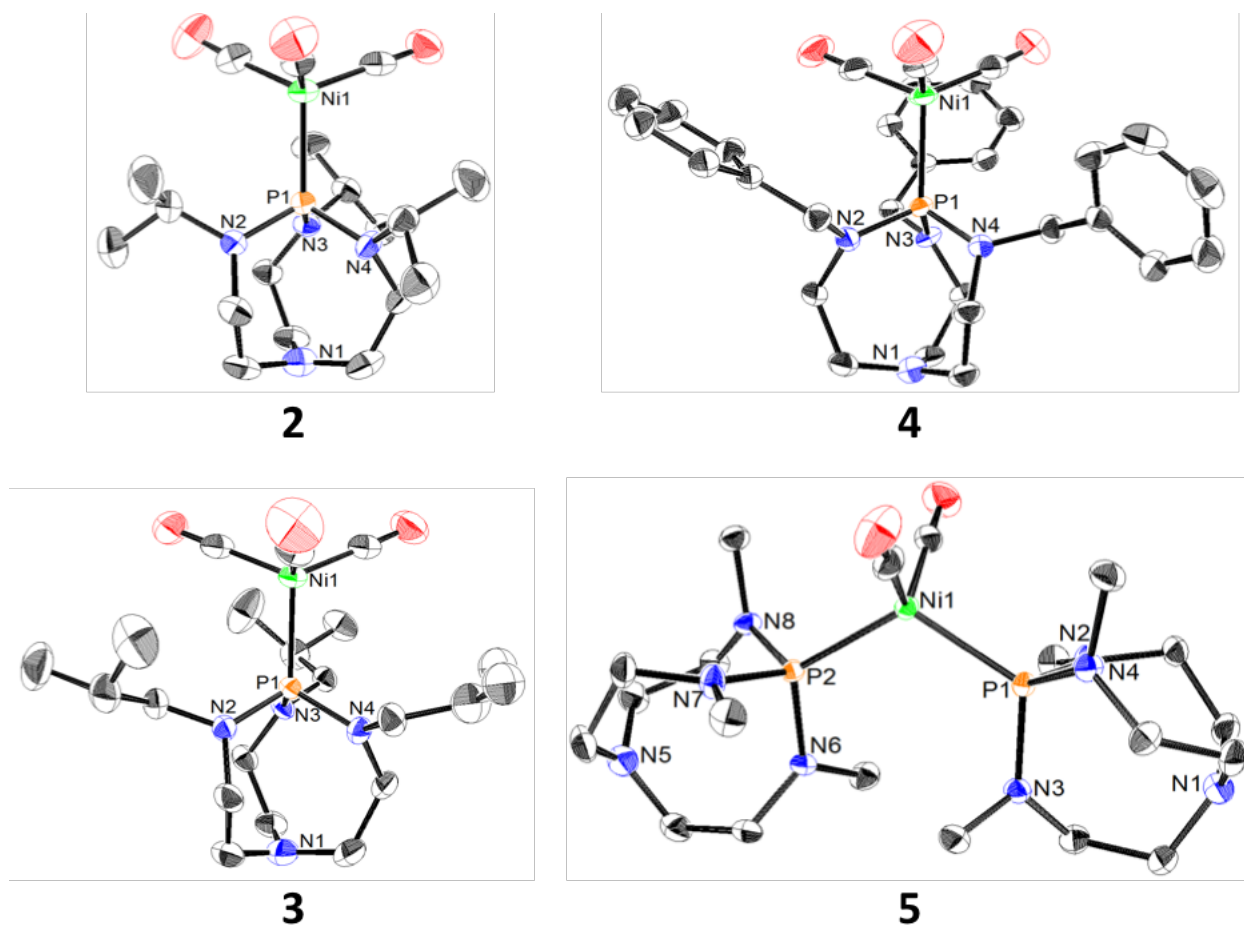


Figure 1.3. Crystal structure of $\text{Ni}(\text{L}^{i\text{Pr}})(\text{CO})_3$ (**2**), $\text{Ni}(\text{L}^{i\text{Bu}})(\text{CO})_3$ (**3**), $\text{Ni}(\text{L}^{\text{Bz}})(\text{CO})_3$ (**4**) and $\text{Ni}(\text{L}^{\text{Me}})_2(\text{CO})_2$ (**5**). Thermal ellipsoids are drawn at 80% probability; hydrogen atoms are omitted for clarity. Carbon atoms from the minor part of a disorder in **3** are also omitted. Reproduced by permission of The Royal Society of Chemistry.

Table 1.2. Crystallographic data and refinement parameters for complexes **2-5**. Reproduced by permission of The Royal Society of Chemistry.

Complex	2	3	4	5
Formula	C ₁₈ H ₃₃ N ₄ O ₃ PNi	C ₂₁ H ₃₉ N ₄ O ₃ PNi	C ₃₀ H ₃₃ N ₄ O ₃ PNi	C ₂₀ H ₄₂ N ₈ O ₂ P ₂ Ni
Molar Mass	443.16	485.24	587.28	547.27
Crystal System	Monoclinic	Monoclinic	Monoclinic	Monoclinic
Space Group	P2(1)/n	P2(1)/n	P2(1)/n	P2(1)/n
T[K]	133(2)	88(2)	133(2)	133(2)
a[Å]	9.4521(6)	10.4524(5)	9.7263(8)	8.5551(5)
b[Å]	16.0515(11)	17.9047(8)	23.412(2)	19.4034(12)
c[Å]	14.5677(10)	13.5993(6)	12.5881(11)	15.9663(1)
α[°]	90.00	90.00	90.00	90.00
β[°]	93.8772(8)	97.2348(6)	99.3160(10)	104.7970(10)
γ[°]	90.00	90.00	90.00	90.00
V[Å ³]	2205.2(3)	2524.8(2)	2828.6(4)	2562.5(3)
Z	4	4	4	4
D(calcd) [Mgm ⁻³]	1.335	1.277	1.379	1.419
μ(Mo-K _α) [mm ⁻¹]	0.977	0.859	0.781	0.916
Index Range	-12 ≤ h ≤ 12 -21 ≤ k ≤ 21 -19 ≤ l ≤ 19	-14 ≤ h ≤ 13 -23 ≤ k ≤ 23 -18 ≤ l ≤ 18	-13 ≤ h ≤ 13 -32 ≤ k ≤ 31 -16 ≤ l ≤ 17	-11 ≤ h ≤ 11 -25 ≤ k ≤ 25 -21 ≤ l ≤ 21
Reflection Collected	24569	31264	70276	62910
Independent Reflections	5360	6479	7270	6562
Data/Restraints/Parameters	5360 / 0 / 250	6479 / 0 / 431	7270 / 0 / 352	6562 / 0 / 304
R ₁ , wR ₂ [I > 2σ(I)]	0.0359, 0.0749	0.0272, 0.0665	0.0400, 0.1283	0.0232, 0.1097
R ₁ , wR ₂ [all data]	0.0544, 0.0810	0.0341, 0.0701	0.0470, 0.1393	0.0242, 0.1122
GOF	1.220	1.029	1.168	1.056

Table 1.3. Selected distances and angles of **2-5**. Reproduced by permission of The Royal Society of Chemistry.

Complex	2	3	4	5^a
P-Ni (Å)	2.2680(5)	2.2519(3)	2.2424(5)	2.2320(3)
P...N1 (Å)	3.330	3.435	3.317	3.478
P-N2 (Å)	1.6927(14)	1.6899(11)	1.6879(13)	1.6892(9)
P-N3 (Å)	1.6900(14)	1.6885(11)	1.6824(13)	1.6902(9)
P-N4 (Å)	1.6894(14)	1.6876(11)	1.6890(13)	1.6939(9)
C-O1 (Å)	1.140(2)	1.1385(17)	1.146(2)	1.1500(15)
C-O2 (Å)	1.143(2)	1.1447(18)	1.140(2)	1.1506(14)
C-O3 (Å)	1.133(2)	1.1404(18)	1.142(2)	-----
N2-P-Ni (°)	114.59(5)	113.93(4)	112.74(5)	112.92(3)
N3-P-Ni (°)	113.96(5)	113.77(4)	114.01(5)	120.25(3)
N4-P-Ni (°)	115.05(5)	115.12(4)	115.49(5)	113.12(3)
N4-P-N3 (°)	103.34(7)	104.00(5)	105.32(6)	102.74(5)
N3-P-N2 (°)	104.07(7)	104.18(5)	103.78(6)	103.10(5)
N2-P-N4 (°)	104.46(7)	104.64(5)	104.32(6)	102.71(4)

^aone of the two L^{Me} measurements in complex **5**

1.3.3. Tolman Electronic Parameters and Cone Angles of Ni(L^R)(CO)₃ Complexes (1-4)

The electronic and steric properties of the strongest electron donating trialkyl substituted phosphines measured by Tolman⁵ are used as a comparison to the proazaphosphatranes summarized in Table 1.1 and shown in Figure 1.4. Complexes of **1-3** display CO vibrational frequencies similar to those reported for the most donating alkyl-phosphine ligand, P(*t*Bu)₃ (Ni(P(*t*Bu)₃)(CO)₃, $\tilde{\nu}_{\text{CO}} = 2056.1 \text{ cm}^{-1}$), while the CO vibrational frequency of complex **4** is closer to those observed for the acyclic triaminophosphine ligand (Ni(P(NMe₂)₃)(CO)₃, $\tilde{\nu}_{\text{CO}} = 2061.9 \text{ cm}^{-1}$).⁵ The trend in electron donor properties of the trisubstituted proazaphosphatranes follows the same trend as the trialkyl substituted phosphines originally measured by Tolman (stronger donor > weaker donor: *i*Pr ≥ *i*Bu > Me > Bz). However, the overall strength of electronic donation for the proazaphosphatranes is greater than that of the equivalently substituted tertiary phosphine.

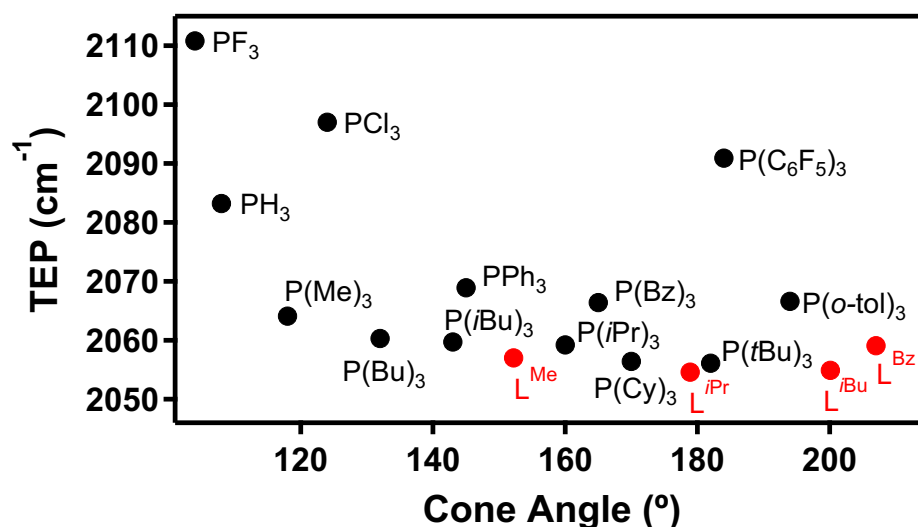


Figure 1.4. Comparison of Tolman electronic parameter (TEP) and cone angles. Red dots (●) represent proazaphosphatranes measured herein and black dots (●) represent phosphines measured by Tolman.⁵ Reproduced by permission of The Royal Society of Chemistry.

The greater overall donor strengths of the proazaphosphatranes are primarily due to the replacement of the alkyl functionalities on the phosphine with alkyl-substituted amine donors. Amine substituents are known to increase the strength of electron donation when bound to phosphorus ligands. A prior study by Woollins *et al.* systematically investigated this effect on acyclic phosphines and determined that the strength of phosphorus electron donation increases after the first and second P–C bonds are replaced by P–N bonds.^{28,29} However, the replacement of the third P–C bond with a P–N bond results in a decrease in the electron donor strength because the effect of a stronger σ donor is outweighed by the electron-withdrawing character of the more electronegative nitrogen atoms due to steric constraints. This phenomenon is observable in the X-ray crystal structure of acyclic tris(dialkylamino)phosphine ligands, where two of the nitrogen atoms are nearly planar (sum of angles at nitrogen $\sim 360^\circ$) and one of the nitrogens is not (sum of the angles at nitrogen $< 350^\circ$) (Figure 1.5).³⁰⁻³² As a result, the two planar nitrogen atoms can donate electron density to the phosphorus through their lone pairs, which are nearly orthogonal to the phosphorus lone pair. However, the third nitrogen only contributes electron-withdrawing character due to its orientation (anti) to the lone pair on phosphorus (Figure 1.5).³³ In contrast, structural characterizations of the cyclic proazaphosphatrane ligands in this chapter (Figure 1.3) demonstrate that all three nitrogens bound to the phosphorus are nearly planar (sum of angles at nitrogen = 358 to 360°). Verkade *et al.* hypothesized that the rigid bicyclic framework of the proazaphosphatrane molecule constrains all three nitrogens to adopt this geometry, resulting in stronger overall electron-donating character compared to the previously studied acyclic tris(dialkylamino)phosphines.⁸

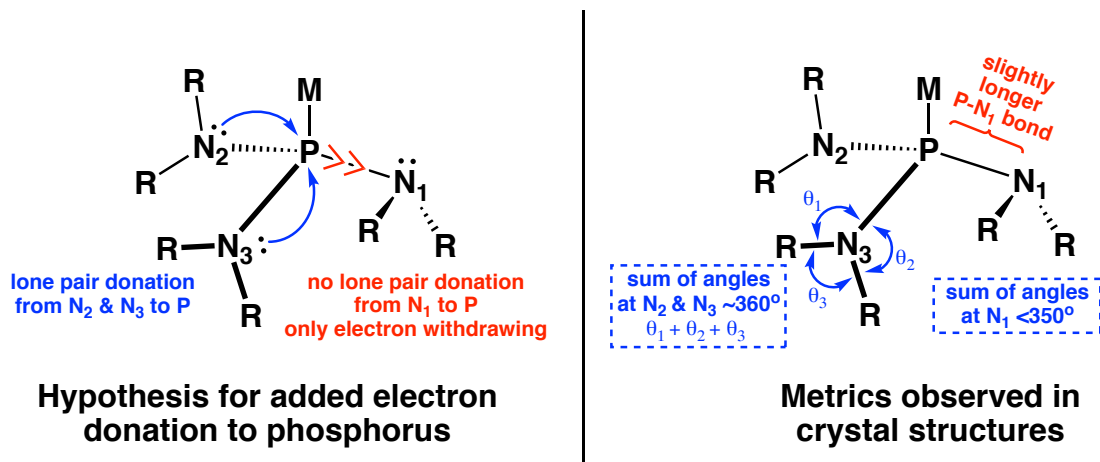


Figure 1.5. Proposed electronic properties of a generic tri(dialkylamino)phosphine and the metrical parameters observed from crystal structures.

Overall, the proazaphosphatranes exhibit greater cone angles compared to the equivalent trialkyl substituted phosphines. In fact, L^{Bz} displayed a cone angle close to the highest cone angle ($P(\text{mesityl})_3 = 212^\circ$) measured by Tolman.⁵ The TEP vs. cone angle for L^R in **1-4** (using Tolman cone angle measured from the structure of **5** for **1**) are graphed along with comparable phosphines in Figure 1.4, which demonstrates that while the cone angle of proazaphosphatranes are highly substituent dependent, they all maintain their strong electron donating character.

1.4. Conclusion

The first experimentally measured Tolman electronic parameters and cone angles for a series of proazaphosphatranes are presented. The proazaphosphatranes in this study display lower TEPs and greater cone angles compared to equivalently substituted trialkyl phosphines. The unique cyclic structure of the proazaphosphatranes contributes to its high donor strength, which is also greater than comparable acyclic triaminophosphines. Another interesting feature of the

proazaphosphatranes is the large effect that alkyl substitution plays on the cone angle while having a negligible effect on the electron donor strength. This property allows the steric bulk to be independently tuned. The quantification of Tolman parameters for proazaphosphatranes permits the rational modification of steric and electronic properties for this synthetically modular class of ligands.

1.5. Experimental Details

General Considerations

The complexes described below are air- and moisture-sensitive, and must be handled under an inert atmosphere of nitrogen using standard glovebox and Schlenk techniques. Unless otherwise noted, all procedures were performed at ambient temperature (21-24 °C). All solvents were sparged with argon and dried using a solvent purification system. Tetrahydrofuran, pentane, diethyl ether, and dichloromethane were passed through two columns of neutral alumina. Compounds 2,8,9-tribenzyl-2,3,8,9-tetraaza-1-phosphabicyclo[3,3,3]undecane (L^{Bz}), and 2,8,9-triisopropyl-2,3,8,9-tetraaza-1-phosphabicyclo[3,3,3]undecane (L^{iPr})³⁴ were synthesized according to established procedures. C_6D_6 was freeze-pump-thawed three times and dried over molecular sieves. 2,8,9-trimethyl-2,3,8,9-tetraaza-1-phosphabicyclo[3,3,3]undecane (L^{Me}) was purchased from Sigma-Aldrich with unspecified purity; therefore further extraction with pentane was necessary to obtain the product in high purity. 2,8,9-triisobutyl-2,3,8,9-tetraaza-1-phosphabicyclo[3,3,3]undecane (L^{iBu}), bis(1,5-cyclooctadiene) nickel(0) (98%), and carbon monoxide (100%) were purchased from commercial sources and used without further purification.

Physical Methods

Nuclear Magnetic Resonance (NMR) Spectroscopy: Nuclear magnetic resonance (NMR) spectra were recorded on a Bruker DRX500 spectrometer fitted with a TCI cryoprobe (^{13}C) or a DRX400 with a switchable QNP probe (^1H and ^{31}P) in dry, degassed solvents. ^1H NMR spectra were referenced to (tetramethylsilane) TMS using the residual proteo impurities of the solvent; ^{13}C NMR spectra were referenced to TMS using the natural abundance ^{13}C of the solvent; ^{31}P NMR spectra were referenced to H_3PO_4 using the Ξ scale with the corresponding ^1H spectra. All chemical shifts are reported in the standard δ notation in parts per million; positive chemical shifts are to a higher frequency from the given reference.

Infrared (IR) Spectroscopy: Infrared (IR) absorption measurements of the solution of **1-5** in CH_2Cl_2 was taken in a OMNI-Cell CaF_2 sealed cell (1.00 mm) on a Thermo Scientific Nicolet iS5 spectrophotometer with an iD1 transmission attachment.

Elemental Analysis (EA): Elemental analyses were performed on a PerkinElmer 2400 Series II CHNS elemental analyzer or on an Exeter Analytical, Inc. CE-440 Elemental Analyzer.

X-ray Crystallography (XRC): X-ray diffraction studies were carried out at the UCI Department of Chemistry X-ray Crystallography Facility on a Bruker SMART APEX II diffractometer. Data was collected at 88K for **3** and 133K for **2**, **4**, and **5** using $\text{Mo K}\alpha$ radiation ($\lambda = 0.71073 \text{ \AA}$). A full sphere of data was collected for each crystal structure. The APEX2 program suite was used to determine unit-cell parameters and for collection. (30 sec/frame scan time for a sphere of diffraction data). The raw frame data were processed

and absorption corrected using the SAINT and SADABS programs, respectively, to yield the reflection data files. Structures were solved by direct methods using SHELXS and refined against F^2 on all data by full-matrix least squares with SHELXL-97. The analytical scattering factors for neutral atoms were used throughout the analysis. All non-hydrogen atoms were refined anisotropically. Hydrogen atoms were placed at geometrically calculated positions and refined using a riding model, and their isotropic displacement parameters were fixed at 1.2 (1.5 for methyl groups) times the U_{eq} of the atoms to which they are bonded. For structure **3**, carbon atoms C(16), C(17) and C(18) were disordered and modeled using multiple components with partial site-occupancy-factors.

General Synthesis of Ni(L^R)(CO)₃ Complexes

In the glove box, a solution of bis(1,5-cyclooctadiene)nickel(0) (1 equiv.) in 5 mL of tetrahydrofuran was added to a solution of L^R (1 equiv.) in 5 mL of tetrahydrofuran. The solution was stirred for 1 hour at room temperature. The solution was then transferred to a 100 mL Schlenk flask and brought out of the glove box and filled with CO gas (1 atm). The solution was stirred overnight under a CO atmosphere, after which the solution became colorless. The solvent was removed under reduced pressure and the resulting light yellow solid was brought back into the glove box and dissolved in diethyl ether or pentane. Colorless crystals were grown from slow evaporation of diethyl ether (**1**) or pentane (**2-4**).

Ni(L^{Me})(CO)₃ (1): L^{Me} (74.5 mg, 0.345 mmol) and bis(1,5-cyclooctadiene)nickel(0) (94.8 mg, 0.345 mmol). 84% Yield. ¹H NMR (C₆D₆, 400 MHz) δ = 2.39 (br, 9H, CH₃NP), 2.47 (s, 6H, NCH₂CH₂NP), 2.50 (s, 6H, NCH₂CH₂NP). ¹³C {¹H} NMR (C₆D₆, 126 MHz) δ = 35.8 (CH₃NP), 50.4 (NCH₂CH₂NP), 50.6 (NCH₂CH₂NP), 199 (CO). ³¹P NMR (C₆D₆, 162 MHz) δ = 136. FTIR (CH₂Cl₂): $\tilde{\nu}$ = 2057.0 (CO-A₁), 1977.7 (CO-E). Analytical Calculation for C₁₂H₂₁N₄NiO₃P: C, 40.15; H, 5.90; N, 15.61 Found: C, 39.67; H, 5.99; N, 15.15.

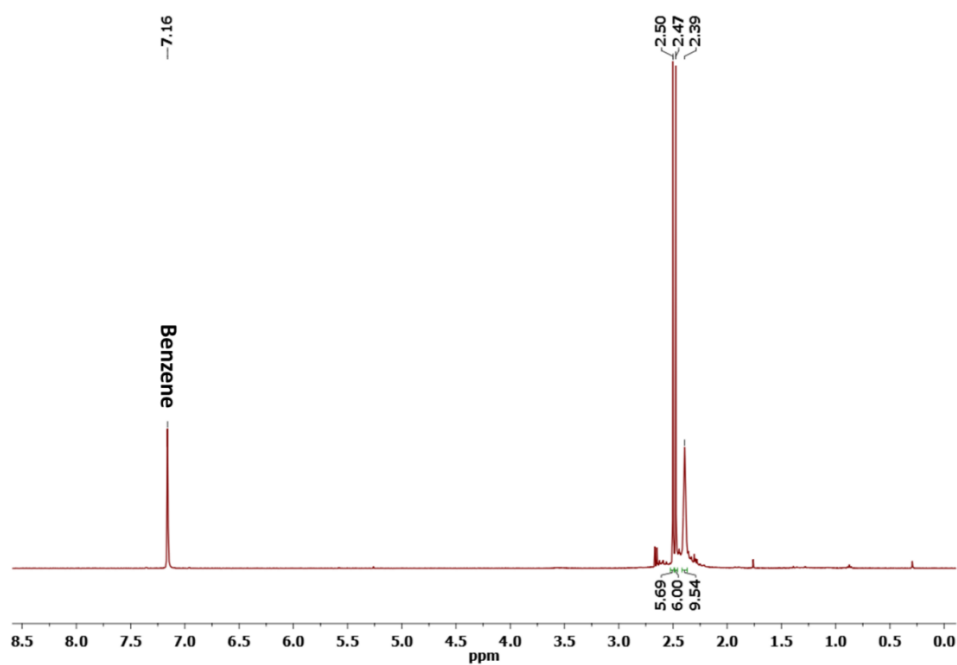


Figure 1.6. ¹H NMR spectrum of Ni(L^{Me})(CO)₃ (1) in C₆D₆.

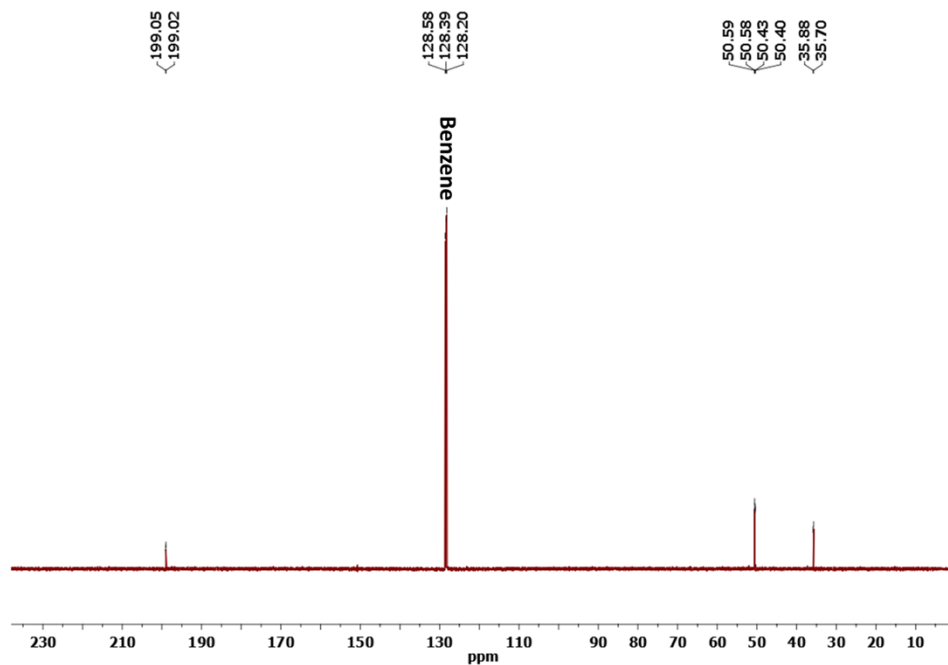


Figure 1.7. ¹³C NMR spectrum of Ni(L^{Me})(CO)₃ (1) in C₆D₆.

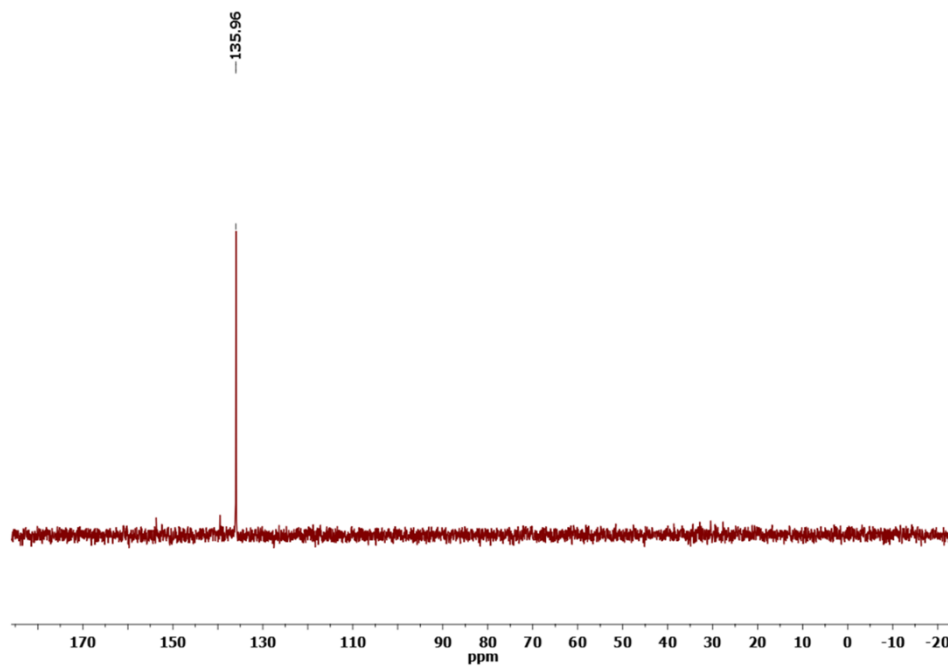


Figure 1.8. ³¹P NMR spectrum of Ni(L^{Me})(CO)₃ (1) in C₆D₆.

Ni(LⁱPr)(CO)₃ (2): LⁱPr (194 mg, 0.647 mmol) and bis(1,5-cyclooctadiene)nickel(0) (178 mg, 0.647 mmol). 87% Yield. ¹H NMR (C₆D₆, 400 MHz) δ = 1.04 (d, *J* = 6.6 Hz, 18H, NCH(CH₃)₂), 2.55-2.69 (A₂B₂, 12H, CH₂CH₂NP), 3.90 (septet, *J* = 6.7 Hz, 3H, NCH(CH₃)₂). ¹³C {¹H} NMR (C₆D₆, 126 MHz) δ = 22.7 (NCH(CH₃)₂), 39.9 (CH₂CH₂NP), 49.7 (NCH(CH₃)₂), 54.8 (CH₂CH₂NP), 199 (CO). ³¹P NMR (C₆D₆, 162 MHz) δ = 137. FTIR (CH₂Cl₂): $\tilde{\nu}$ = 2054.6 (CO-A₁), 1974.7 (CO-E). Analytical Calculation for C₁₈H₃₃N₄NiO₃P: C, 48.79; H, 7.51; N, 12.64 Found: C, 48.75; H, 7.39; N, 12.58.

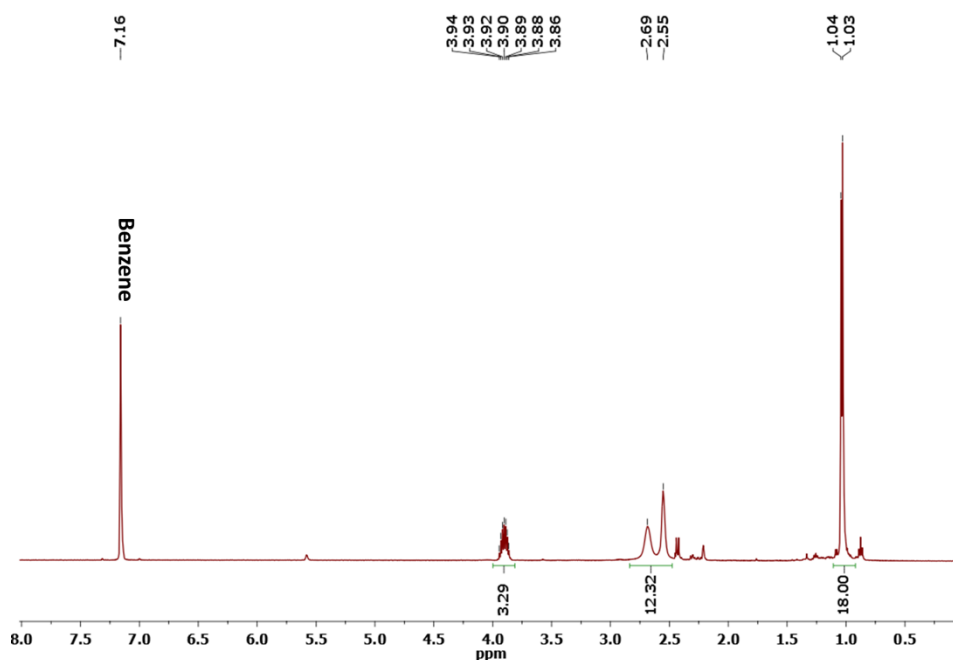


Figure 1.9. ¹H NMR spectrum of Ni(LⁱPr)(CO)₃ (2) in C₆D₆.

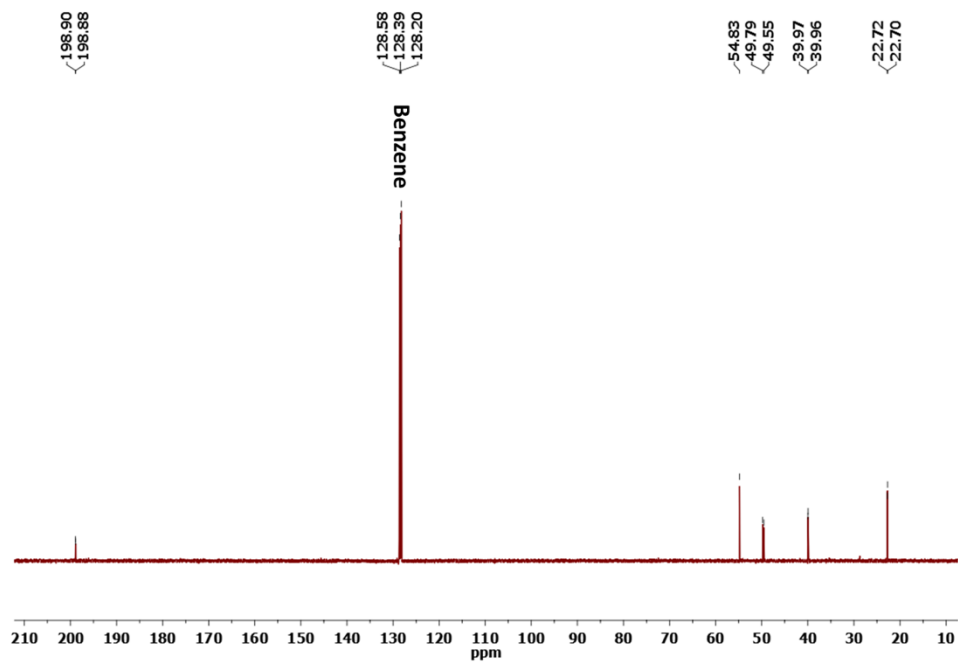


Figure 1.10. ¹³C NMR spectrum of Ni(LⁱPr)(CO)₃ (**2**) in C₆D₆.

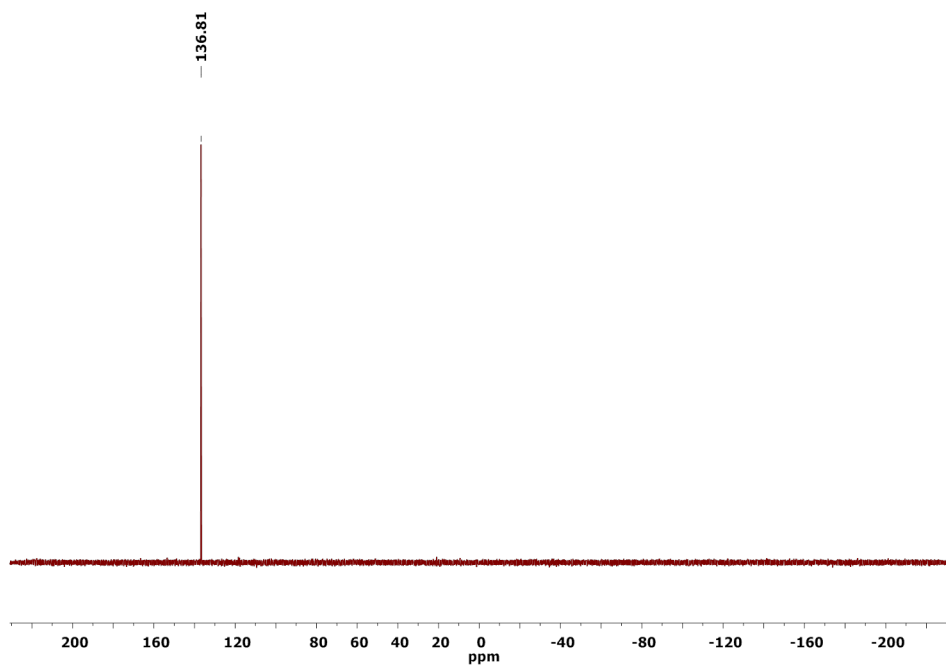


Figure 1.11. ³¹P NMR spectrum of Ni(LⁱPr)(CO)₃ (**2**) in C₆D₆.

Ni(LⁱBu)(CO)₃ (3): LⁱBu (195 mg, 0.569 mmol) and bis(1,5-cyclooctadiene)nickel(0) (157 mg, 0.569 mmol). 74% Yield. ¹H NMR (C₆D₆, 400 MHz) δ = 0.94 (d, *J* = 6.7 Hz, 18H, NCH₂CH(CH₃)₂), 2.06 (septet, *J* = 6.9 Hz, 3H, NCH₂CH(CH₃)₂), 2.55 (t, *J* = 4.8 Hz, 6H, CH₂CH₂NP), 2.82-2.67 (br, 12H, NCH₂CH₂NP, NCH₂CH(CH₃)₂). ¹³C {¹H} NMR (C₆D₆, 126 MHz) δ = 21.1 (NCH₂CH(CH₃)₂), 28.8 (NCH₂CH(CH₃)₂), 48.2 (NCH₂CH₂NP), 50.3 (NCH₂CH₂NP), 55.4 (NCH₂CH(CH₃)₂), 199 (CO). ³¹P NMR (C₆D₆, 162 MHz) δ = 141. FTIR (CH₂Cl₂): $\tilde{\nu}$ = 2054.9 (CO-A₁), 1975.3 (CO-E). Analytical Calculation for C₂₁H₃₉N₄NiO₃P: C, 51.98; H, 8.10; N, 11.55 Found: C, 51.56; H, 7.94; N, 11.86.

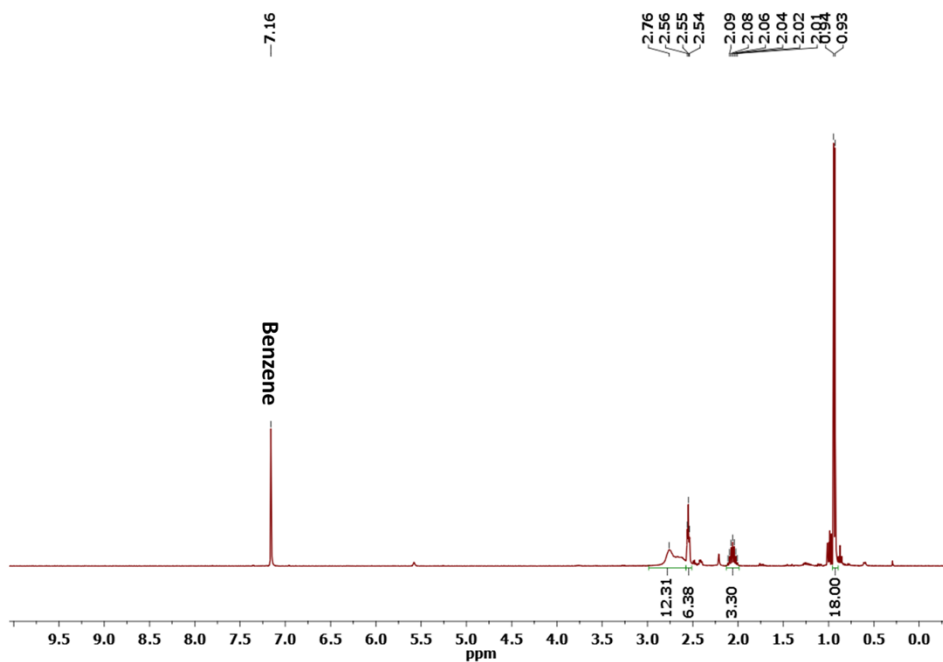


Figure 1.12. ¹H NMR spectrum of Ni(LⁱBu)(CO)₃ (3) in C₆D₆.

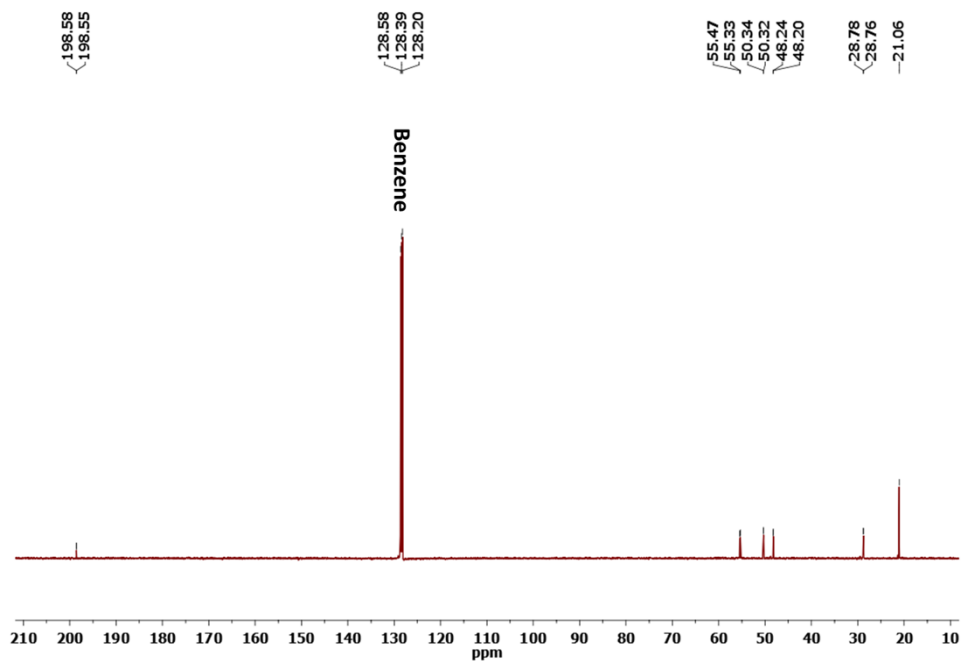


Figure 1.13. ¹³C NMR spectrum of Ni(LⁱBu)(CO)₃ (**3**) in C₆D₆.

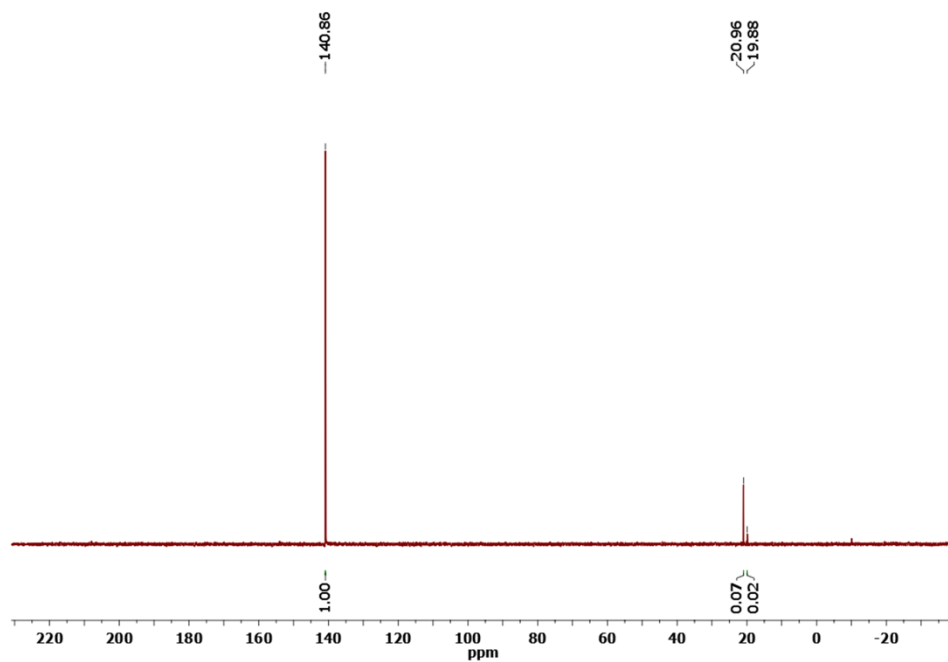


Figure 1.14. ³¹P NMR spectrum of Ni(LⁱBu)(CO)₃ (**3**) in C₆D₆. Resonances around 20 ppm are due to oxidized LⁱBu.³⁵

Ni(L^{Bz})(CO)₃ (4): L^{Bz} (146 mg, 0.328 mmol) and bis(1,5-cyclooctadiene)nickel(0) (90.0 mg, 0.328 mmol). 93% Yield. ¹H NMR (C₆D₆, 400 MHz) δ = 2.45 (t, *J* = 4.8 Hz, 6H, NCH₂CH₂NP), 2.68 (br, 6H, NCH₂CH₂NP), 4.31 (br, 6H, PhCH₂NP), 7.14 (m, 3H, *p*-Ph), 7.30 (t, *J* = 7.7 Hz, 6H, *m*-Ph), 7.40 (d, *J* = 7.3 Hz, 6H, *o*-Ph). ¹³C {¹H} NMR (C₆D₆, 126 MHz) δ = 46.7 (NCH₂CH₂NP), 49.9 (NCH₂Ph), 50.7 (NCH₂CH₂NP), 128 (Ph), 128 (Ph), 129 (Ph), 139 (Ph), 198 (CO). ³¹P NMR (C₆D₆, 162 MHz) δ = 143. FTIR (CH₂Cl₂): $\tilde{\nu}$ = 2059.1 (CO-A₁), 1981.1 (CO-E). Analytical Calculation for C₃₀H₃₃N₄NiO₃P: C, 61.36; H, 5.66; N, 9.54 Found: C, 61.02; H, 5.64; N, 9.48.

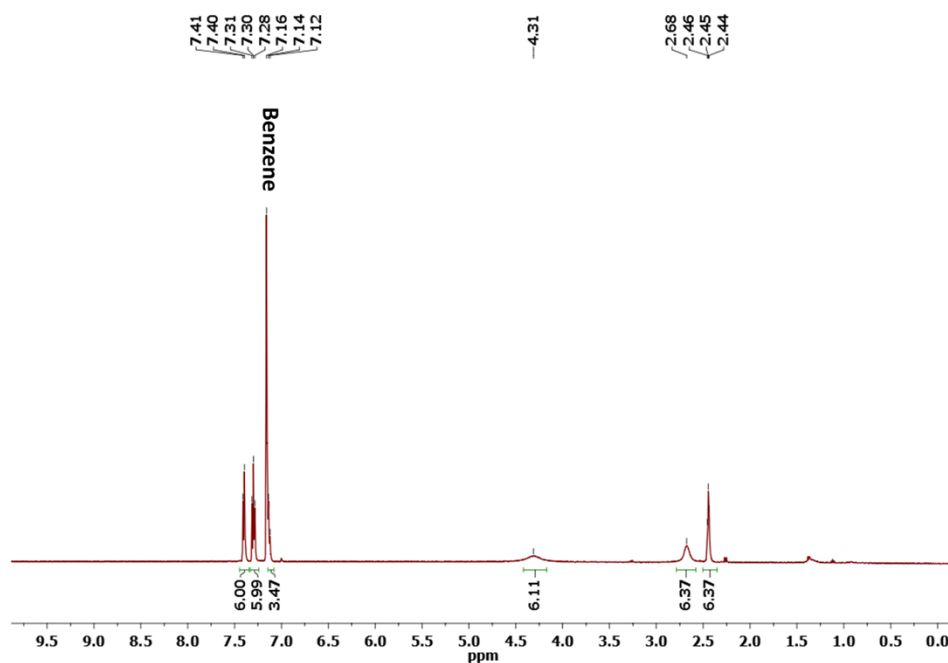


Figure 1.15. ¹H NMR spectrum of Ni(L^{Bz})(CO)₃ (4) in C₆D₆.

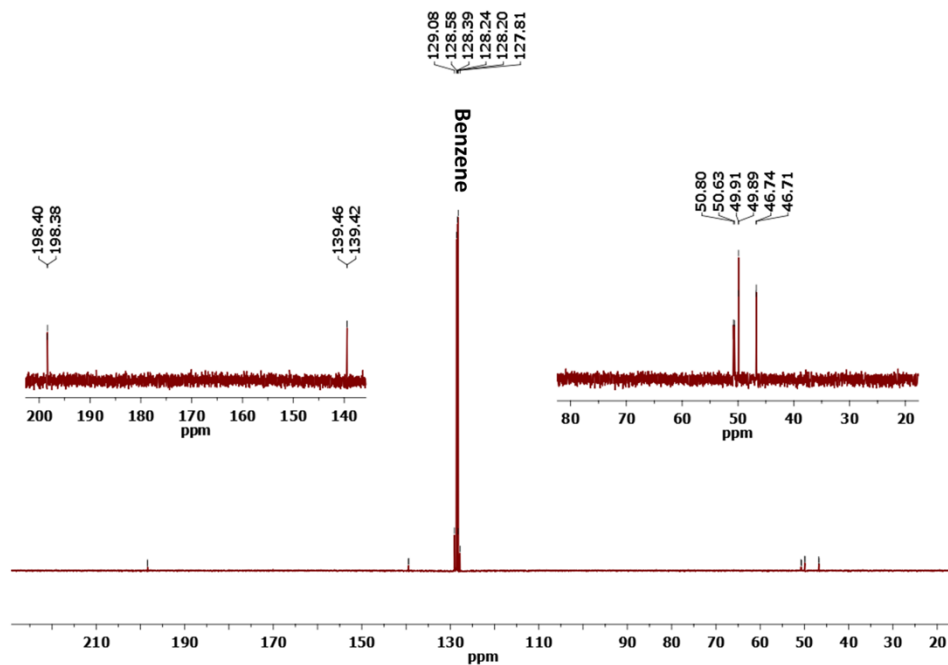


Figure 1.16. ^{13}C NMR spectrum of $\text{Ni}(\text{L}^{\text{Bz}})(\text{CO})_3$ (**4**) in C_6D_6 .

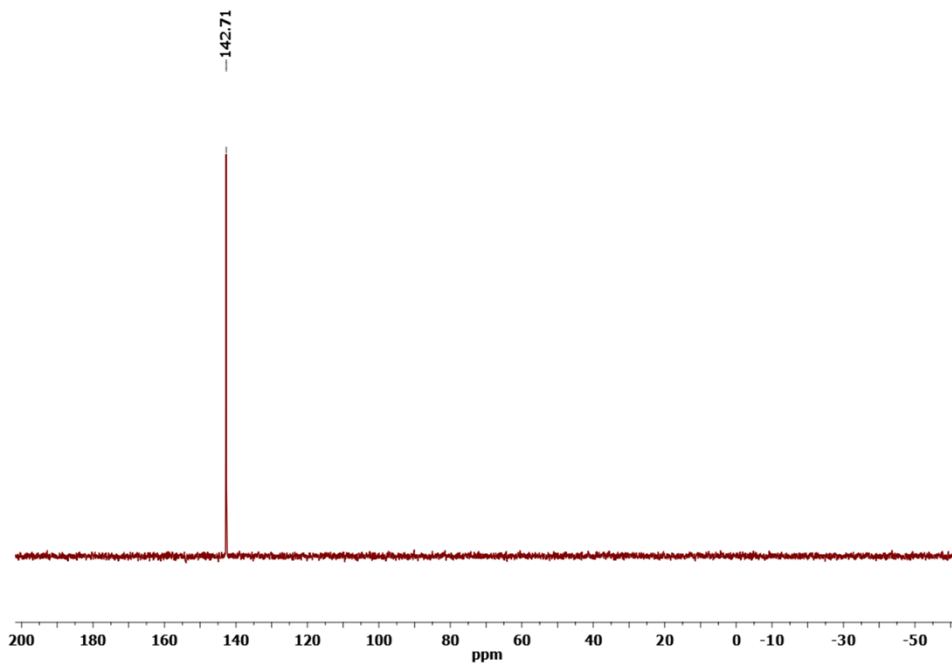


Figure 1.17. ^{31}P NMR spectrum of $\text{Ni}(\text{L}^{\text{Bz}})(\text{CO})_3$ (**4**) in C_6D_6 .

Ni(L^{Me})₂(CO)₂ (5): In the glove box, a solution of bis(1,5-cyclooctadiene)nickel(0) (26.2 mg, 0.093 mmol) in 5 mL of tetrahydrofuran was added to a solution of L^{Me} (41.2 mg, 0.191 mmol) in 5 mL of tetrahydrofuran. The solution was stirred for 1 hour at room temperature. The solution was transferred to a 100 mL Schlenk flask, brought out of the glove box, and filled with CO gas (1 atm). The solution was stirred overnight under a CO atmosphere, during which time the color changed from dark orange to colorless. The solvent was removed under reduced pressure and the resulting light yellow solid was brought back into the glove box and washed with pentane. Colorless crystals of **5** were grown from slow evaporation of dichloromethane to give the product in 62% yield. ¹H NMR (C₆D₆, 400 MHz) δ = 2.61 (s, 18H, CH₃NP), 2.74 (d, *J* = 8.7 Hz, 24H, NCH₂CH₂NP). ¹³C {¹H} NMR (C₆D₆, 126 MHz) δ = 36.2 (CH₃NP), 50.6 (NCH₂CH₂NP), 51.1 (NCH₂CH₂NP), 204 (CO). ³¹P NMR (C₆D₆, 162 MHz) δ = 144. FTIR (CH₂Cl₂): $\tilde{\nu}$ = 1976.8 (CO), 1909.3 (CO). Analytical Calculation for C₂₀H₄₂N₈NiO₂P₂: C, 43.90; H, 7.74; N, 20.48 Found: C, 43.51; H, 7.79; N, 20.49.

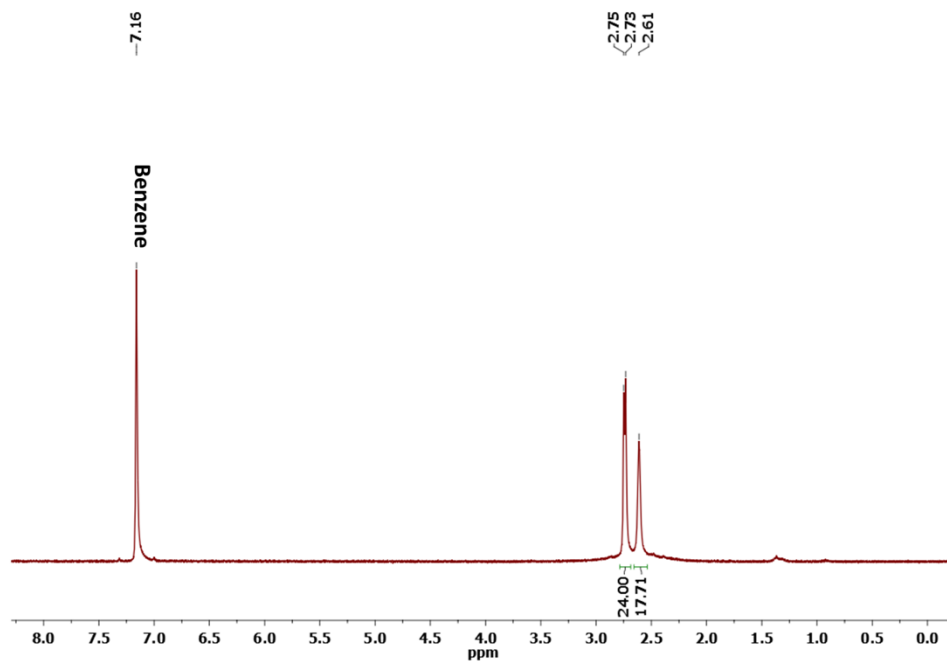


Figure 1.18. ^1H NMR spectrum of $\text{Ni}(\text{L}^{\text{Me}})_2(\text{CO})_2$ (**5**) in C_6D_6 .

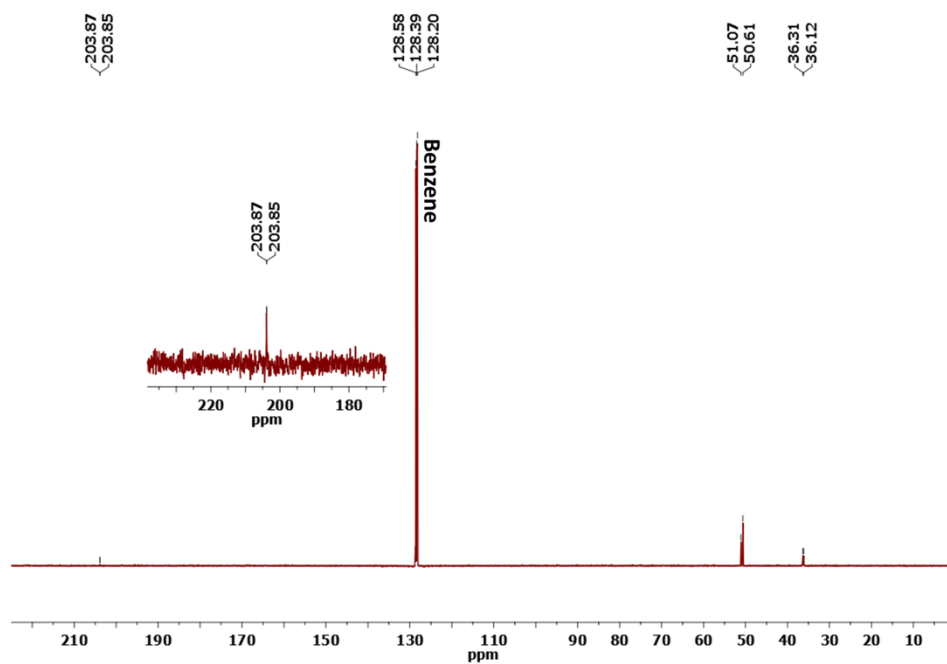


Figure 1.19. ^{13}C NMR spectrum of $\text{Ni}(\text{L}^{\text{Me}})_2(\text{CO})_2$ (**5**) in C_6D_6 .

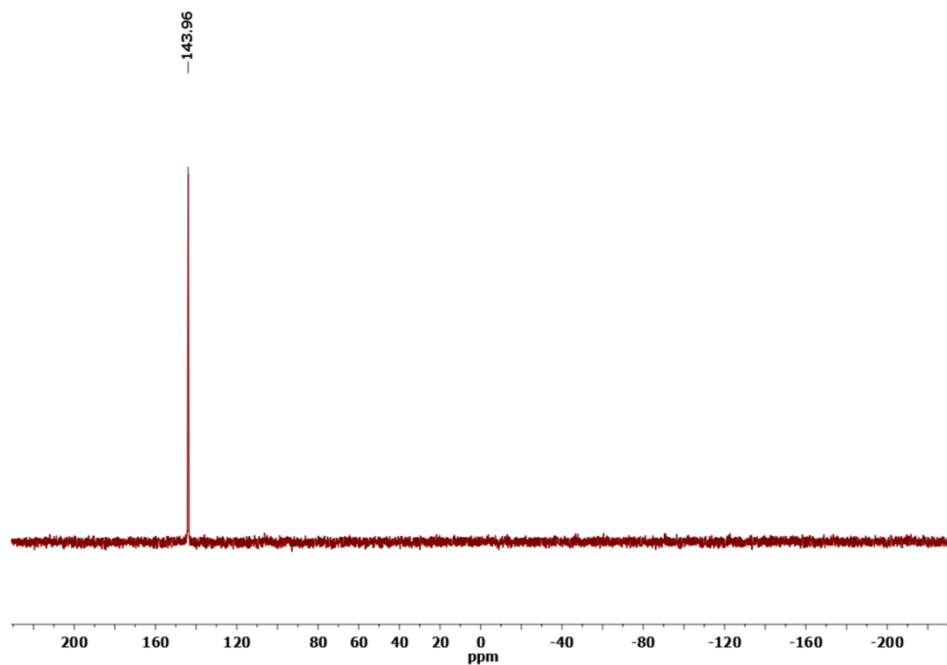


Figure 1.20. ^{31}P NMR spectrum of $\text{Ni}(\text{L}^{\text{Me}})_2(\text{CO})_2$ (**5**) in C_6D_6 .

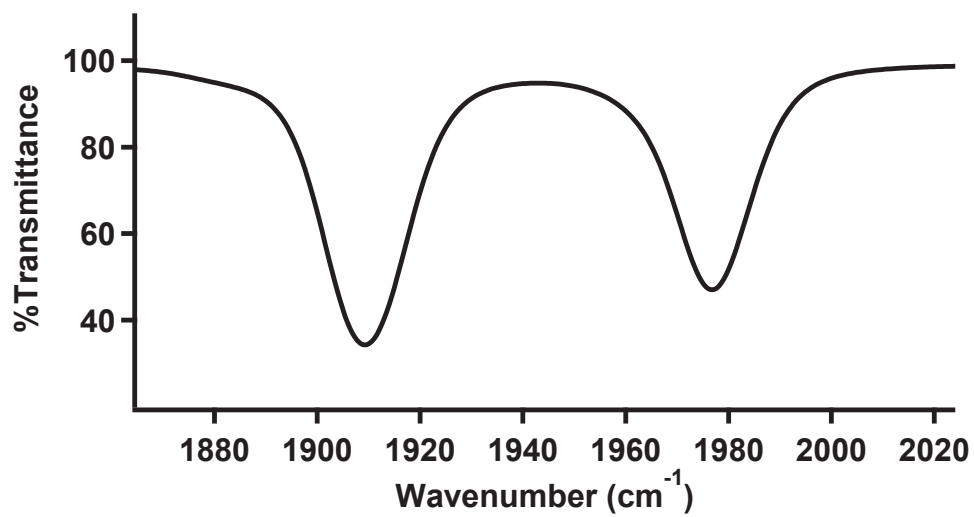


Figure 1.21. IR spectrum $\text{Ni}(\text{L}^{\text{Me}})_2(\text{CO})_2$ (**5**) in CH_2Cl_2 .

1.6. References

1. Crabtree, R. H., Carbonyls, Phosphine Complexes, and Ligand Substitution Reactions. In *The Organometallic Chemistry of the Transition Metals*, Crabtree, R. H., Ed. John Wiley & Sons, Inc: 2005; pp 87-124.
2. Gillespie, J. A.; Zuidema, E., Phosphorus Ligand Effects in Homogeneous Catalysis and Rational Catalyst Design. In *Phosphorus(III) Ligands in Homogeneous Catalysis: Design and Synthesis*, van Leeuwen, P. W.; Kamer, P. C., Eds. John Wiley & Sons, Ltd: 2012; pp 1-26.
3. DeAngelis, A.; Colacot, T. J., CHAPTER 2 Prominent Ligand Types in Modern Cross-Coupling Reactions. In *New Trends in Cross-Coupling: Theory and Applications*, The Royal Society of Chemistry: 2015; pp 20-90.
4. Kendall, A. J.; Tyler, D. R., The synthesis of heteroleptic phosphines. *Dalton Transactions* **2015**, 44 (28), 12473-12483.
5. Tolman, C. A., Steric effects of phosphorus ligands in organometallic chemistry and homogeneous catalysis. *Chemical Reviews* **1977**, 77 (3), 313-348.
6. Thammavongsy, Z.; Khosrowabadi Kotyk, J. F.; Tsay, C.; Yang, J. Y., Flexibility is Key: Synthesis of a Tripyridylamine (TPA) Congener with a Phosphorus Apical Donor and Coordination to Cobalt(II). *Inorganic Chemistry* **2015**, 54 (23), 11505-11510.
7. Matthews, A. D.; Gravalis, G. M.; Schley, N. D.; Johnson, M. W., Synthesis, Structure, and Reactivity of Palladium Proazaphosphatane Complexes Invoked in C–N Cross-Coupling. *Organometallics* **2018**, 37 (18), 3073-3078.
8. Su, W.; Urgaonkar, S.; McLaughlin, P. A.; Verkade, J. G., Highly Active Palladium Catalysts Supported by Bulky Proazaphosphatane Ligands for Stille Cross-Coupling: Coupling of Aryl and Vinyl Chlorides, Room Temperature Coupling of Aryl Bromides, Coupling of Aryl Triflates, and Synthesis of Sterically Hindered Biaryls. *Journal of the American Chemical Society* **2004**, 126 (50), 16433-16439.
9. Urgaonkar, S.; Verkade, J. G., Scope and Limitations of Pd₂(dba)₃/P(i-BuNCH₂CH₂)₃N-Catalyzed Buchwald–Hartwig Amination Reactions of Aryl Chlorides. *The Journal of Organic Chemistry* **2004**, 69 (26), 9135-9142.
10. Urgaonkar, S.; Nagarajan, M.; Verkade, J. G., P[N(i-Bu)CH₂CH₂]₃N: A Versatile Ligand for the Pd-Catalyzed Amination of Aryl Chlorides. *Organic Letters* **2003**, 5 (6), 815-818.
11. Tolman, C. A., Phosphorus ligand exchange equilibria on zerovalent nickel. Dominant role for steric effects. *Journal of the American Chemical Society* **1970**, 92 (10), 2956-2965.
12. Müller, T. E.; Mingos, D. M. P., Determination of the Tolman cone angle from crystallographic parameters and a statistical analysis using the crystallographic data base. *Transition Metal Chemistry* **1995**, 20 (6), 533-539.
13. Wünsche, M. A.; Mehlmann, P.; Witteler, T.; Buß, F.; Rathmann, P.; Dielmann, F., Imidazolin-2-ylidenaminophosphines as Highly Electron-Rich Ligands for Transition-Metal Catalysts. *Angewandte Chemie International Edition* **2015**, 54 (40), 11857-11860.
14. Su, W.; Urgaonkar, S.; Verkade, J. G., Pd₂(dba)₃/P(i-BuNCH₂CH₂)₃N-Catalyzed Stille Cross-Coupling of Aryl Chlorides. *Organic Letters* **2004**, 6 (9), 1421-1424.

15. Urgaonkar, S.; Nagarajan, M.; Verkade, J. G., Pd/P(i-BuNCH₂CH₂)₃N: an efficient catalyst for Suzuki cross-coupling of aryl bromides and chlorides with arylboronic acids. *Tetrahedron Letters* **2002**, *43* (49), 8921-8924.
16. You, J.; Verkade, J. G., P(i-BuNCH₂CH₂)₃N: An Efficient Ligand for the Direct α -Arylation of Nitriles with Aryl Bromides. *The Journal of Organic Chemistry* **2003**, *68* (21), 8003-8007.
17. You, J.; Verkade, J. G., A General Method for the Direct α -Arylation of Nitriles with Aryl Chlorides. *Angewandte Chemie International Edition* **2003**, *42* (41), 5051-5053.
18. Nandakumar, M. V.; Verkade, J. G., One-Pot Sequential N and C Arylations: An Efficient Methodology for the Synthesis of trans 4-N,N-Diaryl Aminostilbenes. *Angewandte Chemie International Edition* **2005**, *44* (20), 3115-3118.
19. Kim, S. H.; Kim, M.; Verkade, J. G.; Kim, Y., A Tuned Bicyclic Proazaphosphatrane for Catalytically Enhanced N-Arylation Reactions with Aryl Chlorides. *European Journal of Organic Chemistry* **2015**, *2015* (9), 1954-1960.
20. Venkat Reddy, C. R.; Urgaonkar, S.; Verkade, J. G., A Highly Effective Catalyst System for the Pd-Catalyzed Amination of Vinyl Bromides and Chlorides. *Organic Letters* **2005**, *7* (20), 4427-4430.
21. Urgaonkar, S.; Verkade, J. G., Palladium/Proazaphosphatrane-Catalyzed Amination of Aryl Halides Possessing a Phenol, Alcohol, Acetanilide, Amide or an Enolizable Ketone Functional Group: Efficacy of Lithium Bis(trimethylsilyl)amide as the Base. *Advanced Synthesis & Catalysis* **2004**, *346* (6), 611-616.
22. Urgaonkar, S.; Nagarajan, M.; Verkade, J. G., P(i-BuNCH₂CH₂)₃N: An Effective Ligand in the Palladium-Catalyzed Amination of Aryl Bromides and Iodides. *The Journal of Organic Chemistry* **2003**, *68* (2), 452-459.
23. Urgaonkar, S.; Verkade, J. G., Synthesis of N-aryl-aza-crown ethers via Pd-catalyzed amination reactions of aryl chlorides with aza-crown ethers. *Tetrahedron* **2004**, *60* (51), 11837-11842.
24. Aneetha, H.; Wu, W.; Verkade, J. G., Stereo- and Regioselective Pt(DVDS)/P(iBuNCH₂CH₂)₃N-Catalyzed Hydrosilylation of Terminal Alkynes. *Organometallics* **2005**, *24* (11), 2590-2596.
25. Tolman, C. A., Electron donor-acceptor properties of phosphorus ligands. Substituent additivity. *Journal of the American Chemical Society* **1970**, *92* (10), 2953-2956.
26. Yang, L.; Powell, D. R.; Houser, R. P., Structural variation in copper(I) complexes with pyridylmethylamide ligands: structural analysis with a new four-coordinate geometry index, τ_4 . *Dalton Transactions* **2007**, (9), 955-964.
27. Davis, M. A., Group electronegativity and polar substituent constants. *The Journal of Organic Chemistry* **1967**, *32* (4), 1161-1163.
28. Clarke, M. L.; Cole-Hamilton, D. J.; Slawin, A. M. Z.; Woollins, J. D., P-N bond formation as a route to highly electron rich phosphine ligands. *Chemical Communications* **2000**, (20), 2065-2066.

29. Clarke, M. L.; Holliday, G. L.; Slawin, A. M. Z.; Woollins, J. D., Highly electron rich alkyl- and dialkyl-N-pyrrolidinyl phosphines: an evaluation of their electronic and structural properties. *Journal of the Chemical Society, Dalton Transactions* **2002**, (6), 1093-1103.
30. Xi, S. K.; Schmidt, H.; Lensink, C.; Kim, S.; Wintergrass, D.; Daniels, L. M.; Jacobson, R. A.; Verkade, J. G., Bridgehead-bridgehead communication in untransannulated phosphatrane ZP(ECH₂CH₂)₃N systems. *Inorganic Chemistry* **1990**, 29 (12), 2214-2220.
31. Socol, S. M.; Jacobson, R. A.; Verkade, J. G., Ligation of phosphorus ligands to silver(I): Coordination of one to four P(NR₂)₃ ligands and the structure of a nonlinear two-coordinate complex. *Inorganic Chemistry* **1984**, 23 (1), 88-94.
32. Cowley, A. H.; Davis, R. E.; Remadna, K., Conformational behavior of ligated tris(dialkylamino)phosphines. X-ray crystal structures of (Me₂N)₃PFe(CO)₄ at 21 degree C and of [(Me₂N)₃P]₂Fe(CO)₃ at -35 degree C. *Inorganic Chemistry* **1981**, 20 (7), 2146-2152.
33. Moloy, K. G.; Petersen, J. L., N-Pyrrolyl Phosphines: An Unexploited Class of Phosphine Ligands with Exceptional pi-Acceptor Character. *Journal of the American Chemical Society* **1995**, 117 (29), 7696-7710.
34. Wróblewski, A. E.; Pinkas, J.; Verkade, J. G., Strongly Basic Proazaphosphatranes: P (EtNCH₂CH₂)₃N and P (iso-PrNCH₂CH₂)₃N. *Main Group Chemistry* **1995**, 1 (1), 69-79.
35. Gudat, D.; Lensink, C.; Schmidt, H.; Xi, S. K.; Verkade, J. G., Novel Properties of New Phosphatranes and Silatranes. *Phosphorus, Sulfur, and Silicon and the Related Elements* **1989**, 41 (1-2), 21-29.

CHAPTER 2

Expanding the Denticity of Proazaphosphatrane:

Ligand Synthesis

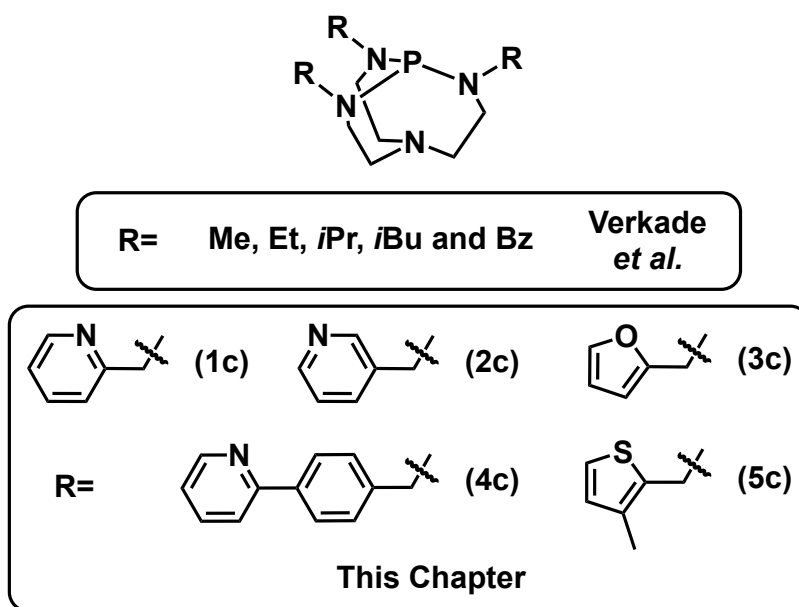
Portions of this chapter have been published:

Thammavongsy, Z.; Khosrowabadi Kotyk, J. F.; Tsay, C.; Yang, J. Y. *Inorg. Chem.* **2015**, *54*, 11505-1151

2.1. Motivation and Specific Aims

Proazaphosphatranes are strong, non-ionic bases that are easily modifiable. However, the functionalization of proazaphosphatranes outside of simple alkyl groups is lacking in the literature. Current interest in proazaphosphatranes has expanded their use outside of simple acid/base chemistry, highlighting the multilateral utility of this electron rich molecule. In this chapter, the facile synthesis of proazaphosphatrane that incorporates heteroatom donors, (2-pyridine, 3-pyridine, 4-(2-pyridinyl-benzene), furan and 2-methylthiophene) for use as ligands in inorganic complexes with primary and secondary coordination effects is reported (Chart 2.1).

Chart 2.1. Series of Proazaphosphatrane Compounds with Various Functional Groups.



^1H , ^{13}C , and ^{31}P NMR spectra, along with high resolution mass spectra of these compounds are presented. A solid state structure from X-ray crystallographic analysis of protonated ([tris(2-pyridylmethyl)proazaphosphatrane-H]chloride) and the unprotonated form (tris(3-pyridylmethyl)proazaphosphatrane) are also included.

2.2. Background

There are numerous publications highlighting the properties⁶⁻¹⁰ and utility^{11, 12} of proazaphosphatranes. The majority of proazaphosphatranes used in these studies have alkyl substituents, due to their commercial availability (Chart 2.1).^{2, 40, 42, 43, 45} However, there have been recent efforts to expand and develop the design of proazaphosphatranes, for use in anion binding,⁴⁶ enhanced organic⁴⁷ and organometallic³⁹ catalysis, and immobilization on solid silica support (See Introduction).^{48, 49} In addition, proazaphosphatranes are highly modular, with facile synthetic approaches to incorporate various functional groups. This chapter seeks to advance the proazaphosphatrane framework, by incorporate multi-donor atom sites, for the purpose of increasing chelating stability and/or potential secondary coordination effects in inorganic complexes.

In this chapter, the facile synthesis of symmetric proazaphosphatranes bearing heteroatoms donors, (2-pyridine, 3-pyridine, 4-(2-pyridinyl-benzene), furan and 2-methylthiophene) is reported (Chart 2.1).

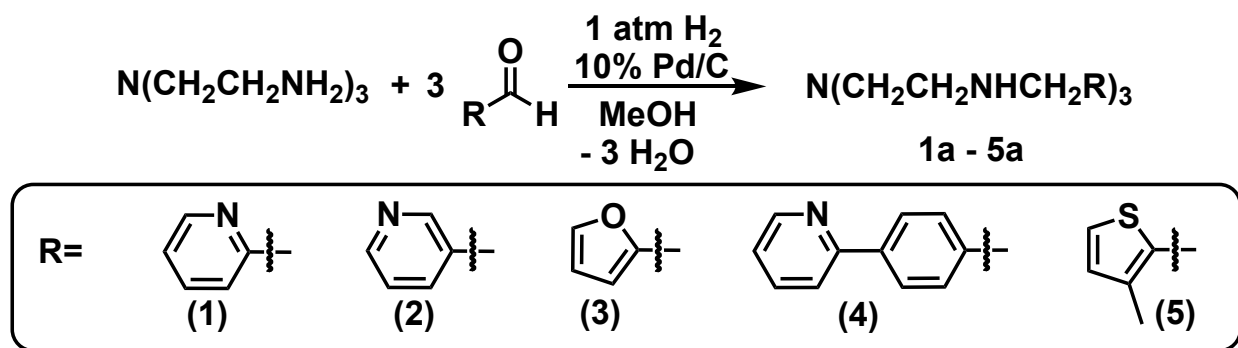
2.3. Results and Discussion

2.3.1. Synthesis of Tri-Substituted Tris(2-aminoethyl)amines

The compounds, tris[(((2-pyridyl)methyl)-amino)ethyl]-amine (**1a**), tris[(((3-pyridyl)methyl)-amino)ethyl]-amine (**2a**), tris[(((furan)methyl)-amino)ethyl]-amine(**3a**) and tris[(((2-methylthiophene))methyl)-amino]ethyl]-amine (**5a**) were synthesized with slight modifications from previously published procedures.⁵⁴⁻⁵⁶ The new compound tris[[(4-(2-pyridyl)benzyl)-amino]ethyl]-amine (**4a**) is synthesized via the Schiff-base condensation of a 3:1

ratio of 4-(2-pyridyl)benzaldehyde to tris(2-aminoethyl)-amine in methanol, followed by hydrogenation with H₂ gas and a Pd/C catalyst (Scheme 2.1). After work-up, a waxy white solid (**4a**) was isolated in a 79.1 percent yield. Spectroscopic and ESI-MS data confirmed the identity of **4a**. This general synthesis works well with aldehydes, providing easy access to various donor groups (R in Scheme 2.1), albeit, only neutral donors have so far been incorporated.

Scheme 2.1. Synthesis of tri-substituted tris(2-aminoethyl)amine.

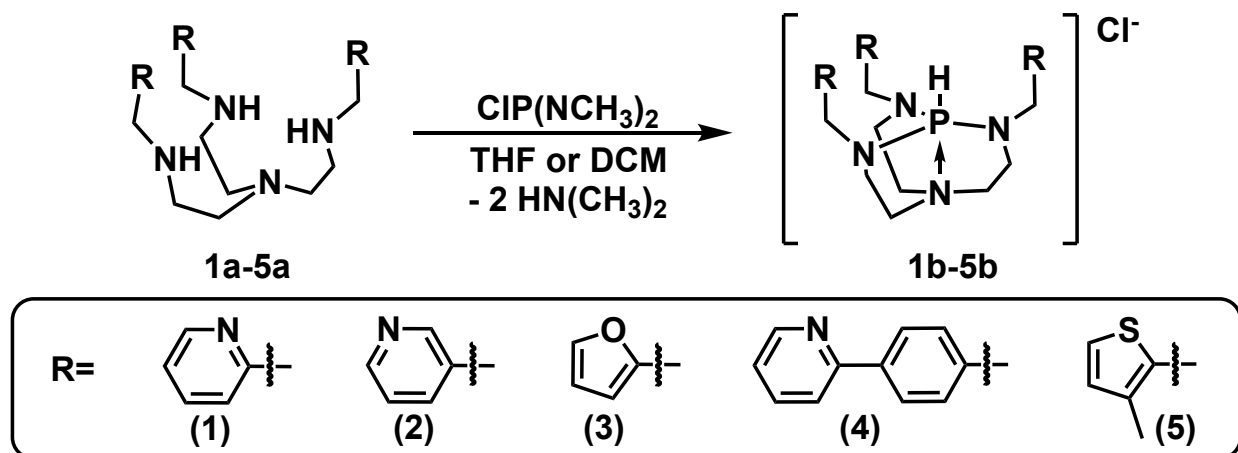


2.3.2. Synthesis of Protonated Tri-Substituted Azaphosphatranes

The addition of excess bis(dimethylamino)chlorophosphine to **1a-5a** yielded the protonated azaphosphatrane compounds **1b-5b** along with the by-product, dimethylamine (Scheme 2.2). The latter can be removed by excessive washing with tetrahydrofuran. Drying the resulting solid under reduced pressure overnight furnishes [HP((2-PyrCH₂)-NCH₂CH₂)₃N][Cl] (**1b**) as a white solid in 61.9 percent yield. The compounds **2b-5b** were not fully characterized due to high levels of impurities of the by-product, dimethylamine. However, the ³¹P{¹H} NMR spectra of **2b-5b** confirmed the presence of one phosphorus atom around -10.0 ppm, corresponding to the product. The ³¹P{¹H} NMR spectrum of **1b** features a singlet at -10.0 ppm, which appears as a

doublet in the ^{31}P NMR spectrum with a J -coupling of 506 Hz, consistent with previously published protonated azaphosphatranes (see Experimental Details).⁶

Scheme 2.2. Synthesis of protonated tri-substituted azaphosphatranes.



Single crystals suitable for X-ray analysis were grown by layering diethyl ether over a solution of **1b** in acetonitrile. The solid-state structure of compound **1b** displayed a P–N1 distance of 1.971(16) Å and a P–H distance of 1.24(2) Å (Figure 2.1). These bond distances are similar to previously reported protonated forms of Verkade’s Superbases.^{2, 18} The significant Brønsted basicity of Verkade’s superbase ($\text{p}K_{\text{a}}$ of protonated superbase = 32.9 in CH_3CN)⁴ is attributed to electron donation from the trans nitrogen atom (N_{ax} , or N1 in structure of **1b**) to the phosphorus, which stabilizes the protonated form. This strong interaction between the P and N_{ax} has been observed in prior structural characterization of protonated versus non-protonated bases.⁵ When protonated, the P– N_{ax} distances are typically 2.0 Å or less, while the corresponding free bases have P– N_{ax} distances of over 3.0 Å.

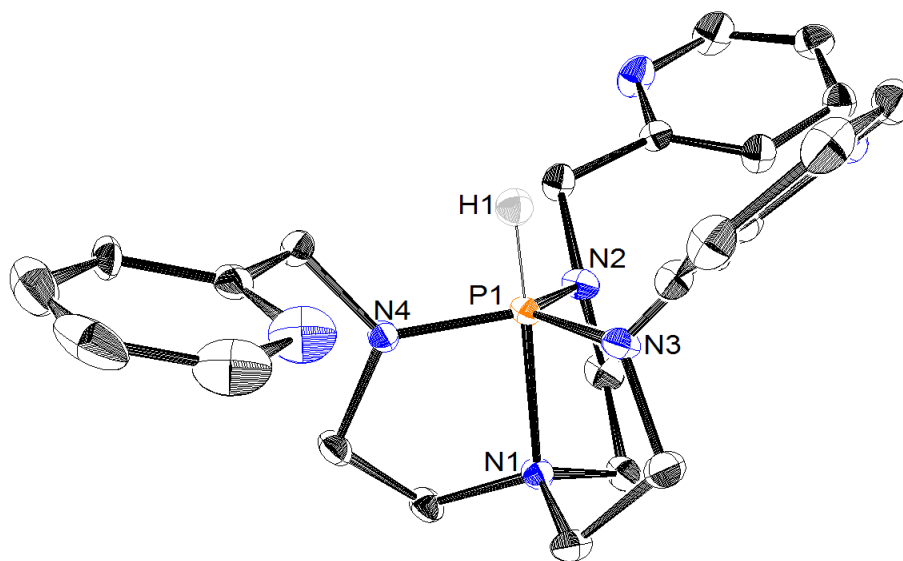
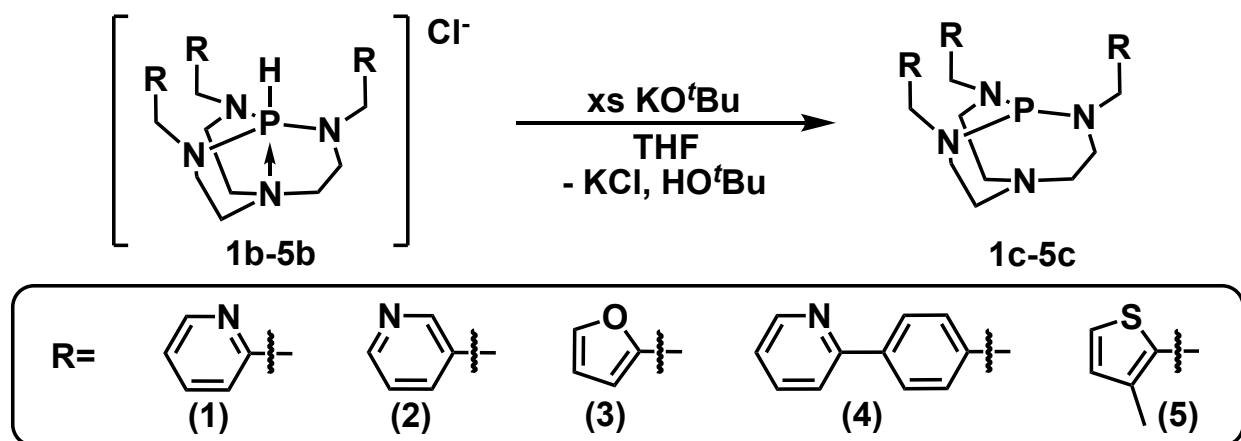


Figure 2.1. Crystal structure of $[\text{HP}((2\text{-PyrCH}_2)\text{-NCH}_2\text{CH}_2)_3\text{N}][\text{Cl}]$ (**1b**). Thermal ellipsoids are drawn at 50% probability; hydrogen atoms except for H1, which is located in the difference map and refined freely, and Cl^- anion were omitted for clarity. Adapted with permission from Thammavongsy, Z.; Khosrowabadi Kotyk, J. F.; Tsay, C.; Yang, J. Y. *Inorg. Chem.* **2015**, 54, 11505-11510. Copyright 2015 American Chemical Society.

2.3.3. Synthesis of Tri-Substituted Proazaphosphatranes

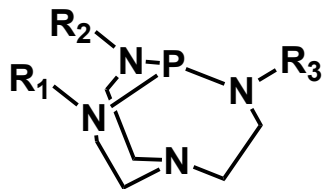
After the isolation of the protonated azaphosphatrane compounds **1b-5b**, excess KO^tBu is added to deprotonate the protonated azaphosphatranes, providing the symmetric tri-substituted proazaphosphatrane compounds **1c-5c**, in 85.4, 55.7, 79.1, 59.1 and 59.1 percent yield (Scheme 2.3). The presence of the dimethylamine by-product in **2b-5b** does not hinder the deprotonation step. Compounds **1c-5c** were characterized by ^1H , $^{13}\text{C}\{^1\text{H}\}$, and $^{31}\text{P}\{^1\text{H}\}$ NMR spectroscopies. The composition of **1c-5c** was confirmed through electrospray ionization mass spectrometry.

Scheme 2.3. Synthesis of Tri-Substituted Proazaphosphatranes



The ^{31}P NMR spectra of **1c-5c** displayed shifts at 126.4, 127.1, 126.9, 127.3 and 125.7 ppm, respectively. Compound **1c-5c** were performed in C_6D_6 in order to compare the ^{31}P NMR shifts to the alkyl-substituted proazaphosphatranes (Table 2.1), measured by Verkade co-workers.^{2, 34, 41-43} The ^{31}P $\{^1\text{H}\}$ NMR shifts of **1c-5c** in C_6D_6 are in the range of the symmetric benzyl substituted proazaphosphatranes (127.9 ppm in Table 2.1), likely due to the aromatic ring system. Compound **1c-5c** are downfield shifted relative to the symmetric methyl (120.8 ppm), ethyl (119.4 ppm) and isopropyl-substituted (118.7 ppm) proazaphosphatranes, except for the symmetric isobutyl-substituted (130.9 ppm) proazaphosphatranane (Table 2.1). Interestingly, the upfield trend observed in the ^{31}P NMR shift from methyl to isopropyl-substitution of Verkade's Superbases does not continue with the isobutyl group. Instead, a downfield shift ($\Delta 12.2$ ppm going from isopropyl to isobutyl-substituted proazaphosphatranane) is observed. This trend is opposite to what is seen with alkyl phosphines.⁵⁷ However, the trend observed for Verkade's asymmetric proazaphosphatranes (where isobutyl groups are replaced with benzyl groups) does fall in line with the expected observation of an upfield ^{31}P NMR shift, due to a less electron donating group.

Table 2.1. ^{31}P NMR values of **1c-5c** and various alkyl- and benzyl-substituted proazaphosphatranes in C_6D_6 reported by Verkade *et al.* Greyed out rows represent asymmetric proazaphosphatranes.



R_1	R_2	R_3	^{31}P NMR δ (C_6D_6)
1	1	1	126.4
2	2	2	127.1
3	3	3	126.9
4	4	4	127.3
5	5	5	125.7
CH_3	CH_3	CH_3	120.8 ²
Et	Et	Et	119.4 ⁴²
<i>i</i> Pr	<i>i</i> Pr	<i>i</i> Pr	118.7 ⁴²
H	<i>i</i> Pr	<i>i</i> Pr	110.5 ⁴¹
H	H	<i>i</i> Pr	101.4 ⁴³
<i>i</i> Bu	<i>i</i> Bu	<i>i</i> Bu	130.9 ⁴³
<i>i</i> Bu	<i>i</i> Bu	Bz	130.0 ³⁴
<i>i</i> Bu	Bz	Bz	128.9 ³⁴
Bz	Bz	Bz	127.9 ³⁴

In addition, an X-ray quality crystal of compound **2c** was grown from a concentrated sample of **2c** in tetrahydrofuran/pentane mixture at -35°C . The crystal structure of **2c** displayed a P1-N6 distance of 3.322 Å, similar to other previously published proazaphosphatranes (Figure 2.2).^{18, 20, 24, 58-60} All three P-N_{eq} distances are close, measuring 1.696, 1.697 and 1.702 Å for P1-N1, P1-N2, and P1-N4, respectively. In addition, the sum of angles at nitrogen (N1, N2, and N4) is $\sim 360^\circ$, due to the rigid cage frame of proazaphosphatrane.³⁴ The combination of these two metrics indicate all three equatorial nitrogen atoms donate their electron density to the phosphorus contributing to its donor strength.

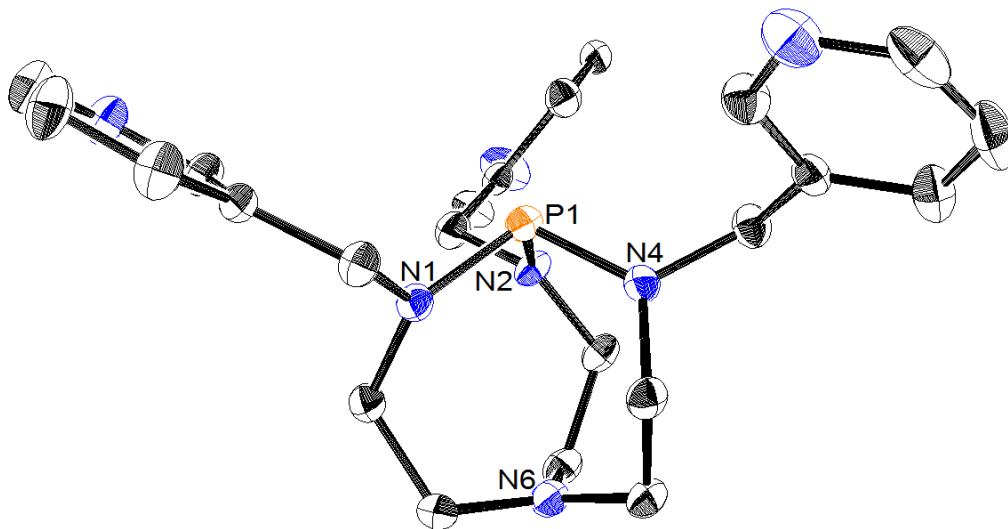


Figure 2.2. Crystal structure of $[P((3\text{-PyrCH}_2)\text{-NCH}_2\text{CH}_2)_3\text{N}]$ (**2c**). Thermal ellipsoids are drawn at 50% probability; hydrogen atoms were omitted for clarity.

2.4. Conclusion

The design of proazaphosphatranes expanded to incorporate heteroatom donors for use as ligands in inorganic complexes. Incorporation of the N, O, and S donors involved a facile synthesis of amine precursors, which goes through a well-known Schiff-based reaction, followed by hydrogenation. Coordination studies of the tris(2-pyridylmethyl)-azaphosphatrane (**1c**) ligand with transition metal ions will be focused on in Chapter 3.

2.5. Experimental Details

General Considerations

Compounds **1c-5c** described below are moisture-sensitive, and must be handled under an inert atmosphere of nitrogen using standard glovebox and Schlenk techniques. Unless otherwise noted, all procedures were performed at ambient temperature (21-24 °C). All solvents were sparged with argon and dried using a solvent purification system.

Tetrahydrofuran, pentane, diethyl ether, and dichloromethane were passed through two columns of neutral alumina. Compounds tris[(((2-pyridyl)methyl)-amino]ethyl]amine, tris[(((3-pyridyl)methyl)-amino]ethyl]amine, tris[(((furan)methyl)-amino]ethyl]amine and tris[(((2-methylthiophene))methyl)-amino]ethyl]amine were synthesized according to established procedures.⁵⁴⁻⁵⁶ C₆D₆ and CD₃N were freeze-pump-thawed three times and dried over molecular sieves. Furfural, 3-methyl-2-thiophenecarboxyaldehyde, 3-pyridinecarboxyaldehyde, 2-pyridinecarboxyaldehyde, 4-(2-pyridyl)benzaldehyde, bis(dimethylamino)chlorophosphine, Pd/C (10%) and potassium tert-butoxide were purchased from commercial sources and used without further purification.

Physical Methods

Nuclear Magnetic Resonance (NMR) Spectroscopy: Nuclear magnetic resonance (NMR) spectra were recorded on a Bruker DRX500 spectrometer fitted with a TCI cryoprobe (¹H and ¹³C), a Bruker AVANCE 600 MHz (¹H, ¹³C, and ³¹P) or a DRX400 with a switchable QNP probe (¹H and ³¹P). ¹H NMR spectra were referenced to (tetramethylsilane) TMS using the residual proton signal of the solvent; ¹³C NMR spectra were referenced to TMS using the natural abundance ¹³C of the solvent; ³¹P NMR spectra were referenced to an internal H₃PO₄ sample in D₂O or to H₃PO₄ using the Ξ scale with the corresponding ¹H spectra. All chemical shifts are reported in the standard δ notation in parts per million.

Mass Spectrometry (MS): High resolution mass spectra (HR-MS) and electrospray ionization mass spectra (ESI-MS) were obtained on a Micromass LCT and collected at the University of California-Irvine Mass Spectrometry Facility.

X-ray Crystallography (XRC): X-ray Crystallography. X-ray diffraction studies were carried out at the UCI Department of Chemistry X-ray Crystallography Facility on a Bruker SMART APEX II diffractometer. Data were collected at 296 K for **1b** and 88 K for **2c** using Mo K α radiation ($\lambda = 0.71073 \text{ \AA}$). A full sphere of data was collected for each crystal structure. The APEX2 program suite was used to determine unit-cell parameters and to collect data. The raw frame data were processed and absorption corrected using the SAINT and SADABS programs, respectively, to yield the reflection data files. Structures were solved by direct methods using SHELXS and refined against F² on all data by full-matrix least-squares with SHELXL-97. All non-hydrogen atoms were refined anisotropically. Hydrogen atoms other than H1 in **1b** were placed at geometrically calculated positions and refined using a riding model, and their isotropic displacement parameters were fixed at 1.2 (1.5 for methyl groups) times the U_{eq} of the atoms to which they are bonded. H1 in **1b** was located in the difference map and refined freely. For the structure of **1b**, checkCIF reports three level B alerts (PLAT230_ALERT_2_B) due to unequal anisotropic displacement parameters (ADPs) along chemical bonds, which can signify an incorrect atom type assignment. However, we are confident in our assignments, as all three alerts involve bonds within a pyridine ring of the TPAP ligand whose identity has been confirmed through other spectroscopic techniques. An additional level B alert (PLAT411_ALERT_2_B) was reported for this structure due to a short nonbonding intermolecular H \cdots H distance between two ligand hydrogen atoms (H21 and H23); this is likely a result of crystal packing. For the structure of **2c**, a finalized structure is yet to be collected. All values are reported using preliminary data.

Tris[[4-(2-pyridyl)benzyl]-amino]ethylamine (4a): 4-(dimethylamino)benzaldehyde (1.00 g, 5.46 mmol) was added to a stirred solution of tris(2-aminoethyl)-amine (266 mg, 1.82 mmol) in 60 mL of dry methanol. A 10% palladium on activated carbon (500 mg) was added and the reaction was brought outside the glovebox and put under one atmosphere of H₂ for 12 h at room temperature. The reaction mixture was filtered off using a Büchner funnel and washed with 15 mL of dry methanol. The filtrate was dried under reduced pressure at 50 °C, producing a waxy solid in 79.1% yield. ¹H NMR (CDCl₃, 500 MHz) δ = 1.75 (b, 3H, NH), 2.62 (t, 6H, CH₂CH₂N), 2.72 (t, 6H, NCH₂CH₂), 3.81 (s, 6H, PhCH₂N), 7.17 (t, 3H, Py), 7.35 (d, 6H, Ph), 7.62 (m, 6H, Py), 7.88 (d, 6H, Ph), 8.65 (d, 3, Py). ¹³C{¹H} NMR (CDCl₃, 126 MHz) δ = 47.39, 53.98, 54.44, 120.6, 122.1, 127.1, 128.6, 136.8, 138.1, 141.6, 149.8, 157.4. ESI-MS (*m/z*): [M+H]⁺ calcd for C₄₂H₄₅N₇: 647.37, Found: 648.59.

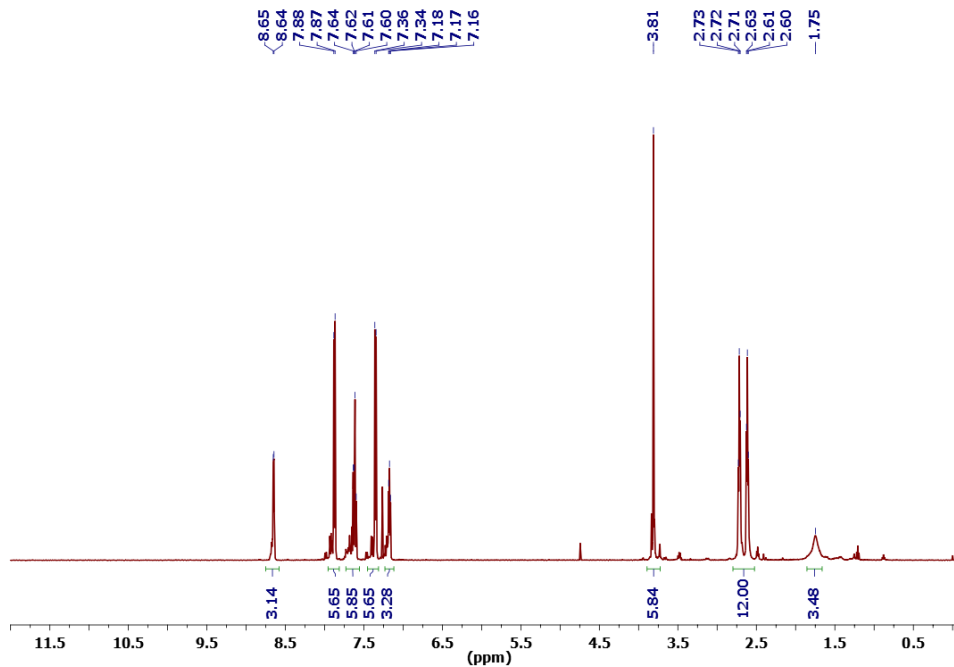


Figure 2.3. ^1H NMR spectrum of tris[[4-(2-pyridyl)benzyl]-amino]ethylamine (**4a**) in CDCl_3 .

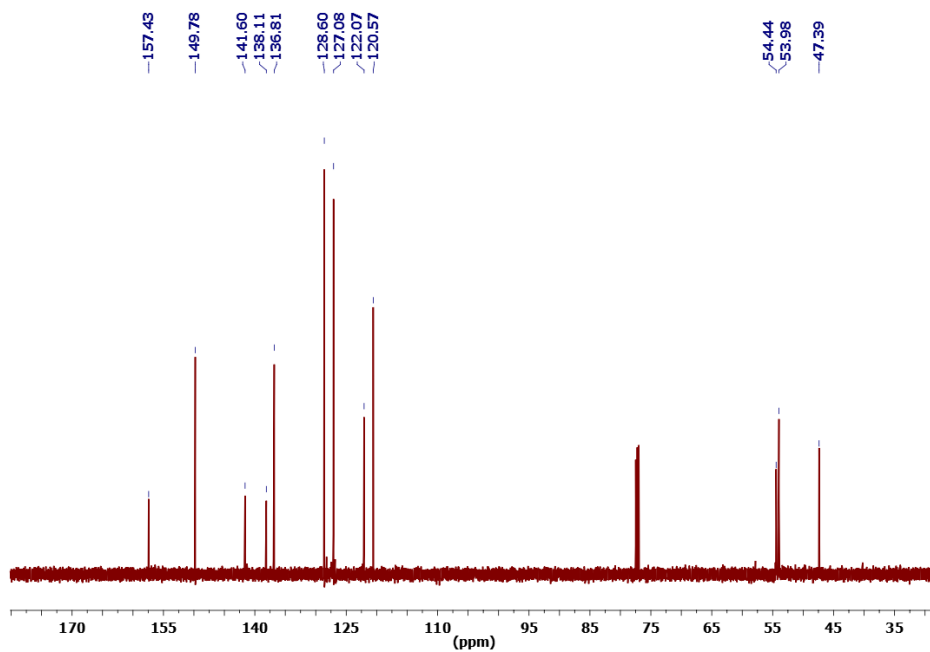


Figure 2.4. $^{13}\text{C}\{^1\text{H}\}$ NMR spectrum of tris[[4-(2-pyridyl)benzyl]-amino]ethylamine (**4a**) in CDCl_3 .

[HP((2-PyrCH₂)-NCH₂CH₂)₃N][Cl] (1b): In the glovebox, a solution of **1a** (200 mg, 0.476 mmol) in 5 mL of tetrahydrofuran was added to a solution of bis(dimethylamino)-chlorophosphine (111 mg, 0.715 mmol) in 10 mL of tetrahydrofuran. The mixture was stirred overnight, at which time a white solid precipitated out of solution. The solution was filtered through a medium fritted funnel, the precipitate was washed with tetrahydrofuran, and the solvent was removed on the high vacuum line to afford a white solid in 61.9% yield. Single crystals suitable for X-ray analysis were grown by layering diethyl ether over a solution of **1b** in acetonitrile. ¹H NMR (CD₃CN, 400 MHz) δ = 3.16 (m, 6H, PNCH₂CH₂N), 3.25 (m, 6H, PNCH₂CH₂N), 4.25 (d, *J* = 19.1 Hz, 6H, PyrCH₂N), 5.84 (d, *J* = 506 Hz, 1H, P-*H*), 7.23 (m, 3H, Pyr), 7.28 (d, *J* = 7.8 Hz, 3H, Pyr), 7.70 (td, *J* = 7.7, 1.9 Hz, 3H, Pyr), 8.51 (d, *J* = 5.5 Hz, 3H, Pyr). ¹³C{¹H} NMR (CD₃CN, 126 MHz) δ = 40.25, 47.91, 53.39, 122.6, 123.4, 137.87, 150.5, 159.2. ³¹P{¹H} NMR (CD₃CN, 162 MHz) δ = -10.00. ³¹P NMR (CD₃CN, 162 MHz) δ = -10.00 (d, ¹*J*_{P-H} = 506 Hz). ESI-MS (*m/z*): [M - Cl]⁺ calcd for C₂₄H₃₁N₇P, 448.27; Found, 448.23.

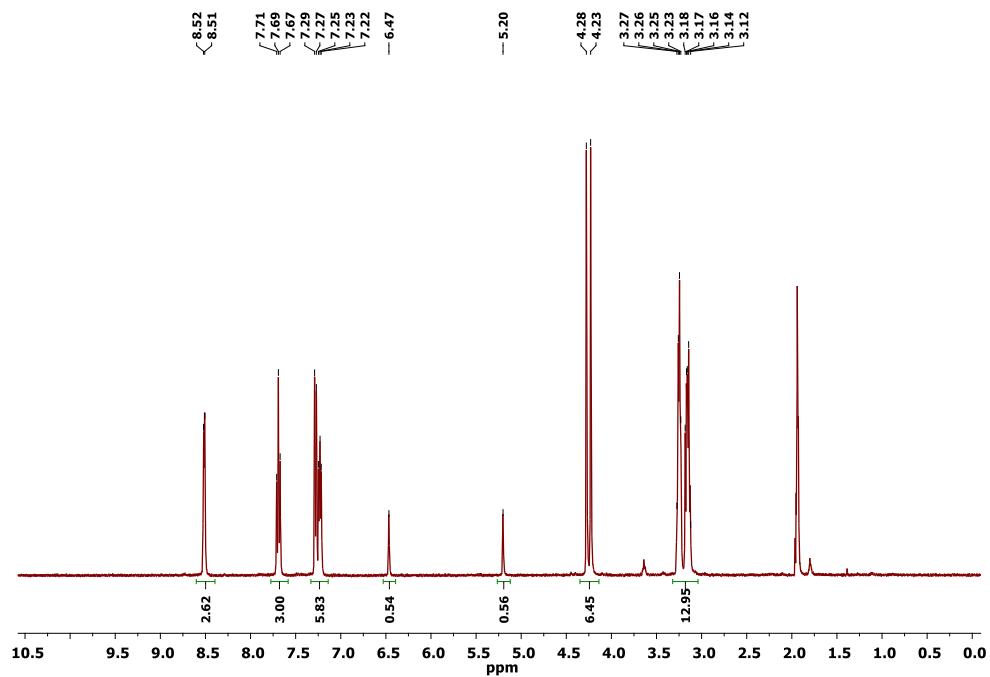


Figure 2.5. ^1H NMR spectrum of $[\text{HP}((2\text{-PyrCH}_2)\text{-NCH}_2\text{CH}_2)_3\text{N}][\text{Cl}]$ (**1b**) in CD_3CN .

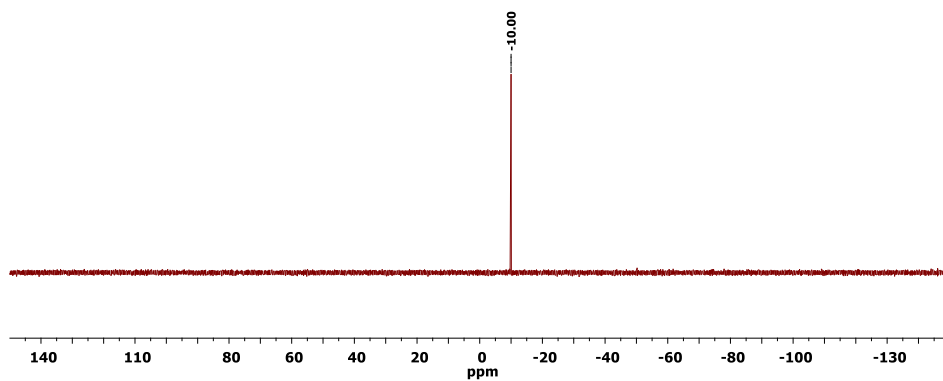


Figure 2.6. $^{31}\text{P}\{^1\text{H}\}$ NMR spectrum of $[\text{HP}((2\text{-PyrCH}_2)\text{-NCH}_2\text{CH}_2)_3\text{N}][\text{Cl}]$ (**1b**) in CD_3CN .

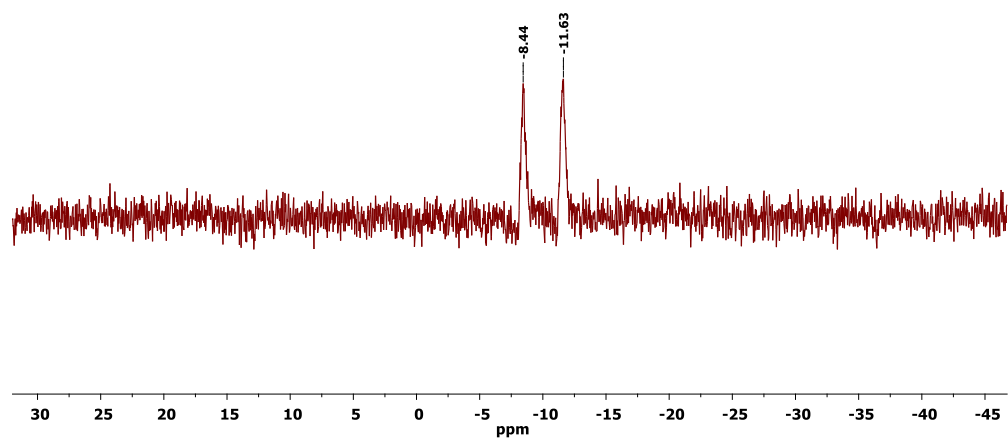


Figure 2.7. ^{31}P NMR spectrum of $[\text{HP}((2\text{-PyrCH}_2)\text{-NCH}_2\text{CH}_2)_3\text{N}][\text{Cl}]$ (**1b**) in CD_3CN .

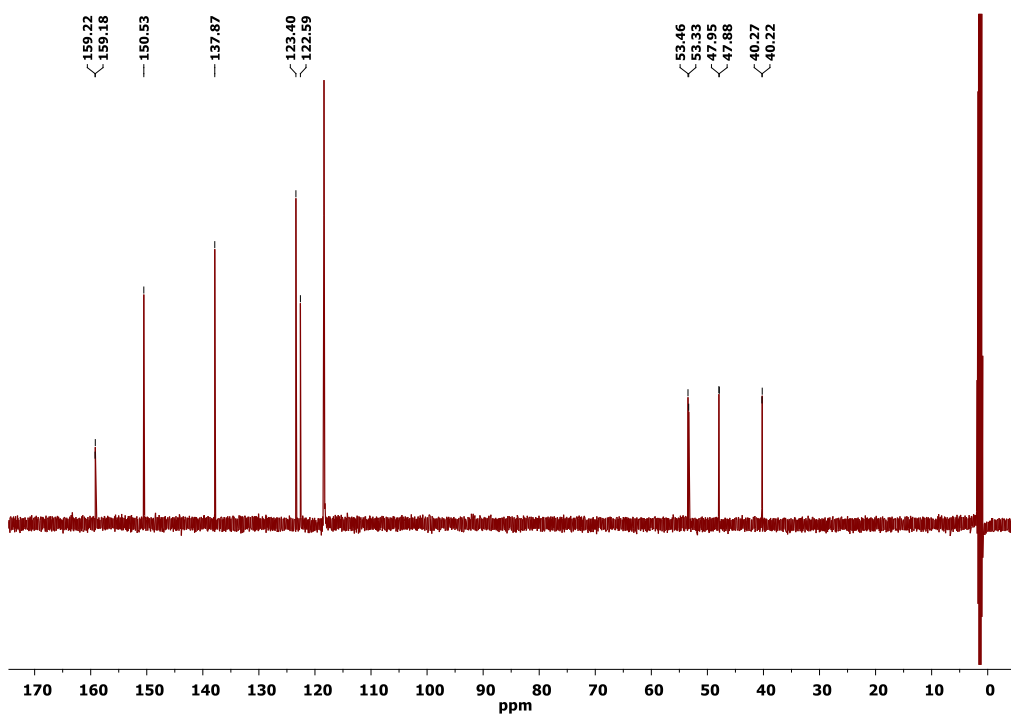


Figure 2.8. $^{13}\text{C}\{^1\text{H}\}$ NMR spectrum of $[\text{HP}((2\text{-PyrCH}_2)\text{-NCH}_2\text{CH}_2)_3\text{N}][\text{Cl}]$ (**1b**) in CD_3CN .

General Synthesis of 1c-5c: In the glove box, ~1.5 equivalents of bis(dimethylamino)chlorophosphine was added to a solution of **1a-5d** in 10 mL of dichloromethane. The mixture was stirred for 1 day. Diethyl ether was added to this solution, producing a white precipitate. The mixture was filtered through a medium fritted funnel to afford a white solid. The white solid was taken to the next step without further purification. In the glove box, ~2 equivalents of potassium *tert*-butoxide were added to a suspension of the white solid in 10 mL of tetrahydrofuran. The mixture was stirred for 1 day, during which time a white solid (KCl) precipitated out of solution. The solution was filtered through a medium fritted funnel. The filtrate was collected and the solvent was removed under reduced pressure. The solid was re-dissolved in acetonitrile and once again filtered through a medium fritted funnel in order to separate out excess potassium *tert*-butoxide and KCl. Acetonitrile was removed under reduced pressure and the solid was re-dissolved in dry tetrahydrofuran and layered with dry pentane. After 1 day of standing, the solution was filtered from crystalline KCl and the solvents from the filtrate were removed under reduced pressure to obtain products (**1c-5c**).

[P((2-PyrCH₂)-NCH₂CH₂)₃N] (1c): Potassium *tert*-butoxide (148 mg, 0.132 mmol) was added in this step of the reaction producing a white solid in 85.4% yield. ¹H NMR (CD₃CN, 400 MHz) δ = 2.76 (m, 6H, PNCH₂CH₂N), 2.84 (m, 6H, PNCH₂CH₂N), 4.29 (d, *J* = 10.8 Hz, 6H, PyrCH₂N), 7.19 (m, 3H, Pyr), 7.47 (m, 3H, Pyr), 7.71 (td, *J* = 7.6, 1.8 Hz, 3H, Pyr), 8.49 (m, 3H, Pyr). ¹³C{¹H} NMR (CD₃CN, 126 MHz) δ = 47.2, 51.7, 55.8, 122.8, 122.9, 137.5, 150.0, 162.5. ³¹P{¹H} NMR (CD₃CN, 162 MHz) δ = 126.6. ³¹P{¹H} NMR (C₆D₆, 243 MHz) δ = 126.6. ESI-MS (*m/z*): [M + H]⁺ calcd for C₂₄H₃₁N₇P, 448.27; Found, 448.27.

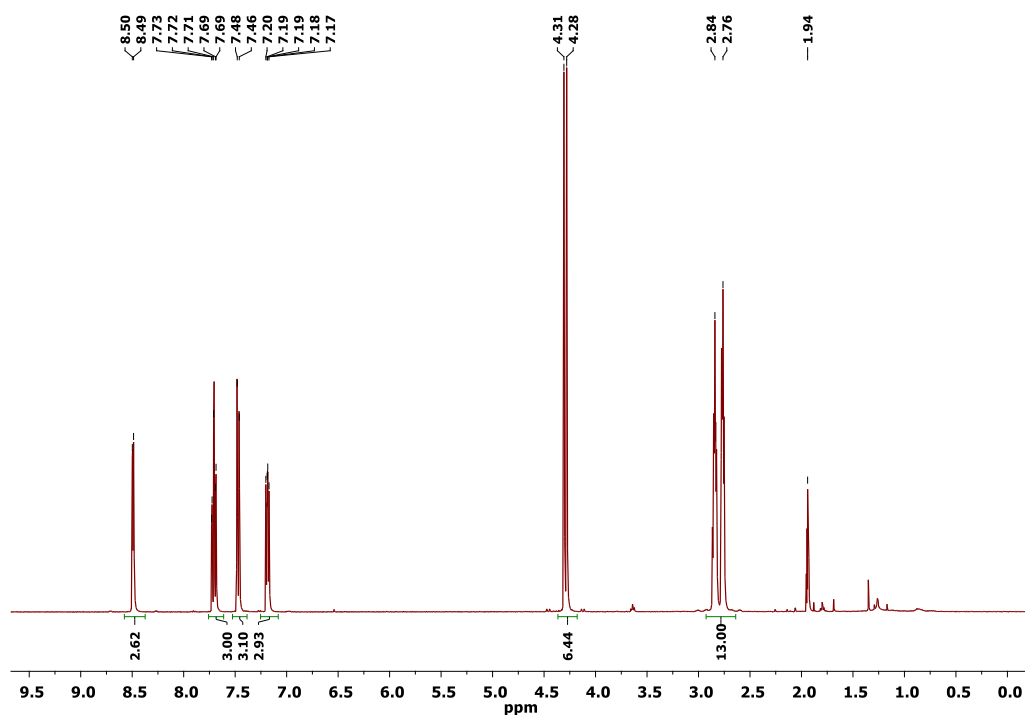


Figure 2.9. ¹H NMR spectrum of [P((2-PyrCH₂)-NCH₂CH₂)₃N] (1c) in CD₃CN.

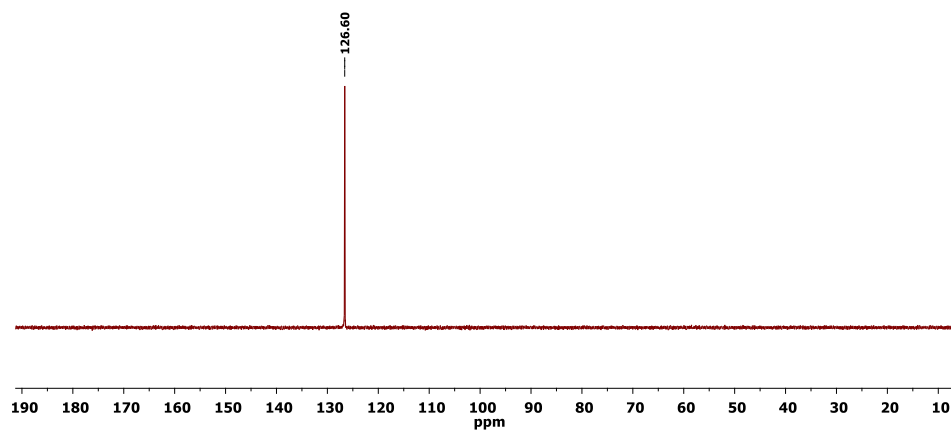


Figure 2.10. ^{31}P NMR spectrum of $[\text{P}((2\text{-PyrCH}_2)\text{-NCH}_2\text{CH}_2)_3\text{N}]$ (**1c**) in CD_3CN .

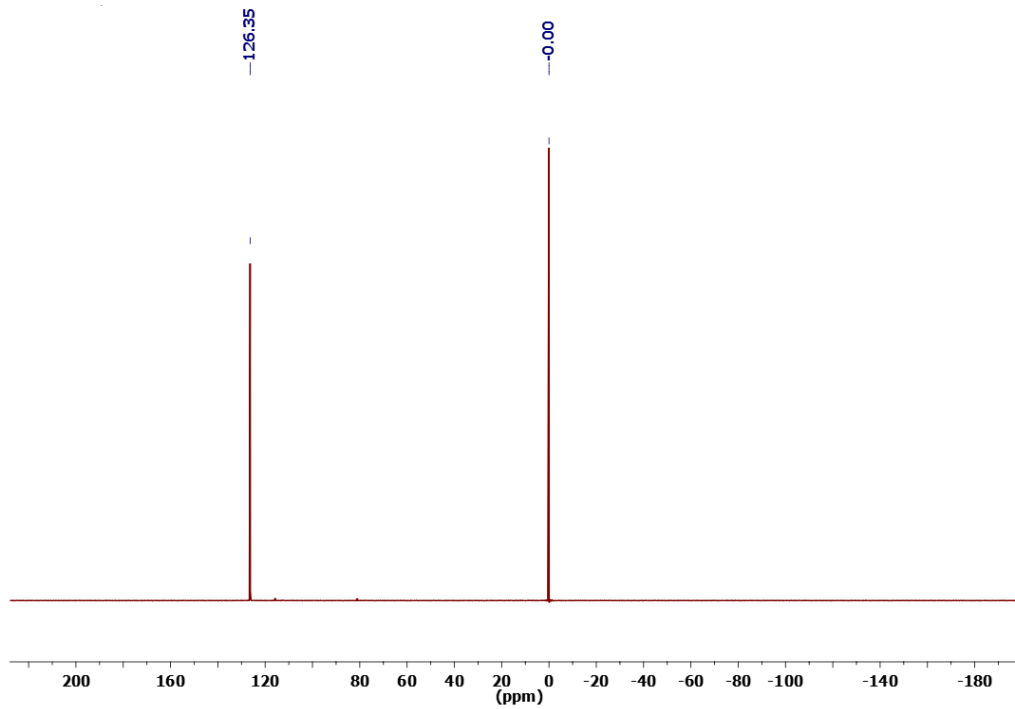


Figure 2.11. $^{31}\text{P}\{^1\text{H}\}$ NMR spectrum of $[\text{P}((2\text{-PyrCH}_2)\text{-NCH}_2\text{CH}_2)_3\text{N}]$ (**1c**) in C_6D_6 .

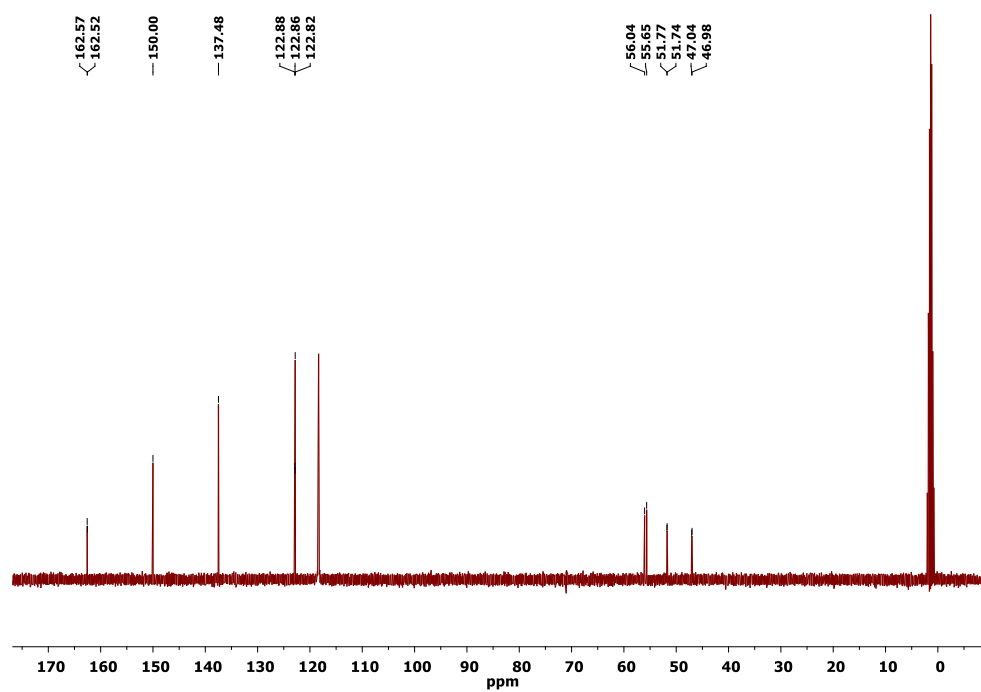


Figure 2.12. $^{13}\text{C}\{^1\text{H}\}$ NMR spectrum of $[\text{P}((2\text{-PyrCH}_2)\text{-NCH}_2\text{CH}_2)_3\text{N}]$ (**1c**) in CD_3CN .

[P((3-PyrCH₂)-NCH₂CH₂)₃N] (2c): Bis(dimethylamino)chlorophosphine (0.690 mg, 0.446 mmol) and **2a** (122 mg, 0.290 mmol) were mixed in the first step. Potassium *tert*-butoxide (0.066 mg, 0.58 mmol) was added in the second step of the reaction producing a white solid in 55.7% yield. Colorless crystals were grown from a concentrated sample of tetrahydrofuran/pentane mixture at -35°C. ¹H NMR (CD₃CN, 500 MHz) δ = 2.75 (s, 12H, CH₂CH₂N), 4.19 (d, 6H, PyrCH₂N), 7.29 (m, 3H, Py), 7.71 (m, 3H, Py), 8.45 (m, 3H, Py), 8.53 (m, 3H, Py). ¹³C{¹H}NMR (CD₃CN, 126 MHz) δ = 46.08, 50.81, 51.37, 124.3, 136.5, 137.5, 149.2, 150.5. ³¹P{¹H}NMR (C₆D₆, 243 MHz) δ = 127.1. HR-ESI-MS (*m/z*): [M+H]⁺ calcd for C₂₄H₃₀N₇P 448.2; found 448.1.

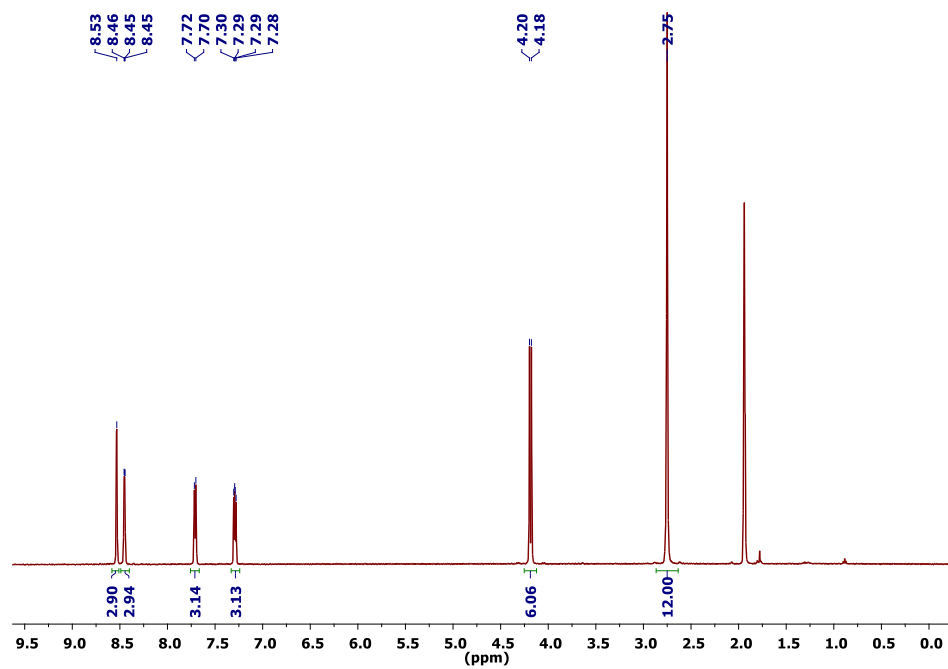


Figure 2.13. ^1H NMR spectrum of $[\text{P}((3\text{-PyrCH}_2)\text{-NCH}_2\text{CH}_2)_3\text{N}]$ (**2c**) in CD_3CN .

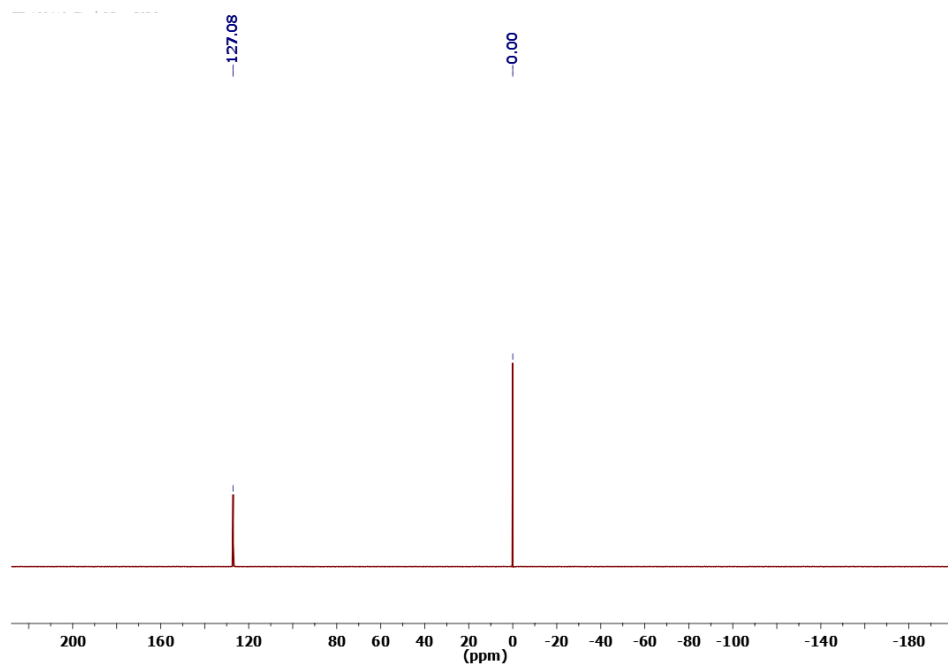


Figure 2.14. $^{31}\text{P}\{^1\text{H}\}$ NMR spectrum of $[\text{P}((3\text{-PyrCH}_2)\text{-NCH}_2\text{CH}_2)_3\text{N}]$ (**2c**) in C_6D_6 .

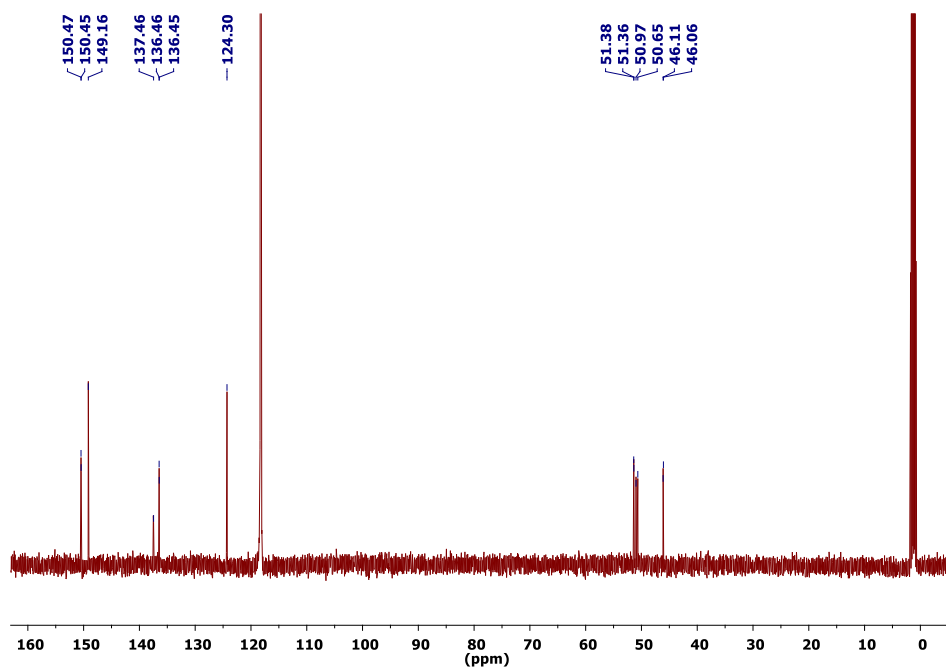


Figure 2.15. $^{13}\text{C}\{^1\text{H}\}$ NMR spectrum of $[\text{P}((3\text{-PyrCH}_2)\text{-NCH}_2\text{CH}_2)_3\text{N}]$ (**2c**) in CD_3CN .

[P((Furan-CH₂)-NCH₂CH₂)₃N] (3c): Bis(dimethylamino)chlorophosphine (0.51 mg, 0.33 mmol) and **3a** (137 mg, 0.211 mmol) were mixed in the first step. Potassium *tert*-butoxide (0.048 mg, 0.43 mmol) was added in the second step of the reaction producing a white solid in 59.1% yield. ¹H NMR (CD₃CN, 600 MHz) δ = 2.82 (m, 12H, CH₂CH₂N), 4.28 (d, 6H, PhCH₂N), 7.27 (m, 3H, Py), 7.48 (d, 6H, Py), 7.80 (m, 6H, Ph), 8.01 (m, 6H, Ph), 8.63 (m, 3H, Py). ¹³C{¹H}NMR (CD₃CN, 151 MHz) δ = 46.48, 51.56, 53.24, 121.1, 123.2, 127.6, 129.4, 137.9, 138.8, 143.6, 150.6, 157.7. ³¹P{¹H}NMR (C₆D₆, 243 MHz) δ = 127.3. HR-ESI-MS (*m/z*): [M+H]⁺ calcd for C₄₂H₄₂N₇P 676.3; found 676.6.

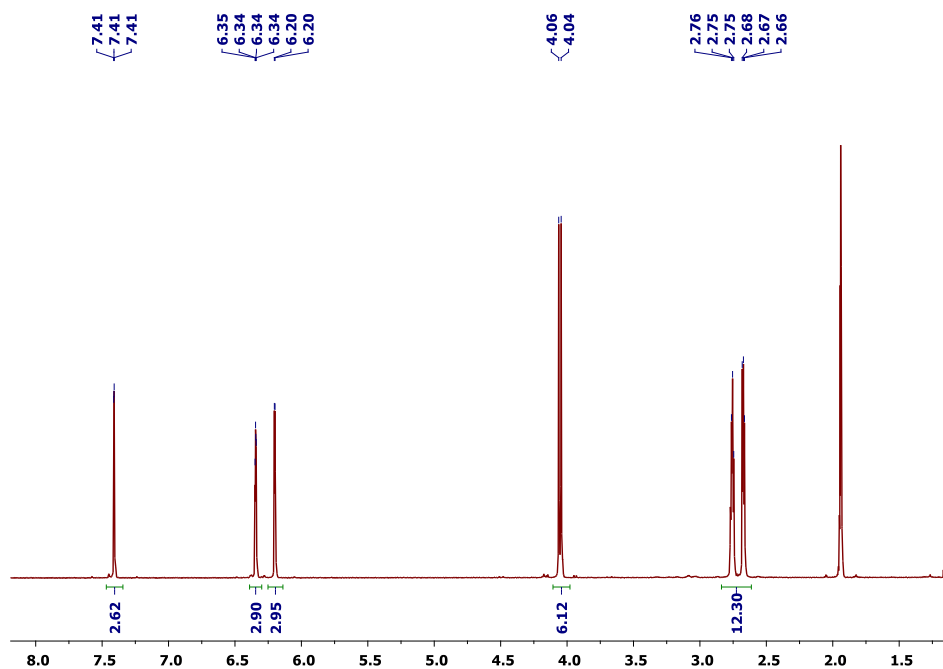


Figure 2.16. ¹H NMR spectrum of [P((Furan-CH₂)-NCH₂CH₂)₃N] (**3c**) in CD₃CN.

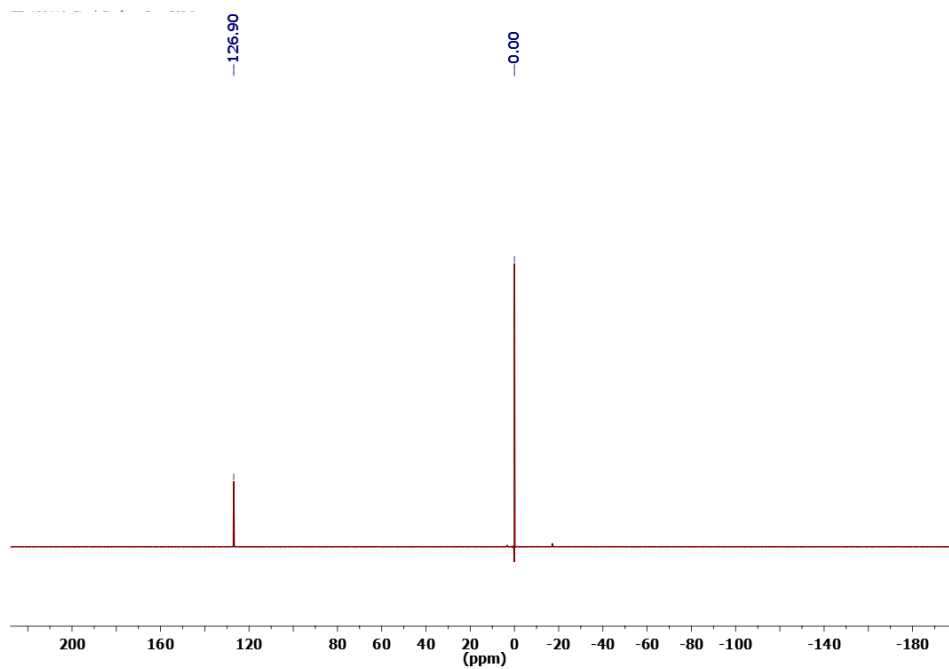


Figure 2.17. $^{31}\text{P}\{^1\text{H}\}$ NMR spectrum of $[\text{P}((\text{Furan-CH}_2)\text{-NCH}_2\text{CH}_2)_3\text{N}]$ (**3c**) in C_6D_6 .

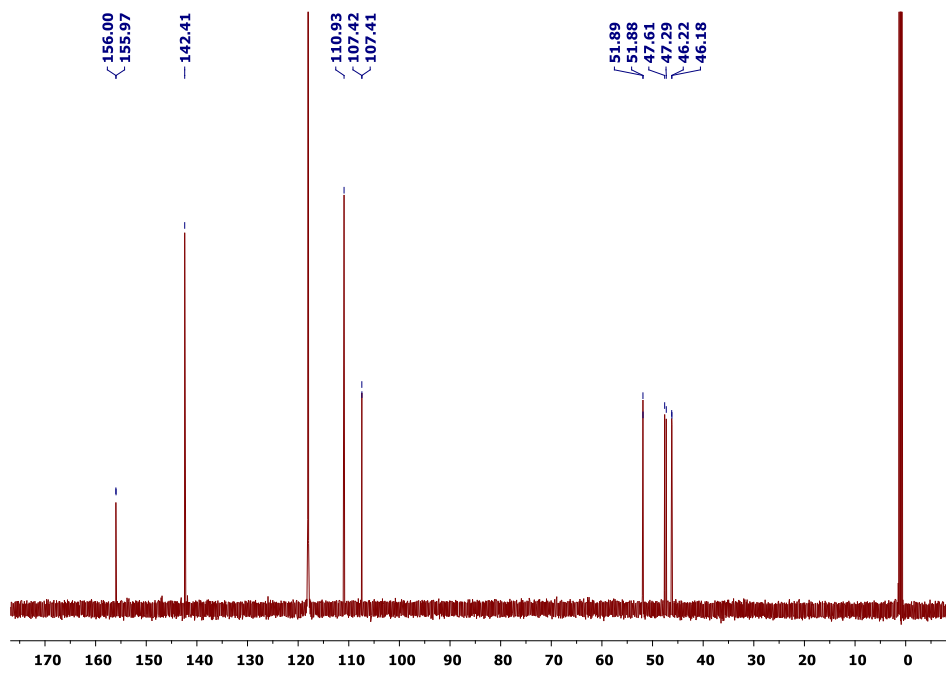


Figure 2.18. $^{13}\text{C}\{^1\text{H}\}$ NMR spectrum of $[\text{P}((\text{Furan-CH}_2)\text{-NCH}_2\text{CH}_2)_3\text{N}]$ (**3c**) in CD_3CN .

[P((2-Pyr-Ph-CH₂)-NCH₂CH₂)₃N] (4c): Bis(dimethylamino)chlorophosphine (138 mg, 0.893 mmol) and **4a** (230 mg, 0.595 mmol) were mixed in the first step. Potassium *tert*-butoxide (148 mg, 1.32 mmol) was added in the second step of the reaction producing a yellow oil in 76.9% yield. ¹H NMR (CD₃CN, 600 MHz) δ = 2.71 (m, 12H, NCH₂CH₂), 4.05 (d, 6H, CH₂N), 6.20 (m, 3H, C₄H₂O), 6.34 (m, 3H, C₄H₂O), 7.41 (m, 3H, C₄H₂O). ¹³C{¹H}NMR (CD₃CN, 151 MHz) δ = 46.20, 47.45, 51.88, 107.4, 110.9, 142.4, 155.9. ³¹P{¹H}NMR (C₆D₆, 243 MHz) δ = 126.9. HR-ESI-MS (*m/z*): [M+H]⁺ calcd for C₂₁H₂₇N₄PO₃ 415.2; found 415.0.

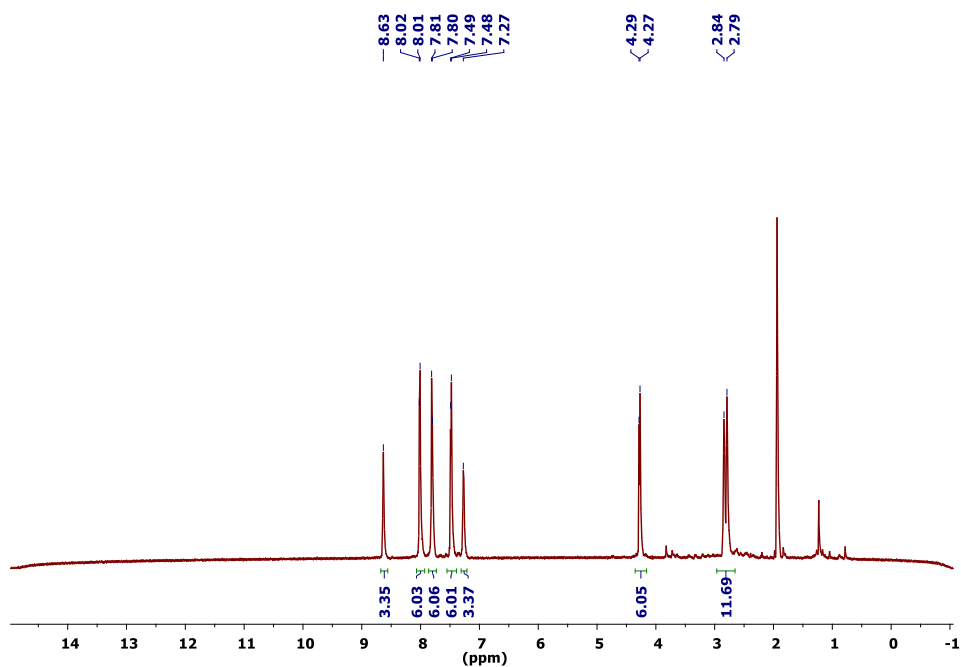


Figure 2.19. ¹H NMR spectrum of [P((2-Pyr-Ph-CH₂)-NCH₂CH₂)₃N] (**4c**) in CD₃CN.

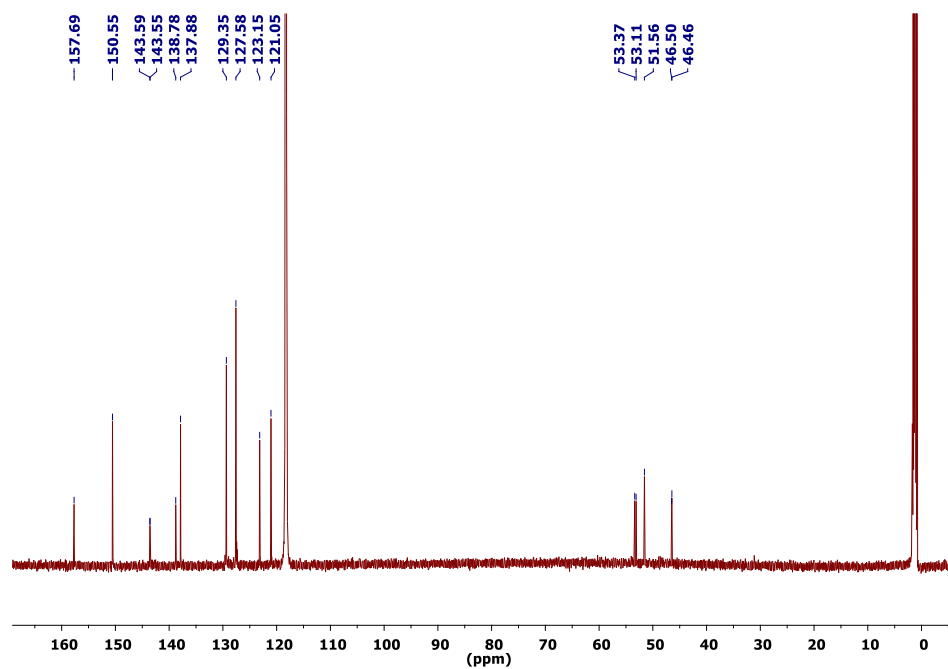


Figure 2.20. $^{13}\text{C}\{^1\text{H}\}$ NMR spectrum of $[\text{P}((2\text{-Pyr-Ph-CH}_2)\text{-NCH}_2\text{CH}_2)_3\text{N}]$ (**4c**) in CD_3CN .

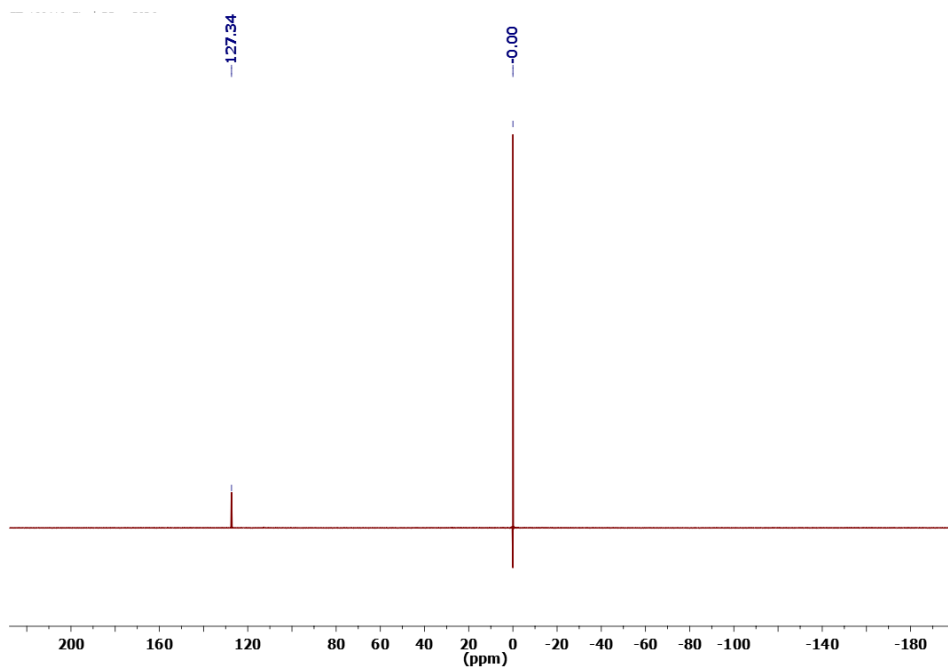


Figure 2.21. $^{31}\text{P}\{^1\text{H}\}$ NMR spectrum of $[\text{P}((2\text{-Pyr-Ph-CH}_2)\text{-NCH}_2\text{CH}_2)_3\text{N}]$ (**4c**) in C_6D_6 .

[P((2-CH₃-Thiophene-CH₂)-NCH₂CH₂)₃N] (5c): Bis(dimethylamino)chlorophosphine (124 mg, 0.801 mmol) and **5a** (253 mg, 0.531 mmol) were mixed in the first step. Potassium *tert*-butoxide (131 mg, 1.17 mmol) was added in the second step of the reaction producing a white oily solid in 59.1% yield. ¹H NMR (CD₃CN, 600 MHz) δ = 2.18 (s, 9H, CH₃), 2.80 (m, 12H, NCH₂CH₂), 4.23 (m, 6H, CH₂N), 6.80 (m, 3H, C₄H₂S), 7.13 (m, 3H, C₄H₂S). ¹³C {¹H}NMR (CD₃CN, 151 MHz) δ = 13.83, 45.99, 46.53, 51.69, 123.5, 131.0, 134.3, 140.2. ³¹P {¹H}NMR (C₆D₆, 243 MHz) δ = 125.7. HR-ESI-MS (*m/z*): [M+H]⁺ calcd for C₂₄H₃₃N₄PS₃ 505.2; found 505.0.

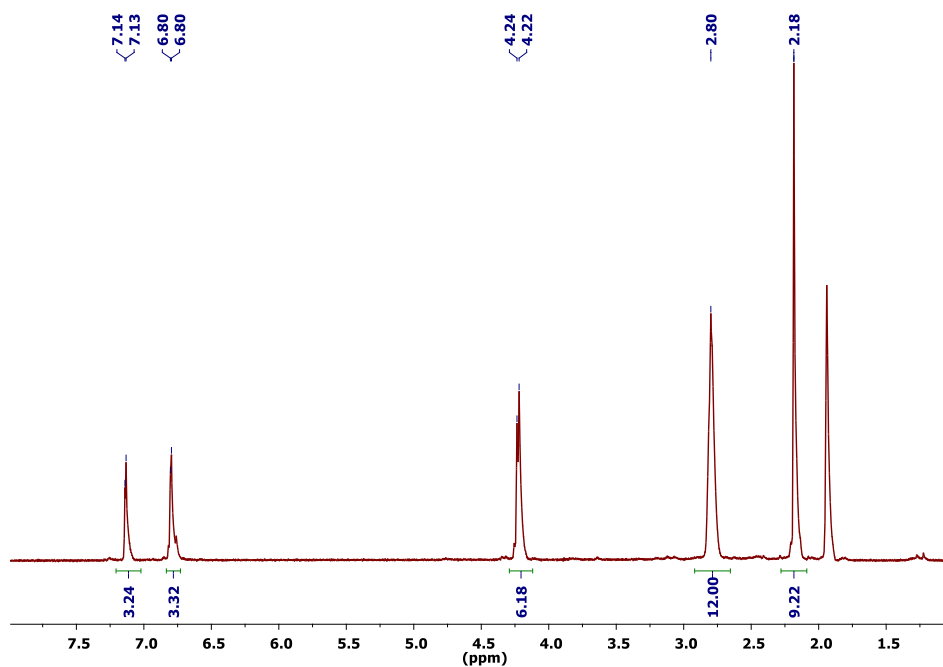


Figure 2.22. ¹H NMR spectrum of [P((2-CH₃-Thiophene-CH₂)-NCH₂CH₂)₃N] (**5c**) in CD₃CN.

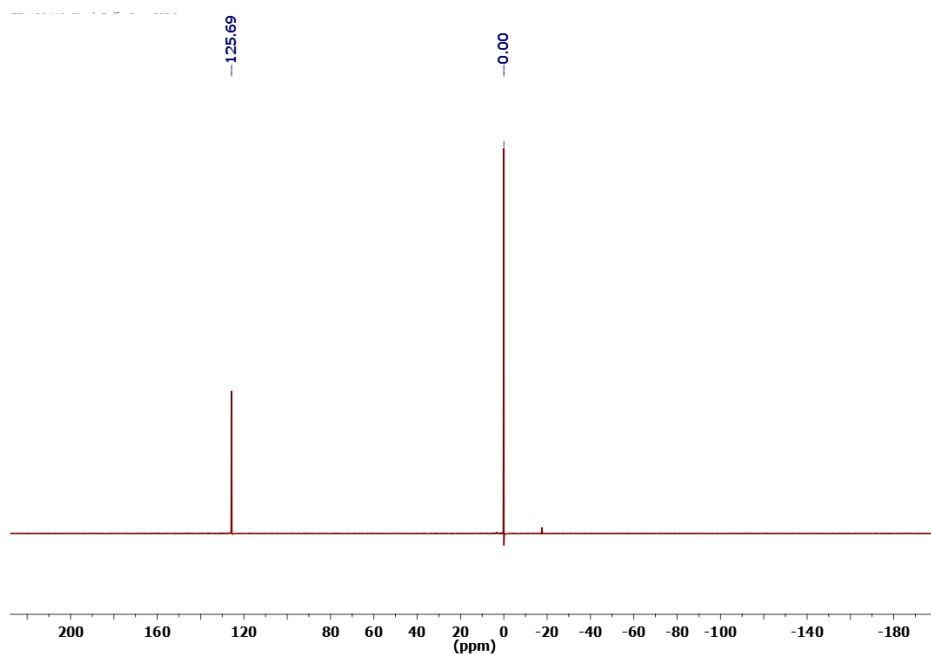


Figure 2.23. $^{31}\text{P}\{^1\text{H}\}$ NMR spectrum of $[\text{P}((2\text{-CH}_3\text{-Thiophene-CH}_2)\text{-NCH}_2\text{CH}_2)_3\text{N}]$ (**5c**) in C_6D_6 .

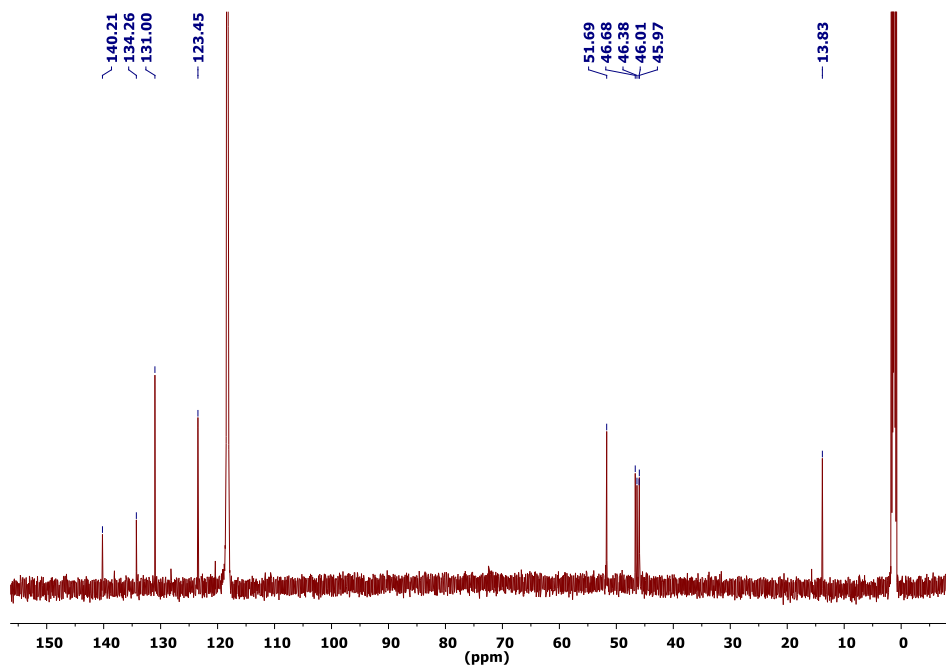


Figure 2.24. $^{13}\text{C}\{^1\text{H}\}$ NMR spectrum of $[\text{P}((2\text{-CH}_3\text{-Thiophene-CH}_2)\text{-NCH}_2\text{CH}_2)_3\text{N}]$ (**5c**) in CD_3CN .

2.6. References

1. Schmidt, H.; Lensink, C.; Xi, S. K.; Verkade, J. G., New Prophosphatranes: Novel intermediates to five-coordinate phosphatranes. *Zeitschrift für anorganische und allgemeine Chemie* **1989**, 578 (1), 75-80.
2. Lensink, C.; Xi, S. K.; Daniels, L. M.; Verkade, J. G., The unusually robust phosphorus-hydrogen bond in the novel cation [cyclic] $\text{HP}(\text{NMeCH}_2\text{CH}_2)_3\text{N}^+$. *Journal of the American Chemical Society* **1989**, 111 (9), 3478-3479.
3. Pinkas, J.; Tang, J.; Wan, Y.; Verkade, J. G., Chemical Games with Molecular Footballs, Darts and Paddlewheels. *Phosphorus, Sulfur, and Silicon and the Related Elements* **1994**, 87 (1-4), 193-207.
4. Kisanga, P. B.; Verkade, J. G.; Schwesinger, R., pK_a Measurements of $\text{P}(\text{RNCH}_2\text{CH}_2)_3\text{N}$. *The Journal of Organic Chemistry* **2000**, 65 (17), 5431-5432.
5. Verkade, J. G., Atranans: new examples with unexpected properties. *Accounts of Chemical Research* **1993**, 26 (9), 483-489.
6. Laramay, M. A. H.; Verkade, J. G., The "anomalous" basicity of $\text{P}(\text{NHCH}_2\text{CH}_2)_3\text{N}$ relative to $\text{P}(\text{NMeCH}_2\text{CH}_2)_3\text{N}$ and $\text{p}(\text{NBzCH}_2\text{CH}_2)_3\text{N}$: a chemical consequence of orbital charge balance? *Journal of the American Chemical Society* **1990**, 112 (25), 9421-9422.
7. Xi, S. K.; Schmidt, H.; Lensink, C.; Kim, S.; Wintergrass, D.; Daniels, L. M.; Jacobson, R. A.; Verkade, J. G., Bridgehead-bridgehead communication in untransannulated phosphatrane $\text{ZP}(\text{ECH}_2\text{CH}_2)_3\text{N}$ systems. *Inorganic Chemistry* **1990**, 29 (12), 2214-2220.
8. Laramay, M. A. H.; Verkade, J. G., Unusually Lewis basic Pro-azaphosphatranes. *Zeitschrift für anorganische und allgemeine Chemie* **1991**, 605 (1), 163-174.
9. Tang, J. S.; Verkade, J. G., Synthesis and reactivity patterns of new proazaphosphatranes and quasi-azaphosphatranes $\text{ZP}(\text{MeNCH}_2\text{CH}_2)_3\text{N}$. *Journal of the American Chemical Society* **1993**, 115 (5), 1660-1664.
10. Kárpáti, T.; Veszprémi, T.; Thirupathi, N.; Liu, X.; Wang, Z.; Ellern, A.; Nyulászi, L.; Verkade, J. G., Synthesis and Photoelectron Spectroscopic Studies of $\text{N}(\text{CH}_2\text{CH}_2\text{NMe})_3\text{PE}$ (E = O, S, NH, CH₂). *Journal of the American Chemical Society* **2006**, 128 (5), 1500-1512.
11. Kisanga, P.; McLeod, D.; Liu, X.; Yu, Z.; Ilankumaran, P.; Wang, Z.; McLaughlin, P. A.; Verkade, J. G., New Chemistry of $\text{ZP}(\text{RNCH}_2\text{CH}_2)_3\text{N}$ Systems. *Phosphorus, Sulfur, and Silicon and the Related Elements* **1999**, 144 (1), 101-104.
12. Verkade, J. G., $\text{P}(\text{RNCH}_2\text{CH}_2)_3\text{N}$: Very Strong Non-Ionic Bases Useful in Organic Synthesis. In *New Aspects in Phosphorus Chemistry II*, Majoral, J.-P., Ed. Springer Berlin Heidelberg: Berlin, Heidelberg, 2003; pp 1-44.
13. Tang, J.; Verkade, J. G., Nonionic Superbase-Promoted Synthesis of Oxazoles and Pyrroles: Facile Synthesis of Porphyrins and alpha-C-Acyl Amino Acid Esters. *The Journal of Organic Chemistry* **1994**, 59 (25), 7793-7802.
14. Arumugam, S.; Verkade, J. G., $\text{P}(\text{CH}_3\text{NCH}_2\text{CH}_2)_3\text{N}$: A Nonionic Superbase for Efficient Dehydrohalogenation. *The Journal of Organic Chemistry* **1997**, 62 (14), 4827-4828.

15. Yang, J.; Chatelet, B.; Dufaud, V.; Hérault, D.; Michaud-Chevallier, S.; Robert, V.; Dutasta, J.-P.; Martinez, A., Endohedral Functionalized Cage as a Tool to Create Frustrated Lewis Pairs. *Angewandte Chemie International Edition* **2018**, *57* (43), 14212-14215.
16. Raytchev, P. D.; Martinez, A.; Gornitzka, H.; Dutasta, J.-P., Encaging the Verkade's Superbases: Thermodynamic and Kinetic Consequences. *Journal of the American Chemical Society* **2011**, *133* (7), 2157-2159.
17. Chatelet, B.; Dufaud, V.; Dutasta, J.-P.; Martinez, A., Catalytic Activity of an Encaged Verkade's Superbase in a Base-Catalyzed Diels-Alder Reaction. *The Journal of Organic Chemistry* **2014**, *79* (18), 8684-8688.
18. Chatelet, B.; Gornitzka, H.; Dufaud, V.; Jeanneau, E.; Dutasta, J.-P.; Martinez, A., Superbases in Confined Space: Control of the Basicity and Reactivity of the Proton Transfer. *Journal of the American Chemical Society* **2013**, *135* (49), 18659-18664.
19. Yu, Z.; Verkade, J. G., P(MeNCH₂CH₂)₃N: An efficient desulfurizing reagent. *Heteroatom Chemistry* **1999**, *10* (7), 544-547.
20. Johnstone, T. C.; Wee, G. N. J. H.; Stephan, D. W., Accessing Frustrated Lewis Pair Chemistry from a Spectroscopically Stable and Classical Lewis Acid-Base Adduct. *Angewandte Chemie International Edition* **2018**, *57* (20), 5881-5884.
21. Johnstone, T. C.; Briceno-Strocchia, A. I.; Stephan, D. W., Frustrated Lewis Pair Oxidation Permits Synthesis of a Fluoroazaphosphatrane, [FP(MeNCH₂CH₂)₃N]⁺. *Inorganic Chemistry* **2018**, *57* (24), 15299-15304.
22. Thammavongsy, Z.; Cunningham, D. W.; Sutthirat, N.; Eisenhart, R. J.; Ziller, J. W.; Yang, J. Y., Adaptable ligand donor strength: tracking transannular bond interactions in tris(2-pyridylmethyl)-azaphosphatrane (TPAP). *Dalton Transactions* **2018**, *47* (39), 14101-14110.
23. Chatelet, B.; Nava, P.; Clavier, H.; Martinez, A., Synthesis of Gold(I) Complexes Bearing Verkade's Superbases. *European Journal of Inorganic Chemistry* **2017**, *2017* (37), 4311-4316.
24. Mummadi, S.; Kenefake, D.; Diaz, R.; Unruh, D. K.; Krempner, C., Interactions of Verkade's Superbase with Strong Lewis Acids: From Labile Mono- and Binuclear Lewis Acid-Base Complexes to Phosphenium Cations. *Inorganic Chemistry* **2017**, *56* (17), 10748-10759.
25. Matthews, A. D.; Gravalis, G. M.; Schley, N. D.; Johnson, M. W., Synthesis, Structure, and Reactivity of Palladium Proazaphosphatrane Complexes Invoked in C–N Cross-Coupling. *Organometallics* **2018**, *37* (18), 3073-3078.
26. You, J.; Verkade, J. G., P(i-BuNCH₂CH₂)₃N: An Efficient Ligand for the Direct α -Arylation of Nitriles with Aryl Bromides. *The Journal of Organic Chemistry* **2003**, *68* (21), 8003-8007.
27. Urgaonkar, S.; Nagarajan, M.; Verkade, J. G., P[N(i-Bu)CH₂CH₂]₃N: A Versatile Ligand for the Pd-Catalyzed Amination of Aryl Chlorides. *Organic Letters* **2003**, *5* (6), 815-818.
28. You, J.; Verkade, J. G., A General Method for the Direct α -Arylation of Nitriles with Aryl Chlorides. *Angewandte Chemie International Edition* **2003**, *42* (41), 5051-5053.
29. Urgaonkar, S.; Verkade, J. G., Synthesis of N-aryl-aza-crown ethers via Pd-catalyzed amination reactions of aryl chlorides with aza-crown ethers. *Tetrahedron* **2004**, *60* (51), 11837-11842.

30. Urgaonkar, S.; Verkade, J. G., Scope and Limitations of Pd₂(dba)₃/P(i-BuNCH₂CH₂)₃N-Catalyzed Buchwald-Hartwig Amination Reactions of Aryl Chlorides. *The Journal of Organic Chemistry* **2004**, *69* (26), 9135-9142.
31. Su, W.; Urgaonkar, S.; Verkade, J. G., Pd₂(dba)₃/P(i-BuNCH₂CH₂)₃N-Catalyzed Stille Cross-Coupling of Aryl Chlorides. *Organic Letters* **2004**, *6* (9), 1421-1424.
32. Urgaonkar, S.; Verkade, J. G., Palladium/Proazaphosphatane-Catalyzed Amination of Aryl Halides Possessing a Phenol, Alcohol, Acetanilide, Amide or an Enolizable Ketone Functional Group: Efficacy of Lithium Bis(trimethylsilyl)amide as the Base. *Advanced Synthesis & Catalysis* **2004**, *346* (6), 611-616.
33. Urgaonkar, S.; Nagarajan, M.; Verkade, J. G., P(i-BuNCH₂CH₂)₃N: An Effective Ligand in the Palladium-Catalyzed Amination of Aryl Bromides and Iodides. *The Journal of Organic Chemistry* **2003**, *68* (2), 452-459.
34. Su, W.; Urgaonkar, S.; McLaughlin, P. A.; Verkade, J. G., Highly Active Palladium Catalysts Supported by Bulky Proazaphosphatane Ligands for Stille Cross-Coupling: Coupling of Aryl and Vinyl Chlorides, Room Temperature Coupling of Aryl Bromides, Coupling of Aryl Triflates, and Synthesis of Sterically Hindered Biaryls. *Journal of the American Chemical Society* **2004**, *126* (50), 16433-16439.
35. Aneetha, H.; Wu, W.; Verkade, J. G., Stereo- and Regioselective Pt(DVDS)/P(iBuNCH₂CH₂)₃N-Catalyzed Hydrosilylation of Terminal Alkynes. *Organometallics* **2005**, *24* (11), 2590-2596.
36. Nandakumar, M. V.; Verkade, J. G., Pd₂dba₃/P(i-BuNCH₂CH₂)₃N: a highly efficient catalyst for the one-pot synthesis of trans-4-*N,N*-diarylamino stilbenes and *N,N*-diarylamino styrenes. *Tetrahedron* **2005**, *61* (41), 9775-9782.
37. Venkat Reddy, C. R.; Urgaonkar, S.; Verkade, J. G., A Highly Effective Catalyst System for the Pd-Catalyzed Amination of Vinyl Bromides and Chlorides. *Organic Letters* **2005**, *7* (20), 4427-4430.
38. Han Kim, S.; Jang, W.; Kim, M.; Verkade, J. G.; Kim, Y., Synergistic Effect of a Bis(proazaphosphatane) in Mild Palladium-Catalyzed Direct α -Arylations of Nitriles with Aryl Chlorides. *European Journal of Organic Chemistry* **2014**, *2014* (27), 6025-6029.
39. Kim, S. H.; Kim, M.; Verkade, J. G.; Kim, Y., A Tuned Bicyclic Proazaphosphatane for Catalytically Enhanced N-Arylation Reactions with Aryl Chlorides. *European Journal of Organic Chemistry* **2015**, *2015* (9), 1954-1960.
40. Tang, J.-s.; Verkade, J. G., An improved synthesis of the strong base P(MeNCH₂CH₂)₃N. *Tetrahedron Letters* **1993**, *34* (18), 2903-2904.
41. D'sa, B. A.; Verkade, J. G., Synthesis of a Novel Exceedingly Strong Nonionic Superbase. *Phosphorus, Sulfur, and Silicon and the Related Elements* **1997**, *123* (1), 301-312.
42. Wróblewski, A. E.; Pinkas, J.; Verkade, J. G., Strongly Basic Proazaphosphatanes: P(EtNCH₂CH₂)₃N and P(iso-PrNCH₂CH₂)₃N. *Main Group Chemistry* **1995**, *1* (1), 69-79.
43. Kisanga, P. B.; Verkade, J. G., Synthesis of new proazaphosphatanes and their application in organic synthesis. *Tetrahedron* **2001**, *57* (3), 467-475.
44. Zhou, Y.; Armstrong, D. W.; Zhang, Y.; Verkade, J. G., First synthesis of P-chirogenic phosphatanes. *Tetrahedron Letters* **2011**, *52* (14), 1545-1548.

45. You, J.; Wróblewski, A. E.; Verkade, J. G., P[(S,S,S)-CH₃NCH(CH₂Ph)CH₂]₃N: a new C₃-symmetric enantiomerically pure proazaphosphatrane. *Tetrahedron* **2004**, *60* (36), 7877-7883.
46. Zhang, D.; Ronson, T. K.; Mosquera, J.; Martinez, A.; Guy, L.; Nitschke, J. R., Anion Binding in Water Drives Structural Adaptation in an Azaphosphatrane-Functionalized Fe^{II}₄L₄ Tetrahedron. *Journal of the American Chemical Society* **2017**, *139* (19), 6574-6577.
47. Yang, J.; Chatelet, B.; Ziarelli, F.; Dufaud, V.; Hérault, D.; Martinez, A., Verkade's Superbase as an Organocatalyst for the Strecker Reaction. *European Journal of Organic Chemistry* **2018**, *2018* (45), 6328-6332.
48. Raytchev, P. D.; Roussi, L.; Dutasta, J.-P.; Martinez, A.; Dufaud, V., Homogeneous and silica-supported azidoproazaphosphatranes as efficient catalysts for the synthesis of substituted coumarins. *Catalysis Communications* **2012**, *28*, 1-4.
49. Raytchev, P. D.; Bendjeriou, A.; Dutasta, J.-P.; Martinez, A.; Dufaud, V., A New Step Towards Solid Base Catalysis: Azidoproazaphosphatranes Immobilized in Nanopores of Mesoporous Silica. *Advanced Synthesis & Catalysis* **2011**, *353* (11-12), 2067-2077.
50. Portnoy, M.; Milstein, D., Chelate effect on the structure and reactivity of electron-rich palladium complexes and its relevance to catalysis. *Organometallics* **1993**, *12* (5), 1655-1664.
51. Cook, S. A.; Hill, E. A.; Borovik, A. S., Lessons from Nature: A Bio-Inspired Approach to Molecular Design. *Biochemistry* **2015**, *54* (27), 4167-4180.
52. DuBois, M. R.; DuBois, D. L., The role of pendant bases in molecular catalysts for H₂ oxidation and production. *Comptes Rendus Chimie* **2008**, *11* (8), 805-817.
53. Thammavongsy, Z.; Kha, I. M.; Ziller, J. W.; Yang, J. Y., Electronic and steric Tolman parameters for proazaphosphatranes, the superbase core of the tri(pyridylmethyl)azaphosphatrane (TPAP) ligand. **2016**.
54. Nisar Ahamed, B.; Ravikumar, I.; Ghosh, P., A new chemosensor that signals Hg(II), Cu(II) and Zn(II) at different emission wavelengths: selectivity toward Hg(II) in acetonitrile. *New Journal of Chemistry* **2009**, *33* (9), 1825-1828.
55. Matyuska, F.; Szorcsik, A.; May, N. V.; Dancs, Á.; Kováts, É.; Bényei, A.; Gajda, T., Tailoring the local environment around metal ions: a solution chemical and structural study of some multidentate tripodal ligands. *Dalton Transactions* **2017**, *46* (26), 8626-8642.
56. Deroche, A.; Morgenstern-Badarau, I.; Cesario, M.; Guilhem, J.; Keita, B.; Nadjó, L.; Houée-Levin, C., A Seven-Coordinate Manganese(II) Complex Formed with a Single Tripodal Heptadentate Ligand as a New Superoxide Scavenger. *Journal of the American Chemical Society* **1996**, *118* (19), 4567-4573.
57. Köhl, O., The Range of Chemical Shifts, Coupling Constants, and What Influences Each. In *Phosphorus-31 NMR Spectroscopy: A Concise Introduction for the Synthetic Organic and Organometallic Chemist*, Köhl, O., Ed. Springer Berlin Heidelberg: Berlin, Heidelberg, 2008; pp 7-23.
58. Liu, X.; Ilankumaran, P.; Guzei, I. A.; Verkade, J. G., P[(S,S,S)-PhHMeCNCH₂CH₂]₃N: A New Chiral ³¹P and ¹H NMR Spectroscopic Reagent for the Direct Determination of ee Values of Chiral Azides. *The Journal of Organic Chemistry* **2000**, *65* (3), 701-706.

59. Liu, X.; Bai, Y.; Verkade, J. G., Synthesis and structural features of new sterically hindered azaphosphatrane systems: $ZP(RNCH_2CH_2)_3N$. *Journal of Organometallic Chemistry* **1999**, 582 (1), 16-24.
60. Raders, S. M.; Verkade, J. G., An Electron-Rich Proazaphosphatrane for Isocyanate Trimerization to Isocyanurates. *The Journal of Organic Chemistry* **2010**, 75 (15), 5308-5311.

CHAPTER 3

Tracking the Transannular Bond Interaction in Tris(2-pyridylmethyl)-azaphosphatrane (TPAP) with Various Transition Metal ions

Portions of this chapter have been published:

Thammavongsy, Z.; Cunningham, D. W.; Sutthirat, N.; Eisenhart, R. J.; Ziller, J. W.; Yang, J. Y. *Dalton Trans.* **2018**, 47, 14101-14110

Thammavongsy, Z.; Kha, I. M.; Ziller, J. W.; Yang, J. Y. *Dalton Trans.* **2016**, 45, 9853-9859

Thammavongsy, Z.; Khosrowabadi Kotyk, J. F.; Tsay, C.; Yang, J. Y. *Inorg. Chem.* **2015**, 54, 11505-11510

Computational analysis in this chapter was performed by graduate student Drew W. Cunningham.

3.1. Motivation and Specific Aims

Flexible ligands that can adapt their donor strength have enabled unique reactivity in a wide range of inorganic complexes. Most examples are composed of flexible multi-dentate ligands containing a donor that can vary its interaction through its distance to the metal center. This chapter describes an alternative type of adaptable ligand interaction in the neutral multi-dentate ligand tris(2-pyridylmethyl)-azaphosphatrane (TPAP) which contains a proazaphosphatrane unit. Proazaphosphatranes can accept additional electron density from a tertiary nitrogen to form a transannular bond upon coordination of the P to more Lewis acidic atoms (Figure 3.1).

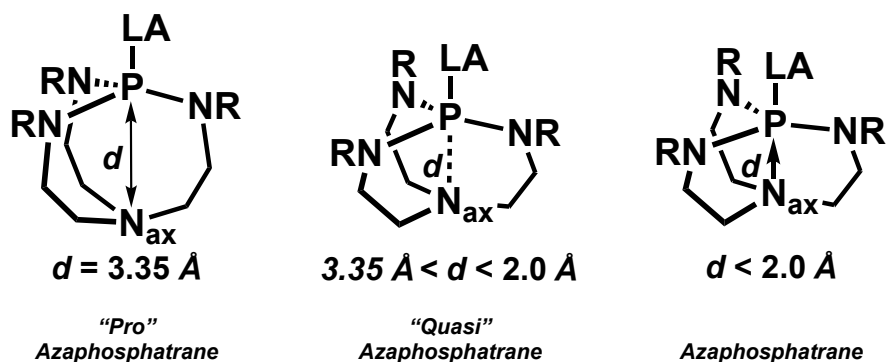


Figure 3.1. Chemdraw structures of azaphosphatranes in three different forms based on the transannular distance of P–N_{ax}.

An experimental investigation of the varying degree of transannular interaction in TPAP coordinated to late transition metals in different oxidation states is reported. The synthesis and characterization of the complexes M(TPAP), where M = Co(I)Cl, [Co(II)(CH₃CN)](BF₄)₂, Ni(0)(1,5-cyclooctadiene), [Ni(II)(CH₃CN)](BF₄)₂, [Pd(II)(CH₃CN)](BF₄)₂, or [Pt(II)Cl](PF₆) are described. Structural characterization and density functional theory of these complexes establish a significant increase in the degree of transannular interaction of the proazaphosphatrane unit when

coordinated to more electron deficient metal ions. Additionally, an effort to synthesize a Co(III)TPAP complex is presented to investigate the transannular bond of CoTPAP in three different oxidation states.

3.2. Background

Ligands that can adapt their donor strength provide a versatile method for adjusting electronic structure in order to access reactive transition metal intermediates. For example, Peters *et al.* extensively explored first row transition metal complexes with tripodal phosphine ligands containing a B, C, or Si heteroatom, where the interaction between the metal and heteroatom adjusts depending on the metal oxidation state and identity of ligands trans to the interaction (Figure 3.2a).¹⁻⁷ Parkin *et al.* demonstrated that the flexible interactions of an apical carbon in atrane-type ligands contributed to unique reactivity,⁸⁻¹⁰ and that the interaction can be modified through ligand design (Figure 3.2b).^{11, 12} Lu *et al.* designed tripodal ligands that encapsulate a Lewis acidic cation that can tune the electronic structure and reactivity at the metal (Figure 3.2c).¹³⁻¹⁶ In addition, the Agapie¹⁷⁻³¹ and Meyer³²⁻³⁴ labs have utilized phenyl or mesitylene linkers strategically positioned near a metal to serve as electron reservoirs to support multi-electron reactivity (Figure 3.2d). In all of the above cases, the adaptable interaction was incorporated into flexible chelating ligands, and the degree of interaction can be evaluated by the metal-donor distance.

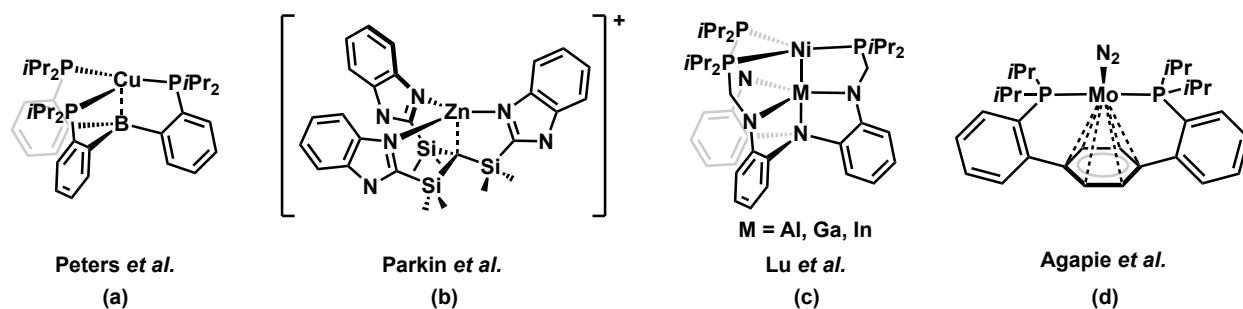


Figure 3.2. Chemdraw structures of (a) Peters', (b) Parkin's, (c) Lu's and (d) Agapie's transition metal complexes, featuring an adaptable ligand platform.

In this chapter, the description of an alternative type of adaptable interaction will be presented. The metal and donor maintain a fixed distance, but the latter can harness electron density through a transannular interaction when coordinated to more electron deficient metals. The ligand is based on proazaphosphatranes, a structurally unique class of neutral organic superbases more commonly known as Verkade's Superbases (Figure 3.1).³⁵⁻³⁹ The pK_a of the protonated form, or azaphosphatrane, ranges from 32.8 to 34.5 in acetonitrile depending on the substituents attached to the equatorial nitrogens (R).⁴⁰⁻⁴³ The extreme basicity of proazaphosphatranes stem from the formation of a stable three-centered four-electron transannular bond⁴⁴ between P and N_{ax} upon protonation.^{36, 45, 46}

Verkade *et al.* previously utilized the $P \cdots N_{ax}$ distance as a useful indicator for evaluating the extent of the transannular interaction. Proazaphosphatranes have $P \cdots N_{ax}$ distances measured by X-ray crystallography of $>3.2 \text{ \AA}$ (3.35 \AA is the sum of the van der Waals radii, which assumes no bonding interactions between P and N_{ax}).^{39, 47-52} In contrast, azaphosphatranes have $P \cdots N_{ax}$ distances of under 2.0 \AA (compared to the two electron covalent radius between P and N_{ax} of 1.72 \AA), providing structural evidence for the transannular interaction. In addition to protons, Verkade

et al. also explored the interaction of azaphosphatranes with Lewis acidic main group acceptors. In these derivatives, the $P\cdots N_{ax}$ distance varies between 2.55 ($X = NPh$) and 3.28 ($X = CH_2$) Å (black circles, Figure 3.3). These intermediate, or “quasi” structures represent distances between the sum of the van der Waals of P and N (3.35 Å) and covalent transannular bond distance in protonated Verkade’s Superbase ($R = Me$, 1.97 Å).^{37,53} Verkade noted a correlation with the degree of transannular interaction and the Lewis acidity of the substituent on P, with the strongest interaction with a proton.⁵⁴

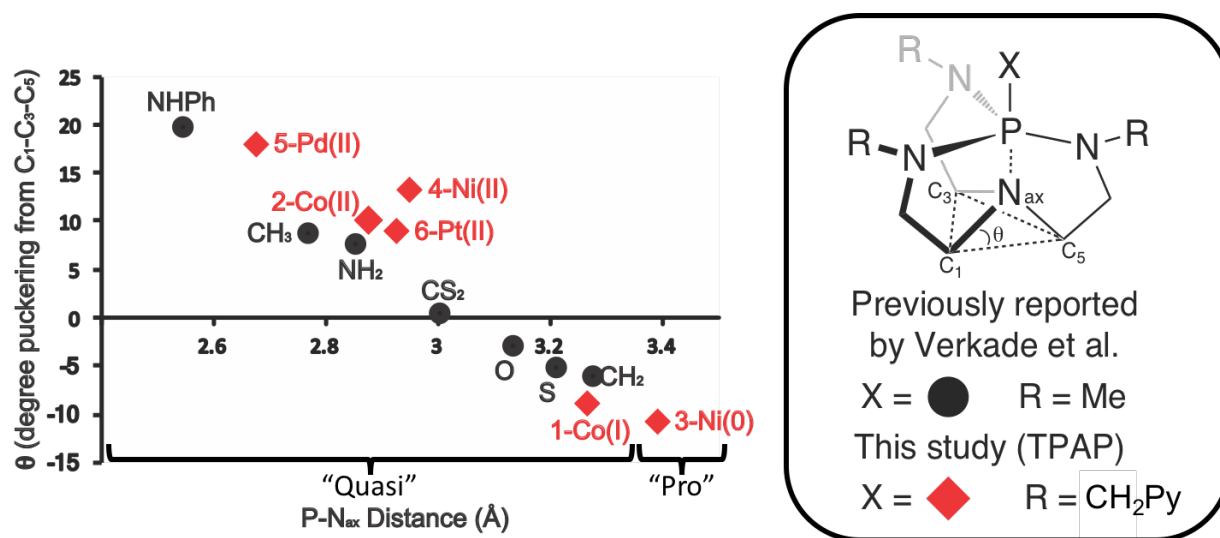
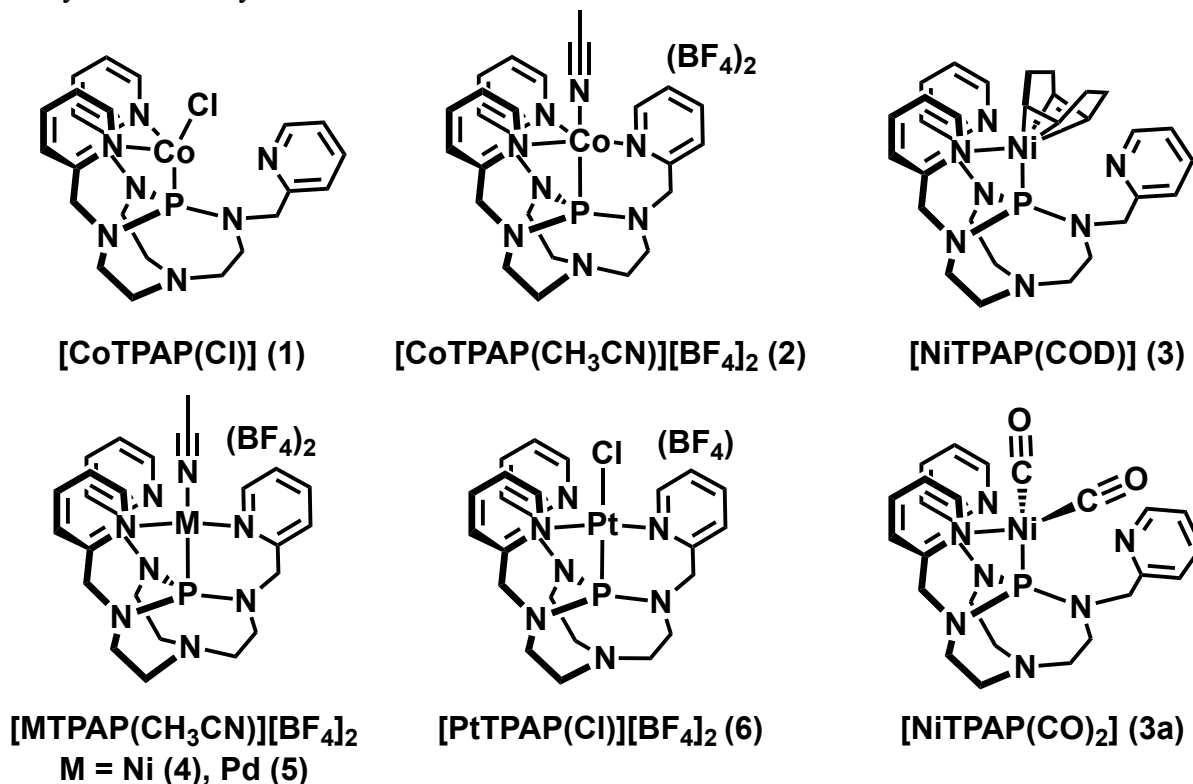


Figure 3.3. (Left) A plot of the transannular distance versus the θ puckering of the axial nitrogen above the plane of the three adjacent carbon atoms for Verkade’s Superbase with various main groups (denoted in black circles ●) and TPAP with various transition metals (denoted in red diamonds ◆). (Right) Depiction of the angle, θ , as the degree of puckering of the axial nitrogen (N_{ax}) out of the $C_1-C_3-C_5$ plane. Values used in this figure are from structural data. Reproduced by permission of The Royal Society of Chemistry.

Although azaphosphatranes have been used as ligands in palladium-catalyzed C–C,⁵⁵⁻⁵⁷ and C–N,⁵⁸⁻⁶⁰ cross-coupling and platinum-catalyzed hydrosilylation,⁶¹ the transannular interaction upon coordination to transition metal complexes had not been systematically interrogated at the time of this study.^{47, 54, 62-64} The dynamic nature of azaphosphatranes motivated this investigation into whether the P···N_{ax} distance would adjust to different metals and oxidation states according to their Lewis acidity. To provide greater coordinative stability, a proazaphosphatrane unit was incorporated in a tetradentate ligand to form tris(2-pyridylmethyl)-azaphosphatrane (TPAP), shown in Chart 3.1.^{62, 63} The proazaphosphatrane in TPAP retains its ability to form a transannular bond; structural characterization of the protonated TPAP has a P···N_{ax} distance of 1.97(16) Å.⁶³ All three pyridine arms in TPAP can potentially coordinate to the metal ion,⁶³ but for some of the complexes reported only one or two pyridine arms are coordinated. In this study, discussion of the structural and computational investigation of TPAP coordinated to two different metals in two different oxidation states: Co(I), Co(II) and Ni(0), Ni(II), as well as the TPAP complexes of Pd(II) and Pt(II), shown in Chart 3.1 as complexes **1-6** (and **3a**). The P···N_{ax} transannular distance was determined through structural characterization by X-ray crystallography. The varying degree of transannular interactions evident in the solid-state was supported by computational studies on the orbital interactions between the P and N_{ax} atoms in complexes **1**, **2**, **4**, **5**, and **6** and an analogue of complex **3**, [NiTPAP(CO)₂] (complex **3a**).

Chart. 3.1. Transition Metal Complexes of TPAP. Reproduced by permission of The Royal Society of Chemistry.



3.3. Results and Discussion

3.3.1. Synthesis and Structure of CoTPAP Complexes (1 & 2)

The ligand TPAP was synthesized as described in chapter 2 and previously reported.⁶³ The purple complex $[\text{CoTPAP}(\text{Cl})]$ (**1**) was prepared by adding stoichiometric amounts of TPAP to $\text{Co}(\text{I})\text{Cl}(\text{PPh}_3)_3$ in tetrahydrofuran. Complex **1** is paramagnetic with a solution μ_{eff} of $3.34 \mu\text{B}$ (C_6D_6), corresponding to an $S = 1$ system. Elemental analysis was used to confirm the analytical purity of the complex. X-ray quality crystals were grown from diethyl ether at -35°C . The solid-state structure of complex **1** is shown in Figure 3.2 and selected bond distances and angles are shown in Table 3.1. The pseudo-tetrahedral cobalt center has a τ_4 parameter of 0.77, where a value

of 1 represents an ideal tetrahedral geometry, and a value of 0 represents an ideal square planar geometry.⁶⁵ The TPAP ligand chelates in a tridentate fashion through the phosphorus donor and two of the three pyridine N atoms. The fourth coordination site is occupied by a chloride ion. In **1**, TPAP has a transannular P...N1 distance of 3.2647(14) Å and θ (puckering of the axial nitrogen above the plane of the three adjacent carbon atoms) of -9.1349° (Figure 3.4, Table 3.1).

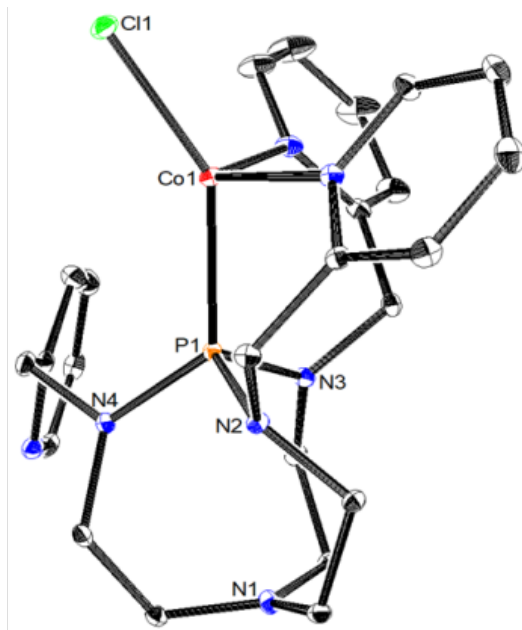


Figure 3.4. Crystal structure of [CoTPAP(Cl)] (**1**). Thermal ellipsoids are drawn at 50% probability. Hydrogen atoms and counteranions are omitted for clarity. Reproduced by permission of The Royal Society of Chemistry.

[CoTPAP(CH₃CN)][BF₄]₂ (**2**) was prepared by reacting stoichiometric quantities of TPAP with [Co(CH₃CN)₆][BF₄]₂ in acetonitrile.⁶³ The product was precipitated and washed with diethyl ether to give the analytically pure product in 56.2% yield. A single crystal for X-ray analysis was grown by layering pentane on a solution of **2** in dichloromethane. The structure is shown in Figure 3.5, and selected bond distances and angles are shown in Table 3.1. The Co–N_{py} distance is similar

for all three pyridines (1.997(2), 2.035(2), and 2.094(2) Å), and the Co–P distance is 2.1693(7) Å. The ligand chelates in a tetradentate fashion, with an acetonitrile solvent taking up a fifth coordination site. The pseudo-square pyramidal cobalt center has a τ_5 parameter of 0.4176, where a value of 0 represents an ideal square pyramid, and a value of 1 represents an ideal trigonal bipyramid.⁶⁶

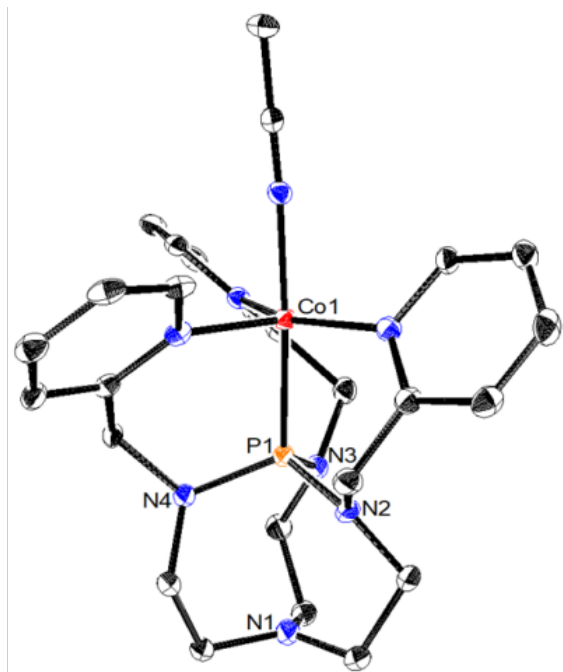


Figure 3.5. Crystal structure of [CoTPAP(CH₃CN)][BF₄]₂ (**2**). Thermal ellipsoids are drawn at 50% probability. Hydrogen atoms and counteranions are omitted for clarity. Adapted with permission from Thammavongsy, Z.; Khosrowabadi Kotyk, J. F.; Tsay, C.; Yang, J. Y. *Inorg. Chem.* **2015**, 54, 11505-11510. Copyright 2015 American Chemical Society.

3.3.2. Attempted Synthesis and Characterization of Co(III)TPAP Complexes (2a-c)

The first attempt of a Co(III)TPAP complex was the metalation of TPAP with Co(III)(acac)₃ (where acac = acetylacetonate) in acetonitrile. The color changed from green to orange after 1 day of mixing. A brown solid was obtained after solvents were removed under reduced pressure. An X-ray quality crystal was grown from the slow evaporation of the brown solid in tetrahydrofuran/diethyl ether mixture. The crystal structure displayed a [Co(II)(acac)]⁻ complex with an outer-sphere protonated TPAP ([TPAPH]⁺) molecule (Figure 3.6). The P–N_{ax} distance in [TPAPH]⁺ is 1.934 Å, consistent with previously published [TPAPH]⁺ structures.⁶³ The [Co(II)(acac)]⁻ is in an octahedral geometry and the Co ion has an assigned oxidation state of +2. The proton source to generate [TPAPH]⁺ could be from adventitious water.

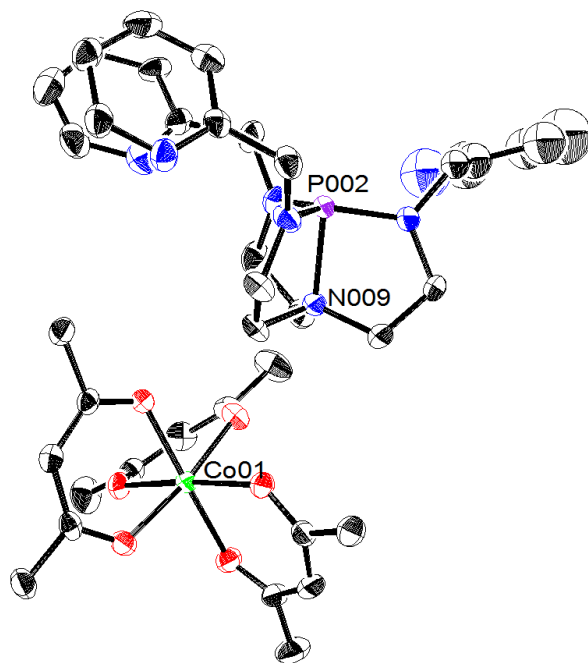


Figure 3.6. Crystal structure of [Co(II)(acac)][TPAPH] (**2a**). Thermal ellipsoids are drawn at 50% probability. Hydrogen atoms are omitted for clarity.

Due to the limited diversity of Co(III) starting materials, attempts were made to oxidize the known $[\text{CoTPAP}(\text{CH}_3\text{CN})][\text{BF}_4]_2$ with AgBF_4 . The reaction of $[\text{CoTPAP}(\text{CH}_3\text{CN})][\text{BF}_4]_2$ with AgBF_4 was performed in the dark due to light sensitivity of AgBF_4 . The reaction was filtered and an orange solution was obtained. The solution was concentrated and the $^{31}\text{P}\{^1\text{H}\}$ NMR spectrum had a resonance at -20 ppm, in the range of a fully transannulated P–N_{ax} bond.⁶⁷ Attempts to recrystallize the product failed, producing orange oils.

Another route was tried, where CoCl_2 , TPAP and FcBF_4 (where Fc = Ferrocenium) were mixed in a 1:1:1 ratio. The mixture of the CoCl_2 and TPAP in acetonitrile were stirred for 1 day before adding FcBF_4 . Once the FcBF_4 was added, the solution turned dark green. The solvent was removed under reduced pressure and the remaining green solid was washed with diethyl ether to remove ferrocene as a yellow solution. An X-ray quality crystal was grown from a slow vapor diffusion of diethyl ether into a solution of the green product in acetonitrile. The crystal structure revealed TPAP with two counter BF_4 anions and an oxidized phosphorus(V) center (Figure 3.7). The P–N_{ax} distance is 1.90 Å, consistent with a full transannulation of the P and N_{ax}.⁴⁰ This structure is unique, as it represents an elusive dicationic azaphosphatrane species proposed by Verkade.⁶⁸

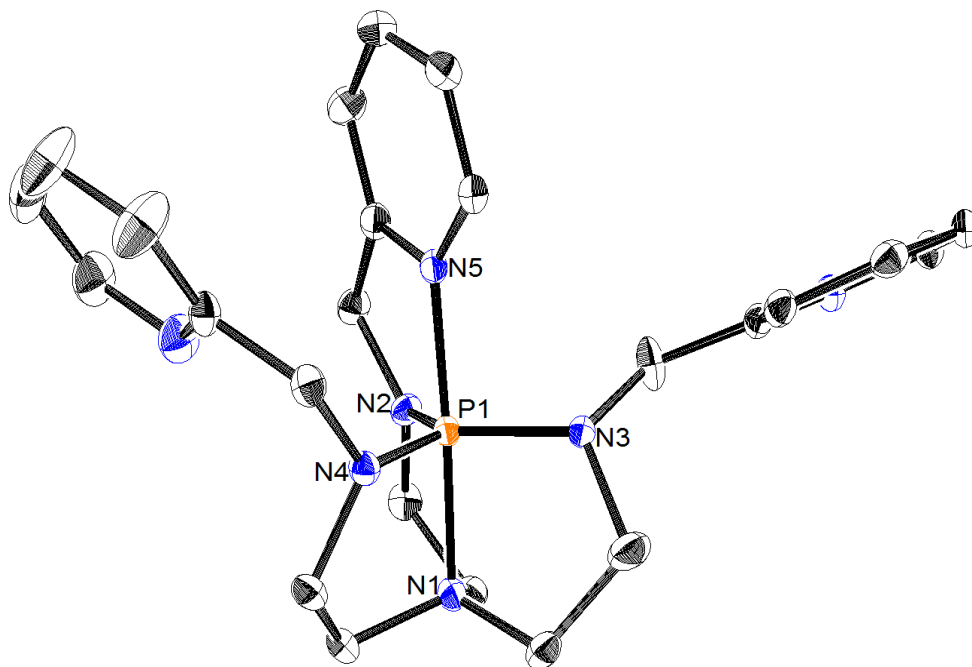


Figure 3.7. Crystal structure of $[\text{TPAP}]^{2+}$ (**2b**). Thermal ellipsoids are drawn at 50% probability. Hydrogen atoms and BF_4 counteranions are omitted for clarity.

Surprisingly, the crystal structure from the reaction of a 1:1 ratio of CoCl_2 and TPAP in acetonitrile produced a $\text{CoCl}_3(\text{TPAPH})$ complex (Figure 3.8). The crystal structure displayed a protonated TPAP ($[\text{TPAPH}]^+$) with a CoCl_3 bound to one of the pyridine donors of TPAP. The Co metal ion is in the +2 oxidation state, where the $[\text{CoCl}_3]^-$ balances the positively charged ligand $[\text{TPAPH}]^+$. The $\text{P}-\text{N}_{\text{ax}}$ distance is 1.941 Å, consistent with previously published protonated TPAP molecules.⁶³

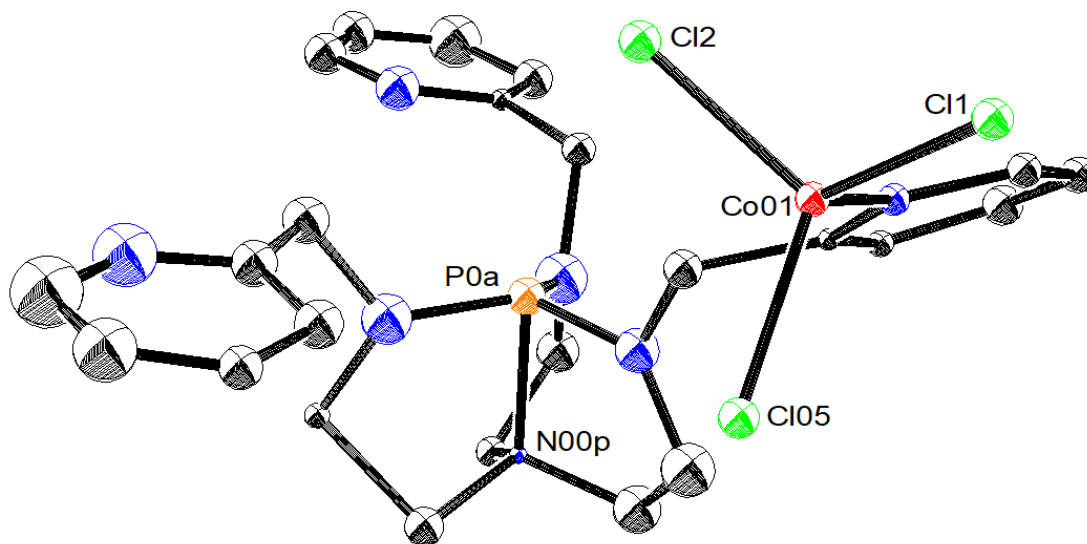


Figure 3.8. Crystal structure of $\text{CoCl}_3(\text{TPAPH})$ (**2c**). Thermal ellipsoids are drawn at 50% probability. Hydrogen atoms are omitted for clarity.

Thus, the attempted synthesis of Co(III)TPAP resulted in a Co(II)TPAP complex with a protonated TPAP ligand or an oxidized TPAP molecule.

3.3.3. Synthesis and Structure of NiTPAP (**3**, **4** & **7**), PdTPAP (**5**) and PtTPAP (**6**) Complexes

$[\text{NiTPAP}(\text{COD})]$ ($\text{COD} = 1,5\text{-cyclooctadiene}$) (**3**) was synthesized through the reaction of stoichiometric amounts of TPAP with $\text{Ni}(\text{COD})_2$ in tetrahydrofuran; the crude product was recrystallized from diethyl ether. Complex **3** is diamagnetic and was characterized by ^1H and $^{31}\text{P}\{^1\text{H}\}$ NMR spectroscopies. X-ray quality crystals of **3** were grown from a concentrated solution in diethyl ether at $-35\text{ }^\circ\text{C}$; the solid-state structure is shown in Figure 3.9. In **3**, TPAP coordinates in a bidentate fashion through the phosphorus donor and one of the pyridines. The $\text{P}\cdots\text{N1}$ distance is $3.3915(17)\text{ \AA}$ and θ is -10.9882° (Table 3.1). The analogue of complex **3**, $[\text{NiTPAP}(\text{CO}_2)]$ (complex **7**) was also synthesized to compare with density functional studies.

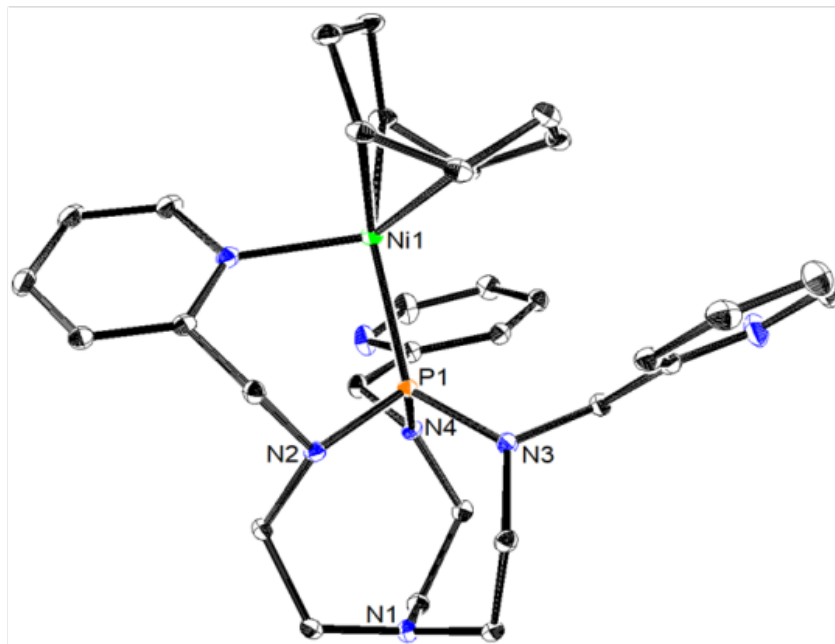


Figure 3.9. Crystal structure of [NiTPAP(COD)] (**3**). Thermal ellipsoids are drawn at 50% probability. Hydrogen atoms are omitted for clarity. Reproduced by permission of The Royal Society of Chemistry.

Complex **3a** was synthesized in a similar fashion as complexes **3**. Bis(1,5-cyclooctadiene)nickel(0) was added to a solution of TPAP in tetrahydrofuran, which produced a green intermediate complex. Once CO gas (1 atm) was introduced, the color changed from dark green to colorless. The solvent was removed and recrystallization of the crude product by slow evaporation in diethyl ether resulted in a 77% yield for **3a**.⁶² Complexes **3a** was characterized by ¹H, ¹³C, ³¹P{¹H} NMR and IR spectroscopies, and the purity was confirmed by elemental analysis. Single crystals suitable for X-ray analysis were grown from slow evaporation of a diethyl ether solution; the solid-state structure of **3a** is shown in Figure 3.10. In this chapter, the structure of complex **3a** is used to computationally model a Ni(0)TPAP complex, due to difficulties in modeling complex **3**.

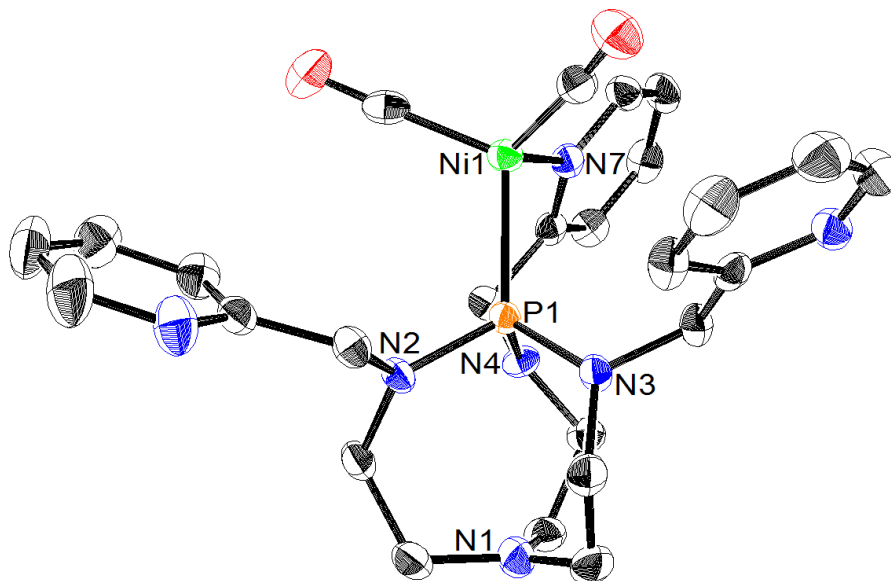


Figure 3.10. Crystal structure of $[\text{NiTPAP}(\text{CO}_2)]$ (**3a**). Thermal ellipsoids are drawn at 80% probability. Hydrogen atoms and counteranions are omitted for clarity. Reproduced by permission of The Royal Society of Chemistry.

The divalent complexes $[\text{NiTPAP}(\text{CH}_3\text{CN})][\text{BF}_4]_2$ (**4**) and $[\text{PdTPAP}(\text{CH}_3\text{CN})][\text{BF}_4]_2$ (**5**) were synthesized by mixing TPAP with $[\text{Ni}(\text{CH}_3\text{CN})_6.5][\text{BF}_4]_2$ and $[\text{Pd}(\text{CH}_3\text{CN})_4][\text{BF}_4]_2$, respectively in acetonitrile. Complexes **4** and **5** are diamagnetic and were characterized by ^1H NMR spectroscopy. X-ray quality crystals were obtained using the same method. The solid-state structures of **4** (Figure 3.11a) and **5** (Figure 3.11b) are displayed below, along with selected bond distances and angles (Table 3.1). Both **4** and **5** are four coordinate square planar complexes with τ_4 values of 0.20 and 0.06, respectively. The $\text{P}\cdots\text{N1}$ distances of **4** and **5** are 2.948(2) and 2.6747(18) Å ($\text{P2}\cdots\text{N9} = 2.6613(18)$ Å), respectively.

$[\text{PtTPAP}(\text{Cl})][\text{PF}_6]$ (**6**) was synthesized in two steps. $\text{PtCl}_2(\text{COD})$ was first added to TPAP in acetonitrile. After one hour, two equivalents of AgPF_6 were added in the dark and the solution was stirred for 5 minutes. A colorless crystal was grown from diethyl ether and acetonitrile.

Complex **6** is diamagnetic and was characterized by ^1H and $^{31}\text{P}\{^1\text{H}\}$ NMR spectroscopies. The solid-state structure of **6** is shown in Figure 3.11c and selected bond distances and angles are shown in Table 3.1. The coordination environment of **6** is similar to that of **4** and **5**, except an acetonitrile ligand is replaced by a chloride anion in the inner sphere. Complex **6** is closer to a square planar coordination geometry, with a τ_4 values of 0.12. TPAP in **6** displayed a $\text{P}\cdots\text{N1}$ distance of 2.927(4) Å ($\text{P2}\cdots\text{N8} = 2.821(4)$ Å), with θ of 8.8644° .

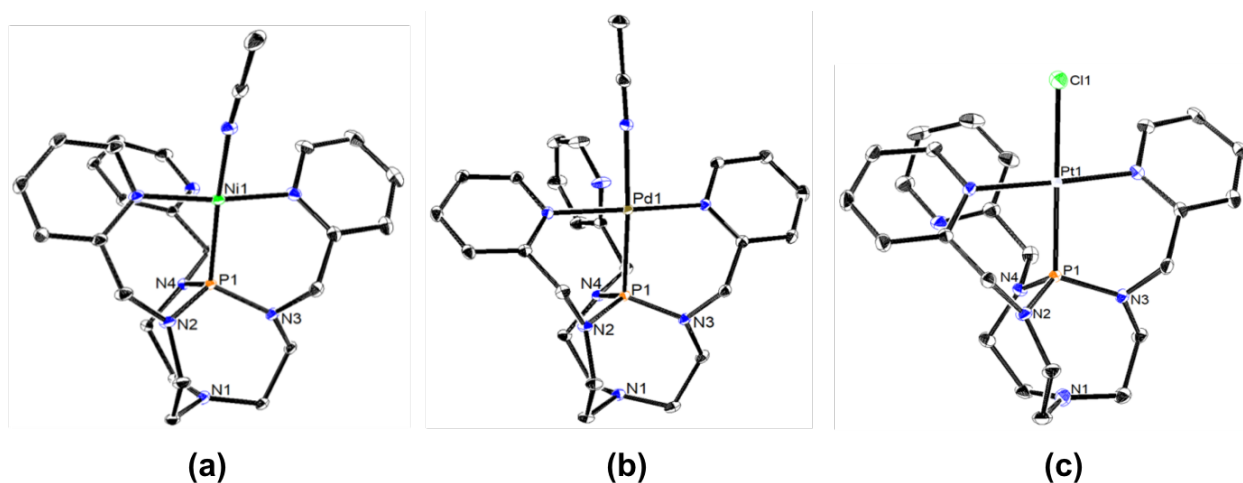


Figure 3.11. Crystal structure of (a) $[\text{NiTPAP}(\text{CH}_3\text{CN})][\text{BF}_4]_2$ (**4**), (b) $[\text{PdTPAP}(\text{CH}_3\text{CN})][\text{BF}_4]_2$ (**5**) and (c) $[\text{PtTPAP}(\text{Cl})][\text{PF}_6]$ (**6**). Structures **5** and **6** display one of two molecules in the asymmetric unit. Thermal ellipsoids are drawn at 50% probability. Hydrogen atoms and counteranions are omitted for clarity. Electron density from the minor disorder of the Pt atom in **6** is also omitted. Reproduced by permission of The Royal Society of Chemistry.

Table 3.1. Bond lengths and angles of complexes **1-6**. Metrics **5** and **6** were taken from one of two molecules in the asymmetric unit. The metal ion is denoted as M. Non-italicized values are from the X-ray structural analysis and italicized values are from the geometry optimized structures calculated using quantum mechanical methods. Reproduced by permission of The Royal Society of Chemistry.

	1	2	3	4	5	6
P₁-N₁ (P---N_{ax}) (Å)	3.2647(14)	2.877(2)	3.3915(17)	2.948(2)	2.6747(18)	2.927(4)
<i>Calc. (P---N_{ax}) (Å)</i>	<i>3.088</i>	<i>2.737</i>	<i>3.306</i>	<i>2.701</i>	<i>2.646</i>	<i>2.815</i>
P₁-N₂ (Å)	1.7089(13)	2.035(2)	1.7101(16)	1.6500(19)	1.6722(17)	1.666(4)
P₁-N₃ (Å)	1.6892(13)	1.997(2)	1.6965(16)	1.6511(19)	1.6528(17)	1.649(4)
P₁-N₄ (Å)	1.6879(13)	2.094(2)	1.7007(16)	1.649(2)	1.6583(16)	1.642(4)
P₁-M (Å)	2.1675(5)	2.1693(7)	2.1642(5)	2.1670(7)	2.2294(5)	2.2245(11)
<i>Calc. P-M (Å)</i>	<i>2.190</i>	<i>2.263</i>	<i>2.323</i>	<i>2.254</i>	<i>2.357</i>	<i>2.354</i>
C₁-C₃-C₅ θ (°)	-9.1349	9.9140	-10.9882	13.0123	17.7932	8.8644
<i>Calc. C₁-C₃-C₅ θ (°)</i>	<i>3.41</i>	<i>16.62</i>	<i>---</i>	<i>17.32</i>	<i>18.62</i>	<i>13.79</i>

3.3.4. Comparison of the Transannular Distance between Co(I)TPAP and Co(II)TPAP

The P···N₁ (or P···N_{ax}) distance of TPAP when bound to a Co(I) ion in complex **1** (3.2647(14) Å) indicates a minimal transannular interaction with a value closer to the “pro” (or free base) rather than the “quasi” form. An additional crystal of **1**, complex **1b** was grown by pentane diffusion into a concentrated tetrahydrofuran solution and exhibited a P···N₁ distance in TPAP of 3.339(2) Å, a difference of 0.0743 Å between structures. Verkade observed that differences in crystal packing could influence the transannular distance by up to 0.1 Å, providing an estimated boundary for error in the solid-state distances.³⁵ The transannular distance observed in both Co(I) structures is comparable to those found when proazaphosphatane is coordinated to main group elements such as sulfur and oxygen (Figure 3.3).⁶⁹

Upon coordination of TPAP to a more Lewis acidic Co(II) ion (complex **2**), the P···N₁ distance shortens to 2.877(2) Å, a significant shift of 0.39 Å. In Figure 3.3, complex **2** is in the middle of the plot (“quasi” form of azaphosphatane).

3.3.5. Comparison of the Transannular Distance between Group 10 TPAP Complexes

Complex **3**, with a Ni(0) ion, has a P \cdots N1 distance of 3.3915(17) Å, outside of the van der Waals radii of P \cdots N and signifying no transannular interaction. The P \cdots N1 distance of **3** falls within the range of four other previously reported Ni(0)azaphosphatrane complexes that bind in a monodentate fashion.⁶² The consistent P \cdots N_{ax} across the series highlights the fact that denticity of TPAP has little influence on the P \cdots N_{ax} transannular interaction compared to monodentate azaphosphatranes when Ni(0) is bound. When TPAP is bound to a Ni(II) ion in complex **4**, the P \cdots N1 distance shortens to 2.948(2) Å, which lies within the “quasi” form of azaphosphatranes. As seen in the CoTPAP case, there is a significant decrease in the P \cdots N1 transannular distance with an increase in the oxidation state of the Ni metal center.

The Pd(II) and Pt(II) TPAP complexes (**5** and **6**) were also investigated in order to determine if the transannular distance changes upon coordination to larger metal ions. The transannular distance decreases by 0.273 Å from Ni(II) to Pd(II), whereas the P \cdots N1 distance in Pt(II) resembles that of Ni(II). The chloride ligand in **6** could increase the P \cdots N1 distance due to the π donation of Cl⁻, which would decrease the Lewis acidity of the Pt metal center.^{37, 70} Attempted isolation of the [Pt(II)TPAP(CH₃CN)]²⁺ was unsuccessful, even when an excess of AgPF₆ was added to complex **6**. Therefore, the effect of the Cl⁻ anion on the Pt(II) center cannot be experimentally quantified.

3.3.6. Metal Ion Oxidation State Effects on TPAP

Verkade found that the $P\cdots N_{ax}$ distance in azaphosphatranes is influenced by the Lewis acidity of the atom or group when bound to the phosphorus. When coordinated to Ni and Co, the $P\cdots N_{ax}$ distance decreases with an increasing oxidation state of the metal (and concomitant increase in Lewis acidity of the metal ion). As the oxidation state increases from Co(I) to Co(II), θ increases by 19.05° and the $P\cdots N1$ distance contracts by 0.39 \AA (Table 3.1, Co(I) and Co(II)). A more prominent trend is observed with Ni(0) and Ni(II), where θ increases by 24° and the $P\cdots N1$ distance shorten by 0.44 \AA upon oxidation (Table 3.1, Ni(0) and Ni(II)).

3.3.7. Quantum Mechanical Calculations

DFT calculations were carried out by Drew W. Cunningham and performed using the Gaussian program suite with the incorporate NBO 3.1 package at the M06⁷¹ level of theory with 6-311G++(3df,3pd) basis set for 3rd row main groups, 6-311G**++ basis set for 2nd row main groups, and LANL2DZ basis set for all metals. Geometry optimizations of the complexes from the X-ray coordinates, followed by harmonic frequency calculations indicated that all of the compounds are minima on the potential energy surface. A comparison of selected calculated and experimental geometrical parameters are tabulated in Table 3.1.

The shortening of the $P\cdots N_{ax}$ distance with concurrent puckering of the axial nitrogen above the plane of the three adjacent carbon atoms (θ in Figure 3.3) is due to electron donation between the axial nitrogen (N_{ax}) and the phosphorus atom of the azaphosphatrane unit. To probe the nature of the $P\cdots N_{ax}$ interaction and observe electron density in a chemically intuitive manner, an analysis utilizing natural bond orbital (NBO) perturbation theory was carried out with a focus

on the NBOs of the M–P–N_{ax} fragment. All calculated values for each metal ion coordinated to TPAP utilized the complexes in Chart 3.1 except [NiTPAP(COD)] (**3**). The latter could not be modeled computationally because the structure failed to converge to a minimum on the potential energy surface. Therefore, [NiTPAP(CO)₂] (**3a**)⁶² was used as an alternative model for the transannular interaction of a Ni(0) bound to TPAP. Table 3.2 summarizes the calculated stabilization energies for each compound.

Table 3.2. Results of NBO analysis of donor-acceptor interactions in compound adducts, estimated by second-order perturbation theory, $E^{(2)}_{i \rightarrow j}$ (kcal mol⁻¹). Reproduced by permission of The Royal Society of Chemistry.

	1	2	4	5	6	7
LP(N_{ax}) → σ*(M–P)	<0.5	1.09	2.09	7.23	3.11	<0.5
LP(N_{ax}) → σ*(P–N_{eq})^a	<1.5	2.86	6.74	8.05	4.22	<1.5

^aThese values are the sum of the three LP(N_{ax}) → σ*(P–N_{eq}).

When the oxidation state of the metal is greater than +1, there is a significant donation from the lone pair (LP) of N_{ax} into unfilled antibonding NBOs. The LP(N_{ax}) → σ*(M–P) stabilization is ca. 2 kcal mol⁻¹ for the case of Ni(II) and Co(II). For Co(I) and Ni(0), where minimal or no transannular interaction is observed experimentally, the stabilization energy is negligible (<0.5 kcal mol⁻¹). For second- and third-row metals the LP(N_{ax}) → σ*(M–P) interaction provides 7.2 kcal mol⁻¹ and 3.1 kcal mol⁻¹ of stabilization energy for Pd(II) and Pt(II), respectively. In addition to the LP(N_{ax}) → σ*(M–P) donation, there is a significant interaction of the axial nitrogen with the three σ*(P–N_{eq}) NBOs (Table 3.2). These calculations suggest the interaction of the axial nitrogen with the phosphorus atom is the dominating factor that influences the puckering angle, θ, and P⋯N_{ax} distance.

The proposed interaction between the phosphorus atom and axial nitrogen can be seen by visualizing the highest occupied molecular orbitals (HOMO) for Ni(0) and Ni(II) (Figure 3.12). In the case of Ni(0), which lacks any significant P \cdots N_{ax} interactions, the axial nitrogen contributes only 7% to the HOMO and does not interact with any orbitals of phosphorus; however, for Ni(II) the axial nitrogen contributes 51% to the HOMO and results in a shortening on the P \cdots N_{ax} as well as a positive value of θ .

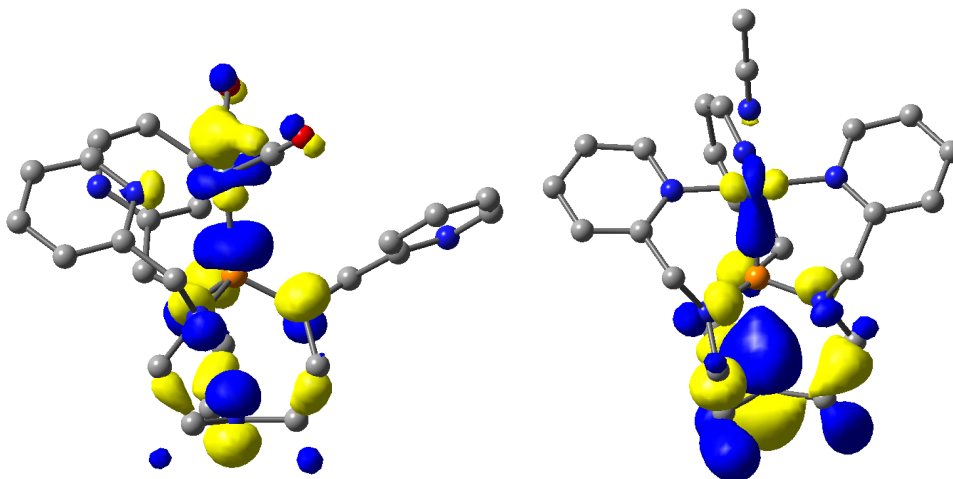


Figure 3.12. (Left) HOMOs of [Ni(0)TPAP(CO)₂] (**3a**) and (Right) [Ni(II)TPAP(CH₃CN)]²⁺ (**4**). All surfaces are at an isovalue of 0.035. Reproduced by permission of The Royal Society of Chemistry.

Additionally, a computational analysis of a Pd(II) analogue with a Cl⁻ anion and a Pt(II) analogue with an acetonitrile ligand was done to probe whether the overall complex charge significantly impacts the M–P and P \cdots N_{ax} distances. The compounds [PdTPAPCl]⁺ and [PtTPAP(CH₃CN)]²⁺ were investigated computationally and compared to their di-cationic (**5**) and mono-cationic (**6**) analogues, respectively. Computational data indicate the P \cdots N_{ax} distance is

close for Pd(II) and Pt(II) when they have the same fourth ligand. However, the P \cdots N_{ax} distance is consistently larger when Pd(II) or Pt(II) is bound by a Cl⁻ anion compared to CH₃CN (Table 3.3).

Table 3.3 shows that the M–P distances are not particularly sensitive to changes in the overall complex charges, as increasing the charge changes the M–P distances at most by ca. 0.01 Å. For both Pt and Pd compounds, the angles θ and P \cdots N_{ax} distances increase by 5.1 ° and 0.15 Å, respectively, when going from mono-cationic to di-cationic. Because the differences in changes of θ and P \cdots N_{ax} are identical for each compound, the complex charge does not account for any non-monotonic trends observed.

Table 3.3. Calculated geometrical parameters for selected mono-cationic and di-cationic comparison. Reproduced by permission of The Royal Society of Chemistry.

	[PtTPAP(CH ₃ CN)] ²⁺	[PtTPAPCl] ⁺	[PdTPAP(CH ₃ CN)] ²⁺	[PdTPAPCl] ⁺
M–P (Å)	2.35025	2.35406	2.35733	2.37091
P \cdots N _{ax} (Å)	2.65028	2.81528	2.64581	2.81892
θ (°)	18.8896	13.78628	18.61757	13.4973

3.4. Conclusion

The use of flexible ligands with adjustable coordinative interactions has shown great utility in accessing reactive metal sites. In this chapter, an azaphosphatrane core was incorporated into a chelating ligand to provide a new type of variable ligand interaction. The metal–ligand distance remains constant for first row transition metals while the non-coordinating nitrogen in the azaphosphatrane can donate additional electron density into the phosphorus ligand. The Tolman electronic parameter measured for azaphosphatranes, described in Chapter 1, establishes that even in the absence of a transannular interaction, they are among the most strongly donating phosphine ligands.⁶² Thus, the TPAP ligand represents an inherently strong ligand that can increase its donor

strength in contrast to prior systems that utilize weaker interactions. The higher donor strength available with TPAP may be valuable for stabilizing more electron deficient metal ions.

3.5. Experimental Details

General Considerations

The complexes described below are air- and moisture-sensitive and must be handled under an inert atmosphere of nitrogen using standard glovebox and Schlenk techniques. Unless otherwise noted, all procedures were performed at ambient temperature (21–24 °C). All solvents were sparged with argon and dried using a solvent purification system. Acetonitrile, diethyl ether, and halogenated solvents were passed through two columns of neutral alumina. Compounds tris(2-pyridylmethyl)proazaphosphatane,⁶³ CoCl(PPh₃)₃,⁷² [Co(CH₃CN)₆][BF₄]₂⁷³ and [Ni(CH₃CN)_{6.5}][BF₄]₂⁷³ were synthesized according to established procedures. CD₃CN and C₆D₆ were freeze–pump–thawed three times and dried over molecular sieves. CoCl₂, [Pd(CH₃CN)₄][BF₄]₂, PtCl₂(COD), Co(acac)₃, AgPF₆, AgBF₄, FcBF₄ and carbon monoxide (100%) were purchased from commercial sources and used without further purification.

Physical Methods

Nuclear Magnetic Resonance (NMR) Spectroscopy: Nuclear magnetic resonance (NMR) spectra were recorded on a DRX400 with a switchable QNP probe (¹H and ³¹P) or a Bruker AVANCE 600 MHz (¹H and ³¹P). ¹H NMR spectra were referenced to (tetramethylsilane) TMS using the residual proteo impurities of the solvent; ¹³C NMR spectra were referenced to TMS using the natural abundance ¹³C of the solvent; ³¹P{¹H} NMR spectroscopy experiments are referenced to the absolute frequency of 0 ppm in the ¹H dimension according to the Xi scale.⁷⁴

Infrared (IR) Spectroscopy: Infrared (IR) absorption measurements of the solution of **1-5** in CH₂Cl₂ was taken in a OMNI-Cell CaF₂ sealed cell (1.00 mm) on a Thermo Scientific Nicolet iS5 spectrophotometer with an iD1 transmission attachment.

Electrospray ionization mass spectrometry (ESI-MS): ESI-MS was performed with an ESI LC-TOF Micromass LCT 3 mass spectrometer in the Department of Chemistry at UC Irvine.

Electrochemistry: Electrochemical experiments were carried out on a Pine Wavedriver 10 potentiostat. Electrochemical experiments were carried out in acetonitrile solutions with 1.0 mM analyte and 0.20 M Bu₄NBF₄. The working electrode was a glassy carbon disc with a diameter of 2 mm, the counter electrode was a glassy carbon rod, and a Ag/AgCl pseudoreference electrode. Potentials were referenced to the ferrocene/ferrocenium couple at 0 V using ferrocene as an internal reference. UV-vis spectrum was collected in acetonitrile solution using an Agilent Technologies Cary 60 UV-vis.

Electron Paramagnetic Resonance (EPR): Perpendicular-mode X-band electron paramagnetic resonance (EPR) spectrum was collected using a Bruker EMX spectrometer.

Elemental Analysis (EA): Elemental analyses were performed on a PerkinElmer 2400 Series II CHNS elemental analyzer.

X-ray Crystallography (XRC): X-ray diffraction studies were carried out at the UCI Department of Chemistry X-ray Crystallography Facility on a Bruker SMART APEX II diffractometer. Data were collected at 133 K for **1**, **3**, **5** and **6**, and 88 K for **2**, **2a-c**, **3a**, and **4** using Mo K α radiation (λ = 0.710 73 Å). The APEX2 program package was used to determine the unit cell parameters and for data collection. The raw frame data was processed using SAINT and SADABS to yield the reflection data file. Subsequent calculations were carried out using the SHELXTL program.

For structure **2**, Hydrogen atoms other than H1 in **2** were placed at geometrically calculated positions and refined using a riding model, and their isotropic displacement parameters were fixed at 1.2 (1.5 for methyl groups) times the U_{eq} of the atoms to which they are bonded. H1 in **2** was located in the difference map and refined freely. For the structure of **2**, checkCIF reports three level B alerts (PLAT230_ALERT_2_B) due to unequal anisotropic displacement parameters (ADPs) along chemical bonds, which can signify an incorrect atom type assignment. However, all three alerts involve bonds within a pyridine ring of the TPAP ligand whose identity has been confirmed through other spectroscopic techniques. An additional level B alert (PLAT411_ALERT_2_B) was reported for this structure due to a short nonbonding intermolecular H \cdots H distance between two ligand hydrogen atoms (H21 and H23); this is likely a result of crystal packing.

For the structure of **4**, checkCIF reports one level B alert (PLAT214_ALERT_2_B) due to a high ratio of maximum to minimum anisotropic displacement parameters (ADPs) for atom F2B, which can signify a substitutional or positional disorder. As this atom is in the minor part of a disordered BF₄ anion, the identity of which is not in question, no further modeling was done. For structure **4**, atoms F(7) and F(8) were disordered and included using multiple components with partial site-occupancy-factors.

For structure **5**, atoms C(54), F(5), F(6), F(7) and F(8) were disordered and included using multiple components with partial site-occupancy-factors.

For structure **6**, there were several high residuals present in the final difference-Fourier map. It was not possible to determine the nature of the residuals although it was probable that

diethyl ether solvent was present. The SQUEEZE routine in the PLATON program package was used to account for the electrons in the solvent accessible voids.

Structural analysis for complex **1b** was carried out at the University of Minnesota, Minneapolis X-ray Crystallography Facility on a Bruker D8 Photon 100 CMOS diffractometer. Data were collected at 123 K. Crystals were grown by a graduate student at the University of Minnesota, Reed J. Eisenhart.

[CoTPAP(Cl)] (1): In the glove box, a solution of TPAP (34.2 mg, 0.0764 mmol) in 5 mL tetrahydrofuran was added to a solution of $\text{CoCl}(\text{PPh}_3)_3$ (67.3 mg, 0.0764 mmol) in 2 mL tetrahydrofuran. The solution immediately turned dark purple and was stirred for 1 day at room temperature. The solvent was removed under reduced pressure. The resulting purple solid was redissolved in diethyl ether and filtered through a glass pipette packed with a glass microfiber filter (22 μm). X-ray quality crystals were grown from a concentrated solution of **1** in diethyl ether at $-35\text{ }^\circ\text{C}$ (28.7 mg, 0.053 mmol, 69.4% yield). Analytical calculation for $\text{C}_{24}\text{H}_{30}\text{ClCoN}_7\text{P}$: C, 53.19; H, 5.58; N, 18.09. Found: C, 53.67; H, 5.25; N, 17.45. μ_{eff} (solution) = $3.34\mu\text{B}$. ESI-MS data could not be obtained due to the air sensitivity of complex **1** in solution.

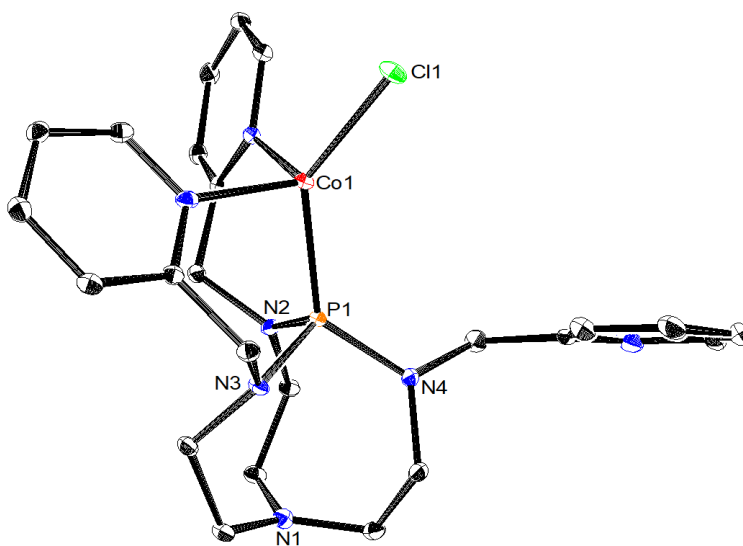


Figure 3.13. Crystal structure of $[\text{CoTPAP}(\text{Cl})]$ (**1b**) Thermal ellipsoids are drawn at 50% probability. Hydrogen atoms are omitted for clarity. Grown from a pentane diffusion into a concentrated THF solution by Reed J. Eisenhart from the University of Minnesota.

[CoTPAP(CH₃CN)][BF₄]₂ (2): In the glovebox, [Co(CH₃CN)₆][BF₄]₂ (23.8 mg, 0.0496 mmol) was added to a solution of TPAP (22.2 mg, 0.0496 mmol) in 3 mL of acetonitrile. The solution immediately turned dark greenish brown and was stirred for 6 h at room temperature. The solvent was removed under reduced pressure, and the resulting green solid was washed with diethyl ether. The green solid was redissolved in dichloromethane and filtered through a glass pipet packed with a glass microfiber filter. To this solution, diethyl ether was layered to afford green crystals that were isolated in 56.2% yield. ESI-MS (m/z): [M - BF₄ - CH₃CN]⁺ Calculation for C₂₄H₃₀BCoF₄N₇P, 593.17; Found, 593.17. UV-vis (CH₃CN) λ_{max}, nm (ε): 255 (8064), 400 (3058), 595 (212) and 975 (50.3). Analytical Calculation for C₂₆H₃₃B₂CoF₈N₈P: C, 43.31; H, 4.61; N, 15.54. Found: C, 42.64; H, 4.58; N, 15.01. μ_{eff} (solution) = 2.67 μB. (⊥)-Mode EPR (CH₃CN, 77K) g = 2.18.

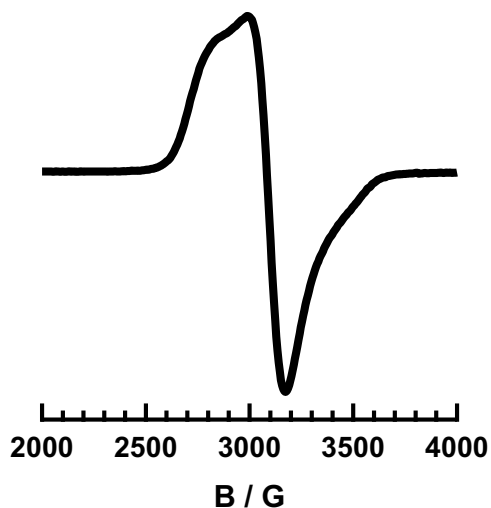


Figure 3.14. EPR spectrum of [CoTPAP(CH₃CN)][BF₄]₂ (2) in a frozen solution of acetonitrile at 77 K. The spectrum display a g = 2.18, which corresponds to an S = ½ system with a Co(II) d⁷ low spin complex.

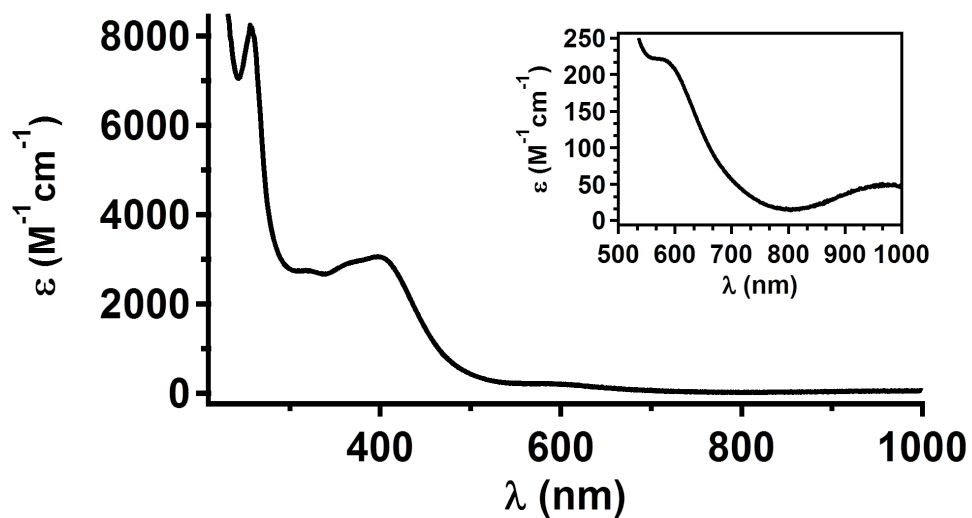


Figure 3.15. UV-vis spectrum of $[\text{CoTPAP}(\text{CH}_3\text{CN})][\text{BF}_4]_2$ (**2**) in acetonitrile at 22°C . An inset display a close up of the bands between 500 and 1000 nm.

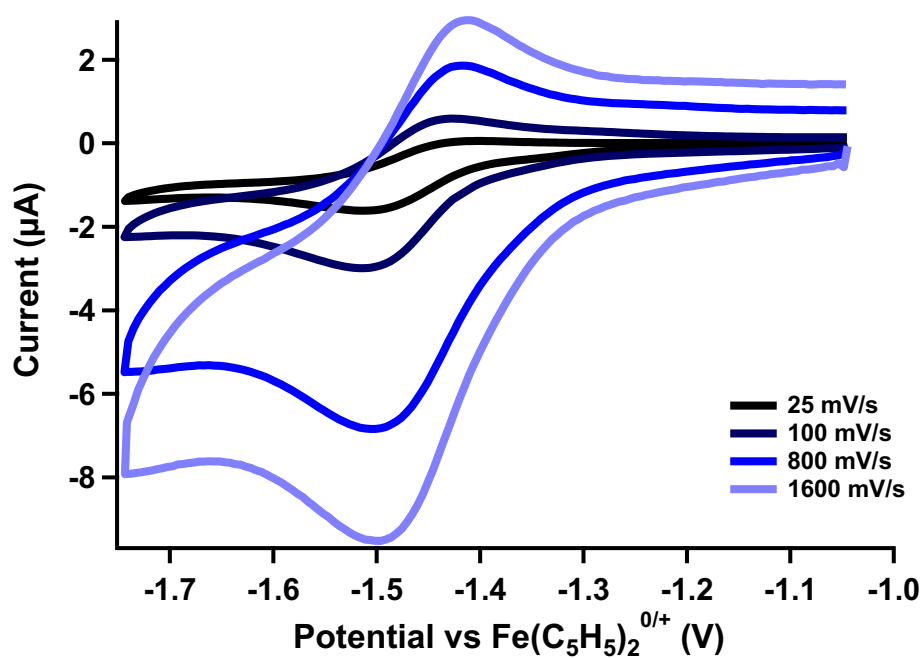


Figure 3.16. Variable scan rate cyclic voltammograms of $[\text{CoTPAP}(\text{CH}_3\text{CN})][\text{BF}_4]_2$ (**2**) with 1.0 mM analyte in acetonitrile with 0.02 M Bu_4NPF_6 . The voltammograms display a reversible event at -1.47 V (vs $\text{Fe}(\text{C}_5\text{H}_5)_2^{0/+}$) and is assigned as the $\text{Co}^{+/+2}$ couple.

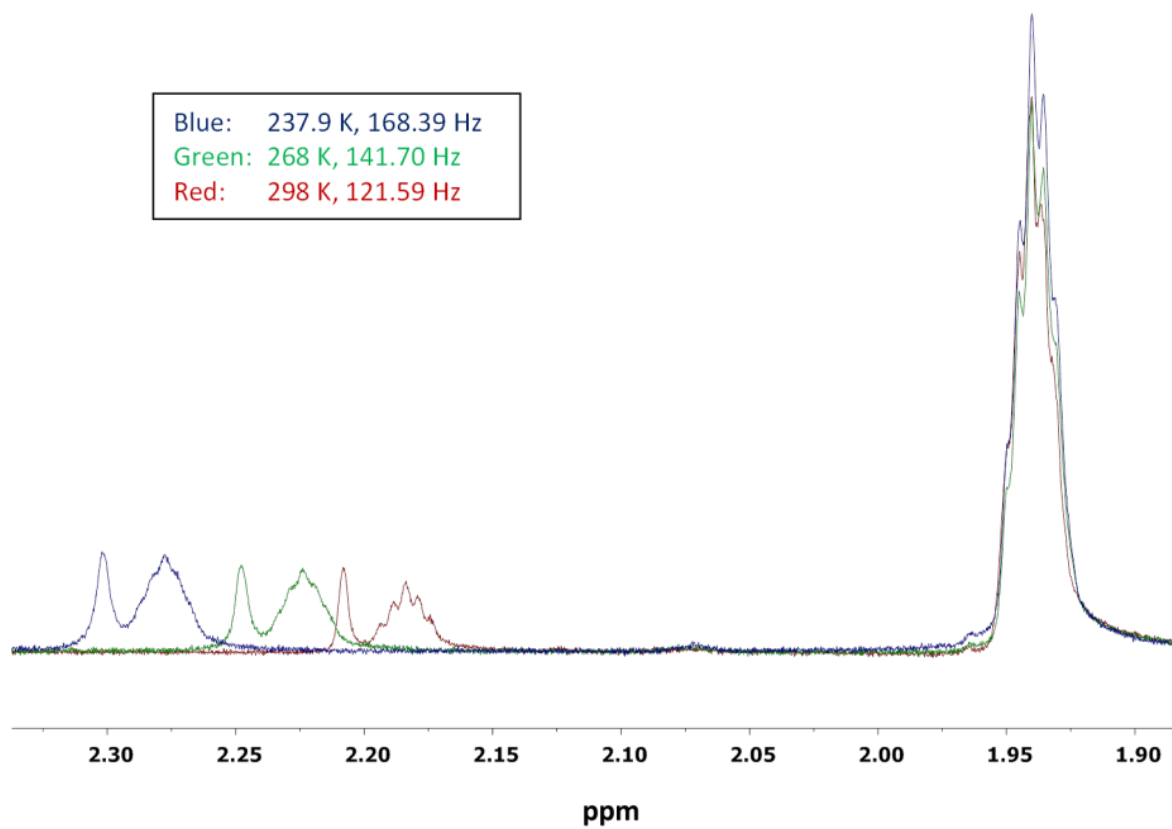


Figure 3.17. Solution magnetic susceptibility. ¹H NMR spectra of [CoTPAP(CH₃CN)][BF₄]₂ (2) at 237, 268 and 298 K in in CD₃CN.

[NiTPAP(COD)] (3): In the glove box, a solution of TPAP (100 mg, 0.223 mmol) in 3 mL tetrahydrofuran was added to a solution of Ni(COD)₂ (61.5 mg, 0.223 mmol) in 7 mL tetrahydrofuran. The solution immediately turned dark green and was stirred for 1 day at room temperature. The solvent was removed under reduced pressure. The resulting green solid was re-dissolved in diethyl ether and filtered through a glass pipette packed with a glass microfiber filter (22 μm). X-ray quality crystals were grown from a concentrated solution of **3** in diethyl ether at -35 °C. ¹H NMR (C₆D₆, 600 MHz) δ = 2.07 (s, 8H, COD), 2.64–2.84 (br, 12H, NCH₂CH₂N), 4.30 (s, 6H, PyCH₂), 4.43 (br, 4H, COD), 6.59 (t, 3H, Py), 7.08 (m, 3H, Py), 7.12 (t, 3H, Py), 8.68 (m, 3H, Py). ³¹P{¹H} NMR (C₆D₆, 243 MHz) δ = 150.7. Analytical calculation for C₂₄H₃₀N₇NiP·(C₈H₁₂)_{0.5}: C, 64.68; H, 7.24; N, 14.67. Found: C, 64.04; H, 6.77; N, 14.29. ESI-MS data could not be obtained due to the air sensitivity of complex **3** in solution. The yield is not reported due to the presence of COD impurities in both the ¹H NMR and elemental analysis data.

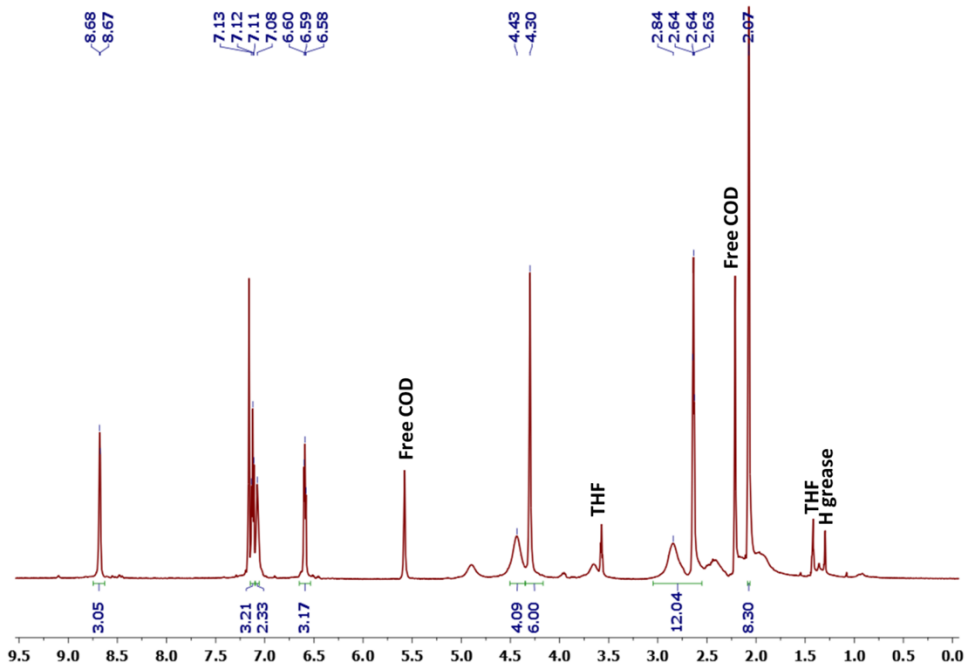


Figure 3.18. ^1H NMR spectrum of $[\text{NiTPAP}(\text{COD})]$ (**3**) in C_6D_6 .

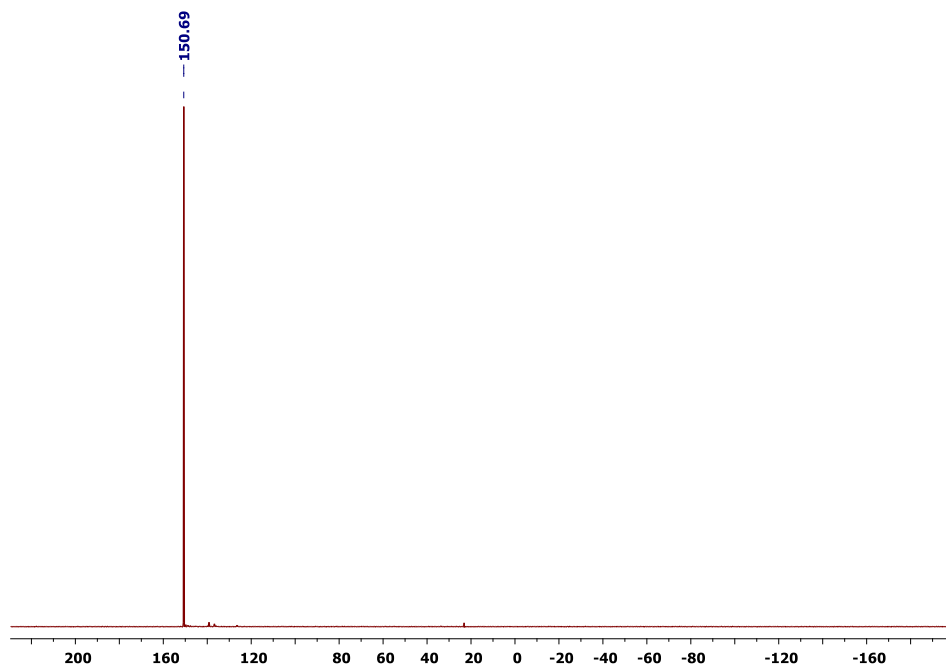


Figure 3.19. $^{31}\text{P}\{^1\text{H}\}$ spectrum of $[\text{NiTPAP}(\text{COD})]$ (**3**) in C_6D_6 .

[NiTPAP(CO)₂] (3a): In the glove box, a solution of bis(1,5- cyclooctadiene)nickel(0) (13.8 mg, 0.0503 mmol) in 5 mL of tetrahydrofuran was added to a solution of TPAP (22.5 mg, 0.0503 mmol) in 5 mL of tetrahydrofuran. The solution was stirred for 1 hour at room temperature. The solution was then transferred to a 100 mL Schlenk flask and brought out of the glove box and filled with CO gas (1 atm). The solution was stirred overnight under a CO atmosphere, after which the color changed from dark green to colorless. The CO gas was removed under reduced pressure with four cycles of freeze– pump–thaw and the resulting light yellow solution was brought back into the glove box. The oil that remained after solvent evaporation was washed with cold pentane to yield a yellow solid. Yellow crystals of **3a** were grown from a slow evaporation of diethyl ether to give the product in 77% yield. NMR studies of **3a** were conducted in a J. Young tube, in 1 atm of CO gas. ¹H NMR (C₆D₆, 400 MHz) δ = 2.46 (t, J = 10.8 Hz, 6H, NCH₂CH₂NP), 2.76 (br, 6H, NCH₂CH₂NP), 4.58 (br, 6H, PyrCH₂N), 6.67 (dd, J = 7.1, 5.1 Hz, 3H, Pyr), 7.25 (td, J = 7.7, 1.7 Hz, 3H, Pyr), 7.38 (d, J = 7.8 Hz, 3H, Pyr), 8.53 (m, 3H, Pyr). ¹³C{¹H} NMR (C₆D₆, 126 MHz) δ = 47.7 (NCH₂CH₂NP), 50.2 (PyrCH₂N), 53.3 (NCH₂CH₂NP), 122 (Pyr), 122 (Pyr), 136 (Pyr), 150 (Pyr), 160 (Pyr), 198 (CO). ³¹P NMR (C₆D₆, 162 MHz) δ = 142. FTIR (CH₂Cl₂): ν = 1981.7 (CO), 1906.5 (CO). Analytical Calculation for C₂₆H₃₀N₇NiO₂P: C, 55.54; H, 5.38; N, 17.44 Found: C, 55.02; H, 5.19; N, 17.50.

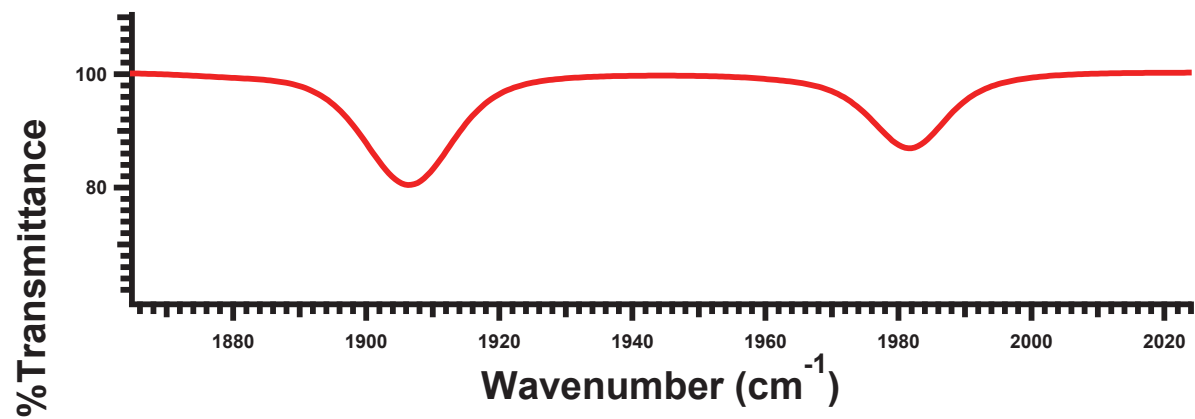


Figure 3.20. IR spectrum of $[\text{NiTPAP}(\text{CO})_2]$ (**3a**) in CH_2Cl_2 .

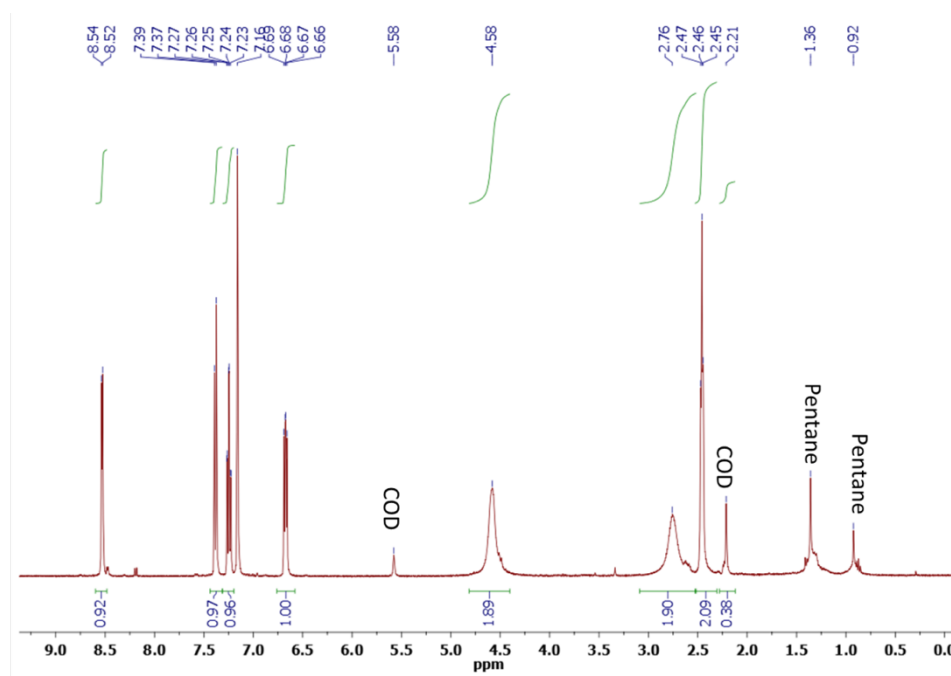


Figure 3.21. ^1H NMR spectrum of $[\text{NiTPAP}(\text{CO})_2]$ (**3a**) in C_6D_6 .

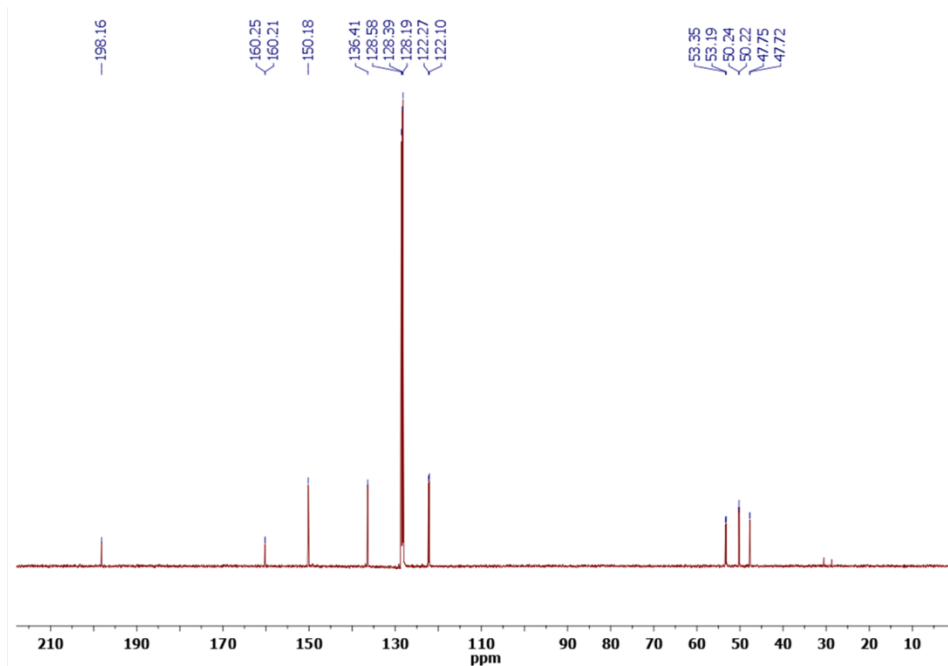


Figure 3.22. ^{13}C NMR spectrum of $[\text{NiTPAP}(\text{CO})_2]$ (**3a**) in C_6D_6 .

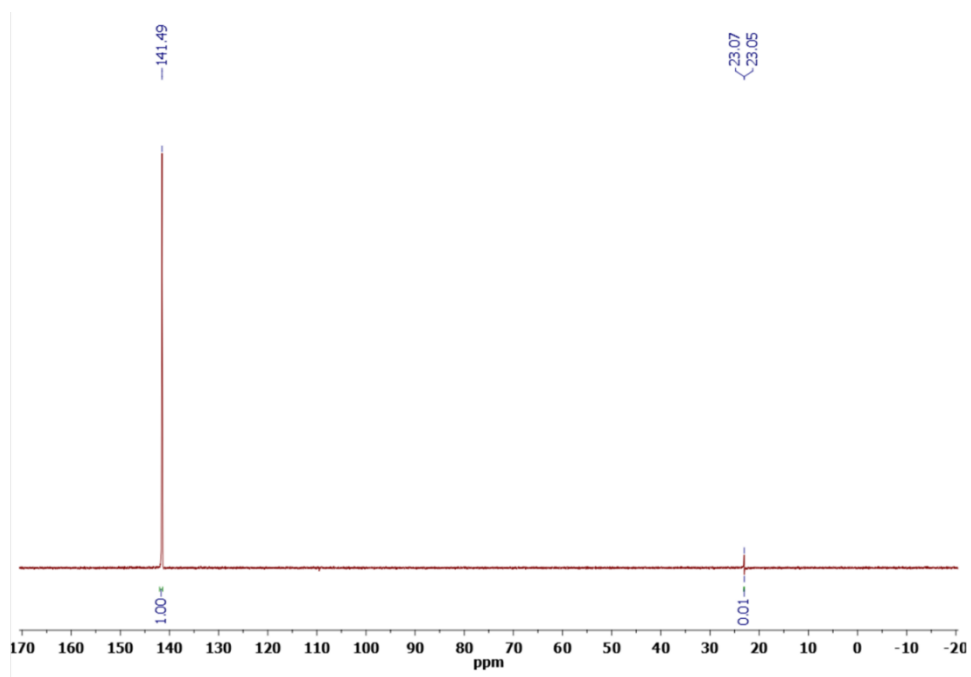


Figure 3.23. $^{31}\text{P}\{^1\text{H}\}$ NMR spectrum of $[\text{NiTPAP}(\text{CO})_2]$ (**3a**) in C_6D_6 .

[NiTPAP(CH₃CN)][BF₄]₂ (4): In the glove box, a solution of TPAP (109 mg, 0.250 mmol) in 7 mL of acetonitrile was added to a solution of [Ni(CH₃CN)_{6.5}][BF₄]₂ (122 mg, 0.250 mmol) in 2 mL of acetonitrile. The solution immediately turned dark orange and was stirred for 1 day at room temperature. The solvent was removed under reduced pressure. The resulting orange solid was redissolved in dichloromethane, filtered through a glass pipette packed with a glass microfiber filter (22 μm). X-ray quality crystals of **4** were grown from acetonitrile and diethyl ether (97.5 mg, 0.135 mmol, 55.1% yield). ¹H NMR (CD₃CN, 400 MHz) δ = 2.82 (t, 6H, NCH₂CH₂N), 2.94 (t, 6H, NCH₂CH₂N), 4.50 (s, 6H, PyCH₂), 7.61 (m, 6H, Py), 7.97 (t, 3H, Py), 9.51(s, 3H, Py). ESI-MS (m/z): [M - 2BF₄ - CH₃CN + Cl]⁺. Calculation for C₂₄H₃₀N₇PNiCl, 540.13; found, 540.20. Analytical calculation for C₂₆H₃₃B₂F₈N₈NiP: C, 43.32; H, 4.61; N, 15.54. Found: C, 43.65; H, 5.02; N, 15.18. Although the sample is analytically pure and the ¹H NMR is consistent with the proposed structure, a ³¹P{¹H} NMR resonance was unable to be resolved. The lack of resonance may be due to fluxional coordination in solution.

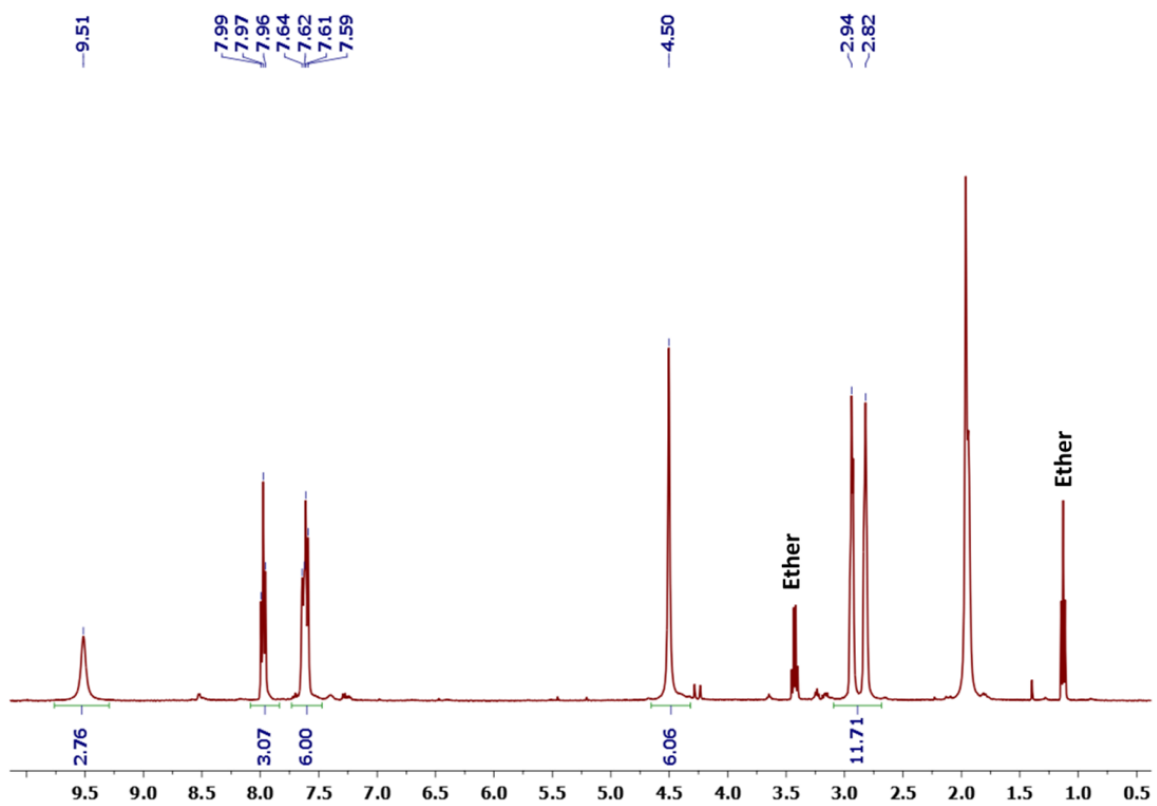


Figure 3.24. ^1H NMR of spectrum of $[\text{NiTPAP}(\text{CH}_3\text{CN})][\text{BF}_4]_2$ (**4**) in CD_3CN .

[PdTPAP(CH₃CN)][BF₄]₂ (5): In the glove box, a solution of TPAP (81.0 mg, 0.181 mmol) in 6 mL of acetonitrile was added to a solution of [Pd(CH₃CN)₄][BF₄]₂ (80.1 mg, 0.181 mmol) in 2 mL of acetonitrile. The solution immediately turned orange and was stirred for 1 day at room temperature. The solvent was removed under reduced pressure. The resulting yellow solid was redissolved in acetonitrile, filtered through a glass pipette packed with a glass microfiber filter (22 μm). X-ray quality crystals of **5** were grown from acetonitrile and diethyl ether (121 mg, 157 mmol, 86.9% yield). ¹H NMR (CD₃CN, 400 MHz) δ = 2.72 (t, 6H, NCH₂CH₂N), 2.94 (m, 6H, NCH₂CH₂N), 4.45 (d, 6H, PyCH₂), 7.46 (m, 6H, Py), 7.97 (dt, 3H, Py), 8.66 (d, 3H, Py). ³¹P{¹H} NMR (CD₃CN, 162 MHz) δ = 50.8. ESI-MS (m/z): [M - 2BF₄ - CH₃CN + Cl]⁺. Calculation for C₂₄H₃₀N₇PPdCl, 588.1; found, 588.0. Analytical calculation for C₂₆H₃₃B₂F₈N₈PdP: C, 40.63; H, 4.33; N, 14.58. Found: C, 40.35; H, 4.20; N, 14.37.

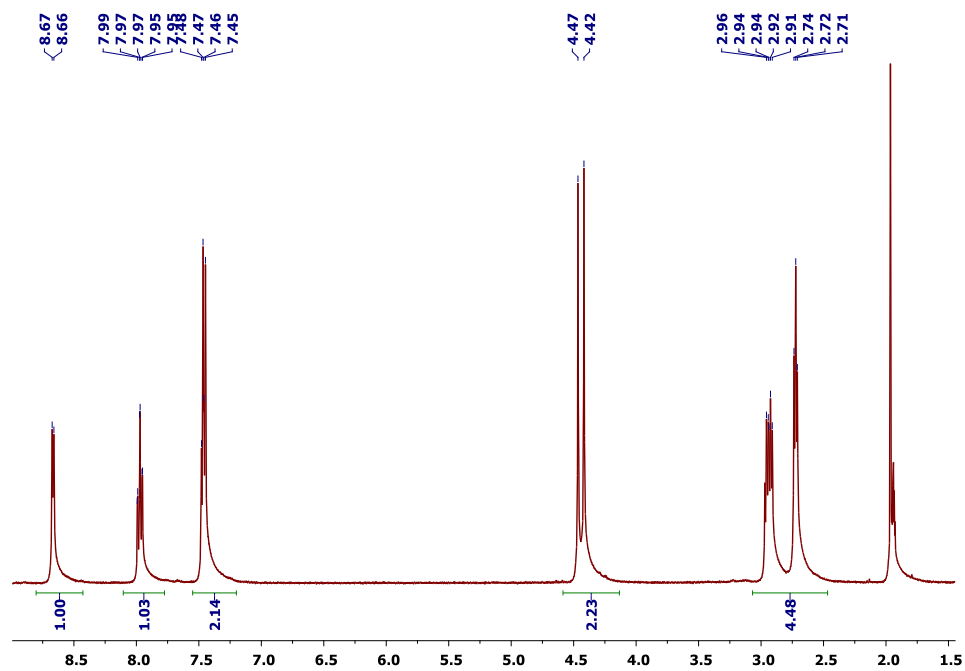


Figure 3.25. ^1H NMR spectrum of $[\text{PdTPAP}(\text{CH}_3\text{CN})][\text{BF}_4]_2$ (**5**) in CD_3CN .

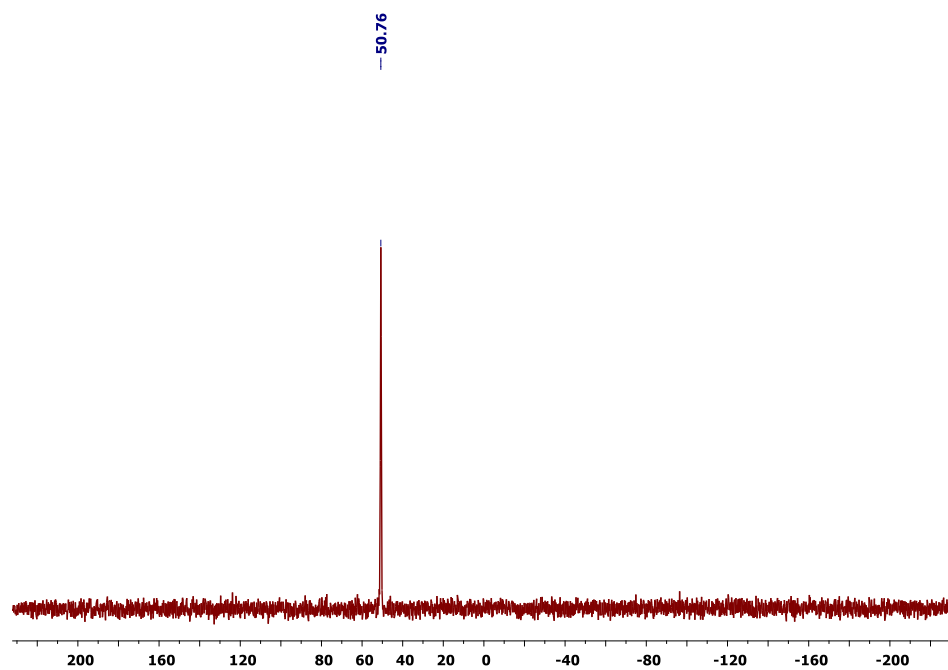


Figure 3.26. $^{31}\text{P}\{^1\text{H}\}$ NMR spectrum of $[\text{PdTPAP}(\text{CH}_3\text{CN})][\text{BF}_4]_2$ (**5**) in CD_3CN .

[PtTPAP(Cl)][PF₆]₂ (6): In the glove box, a solution of TPAP (78.1 mg, 0.175 mmol) in 6 mL of acetonitrile was added to a solution of PtCl₂(COD) (65.3 mg, 0.175 mmol) in 6 mL acetonitrile. The solution immediately turned tan and was stirred for 1 h at room temperature. Then a solution of AgPF₆ (68.0 mg, 0.350 mmol) in 2 mL acetonitrile was added in the dark and stirred for 5 min. The solvent was removed under reduced pressure. The white solid was re-dissolved in dichloromethane and filtered through a medium fritted funnel. The solvent was removed under reduced pressure. The resulting white solid was re-dissolved in acetonitrile and filtered through a glass pipette packed with a glass microfiber filter (22 μm). The filtrate was recrystallized by addition of diethyl ether. Only single crystals of **6** were collected which contributed to the low yield of the pure sample. No attempts were made to further purify the crude product in order to increase the yield. X-ray quality crystals of **6** were grown from the same conditions as the recrystallization (17.3 mg, 0.021 mmol, 12.1% yield). ¹H NMR (CD₃CN, 600 MHz) δ = 2.64 (t, 2H, NCH₂CH₂N), 2.78 (m, 2H, NCH₂CH₂N), 2.89 (m, 6H, NCH₂CH₂N), 3.17 (m, 2H, NCH₂CH₂N), 3.97 (d, 2H, PyCH₂), 4.25 (dd, 2H, PyCH₂), 4.88 (dd, 2H, PyCH₂), 6.75 (d, 1H, Py), 7.27 (m, 1H, Py), 7.46 (t, 2H, Py), 7.61 (m, 3H, Py), 8.08 (t, 2H, Py), 8.42 (m, 1H, Py), 8.95 (m, 2H, Py). ³¹P{¹H} NMR (CD₃CN, 243 MHz) δ = 39.8. ESI-MS (m/z): [M - PF₄]⁺. Calculation for C₂₄H₃₀N₇PPtCl, 677.2; found, 677.1. Analytical calculation for C₂₄H₃₀ClF₆N₇P₂Pt: C, 35.02; H, 3.67; N, 11.91. Found: C, 34.96; H, 3.51; N, 11.84.

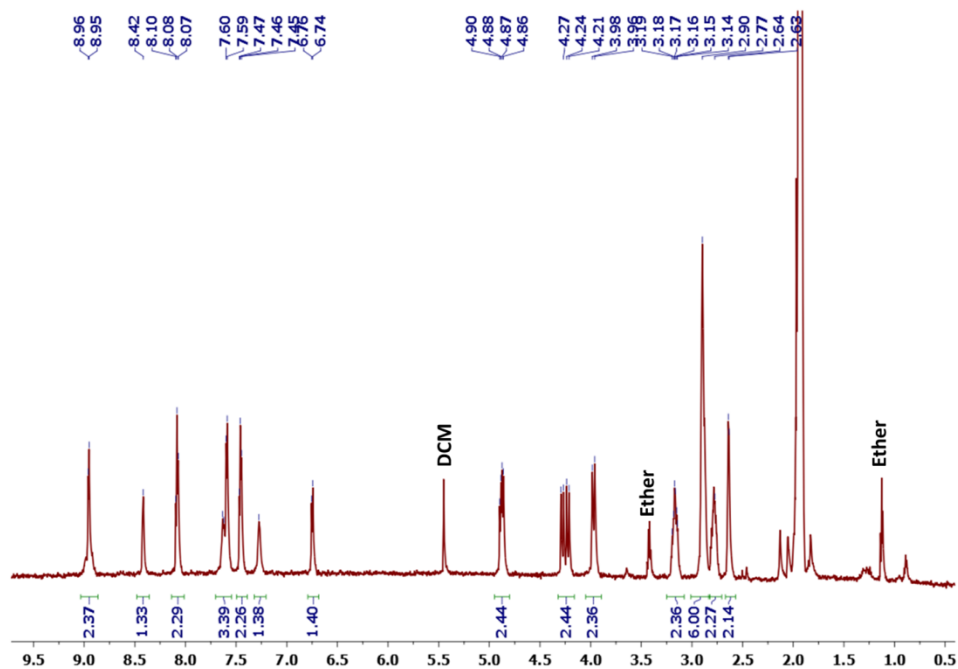


Figure 3.27. ^1H NMR spectrum of $[\text{PtTPAPCl}][\text{PF}_6]_2$ (**6**) in CD_3CN .

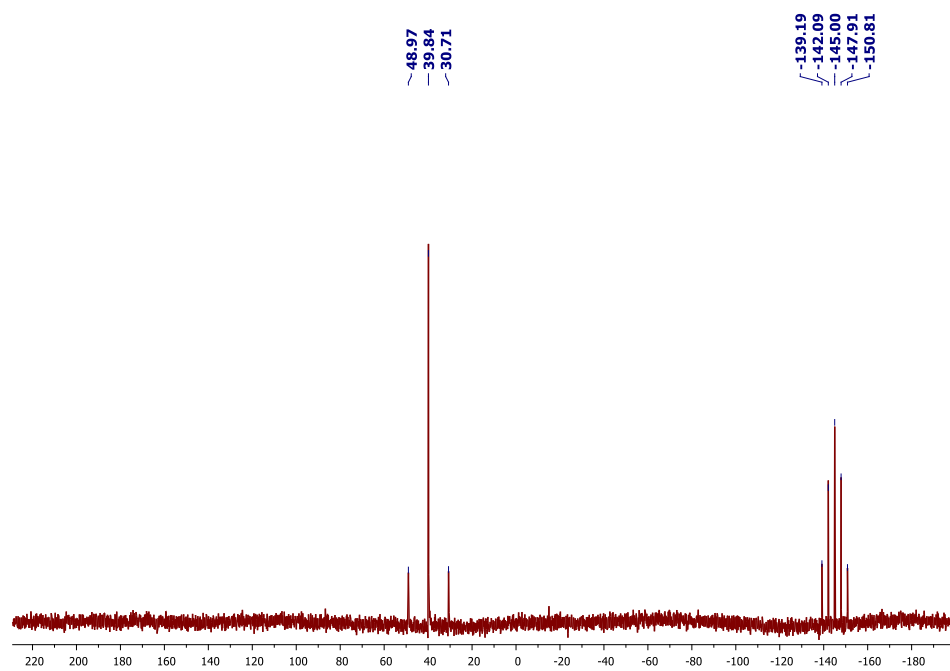


Figure 3.28. $^{31}\text{P}\{^1\text{H}\}$ NMR spectrum of $[\text{PtTPAPCl}][\text{PF}_6]_2$ (**6**) in CD_3CN .

3.6. References

1. Moret, M.-E.; Zhang, L.; Peters, J. C., A Polar Copper–Boron One-Electron σ -Bond. *Journal of the American Chemical Society* **2013**, *135* (10), 3792-3795.
2. Anderson, J. S.; Rittle, J.; Peters, J. C., Catalytic conversion of nitrogen to ammonia by an iron model complex. *Nature* **2013**, *501*, 84.
3. Rittle, J.; Peters, J. C., Fe–N₂/CO complexes that model a possible role for the interstitial C atom of FeMo-cofactor (FeMoco). *Proceedings of the National Academy of Sciences* **2013**, *110* (40), 15898.
4. Creutz, S. E.; Peters, J. C., Catalytic Reduction of N₂ to NH₃ by an Fe–N₂ Complex Featuring a C-Atom Anchor. *Journal of the American Chemical Society* **2014**, *136* (3), 1105-1115.
5. Moret, M.-E.; Peters, J. C., N₂ Functionalization at Iron Metallaboratranes. *Journal of the American Chemical Society* **2011**, *133* (45), 18118-18121.
6. Anderson, J. S.; Moret, M.-E.; Peters, J. C., Conversion of Fe–NH₂ to Fe–N₂ with release of NH₃. *Journal of the American Chemical Society* **2013**, *135* (2), 534-537.
7. Del Castillo, T. J.; Thompson, N. B.; Suess, D. L. M.; Ung, G.; Peters, J. C., Evaluating Molecular Cobalt Complexes for the Conversion of N₂ to NH₃. *Inorganic Chemistry* **2015**, *54* (19), 9256-9262.
8. Rauch, M.; Parkin, G., Zinc and Magnesium Catalysts for the Hydrosilylation of Carbon Dioxide. *Journal of the American Chemical Society* **2017**, *139* (50), 18162-18165.
9. Rauch, M.; Rucolo, S.; Parkin, G., Synthesis, Structure, and Reactivity of a Terminal Magnesium Hydride Compound with a Carbatrane Motif, [TismPriBenz]MgH: A Multifunctional Catalyst for Hydrosilylation and Hydroboration. *Journal of the American Chemical Society* **2017**, *139* (38), 13264-13267.
10. Chakrabarti, N.; Rucolo, S.; Parkin, G., Cadmium Compounds with an [N₃C] Atrane Motif: Evidence for the Generation of a Cadmium Hydride Species. *Inorganic Chemistry* **2016**, *55* (23), 12105-12109.
11. Rucolo, S.; Sattler, W.; Rong, Y.; Parkin, G., Modulation of Zn–C Bond Lengths Induced by Ligand Architecture in Zinc Carbatrane Compounds. *Journal of the American Chemical Society* **2016**, *138* (44), 14542-14545.
12. Rucolo, S.; Rauch, M.; Parkin, G., Tris[(1-isopropylbenzimidazol-2-yl)dimethylsilyl]methyl metal complexes, [TismPriBenz]M: a new class of metallacarbatranes, isomerization to a tris(N-heterocyclic carbene) derivative, and evidence for an inverted ligand field. *Chemical Science* **2017**, *8* (6), 4465-4474.
13. Rudd, P. A.; Planas, N.; Bill, E.; Gagliardi, L.; Lu, C. C., Dinitrogen Activation at Iron and Cobalt Metallalumatrane. *European Journal of Inorganic Chemistry* **2013**, *2013* (22-23), 3898-3906.
14. Vollmer, M. V.; Xie, J.; Lu, C. C., Stable Dihydrogen Complexes of Cobalt(–I) Suggest an Inverse trans-Influence of Lewis Acidic Group 13 Metalloligands. *Journal of the American Chemical Society* **2017**, *139* (19), 6570-6573.

15. Cammarota, R. C.; Lu, C. C., Tuning Nickel with Lewis Acidic Group 13 Metalloligands for Catalytic Olefin Hydrogenation. *Journal of the American Chemical Society* **2015**, *137* (39), 12486-12489.
16. Cammarota, R. C.; Vollmer, M. V.; Xie, J.; Ye, J.; Linehan, J. C.; Burgess, S. A.; Appel, A. M.; Gagliardi, L.; Lu, C. C., A Bimetallic Nickel–Gallium Complex Catalyzes CO₂ Hydrogenation via the Intermediacy of an Anionic d¹⁰ Nickel Hydride. *Journal of the American Chemical Society* **2017**, *139* (40), 14244-14250.
17. Buss, J. A.; Agapie, T., Four-electron deoxygenative reductive coupling of carbon monoxide at a single metal site. *Nature* **2015**, *529*, 72.
18. Buss, J. A.; Agapie, T., Mechanism of Molybdenum-Mediated Carbon Monoxide Deoxygenation and Coupling: Mono- and Dicarbonyl Complexes Precede C–O Bond Cleavage and C–C Bond Formation. *Journal of the American Chemical Society* **2016**, *138* (50), 16466-16477.
19. Horak, K. T.; VanderVelde, D. G.; Agapie, T., Tuning of Metal Complex Electronics and Reactivity by Remote Lewis Acid Binding to π -Coordinated Pyridine Diphosphine Ligands. *Organometallics* **2015**, *34* (19), 4753-4765.
20. Horak, K. T.; Lin, S.; Rittle, J.; Agapie, T., Heterometallic Effects in Trinuclear Complexes Supported by p-Terphenyl Diphosphine Ligands. *Organometallics* **2015**, *34* (18), 4429-4432.
21. Edouard, G. A.; Kelley, P.; Herbert, D. E.; Agapie, T., Aryl Ether Cleavage by Group 9 and 10 Transition Metals: Stoichiometric Studies of Selectivity and Mechanism. *Organometallics* **2015**, *34* (21), 5254-5277.
22. Horak, K. T.; Agapie, T., Dioxygen Reduction by a Pd(0) Hydroquinone Diphosphine Complex. *Journal of the American Chemical Society* **2016**, *138* (10), 3443-3452.
23. Buss, J. A.; Edouard, G. A.; Cheng, C.; Shi, J.; Agapie, T., Molybdenum Catalyzed Ammonia Borane Dehydrogenation: Oxidation State Specific Mechanisms. *Journal of the American Chemical Society* **2014**, *136* (32), 11272-11275.
24. Henthorn, J. T.; Agapie, T., Modulation of Proton-Coupled Electron Transfer through Molybdenum–Quinonoid Interactions. *Inorganic Chemistry* **2016**, *55* (11), 5337-5342.
25. Henthorn, J. T.; Lin, S.; Agapie, T., Combination of Redox-Active Ligand and Lewis Acid for Dioxygen Reduction with π -Bound Molybdenum-Quinonoid Complexes. *Journal of the American Chemical Society* **2015**, *137* (4), 1458-1464.
26. Tsui, E. Y.; Agapie, T., Carbon dioxide cleavage by a Ni₂ complex supported by a binucleating bis(N-heterocyclic carbene) framework. *Polyhedron* **2014**, *84*, 103-110.
27. Lin, S.; Herbert, D. E.; Velian, A.; Day, M. W.; Agapie, T., Dipalladium(I) Terphenyl Diphosphine Complexes as Models for Two-Site Adsorption and Activation of Organic Molecules. *Journal of the American Chemical Society* **2013**, *135* (42), 15830-15840.
28. Suseno, S.; Horak, K. T.; Day, M. W.; Agapie, T., Trinuclear Nickel Complexes with Metal–Arene Interactions Supported by Tris- and Bis(phosphinoaryl)benzene Frameworks. *Organometallics* **2013**, *32* (23), 6883-6886.
29. Horak, K. T.; Velian, A.; Day, M. W.; Agapie, T., Arene non-innocence in dinuclear complexes of Fe, Co, and Ni supported by a para-terphenyl diphosphine. *Chemical Communications* **2014**, *50* (34), 4427-4429.

30. Lin, S.; Day, M. W.; Agapie, T., Nickel Hydrides Supported by a Non-Innocent Diphosphine Arene Pincer: Mechanistic Studies of Nickel–Arene H-Migration and Partial Arene Hydrogenation. *Journal of the American Chemical Society* **2011**, *133* (11), 3828-3831.
31. Chao, S. T.; Lara, N. C.; Lin, S.; Day, M. W.; Agapie, T., Reversible Halide-Modulated Nickel–Nickel Bond Cleavage: Metal–Metal Bonds as Design Elements for Molecular Devices. *Angewandte Chemie International Edition* **2011**, *50* (33), 7529-7532.
32. Halter, D. P.; Heinemann, F. W.; Bachmann, J.; Meyer, K., Uranium-mediated electrocatalytic dihydrogen production from water. *Nature* **2016**, *530*, 317.
33. Bart, S. C.; Heinemann, F. W.; Anthon, C.; Hauser, C.; Meyer, K., A New Tripodal Ligand System with Steric and Electronic Modularity for Uranium Coordination Chemistry. *Inorganic Chemistry* **2009**, *48* (19), 9419-9426.
34. Fieser, M. E.; Palumbo, C. T.; La Pierre, H. S.; Halter, D. P.; Voora, V. K.; Ziller, J. W.; Furche, F.; Meyer, K.; Evans, W. J., Comparisons of lanthanide/actinide +2 ions in a tris(aryloxy)arene coordination environment. *Chemical Science* **2017**, *8* (11), 7424-7433.
35. Kárpáti, T.; Veszprémi, T.; Thirupathi, N.; Liu, X.; Wang, Z.; Ellern, A.; Nyulászi, L.; Verkade, J. G., Synthesis and Photoelectron Spectroscopic Studies of N(CH₂CH₂NMe)₃PE (E = O, S, NH, CH₂). *Journal of the American Chemical Society* **2006**, *128* (5), 1500-1512.
36. Tang, J. S.; Verkade, J. G., Synthesis and reactivity patterns of new proazaphosphatranes and quasi-azaphosphatranes ZP(MeNCH₂CH₂)₃N. *Journal of the American Chemical Society* **1993**, *115* (5), 1660-1664.
37. Liu, X.-D.; Verkade, J. G., Unusual Phosphoryl Donor Properties of OP(MeNCH₂CH₂)₃N. *Inorganic Chemistry* **1998**, *37* (20), 5189-5197.
38. Laramay, M. A. H.; Verkade, J. G., The "anomalous" basicity of P(NHCH₂CH₂)₃N relative to P(NMeCH₂CH₂)₃N and p(NBzCH₂CH₂)₃N: a chemical consequence of orbital charge balance? *Journal of the American Chemical Society* **1990**, *112* (25), 9421-9422.
39. Liu, X.; Bai, Y.; Verkade, J. G., Synthesis and structural features of new sterically hindered azaphosphatranes systems: ZP(RNCH₂CH₂)₃N. *Journal of Organometallic Chemistry* **1999**, *582* (1), 16-24.
40. Lensink, C.; Xi, S. K.; Daniels, L. M.; Verkade, J. G., The unusually robust phosphorus-hydrogen bond in the novel cation [cyclic] HP(NMeCH₂CH₂)₃N⁺. *Journal of the American Chemical Society* **1989**, *111* (9), 3478-3479.
41. Kisanga, P. B.; Verkade, J. G.; Schwesinger, R., pK_a Measurements of P(RNCH₂CH₂)₃N. *The Journal of Organic Chemistry* **2000**, *65* (17), 5431-5432.
42. D'Sa, B.; Kisanga, P.; McLeod, D.; Verkade, J., P(RNCH₂CH₂)₃N: Superbasic and Catalytic Cages. *Phosphorus, Sulfur, and Silicon and the Related Elements* **1997**, *124* (1), 223-232.
43. Wróblewski, A. E.; Pinkas, J.; Verkade, J. G., Strongly Basic Proazaphosphatranes: P(EtNCH₂CH₂)₃N and P(iso-PrNCH₂CH₂)₃N. *Main Group Chemistry* **1995**, *1* (1), 69-79.
44. Green, M. L. H.; Parkin, G., The classification and representation of main group element compounds that feature three-center four-electron interactions. *Dalton Transactions* **2016**, *45* (47), 18784-18795.

45. Liu, X.; Verkade, J. G., Free and Polymer-Bound Tricyclic Azaphosphatranes $\text{HP}(\text{RNCH}_2\text{CH}_2)_3\text{N}^+$: Pro-catalysts in Dehydrohalogenations and Debrominations with NaH. *The Journal of Organic Chemistry* **1999**, *64* (13), 4840-4843.
46. Kisanga, P.; McLeod, D.; Liu, X.; Yu, Z.; Ilankumaran, P.; Wang, Z.; McLaughlin, P. A.; Verkade, J. G., New Chemistry of $\text{ZP}(\text{RNCH}_2\text{CH}_2)_3\text{N}$ Systems. *Phosphorus, Sulfur, and Silicon and the Related Elements* **1999**, *144* (1), 101-104.
47. Xi, S. K.; Schmidt, H.; Lensink, C.; Kim, S.; Wintergrass, D.; Daniels, L. M.; Jacobson, R. A.; Verkade, J. G., Bridgehead-bridgehead communication in untransannulated phosphatrane $\text{ZP}(\text{ECH}_2\text{CH}_2)_3\text{N}$ systems. *Inorganic Chemistry* **1990**, *29* (12), 2214-2220.
48. Windus, T. L.; Schmidt, M. W.; Gordon, M. S., Theoretical Investigation of Azaphosphatrane Bases. *Journal of the American Chemical Society* **1994**, *116* (25), 11449-11455.
49. Laramay, M. A. H.; Verkade, J. G., Unusually Lewis basic Pro-azaphosphatranes. *Zeitschrift für anorganische und allgemeine Chemie* **1991**, *605* (1), 163-174.
50. Chatelet, B.; Gornitzka, H.; Dufaud, V.; Jeanneau, E.; Dutasta, J.-P.; Martinez, A., Superbases in Confined Space: Control of the Basicity and Reactivity of the Proton Transfer. *Journal of the American Chemical Society* **2013**, *135* (49), 18659-18664.
51. Raytchev, P. D.; Martinez, A.; Gornitzka, H.; Dutasta, J.-P., Encaging the Verkade's Superbases: Thermodynamic and Kinetic Consequences. *Journal of the American Chemical Society* **2011**, *133* (7), 2157-2159.
52. Galasso, V., Theoretical Study of the Structure and Bonding in Phosphatrane Molecules. *The Journal of Physical Chemistry A* **2004**, *108* (20), 4497-4504.
53. Verkade, J. G., Five-Coordinate and Quasi-Five-Coordinate Phosphorus. In *Phosphorus Chemistry*, American Chemical Society: 1992; Vol. 486, pp 64-75.
54. Tang, J. S.; Laramay, M. A. H.; Young, V.; Ringrose, S.; Jacobson, R. A.; Verkade, J. G., Stepwise transannular bond formation between the bridgehead atoms in $\text{Z-P}(\text{MeNCH}_2\text{CH}_2)_3\text{N}$ systems. *Journal of the American Chemical Society* **1992**, *114* (8), 3129-3131.
55. Su, W.; Urgaonkar, S.; Verkade, J. G., $\text{Pd}_2(\text{dba})_3/\text{P}(\text{i-BuNCH}_2\text{CH}_2)_3\text{N}$ -Catalyzed Stille Cross-Coupling of Aryl Chlorides. *Organic Letters* **2004**, *6* (9), 1421-1424.
56. Urgaonkar, S.; Nagarajan, M.; Verkade, J. G., $\text{Pd}/\text{P}(\text{i-BuNCH}_2\text{CH}_2)_3\text{N}$: an efficient catalyst for Suzuki cross-coupling of aryl bromides and chlorides with arylboronic acids. *Tetrahedron Letters* **2002**, *43* (49), 8921-8924.
57. You, J.; Verkade, J. G., $\text{P}(\text{i-BuNCH}_2\text{CH}_2)_3\text{N}$: An Efficient Ligand for the Direct α -Arylation of Nitriles with Aryl Bromides. *The Journal of Organic Chemistry* **2003**, *68* (21), 8003-8007.
58. Nandakumar, M. V.; Verkade, J. G., One-Pot Sequential N and C Arylations: An Efficient Methodology for the Synthesis of trans 4-*N,N*-Diaryl Aminostilbenes. *Angewandte Chemie International Edition* **2005**, *44* (20), 3115-3118.
59. Venkat Reddy, C. R.; Urgaonkar, S.; Verkade, J. G., A Highly Effective Catalyst System for the Pd-Catalyzed Amination of Vinyl Bromides and Chlorides. *Organic Letters* **2005**, *7* (20), 4427-4430.

60. Urgaonkar, S.; Nagarajan, M.; Verkade, J. G., P(i-BuNCH₂CH₂)₃N: An Effective Ligand in the Palladium-Catalyzed Amination of Aryl Bromides and Iodides. *The Journal of Organic Chemistry* **2003**, *68* (2), 452-459.
61. Aneetha, H.; Wu, W.; Verkade, J. G., Stereo- and Regioselective Pt(DVDS)/P(iBuNCH₂CH₂)₃N-Catalyzed Hydrosilylation of Terminal Alkynes. *Organometallics* **2005**, *24* (11), 2590-2596.
62. Thammavongsy, Z.; Kha, I. M.; Ziller, J. W.; Yang, J. Y., Electronic and steric Tolman parameters for proazaphosphatranes, the superbases core of the tri(pyridylmethyl)azaphosphatrane (TPAP) ligand. **2016**.
63. Thammavongsy, Z.; Khosrowabadi Kotyk, J. F.; Tsay, C.; Yang, J. Y., Flexibility is Key: Synthesis of a Tripyridylamine (TPA) Congener with a Phosphorus Apical Donor and Coordination to Cobalt(II). *Inorganic Chemistry* **2015**, *54* (23), 11505-11510.
64. Chatelet, B.; Nava, P.; Clavier, H.; Martinez, A., Synthesis of Gold(I) Complexes Bearing Verkade's Superbases. *European Journal of Inorganic Chemistry* **2017**, *2017* (37), 4311-4316.
65. Yang, L.; Powell, D. R.; Houser, R. P., Structural variation in copper(I) complexes with pyridylmethanamide ligands: structural analysis with a new four-coordinate geometry index, τ_4 . *Dalton Transactions* **2007**, (9), 955-964.
66. Addison, A. W.; Rao, T. N.; Reedijk, J.; van Rijn, J.; Verschoor, G. C., Synthesis, structure, and spectroscopic properties of copper(II) compounds containing nitrogen-sulphur donor ligands; the crystal and molecular structure of aqua[1,7-bis(*N*-methylbenzimidazol-2'-yl)-2,6-dithiaheptane]copper(II) perchlorate. *Journal of the Chemical Society, Dalton Transactions* **1984**, (7), 1349-1356.
67. Pinkas, J.; Tang, J.; Wan, Y.; Verkade, J. G., Chemical Games with Molecular Footballs, Darts and Paddlewheels. *Phosphorus, Sulfur, and Silicon and the Related Elements* **1994**, *87* (1-4), 193-207.
68. Kingston, J. V.; Verkade, J. G.; Espenson, J. H., 3/2-Order Chain Kinetics Involving a Postulated Dicationic Intermediate in the Isomerization of a P-Isocyano to a P-Cyano Azaphosphatrane Monocation. *Journal of the American Chemical Society* **2005**, *127* (43), 15006-15007.
69. Verkade, J. G., P(RNCH₂CH₂)₃N: Very Strong Non-Ionic Bases Useful in Organic Synthesis. In *New Aspects in Phosphorus Chemistry II*, Majoral, J.-P., Ed. Springer Berlin Heidelberg: Berlin, Heidelberg, 2003; pp 1-44.
70. Aghazadeh Meshgi, M.; Zitz, R.; Walewska, M.; Baumgartner, J.; Marschner, C., Tuning the Si-N Interaction in Metalated Oligosilanyl silatranes. *Organometallics* **2017**, *36* (7), 1365-1371.
71. Zhao, Y.; Truhlar, D. G., The M06 suite of density functionals for main group thermochemistry, thermochemical kinetics, noncovalent interactions, excited states, and transition elements: two new functionals and systematic testing of four M06-class functionals and 12 other functionals. *Theoretical Chemistry Accounts* **2008**, *120* (1), 215-241.
72. Brennan, M. R.; Kim, D.; Fout, A. R., A synthetic and mechanistic investigation into the cobalt(I) catalyzed amination of aryl halides. *Chemical Science* **2014**, *5* (12), 4831-4839.

73. Coucouvanis, D., Useful Reagents and Ligands. In *Inorganic Syntheses*, Coucouvanis, D., Ed. John Wiley & Sons, Inc.: 2002; Vol. 33, pp 75-121.
74. Harris Robin, K.; Becker Edwin, D.; Cabral de Menezes Sonia, M.; Goodfellow, R.; Granger, P., NMR nomenclature. Nuclear spin properties and conventions for chemical shifts(IUPAC Recommendations 2001). In *Pure and Applied Chemistry*, 2001; Vol. 73, p 1795.

CHAPTER 4

Small Molecule Activation with Transition Metal

Tris(2-pyridylmethyl)azaphosphatrane Complexes

4.1. Motivation and Specific Aims

This chapter is divided into three sections and concentrates on individual small molecule activation reactions with transition metal tris(2-pyridylmethyl)azaphosphatrane (TPAP) complexes. The first section will focus on CO₂ reduction to CO on a Ni(0)(TPAP) complex, followed by O₂ reactivity with a Cu(I)(TPAP) complex, and the last section will highlight hydride complexes of Ir(III)(TPAP) for H₂ activation.

4.1.1. CO₂ Reduction

The rapid burning of fossil fuels has led to increasing concentration of CO₂ in our atmosphere, causing adverse effects on our planet. Research on converting CO₂ to valued chemical commodities is the goal for a net carbon neutral cycle. A fundamental step to accomplish this task is to activate the CO₂ molecule by binding it to a transition metal center. In this chapter, efforts are made to bind and reduce CO₂ to CO with a Ni(0)(TPAP) complex.

4.1.2. O₂ Reactivity

Metalloenzymes serve as models for chemists who seek to mimic their functionality and understand their structures. One example is the tyrosinase enzyme, which controls the production of melanin by oxidation of phenolic precursors to form ortho-quinones. Chemists had synthesized model complexes of the dicopper active site of tyrosinase to investigate potential key intermediates in its reaction with O₂. This chapter aims to add to the rich bioinorganic reactivity of tyrosinase biomimics through studying the reaction of O₂ with a Cu(I)(TPAP) complex. Copper complexes with strong donor ligands have previously been hypothesized to trigger O-O bond cleavage to yield more reactive species.¹

4.1.3. Hydrogenation (H₂)

Hydrogenation is one of the most important reactions in chemistry. Nobel prizes have been issued to organometallic chemists in two separate years for their work in this area; Wilkinson's Rh catalyst for the hydrogenation of olefins and the Noyori chiral Ru catalyst for the asymmetric hydrogenation of carbonyls. Homogenous hydrogenation catalysis is still an active research area, with chemists designing and synthesizing intricate ligands to push the efficiency and selectivity of hydrogenation reactions. This chapter aims to add to the rich chemistry of Ir hydrogenation catalysts by synthesizing Ir-hydride complexes with TPAP, a strong σ donating azaphosphatrane ligand.

4.2. Background

4.2.1. Ni-CO₂ Complexes

Aresta structurally characterized the first Ni-CO₂ complex in 1975, which demonstrated the importance of strong donor ligands to generate an electron rich Ni(0) center for CO₂ binding (Figure 4.1).² Aresta suggested that "the strength of the Ni-CO₂ bond should decrease on increasing the acidity of the phosphorus ligand." This meant that a very strong donor, such as the proazaphosphatrane molecule, could strengthen the Ni-CO₂ bond, and consequently weaken the double bond of CO₂. Years later, Hillhouse³ and Lee⁴ structurally characterized the second and third mononuclear Ni-CO₂ complexes, respectively (Figure 4.1). In Hillhouse's system, he demonstrated the reduction of CO₂ to CO on a Ni complex with bidentate diphosphines, while Lee and coworkers utilized a tridentate triphosphine ligand system with Ni. In all three systems, phosphine donors are used with a Ni(0) metal center.

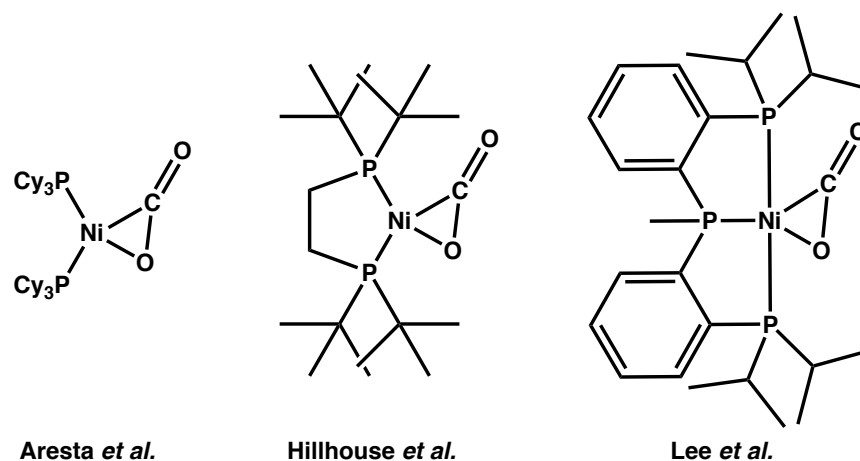


Figure 4.1. Structurally characterized Ni-CO₂ mononuclear complexes.

In this chapter, the reactivity of Ni(0)(TPAP)(COD) complex from chapter 3 is explored with CO₂ in order to investigate its CO₂ binding and reduction activity.

4.2.2. Cu₂O₂ Complexes

The supporting ligand plays a big role in stabilizing the bis(μ-oxo)dicopper core. The characterized structures of bis(μ-oxo)dicopper complexes have been with bi- or tri-dentate nitrogen donating ligand systems. Work from Tolman and coworkers confirmed the structure of a bis(μ-oxo)dicopper complex with a tridentate N ligand. The Cu₂O₂ core was isolated in the isomeric form that is pivotal to the activation of O₂ (Figure 4.2).⁵ Stack later noticed that square-planar coordination geometries dominated trivalent Cu complexes; therefore, he opted for sterically demanding bidentate N ligands for isolation of Cu₂O₂ complexes (Figure 4.2). This ligand design proved useful as Stack was able to study multiple bis(μ-oxo)dicopper complexes with variations of the *N*-peralkylated diamine ligand.⁶ Meyer⁷ was also successful in using a bidentate ligand system and was able to structurally characterize a bis(μ-oxo)dicopper complex (Figure 4.2).

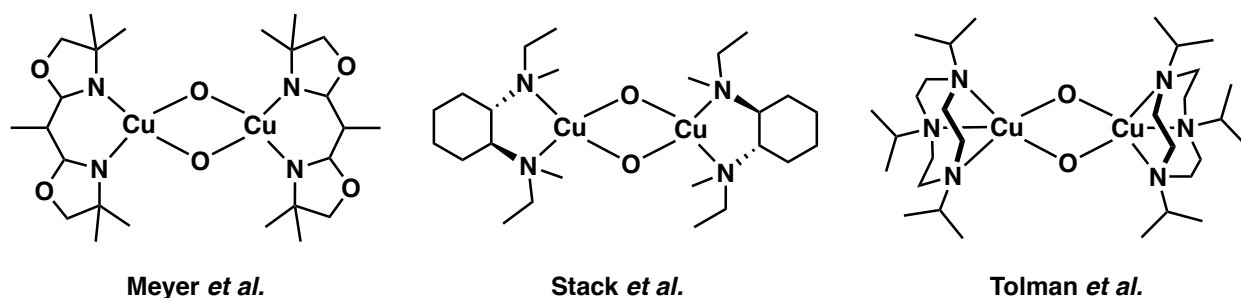


Figure 4.2. Structurally characterized Cu_2O_2 complexes with di- and tri-dentate N ligands.

Another ligand design tip from Stack was to use “bidentate strong sigma-donors” for “optimal thermodynamic stabilization of the d^8 Cu(III) site” in bis(μ -oxo)dicopper complexes.⁶ The TPAP system is a strong sigma donor ligand and is flexible to coordinate in a bi-, tri- or tetradentate fashion to a transition metal ion.

4.2.3. Ir- H_2 Complexes

Strong sigma donating ligands have been shown to increase the rate of hydrogenation in organometallic chemistry. Bercaw and coworkers demonstrated the hydrogenation of cyclooctene to cyclooctane with an Ir(III) N-heterocyclic carbene (NHC) complex and H_2 .⁸ Although they were not able to isolate the activated H_2 intermediate, the Ir-hydride complex was hypothesized to be the active catalyst (Figure 4.3), as most Ir catalyzed hydrogenation reactions often involve hydridoiridium(III) catalytic precursors.⁹⁻¹¹ Another strongly donating NHC system was used in Nozaki’s work for the hydrogenation of CO_2 with an Ir-PCP pincer complex (Figure 4.3). The high catalytic turnover (TON = 230,000) was “attributed to the stabilization of the cationic key transition state by the higher electron-donating nature of the PCP ligand.”¹² Lastly, Jagirdar and coworkers used a tris(pyrazolyl)methane sulfonate complex to stabilize an Ir(III) dihydride complex, which was the active catalyst in their study of olefin hydrogenation with H_2 .¹³ The crystal

structure displayed an octahedral geometry where two hydrides were positioned trans to two strongly donating pyrazolyl donors (Figure 4.3).

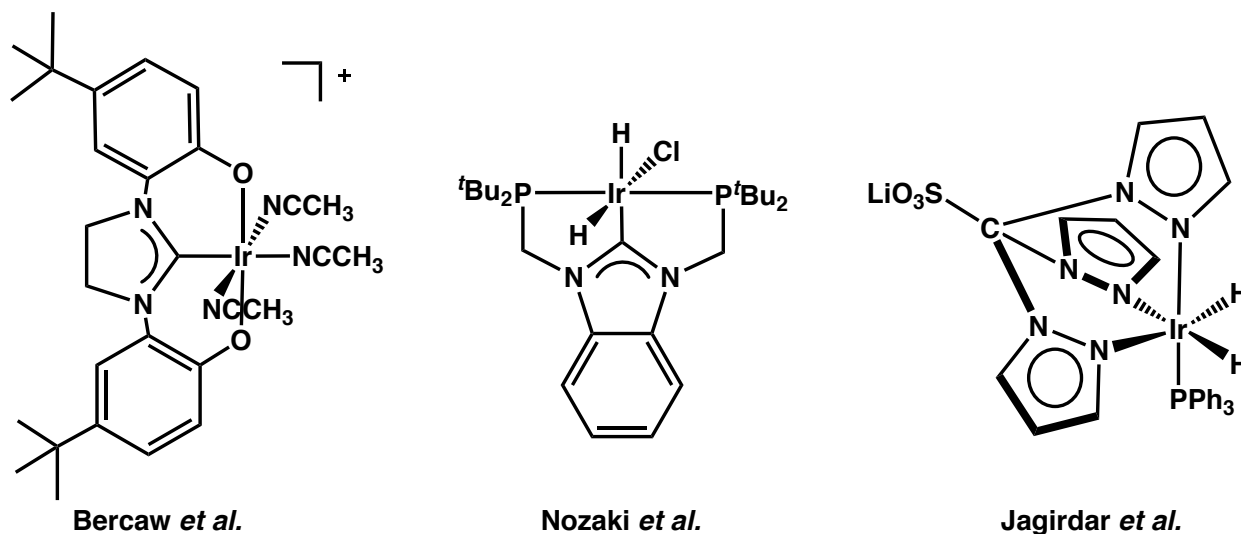


Figure 4.3. Ir(III) complexes bearing strong sigma donor ligands.

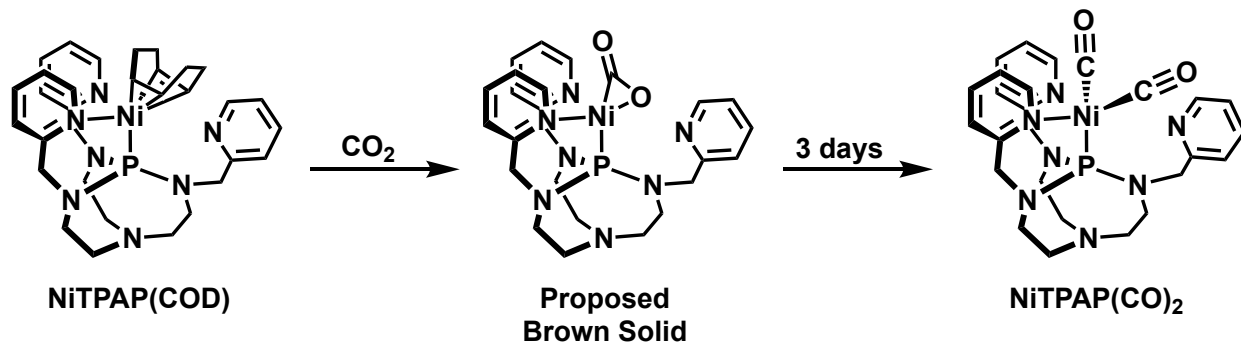
In this chapter, the Ir(III) monohydride (IrH(TPAP)Cl) and dihydride (Ir(H)₂(TPAP)) are synthesized for their potential use as hydrogenation catalysts.

4.3. Results and Discussion

4.3.1. Reaction of Ni(TPAP)(COD) with CO₂

A solution of Ni(TPAP)(COD) (characterized in Chapter 3) in C₆H₆ was added into a Schlenk tube and filled with CO₂ gas (Scheme 4.1). The color of the solution changed from dark green to brown. A brown solid was obtained when the solvent was removed under reduced pressure.

Scheme 4.1. Proposed reactivity of CO₂ with Ni(TPAP)(COD).



The brown solid displayed an IR stretching frequency at 1696 cm⁻¹ (Figure 4.4), which is in the range of structurally characterized Ni-CO₂ complexes.²⁻⁴ Multiple attempts to crystallize the brown solid via layering were unsuccessful.

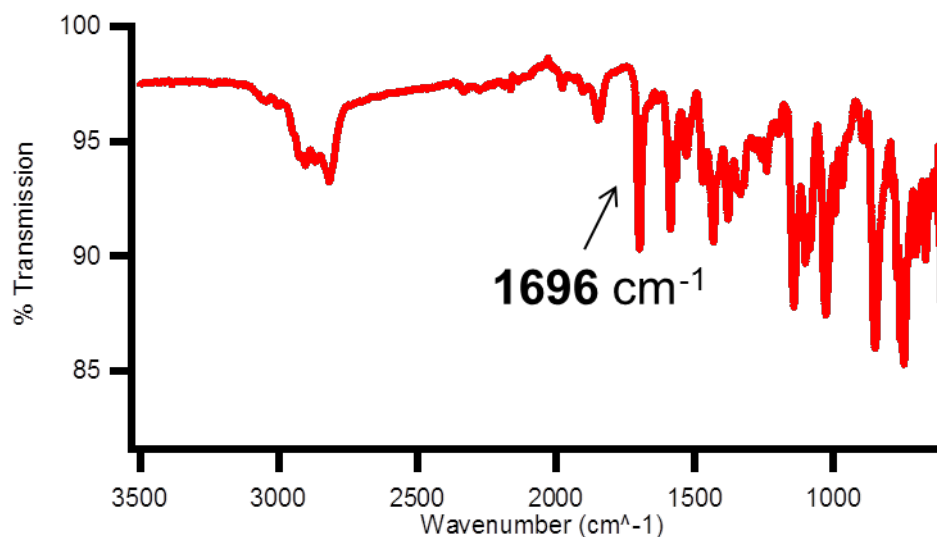


Figure 4.4. IR spectrum of brown solid from the reactivity of Ni(TPAP)(COD) with CO₂.

After 3 days at room temperature, the brown complex decomposed and the IR stretching frequency displayed two carbonyl stretching frequencies at 1981.7 and 1906.5 cm⁻¹ (Figure 4.5), matching the IR stretching frequency of Ni(TPAP)(CO)₂ (see Chapter 3). The reduction of CO₂ to

CO was seen in Hillhouse's system, where the electron rich phosphine ligands were oxidized by the oxygen of the CO₂ molecule. A similar reaction might also be possible with the TPAP system, given their strong donating ability.¹⁴ No further studies were performed to ascertain if TPAP=O was made. The ³¹P NMR signal of TPAP=O would be expected at 23.95 ppm (see Appendix B). In addition, the TPAP molecule can also react with CO₂, without the help of a transition metal ion. Verkade and coworkers previously showed the reactivity of proazaphosphatranes with CO₂ and CS₂.^{15, 16}

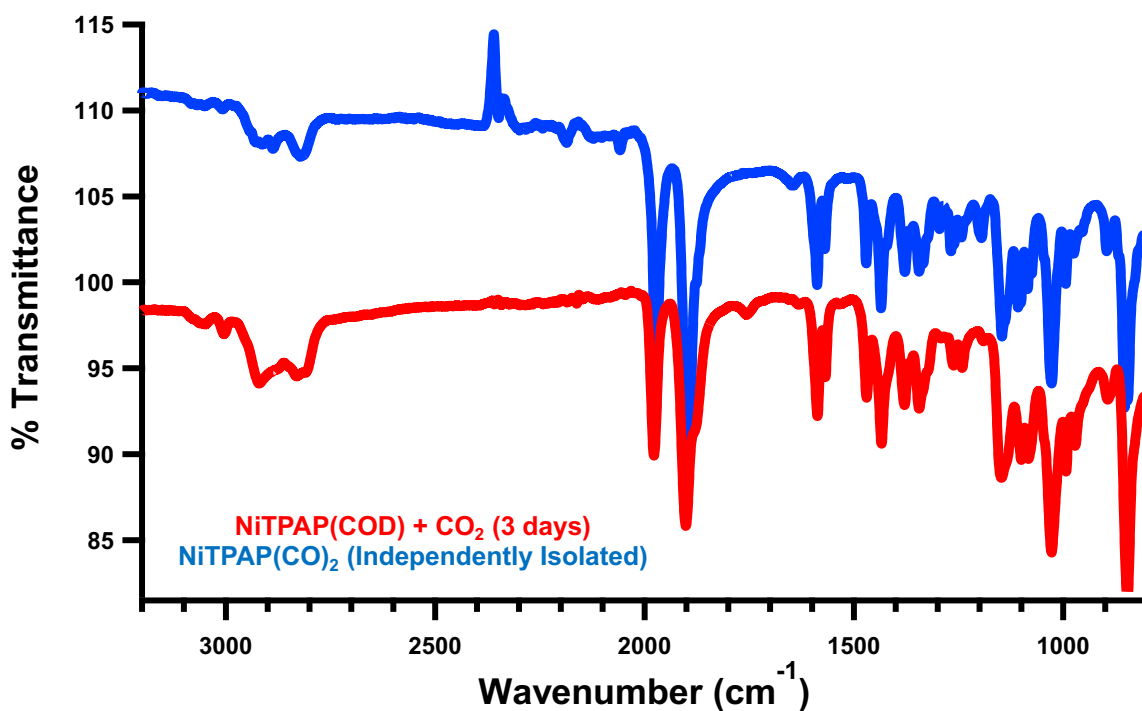


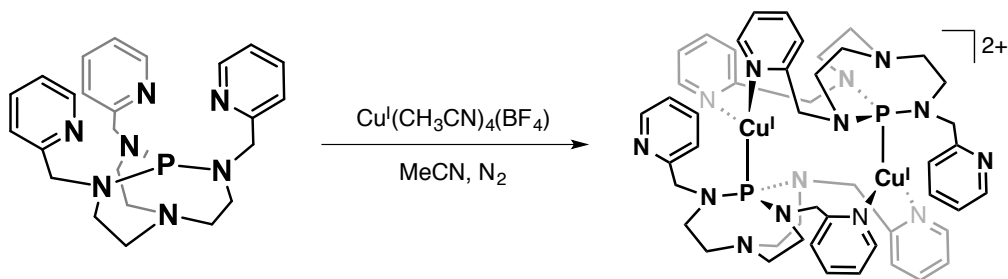
Figure 4.5. IR spectra of (blue) Ni(TPAP)(CO)₂ and (red) Ni(TPAP)(COD) + CO₂ after 3 days of sitting at room temperature.

4.3.2. Synthesis and Structure of Cu(TPAP) Complex

In the glove box, [Cu(CH₃CN)₄][BF₄] and TPAP were mixed in a 1:1 ratio in acetonitrile (Scheme 4.2). After 1 day of stirring, the solution change from colorless to light yellow. A yellow

solid was isolated after acetonitrile was removed. The ^1H NMR spectrum of the yellow solid exhibited resonances corresponding to equivalent protons from the pyridine and azaphosphatrane core, suggesting either coordination of all three pyridine donors to Cu(I) ion or a dynamic system where pyridine donors are rapidly binding and unbinding to the Cu(I) ion.

Scheme 4.2. Synthesis of $[\text{Cu}(\text{TPAP})]_2[\text{BF}_4]_2$ complex.



An X-ray quality crystal of $[\text{Cu}(\text{TPAP})]_2[\text{BF}_4]_2$ was grown by layering a solution of the yellow solid in dichloromethane with diethyl ether. The crystal structure displayed a bimetallic-Cu(TPAP) system with two Cu and two TPAP ligands, $[\text{Cu}(\text{TPAP})]_2[\text{BF}_4]_2$, where one TPAP ligand is coordinated to one Cu(I) site through the P, and coordinated to another Cu(I) site through two pyridine Ns (Figure 4.6). Both Cu(I) ions in the crystal structure displayed a trigonal geometry, and the Cu–Cu distance is 3.018 Å. The combined data of the ^1H NMR spectrum and crystal structure suggest the Cu(I) ion is in a different coordination environment in solution than the solid state.¹⁷

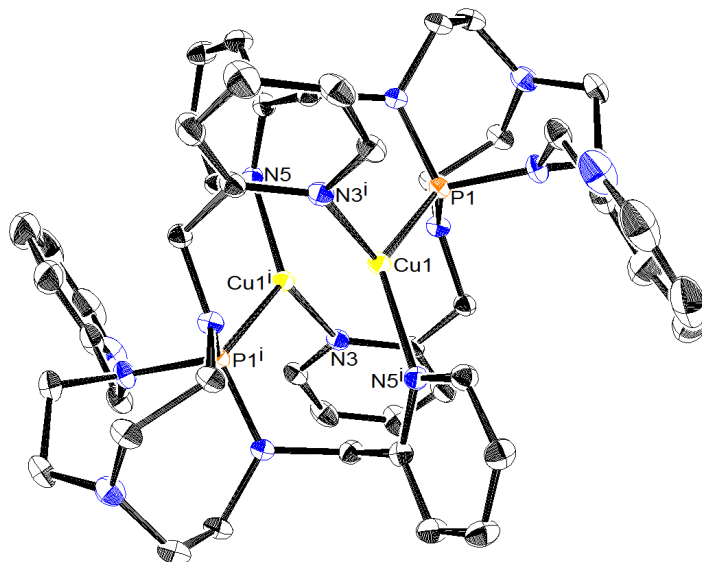


Figure 4.6. Crystal structure of $[\text{Cu}(\text{TPAP})]_2[\text{BF}_4]_2$. Thermal ellipsoids are drawn at 50% probability; hydrogen atoms and counter anions omitted for clarity.

4.3.3. Reaction of Cu(TPAP) with O_2

To a cuvette with 2.0 mmol solution of $[\text{Cu}(\text{TPAP})]_2[\text{BF}_4]_2$ in acetonitrile was added 1 mL of O_2 gas at room temperature. A color change from light yellow to green occurred overnight. The green solution was analyzed by UV-vis (Figure 4.7) and EPR spectroscopy (Figure 4.8). The UV-vis spectrum of $\text{Cu}(\text{TPAP}) + \text{O}_2$ displayed a d-d transition band at 666 nm, characteristic of a Cu(II) metal ion. For comparison, a UV-vis spectrum of Cu(TPAP) is displayed in Figure 4.7, which showed no d-d transition band due to the full shell of the d^{10} Cu(I) metal ion.

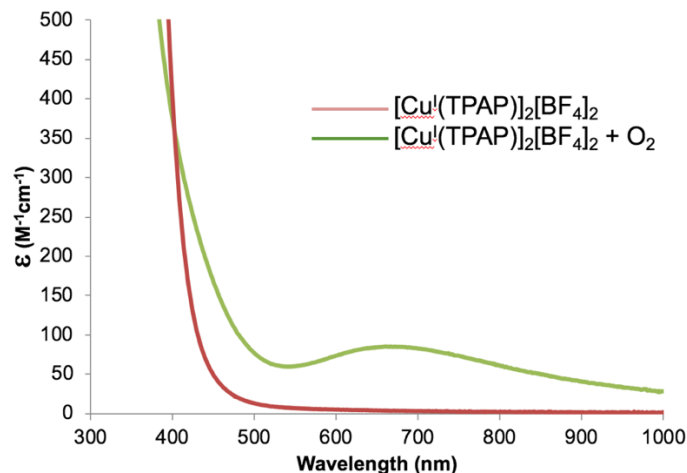


Figure 4.7. UV-vis spectra of (red) Cu(TPAP) and (green) Cu(TPAP) + O₂ in CH₃CN.

An EPR measurement was performed on the green product of Cu(TPAP) + O₂ at 77K, displaying a signal centered at $g = 2.07$. The g value of 2.07 corresponds to an $S = 1/2$, one unpaired electron Cu(II) metal ion. Additional features in the EPR presented a 4-line hyperfine coupling due to $I(\text{Cu}^{63}) = 3/2$. The attempted crystallization of the green product proved unsuccessful as the product decomposes within days.

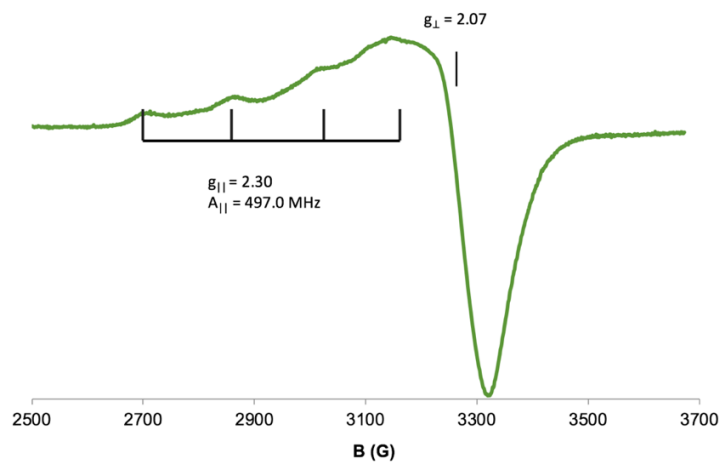
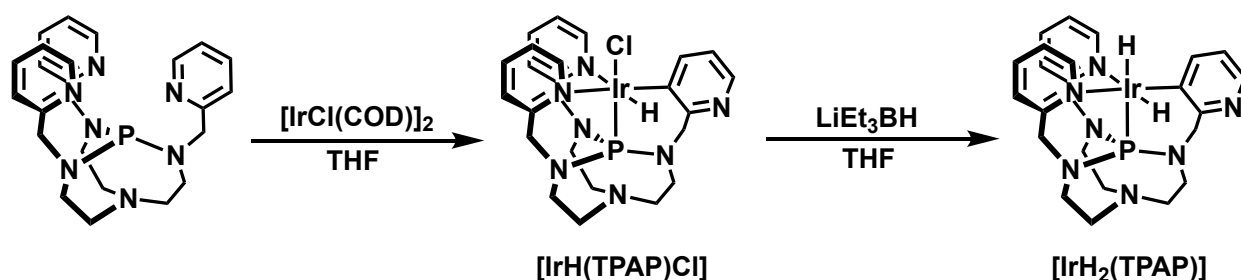


Figure 4.8. EPR spectrum of green product from the reaction of Cu(TPAP) with O₂ in CH₃CN at 77K.

4.3.4. Synthesis of IrH(TPAP)Cl

An IrH(TPAP)Cl complex was synthesized by stirring [Ir(COD)Cl]₂ (COD = 1,5-cyclooctadiene) and TPAP in a 1:1 ratio in tetrahydrofuran (Scheme 4.3). As the reaction was stirring, light orange solids precipitated out of solution. The solution was filtered through a medium fritted filter and the orange solid was washed with tetrahydrofuran. Colorless crystals were grown from a layered solution of the orange solid in dichloromethane with diethyl ether.

Scheme 4.3. Synthesis of IrH(TPAP)Cl and IrH₂(TPAP).



The ¹H NMR spectrum of the colorless crystals displayed a doublet at -21.62 ppm (*J*-coupling of 16.5 Hz), which is in the region of metal hydrides. The ³¹P{¹H} NMR spectrum displayed a doublet at 66.4 ppm, with a matching *J*-coupling of 16.5 Hz to that of the metal hydride signal in the ¹H NMR spectrum. This is consistent with other P-Ir-H *J*-coupling constant, where coupling is observed due to ¹H resonance residing outside of the decoupling window.¹⁸ X-ray analysis of the complex was performed and the structure revealed an octahedral coordination environment around the Ir(III) ion (Figure 4.9). The P, two pyridine Ns, and a Cl anion are coordinated to Ir(III), along with a C-H activated pyridine, where the C of the pyridine ring and a hydride are bound. The P⋯N_{ax} distance is 3.22 Å, which falls closer towards the “Pro” form of azaphosphatranes.

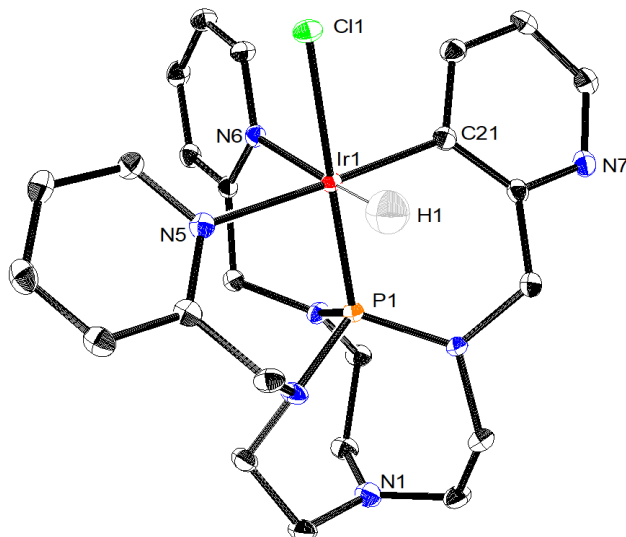


Figure 4.9. Crystal structure of IrH(TPAP)Cl. Solvents molecules (dichloromethane and diethyl ether) and hydrogens are omitted for clarity except for H1, which was located in the difference map and refined freely.

4.3.5. Synthesis of IrH₂(TPAP)

The Ir(III)-dihydride complex, IrH₂(TPAP), was synthesized by adding LiEt₃BH (1.0 M in tetrahydrofuran) into a cold mixture of IrH(TPAP)Cl (-35°C) in tetrahydrofuran via syringe (Scheme 4.3). The solution changed color from colorless to light yellow and was stirred for one hour before adding diethyl ether, during which time a white precipitate appeared. X-ray quality crystals were grown from slow vapor diffusion of pentane into a solution of IrH₂(TPAP) in tetrahydrofuran. The structure displayed similar coordination geometry as the IrH(TPAP)Cl complex, except the Cl anion was substituted with a hydride. The P⋯N_{ax} distance is 3.17 Å, similar to the P⋯N_{ax} distance of IrH(TPAP)Cl, due to the same Ir(III) oxidation state (Figure 4.10).¹⁹

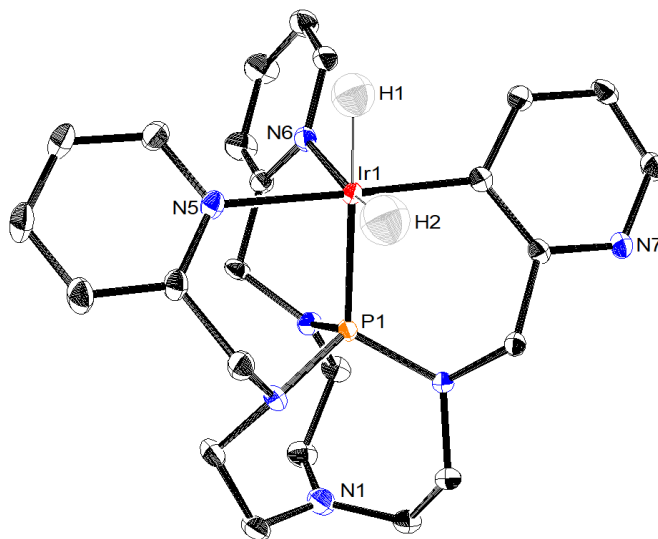


Figure 4.10. Crystal Structure of $[\text{IrH}_2(\text{TPAP})]$. Solvents molecule (tetrahydrofuran), LiCl , and hydrogens are omitted for clarity except for H1 and H2, which were located in the difference map and refined freely.

The ^1H NMR spectrum of crystalline $\text{IrH}_2(\text{TPAP})$ displayed two resonances in the metal-hydride region, a doublet at -3.90 ppm (J -coupling of 183 Hz) and a broad singlet at -21.2 ppm. The $^{31}\text{P}\{^1\text{H}\}$ NMR spectrum displayed a major resonance at 105.6 ppm and smaller resonances at 72.6 , 67.1 and 64.1 ppm, potentially due to unreacted starting material and impurities.

4.3.6. Reactivity of $\text{IrH}(\text{TPAP})\text{Cl}$ with H_2

No reaction was observed when H_2 was added directly to $\text{IrH}(\text{TPAP})\text{Cl}$. The $\text{IrH}(\text{TPAP})\text{Cl}$ complex must be treated with AgBF_4 first before H_2 addition, in order to provide an open coordination site for H_2 to bind. When AgBF_4 was added to $\text{IrH}(\text{TPAP})\text{Cl}$, grey solids appear in solution, likely due to AgCl . The solution was filtered and added into a J. Young tube, followed by the addition of H_2 gas. The ^1H NMR spectrum of the reaction displayed new resonances around the metal-hydride region (Figure 4.11). In addition, the $^{31}\text{P}\{^1\text{H}\}$ NMR spectrum is shifted from

66.4 ppm in IrH(TPAP)Cl to 89.6 ppm. Potential future reactions include adding CO₂ to this new Ir-hydride complex or IrH₂(TPAP).

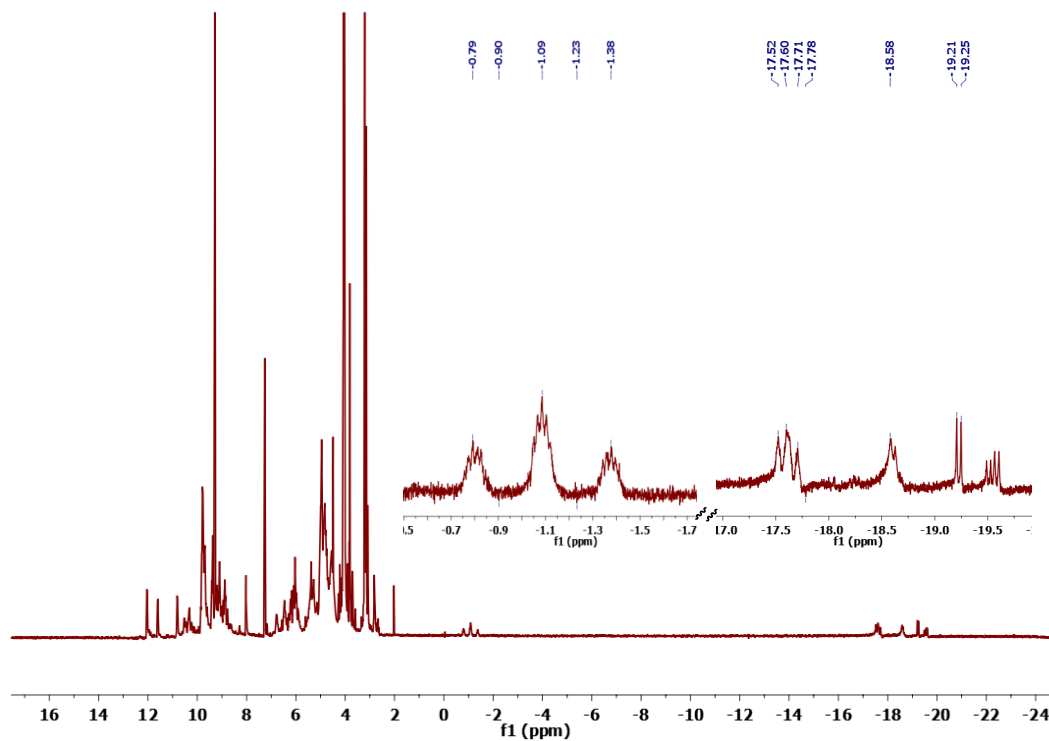


Figure 4.11. ¹H NMR spectrum of IrH(TPAP)Cl + AgBF₄ + H₂ in CD₂Cl₂. Inset displays a close-up view of the hydride region.

4.4. Conclusion

4.4.1. Ni(TPAP)(COD) + CO₂

The reactivity of CO₂ with Ni(TPAP)(COD) produced a brown solid with an IR vibrational frequency consistent with a CO₂ bound Ni(0) complex. The brown solid decomposed to Ni(TPAP)(CO)₂, which demonstrates the ability of the Ni(TPAP) system to activate and reduce CO₂ to CO.

4.4.2. Cu(TPAP) + O₂

A Cu(TPAP) complex was synthesized and characterized. In the solid state, the Cu(TPAP) complex is a dimeric complex, with a molecular formula of [Cu₂(TPAP)₂][BF₄]₂. In solution, all three pyridine donors are equivalent at room temperature. The Cu(TPAP) complex showed O₂ reactivity and the product was characterized as a Cu(II) metal ion by UV-vis and EPR spectroscopies.

4.4.3. IrH(TPAP)Cl + H₂

The synthesis and characterization of IrH(TPAP)Cl and IrH₂(TPAP) are presented. The reactivity of IrH(TPAP)Cl with H₂ was attempted but no reactions occurred until AgBF₄ was added. The cleavage of the Ir-Cl bond is important in order to provide an open coordination site for H₂ binding to the Ir(III) metal center.

4.5. Experimental Details

General Considerations

All manipulations were performed in the glovebox, as the complexes are air- and moisture-sensitive. All solvents were first purged with argon and dried using a solvent purification system. [Ir(COD)Cl]₂, [Cu(CH₃CN)₄][BF₄], Ni(0)(COD)₂, AgBF₄, CO₂, O₂ and H₂ were commercially purchased and used without further purification. Ni(TPAP)(COD) was synthesized according to an established procedure.¹⁹

Physical Methods

Nuclear Magnetic Resonance (NMR) Spectroscopy: Nuclear magnetic resonance (NMR) spectra were recorded on a DRX400 with a switchable QNP probe (¹H) or a Bruker AVANCE 600 MHz (³¹P). ¹H NMR spectra were referenced to (tetramethylsilane) TMS using the residual proteo

impurities of the solvent; $^{31}\text{P}\{^1\text{H}\}$ NMR spectroscopy experiments are referenced to an internal H_3PO_4 sample in D_2O or to H_3PO_4 using the Ξ scale with the corresponding ^1H spectra or referenced to the absolute frequency of 0 ppm in the ^1H dimension according to the Xi scale.²⁰

Infrared (IR) Spectroscopy: IR absorption was taken on a Thermo Scientific Nicolet iS5 spectrophotometer with an iD5 ATR attachment.

Ultraviolet-visible (UV-vis): UV-vis was collected in a 1cm fluoro cell in acetonitrile solution using Agilent Technologies Cary 60 UV-vis spectrometer and 8453 Diode-array UV-vis spectrometer equipped with Unisoku cryostat.

Electron Paramagnetic Resonance (EPR): Perpendicular-mode X-band electron paramagnetic resonance (EPR) spectrum was collected using a Bruker EMX spectrometer.

X-ray Crystallography (XRC): X-ray diffraction studies were carried out at the UCI Department of Chemistry X-ray Crystallography Facility on a Bruker SMART APEX II diffractometer. Data were collected at 88 K using Mo $\text{K}\alpha$ radiation ($\lambda = 0.71073 \text{ \AA}$). The APEX2 program package was used to determine the unit cell parameters and data collection. The raw frame data was processed using SAINT and SADABS to yield the reflection data file. Subsequent calculations were carried out using the SHELXTL program.

[Cu(TPAP)]₂[BF₄]₂: In the glove box, [Cu(CH₃CN)₄][BF₄] (40.9 mg, 0.130 mmol) was added to a solution of TPAP (58.2 mg, 0.130 mmol) in 3 mL of acetonitrile. The solution immediately turned light yellow and was stirred for 2 hours at room temperature. The solvent was removed under vacuum and the resulting yellow solid was washed with diethyl ether. The yellow solid was re-dissolved in dichloromethane and filtered through a glass pipette packed with a glass microfiber filter. Diethyl ether was layered on top of this solution to afford yellow crystals that were isolated in 81.18% yield. ¹H NMR (CD₃CN, 400 MHz) δ = 2.83 (m, 12H, NCH₂CH₂N), 4.03 (d, 6H, PyrCH₂N), 7.31 (t, 3H, Py), 7.39 (d, 3H, Py), 7.80 (t, 3H, Py), 8.51 (d, 3H, Py). ³¹P{¹H}NMR (CD₃CN, 243 MHz) δ = -11.78.

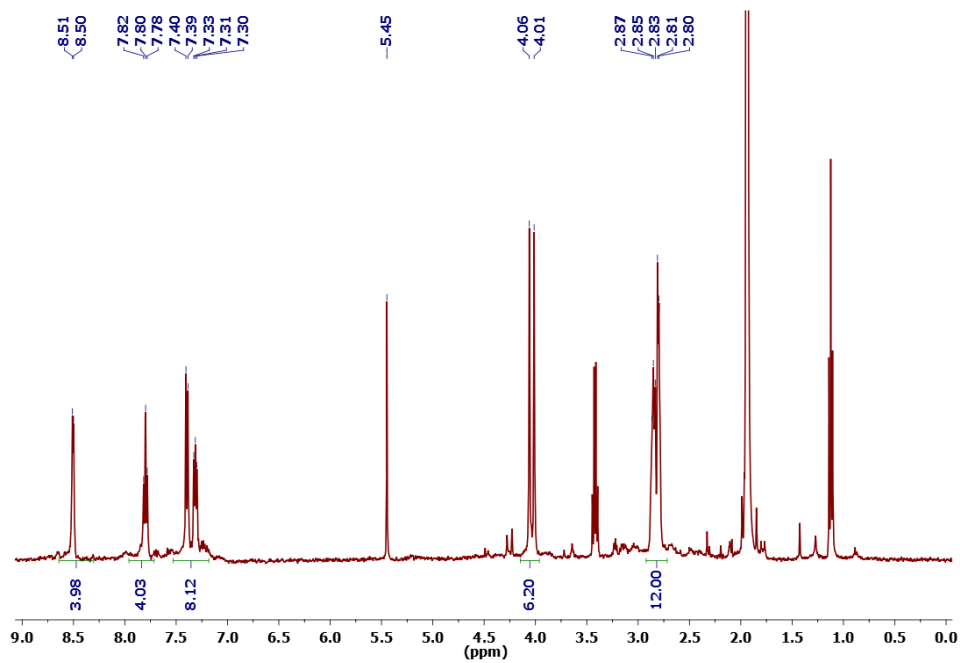


Figure 4.12. ^1H NMR spectrum of Cu(TPAP) complex in CD_3CN .

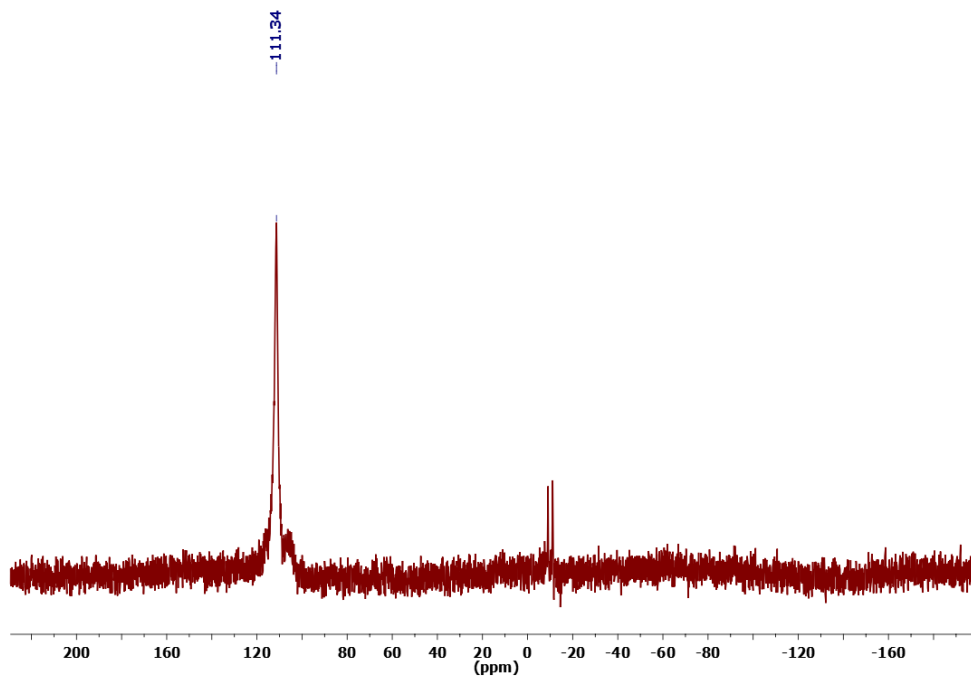


Figure 4.13. $^{31}\text{P}\{^1\text{H}\}$ NMR spectrum of Cu(TPAP) complex in CD_3CN .

IrH(TPAP)Cl: In the glove box, a solution of TPAP (80.0 mg, 0.223 mmol) in 5 mL tetrahydrofuran was added to a solution of [Ir(COD)Cl]₂ (61.5 mg, 0.223 mmol) in 8 mL tetrahydrofuran. An orange precipitate appeared after 30 min of stirring. The orange mixture was stirred for 1 day at room temperature. The solution was filtered through a medium fritted filter and washed with tetrahydrofuran, yielding a light orange solid. Colorless crystals were grown from a layered solution of the orange solid in dichloromethane with diethyl ether. ¹H NMR (CD₂Cl₂, 600 MHz) δ = -21.6. (d, *J*_{PH} = 6.5 Hz, P-Ir-H). ³¹P{¹H} NMR (CD₂Cl₂, 243 MHz) δ = 66.4. The yield is not reported due to the presence of solvent impurities in the ¹H NMR data.

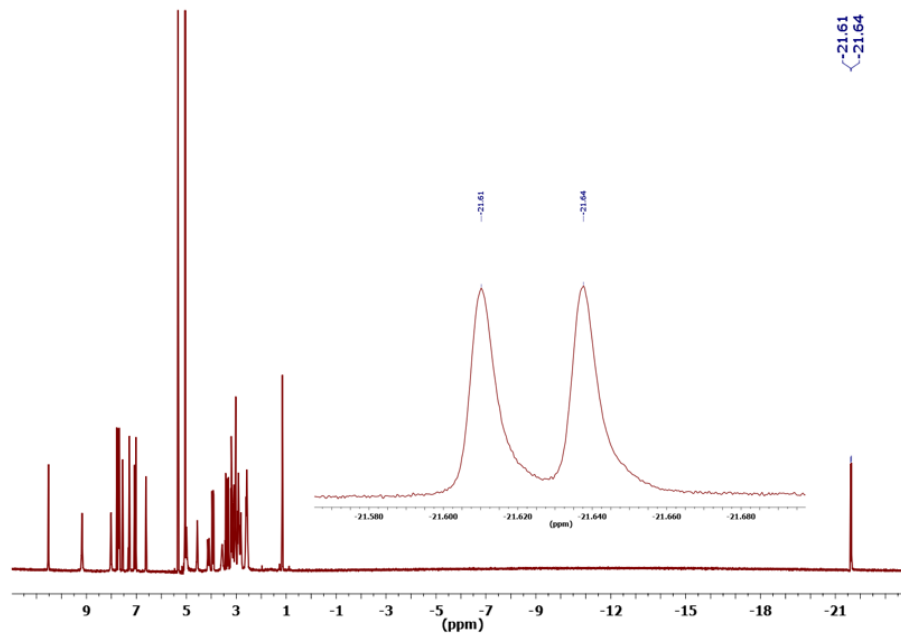


Figure 4.14. ^1H NMR spectrum of $\text{IrH}(\text{TPAP})\text{Cl}$ in CD_2Cl_2 . Inset display close up view of hydride region.

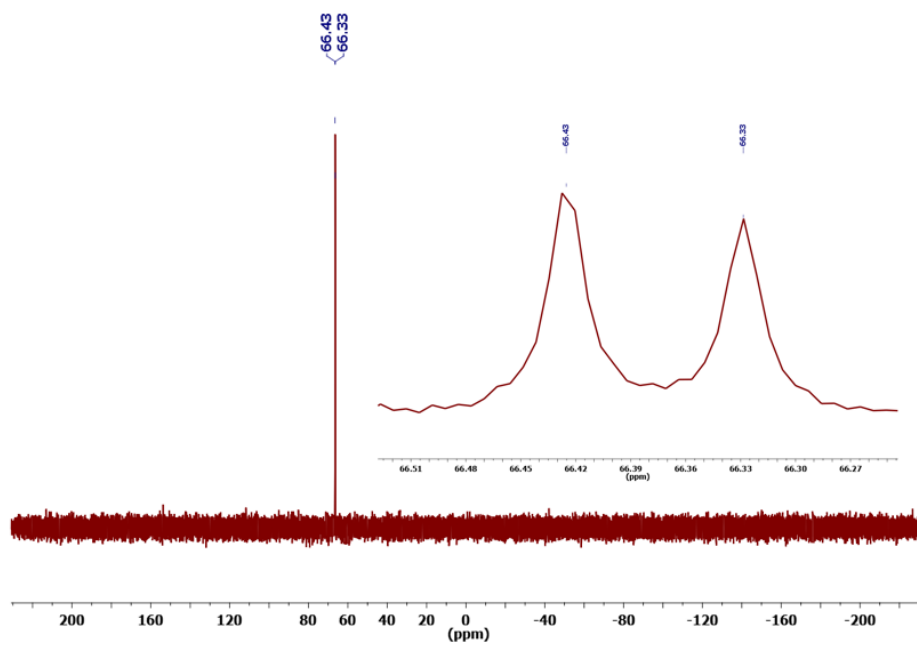


Figure 4.15. $^{31}\text{P}\{^1\text{H}\}$ NMR spectrum of $\text{IrH}(\text{TPAP})\text{Cl}$ in CD_2Cl_2 . Inset display close up view of resonance.

IrH₂(TPAP): In the glove box, a mixture of IrH(TPAP)Cl (50.0 mg, 0.160 mmol) in 3 mL tetrahydrofuran was cooled in a -35 °C freezer for 2 hours before adding LiEt₃BH 0.2 mL, 1.0 M in tetrahydrofuran) via 1 mL syringe. The mixture went into solution and a color change to light yellow occurred within 30 minutes. After 1 h, diethyl ether was added to the solution to produce a white solid. X-ray quality crystals were grown from slow vapor diffusion of pentane into a solution of IrH₂(TPAP) in tetrahydrofuran. ¹H NMR (CD₃CN, 600 MHz) δ = -3.90. (d, P-Ir-H_{ax}) and -21.2. (d, P-Ir-H_{eq}). ³¹P{¹H} NMR (CD₃CN, 243 MHz) δ = 105.6. The yield is not reported due to the presence of solvent impurities in the ¹H NMR data.

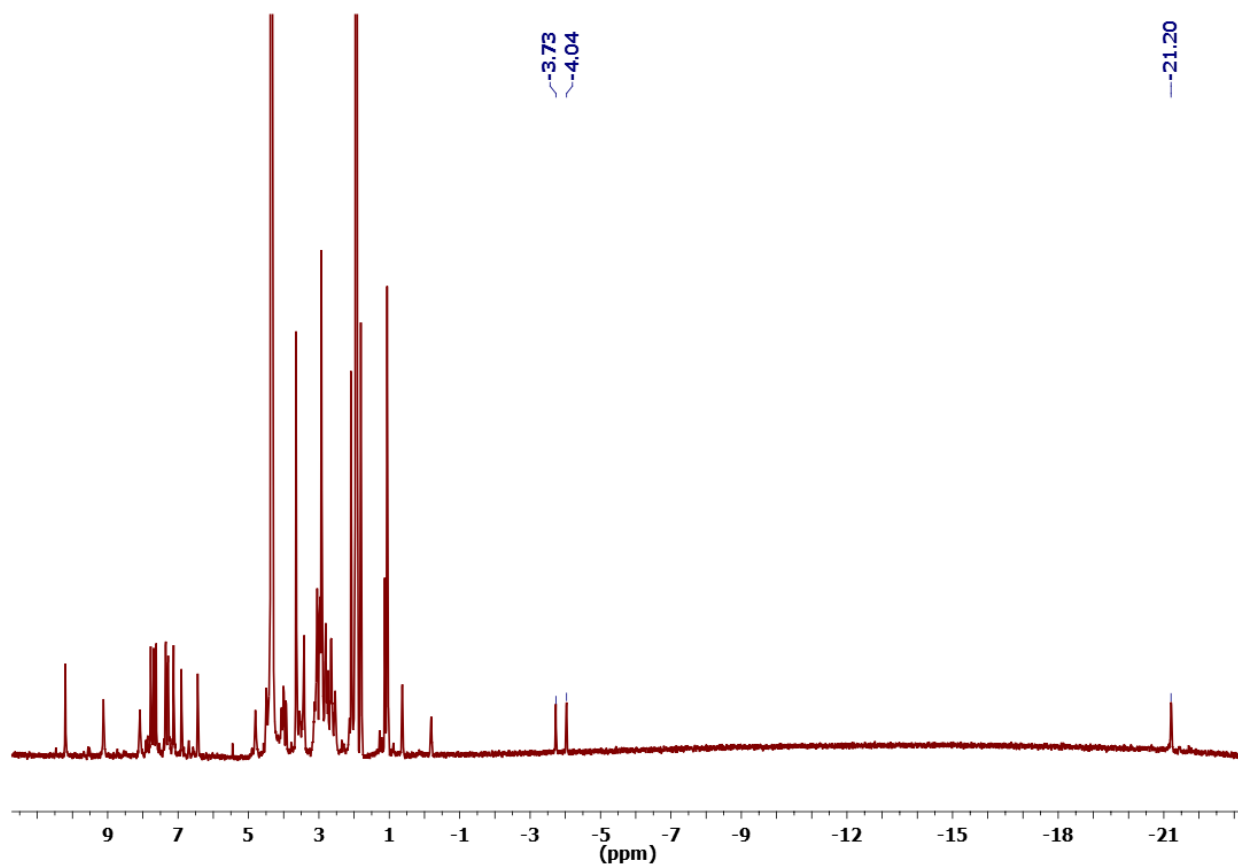


Figure 4.16. ¹H NMR spectrum of IrH₂(TPAP) in CD₂Cl₂.

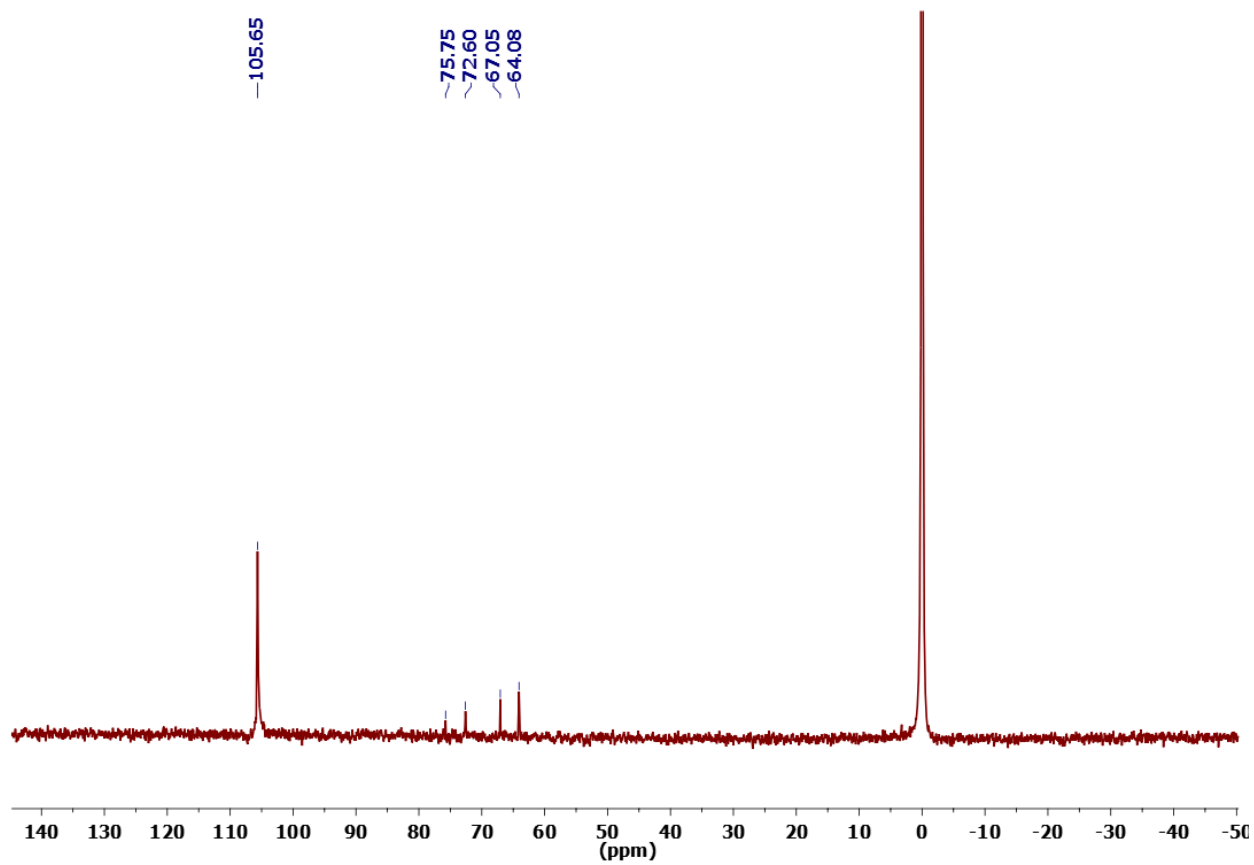


Figure 4.17. $^{31}\text{P}\{^1\text{H}\}$ NMR spectrum of $\text{IrH}_2(\text{TPAP})$ in CD_2Cl_2 .

IrH(TPAP)Cl + AgBF₄ + H₂: In the glove box, a solution of AgBF₄ (80.0 mg, 0.400 mmol) in acetone was added to a solution of IrH(TPAP)Cl (103 mg, 0.401 mmol) in CD₂Cl₂. The reaction was stirred in the dark for 1 hour before filtrating through a medium fritted funnel. The collected solution was added to a J. Young tube and taken outside the box to be charged with H₂ gas. No color change occurred. Gray solids precipitated out of solution after sitting in the J. Young tube for 1 day.

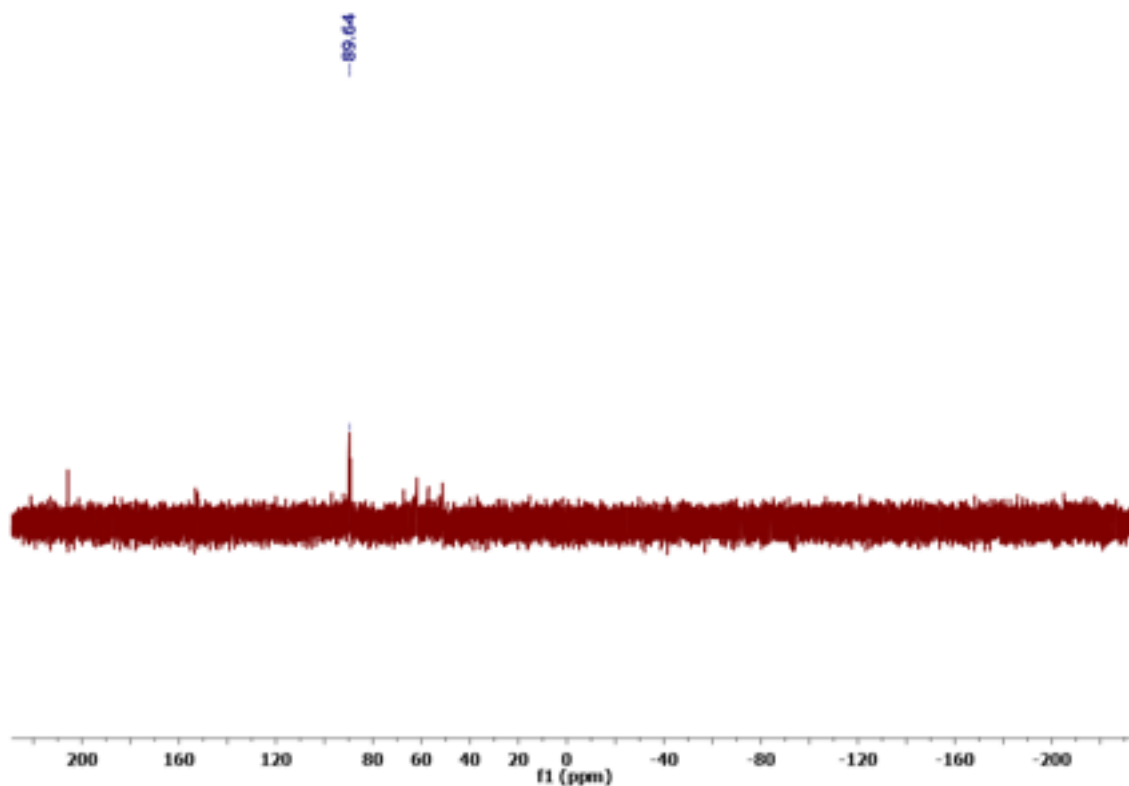


Figure 4.18. ³¹P{¹H} NMR spectrum of [IrH(TPAP)Cl] + AgBF₄ + H₂ in CD₂Cl₂.

4.6. References

1. Ottenwaelder, X.; Rudd, D. J.; Corbett, M. C.; Hodgson, K. O.; Hedman, B.; Stack, T. D. P., Reversible O–O Bond Cleavage in Copper–Dioxygen Isomers: Impact of Anion Basicity. *Journal of the American Chemical Society* **2006**, *128* (29), 9268-9269.
2. Aresta, M.; Nobile, C. F.; Albano, V. G.; Forni, E.; Manassero, M., New nickel–carbon dioxide complex: synthesis, properties, and crystallographic characterization of (carbon dioxide)-bis(tricyclohexylphosphine)nickel. *Journal of the Chemical Society, Chemical Communications* **1975**, (15), 636-637.
3. Anderson, J. S.; Iluc, V. M.; Hillhouse, G. L., Reactions of CO₂ and CS₂ with 1,2-Bis(di-tert-butylphosphino)ethane Complexes of Nickel(0) and Nickel(I). *Inorganic Chemistry* **2010**, *49* (21), 10203-10207.
4. Kim, Y.-E.; Kim, J.; Lee, Y., Formation of a nickel carbon dioxide adduct and its transformation mediated by a Lewis acid. *Chemical Communications* **2014**, *50* (78), 11458-11461.
5. Halfen, J. A.; Mahapatra, S.; Wilkinson, E. C.; Kaderli, S.; Young, V. G.; Que, L.; Zuberbühler, A. D.; Tolman, W. B., Reversible Cleavage and Formation of the Dioxygen O-O Bond Within a Dicopper Complex. *Science* **1996**, *271* (5254), 1397.
6. Cole, A. P.; Mahadevan, V.; Mirica, L. M.; Ottenwaelder, X.; Stack, T. D. P., Bis(μ -oxo)dicopper(III) Complexes of a Homologous Series of Simple Peralkylated 1,2-Diamines: Steric Modulation of Structure, Stability, and Reactivity. *Inorganic Chemistry* **2005**, *44* (21), 7345-7364.
7. Goswami, V. E.; Walli, A.; Förster, M.; Dechert, S.; Demeshko, S.; Holthausen, M. C.; Meyer, F., Acid/base triggered interconversion of μ - η^2 : η^2 -peroxido and bis(μ -oxido) dicopper intermediates capped by proton-responsive ligands. *Chemical Science* **2017**, *8* (4), 3031-3037.
8. Weinberg, D. R.; Hazari, N.; Labinger, J. A.; Bercaw, J. E., Iridium(I) and Iridium(III) Complexes Supported by a Diphenolate Imidazolyl-Carbene Ligand. *Organometallics* **2010**, *29* (1), 89-100.
9. Lee, D.-H.; P. Patel, B.; H. Crabtree, R.; Clot, E.; Eisenstein, O., Heterolytic dihydrogen activation in an iridium complex with a pendant basic group. *Chemical Communications* **1999**, (3), 297-298.
10. Ogo, S.; Kabe, R.; Hayashi, H.; Harada, R.; Fukuzumi, S., Mechanistic investigation of CO₂ hydrogenation by Ru(II) and Ir(III) aqua complexes under acidic conditions: two catalytic systems differing in the nature of the rate determining step. *Dalton Transactions* **2006**, (39), 4657-4663.
11. Roseblade, S. J.; Pfaltz, A., Iridium-Catalyzed Asymmetric Hydrogenation of Olefins. *Accounts of Chemical Research* **2007**, *40* (12), 1402-1411.
12. Takaoka, S.; Eizawa, A.; Kusumoto, S.; Nakajima, K.; Nishibayashi, Y.; Nozaki, K., Hydrogenation of Carbon Dioxide with Organic Base by PC^{II}P-Ir Catalysts. *Organometallics* **2018**, *37* (18), 3001-3009.
13. Nagaraja, C. M.; Nethaji, M.; Jagirdar, B. R., Tris(pyrazolyl)methane Sulfonate Complexes of Iridium: Catalytic Hydrogenation of 3,3-Dimethyl-1-butene. *Organometallics* **2007**, *26* (25), 6307-6311.

14. Thammavongsy, Z.; Kha, I. M.; Ziller, J. W.; Yang, J. Y., Electronic and steric Tolman parameters for proazaphosphatranes, the superbase core of the tri(pyridylmethyl)azaphosphatrane (TPAP) ligand. **2016**.
15. Chatelet, B.; Joucla, L.; Dutasta, J.-P.; Martinez, A.; Dufaud, V., Azaphosphatrane Organocatalysts in Confined Space: Cage Effect in CO₂ Conversion. *Chemistry – A European Journal* **2014**, *20* (28), 8571-8574.
16. Xi, S. K.; Schmidt, H.; Lensink, C.; Kim, S.; Wintergrass, D.; Daniels, L. M.; Jacobson, R. A.; Verkade, J. G., Bridgehead-bridgehead communication in untransannulated phosphatrane ZP(ECH₂CH₂)₃N systems. *Inorganic Chemistry* **1990**, *29* (12), 2214-2220.
17. Sánchez-Eguía, B. N.; Flores-Alamo, M.; Orio, M.; Castillo, I., Side-on cupric–superoxo triplet complexes as competent agents for H-abstraction relevant to the active site of PHM. *Chemical Communications* **2015**, *51* (55), 11134-11137.
18. Millard, M. D.; Moore, C. E.; Rheingold, A. L.; Figueroa, J. S., Four-Coordinate Iridium(I) Monohydrides: Reversible Dinitrogen Binding, Bond Activations, and Deprotonations. *Journal of the American Chemical Society* **2010**, *132* (26), 8921-8923.
19. Thammavongsy, Z.; Cunningham, D. W.; Sutthirat, N.; Eisenhart, R. J.; Ziller, J. W.; Yang, J. Y., Adaptable ligand donor strength: tracking transannular bond interactions in tris(2-pyridylmethyl)-azaphosphatrane (TPAP). *Dalton Transactions* **2018**, *47* (39), 14101-14110.
20. Harris Robin, K.; Becker Edwin, D.; Cabral de Menezes Sonia, M.; Goodfellow, R.; Granger, P., NMR nomenclature. Nuclear spin properties and conventions for chemical shifts(IUPAC Recommendations 2001). In *Pure and Applied Chemistry*, 2001; Vol. 73, p 1795.

APPENDIX A

Crystal Structure of

NiFe(CO)₅(Tris(2-pyridylmethyl)azaphosphatrane);

A Synthetic Mimic of the NiFe Hydrogenase Active Site

Incorporating a Pendant Pyridine Base

Portions of this chapter have been published:

Sutthirat, N.; Ziller, J. W.; Yang, J. Y.; Thammavongsy, Z.* *Acta Cryst.* **2019**, E75, 438-442

Data in this appendix was collected by undergraduate Natwara Sutthirat under the guidance and supervision of Zachary Thammavongsy

A.1. Motivation and Specific Aims

The reaction of Ni(TPAP)(COD) {where TPAP = [(NC₅H₄)CH₂]₃P(NC₂H₄)₃N} with Fe(CO)₅ resulted in the isolation of the title heterobimetallic NiFe(TPAP)(CO)₅ complex dicarbonyl-tricarbonyl[2,8,9-tris(pyridin-2-ylmethyl)-2,5,8,9-tetraaza-1-phosphabicyclo[3.3.3]undecane]-iron-nickel, [FeNi(C₂₄H₃₀N₇P)(CO)₅]. Characterization of the complex by ¹H and ³¹P NMR as well as IR spectroscopies are presented. The structure of NiFe(TPAP)(CO)₅ reveals three terminally bound CO molecules on Fe(0), two bridging CO molecules between Ni(0) and Fe(0), and TPAP coordinated to Ni(0). The Ni—Fe bond length is 2.4828 (4) Å, similar to that of the reduced form of the active site of NiFe hydrogenase (2.5 Å). Additionally, a proximal pendant base from one of the non-coordinating pyridine groups of TPAP is also present. Although the involvement of a pendant base has been cited in the mechanism of NiFe hydrogenase, this moiety has yet to be incorporated in a structurally characterized synthetic mimic with key structural motifs (terminally bound CO or CN⁻ ligands on Fe). Thus, the title complex NiFe(TPAP)(CO)₅ is a unique synthetic model for NiFe hydrogenase.

A.2. Background

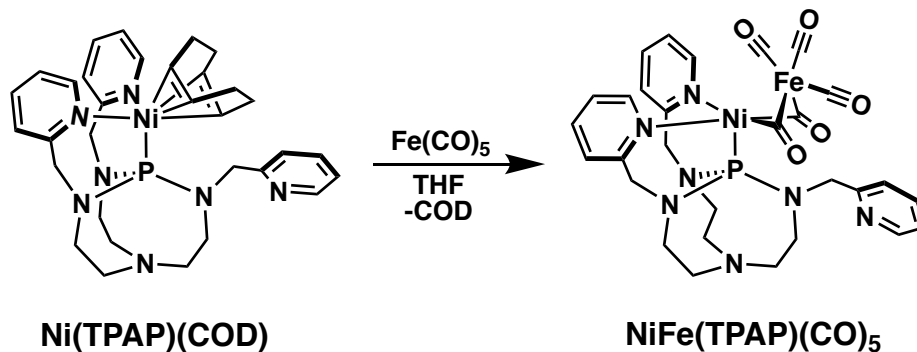
Rare and expensive metals such as Pt are often used to catalyze the production and oxidation of H₂ for utilization in electrolyzers or fuel cells, respectively. Because of this, the production and utilization of H₂ for clean energy applications have motivated scientists to produce efficient catalysts made from abundant metals. In nature, hydrogenase enzymes catalyze the reversible production and oxidation of H₂ with the metals Ni and Fe.¹ Inspired by nature, this work aimed to structurally mimic the active site of the NiFe hydrogenase enzyme.² NiFe hydrogenase contains a NiFe active center, where Fe is coordinated with three different types of ligand (C≡O, C≡N, and a sulfur atom) while Ni is coordinated by four cysteine residues. The C≡O, C≡N, and the sulfur-atom ligands play a role in maintaining the oxidation state of Fe(II) and stabilizing the oxidation state changes of the Ni ion during the catalytic cycle.³ Prior work in this thesis discussed the transannular interaction of bridgehead N and P atoms in the tris(2-pyridylmethyl)-azaphosphatrane (TPAP) ligand in the stabilization of metal ions in different oxidation states.⁴

A recent study by Johnson and co-workers found that the transannular interaction in azaphosphatranes plays a potential role in Pd cross-coupling reactions, where the oxidative addition event ‘is promoted due to electron donation to the metal center from transannulation’.⁵ The transannular interaction in TPAP could play a similar role in stabilizing the Ni ion.

Additionally, a study by Armstrong and collaborators found a conserved arginine residue was vital for catalysis in NiFe hydrogenase.⁶ They propose the guanidine base of arginine participates in the activation of H₂. As a result of this conserved motif, the incorporation of pendant bases into the ligand design of synthetic models of NiFe hydrogenase is important but has been

rarely observed in reported synthetic models of NiFe hydrogenase (as opposed to those of FeFe hydrogenase). In the title complex, NiFe(TPAP)(CO)₅, whose synthesis is illustrated in Scheme A.1, the TPAP ligand features a pendant pyridine base, providing a close structural mimic of the NiFe hydrogenase enzyme.

Scheme A.1. Synthesis of NiFe(TPAP)(CO)₅.



A.3. Results and Discussion

A.3.1. Structural Commentary

The title heterobimetallic NiFe(TPAP)(CO)₅ complex (Figure A.1), displays two bridging CO molecules between the Ni and Fe metal centers. Selected bond lengths and bond angles are given in Table A.1. The Fe(0) center shows a five-coordinate pseudo square-pyramidal geometry comprising three terminally bound CO and two bridging CO molecules. The τ_5 value of the Fe(0) atom is 0.40, where $\tau_5 = 0$ represents an ideal square pyramidal and 1 represents an ideal trigonal–bipyramidal geometry.⁷ The Ni(0) center is also coordinated by the two bridging CO molecules and the TPAP ligand, where the two nitrogens from two pyridines and the phosphorus of the azaphosphatranine are coordinated. The Ni(0) ion displays a five-coordinated square-pyramidal geometry with a τ_5 value of 0.06. The bond lengths of the CO molecules bridging between the Ni

and Fe ions are 1.1821 (16) and 1.1754 (17) Å for O1—C25 and O2—C26, respectively. These bond lengths are longer than the terminally bound CO molecules on Fe, which are 1.1509 (17), 1.148 (2) and 1.1531 (19) Å for O3—C27, O4—C28 and O5—C29, respectively. The shorter bond distances in the bridging CO molecules is indicative of π -back-bonding from the two metal centers to the bridging CO ligands. The Ni—Fe bond length is 2.4828 (4) Å, similar to the Ni—Fe bond length (2.5 Å) in the reduced state of NiFe hydrogenase.⁸ The distance between atoms P1 and N1 in TPAP is 3.2518 (13) Å, consistent with a fully relaxed, pro-form of azaphosphatrane.⁹ One pyridine group from TPAP is uncoordinated to the Ni or Fe metals. Atom N5 of the non-coordinating pyridine is not facing directly towards the metal ions, resulting in an approximate distance of 5.61 and 5.93 Å from Ni and Fe, respectively. In comparison, the arginine side chain lies less than 4.5 Å from both the Ni and Fe in NiFe hydrogenase.⁶

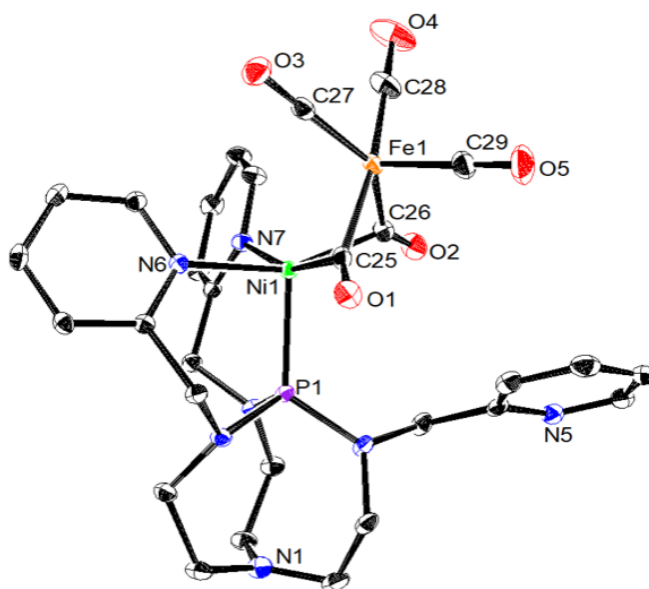


Figure A.1. The molecular structure of complex NiFe(TPAP)(CO)₅. The displacement ellipsoids are drawn at the 50% probability level. For clarity, the hydrogen atoms have been omitted.

Table A.1. Selected geometric parameters NiFe(TPAP)(CO)₅ (Å, °).

Ni1—Fe1	2.4828 (4)	Ni1—N6	2.1167 (11)
Ni1—C25	1.8983 (13)	Ni1—N7	2.1394 (11)
Ni1—C26	1.9805 (13)	Ni1—P1	2.2276 (4)
C28—Fe1—C25	168.88 (6)	C25—Ni1—N7	159.65 (5)
C27—Fe1—C26	144.68 (6)	Ni1—C25—Fe1	80.85 (5)
C26—Ni1—N6	155.94 (5)	Fe1—C26—Ni1	79.42 (5)

A.3.2. Database Survey

A search was performed to compare previously published structures of molecular NiFe bimetallic complexes that are potential biological mimics of NiFe hydrogenase. Specifically, the search was for molecular NiFe that contained three terminally bound CO or CN⁻ ligands to Fe and any bridging ligand(s) between the Ni and Fe metal ions. This search was limited to these features because of their importance in the active site of NiFe hydrogenase. A search of the Cambridge Structural Database (CSD, Version 5.40, update November 2018), gave 32 hits with these attributes. Only 12 structures have Ni—Fe bond lengths relatively close (within 0.2 Å) to those of the reduced form of NiFe hydrogenase (2.5 Å). However, the NiFe complexes of these 12 structures [CSD refcodes: FANHEK, FANHEK01, FANGUZ, FANHAG, FANHIO and FANHUA,¹⁰ LAZWEP,¹¹ SUQQOL,¹² UCUXOH and UCUXUN,¹³ UQAJAZ¹⁴ and YOKWIE¹⁵; do not feature a pendant base, which has been demonstrated by Armstrong and collaborators to play a key role in the function of NiFe hydrogenase.⁶ Structural models of NiFe hydrogenase which incorporate a pendant base but lack the three terminally bound CO or CN ligands of the NiFe hydrogenase active site can be found here [CSD refcodes: EJUSEJ and EJUSUZ,¹⁶ FOTKOP¹⁷ and QEKLAT].¹⁸

A.4. Conclusion

The heterobimetallic complex, NiFe(TPAP)(CO)₅, was characterized by X-ray crystallography. The structure revealed a proximal pendant base from one of the non-coordinating pyridine groups of TPAP. The NiFe(TPAP)(CO)₅ is a rare synthetic mimic of NiFe hydrogenase where pendant bases are incorporated into the design.

A.5. Experimental Details

General Considerations

All manipulations were performed in the glovebox, as the title complex is air- and moisture-sensitive. All solvents (except for C₆D₆) were first purged with argon and dried using a solvent purification system. Iron(0) pentacarbonyl was purchased from Sigma–Aldrich and used without further purification. Ni(TPAP)(COD) was synthesized according to an established procedure.⁴

Physical Methods

Nuclear Magnetic Resonance (NMR) Spectroscopy:

¹H and ³¹P NMR spectra were recorded on a Bruker AVANCE 600 MHz and were referenced to the residual protio solvent peak (except for ³¹P, which was referenced to the absolute frequency of 0 ppm in the ¹H dimension according to the Xi scale).

Infrared (IR) Spectroscopy: IR absorption was taken on a Thermo Scientific Nicolet iS5 spectrophotometer with an iD5 ATR attachment.

Elemental analyses (EA): EA were performed on a PerkinElmer 2400 Series II CHNS elemental analyzer.

X-ray Crystallography (XRC): X-ray diffraction studies were carried out at the UCI Department of Chemistry X-ray Crystallography Facility on a Bruker SMART APEX II diffractometer. Data

were collected at 88 K using Mo K α radiation ($\lambda = 0.71073 \text{ \AA}$). A pink crystal of approximate dimensions 0.230 x 0.342 x 0.354 mm was mounted in a cryo-loop and transferred to a Bruker SMART APEX II diffractometer. The APEX2 program package was used to determine the unit cell parameters and for data collection (30 sec/frame scan time for a sphere of diffraction data). The raw frame data was processed using SAINT and SADABS to yield the reflection data file. Subsequent calculations were carried out using the SHELXTL program. The diffraction symmetry was $2/m$ and the systematic absences were consistent with the monoclinic space group P21/c that was later determined to be correct. The structure was solved by dual space methods and refined on F2 by full-matrix least-squares techniques. The analytical scattering factors for neutral atoms were used throughout the analysis. Hydrogen atoms were included using a riding model. Least-squares analysis yielded $wR2 = 0.0645$ and $Goof = 1.039$ for 397 variables refined against 7655 data, $R1 = 0.0249$ for those 6933 data with $I > 2\sigma(I)$.

NiFe(TPAP)(CO)₅: In a glove box, a solution of TPAP (61.2 mg, 0.136 mmol) in 3 ml of tetrahydrofuran was added to a solution of bis(1,5- cyclooctadiene)nickel(0) (37.4 mg, 0.136 mmol) in tetrahydrofuran. The solution immediately turned dark forest green and was stirred for 1 h at room temperature. To this solution, iron(0) pentacarbonyl (26.6 mg, 0.136 mmol) in 3 ml of tetrahydrofuran was added. The solution turned dark orange–brown and was stirred for 1 h. The solvent was removed under reduced pressure and re-dissolved in diethyl ether. The re-dissolved product was filtered through a glass disposable Pasteur pipette packed with a 25 mm glass microfiber filter and celite (3 cm). Slow evaporation of NiFe(TPAP)(CO)₅ in diethyl ether lead to the formation of pink block-like crystals of the title complex (52% yield). ¹H NMR (C₆D₆, 600 MHz): 2.45–2.58 (m, 12H, NCH₂CH₂N), 4.09 (s, 6H, PyrCH₂), 6.58 (t, 3H, Pyr), 6.96 (t, 3H, Pyr), 7.09 (t, 3H, Pyr), 8.93 (m, 3H, Pyr). ³¹P{¹H} NMR (C₆D₆, 242.94 MHz): 118.6. IR (CO): 1745, 1770, 1919 and 2001 cm⁻¹. Elemental Analysis for C₂₉H₃₀FeN₇NiO₅P: C, 49.61; H, 4.31; N, 13.96; found: C, 49.52; H, 4.28; N, 13.63.

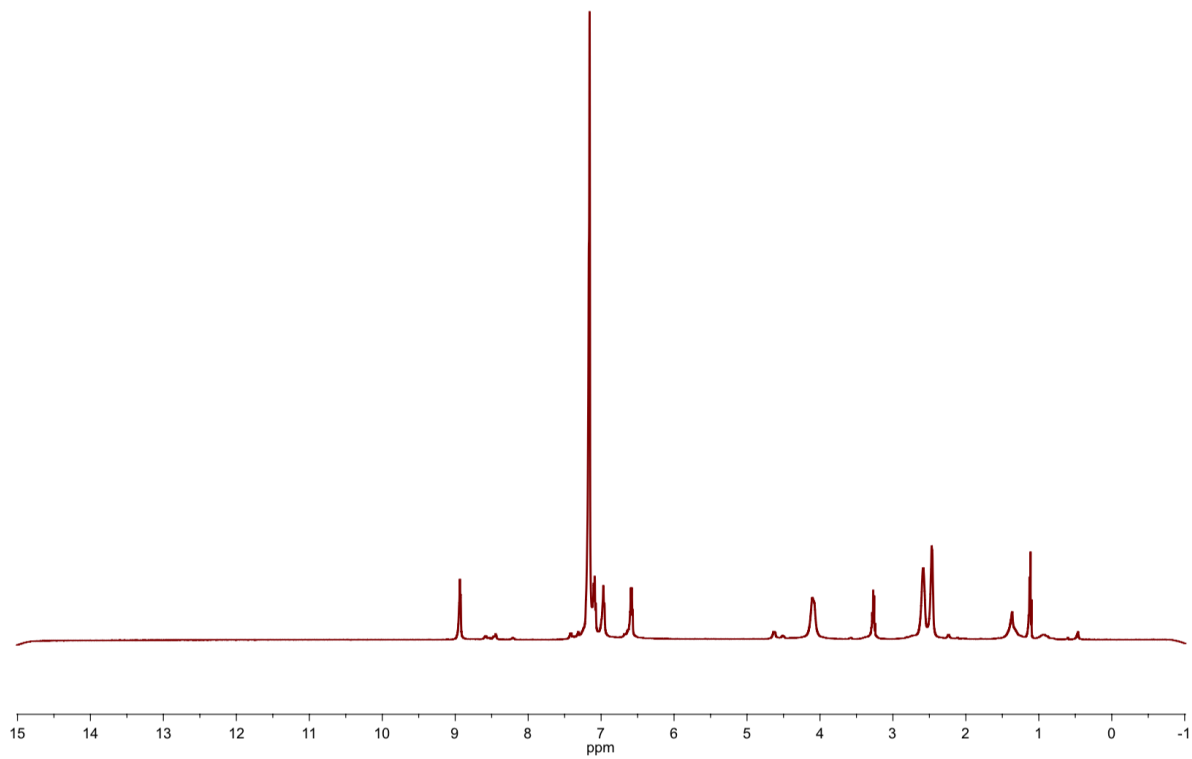


Figure A.2. ^1H NMR spectrum of $\text{NiFe}(\text{TPAP})(\text{CO})_5$ in C_6D_6 .

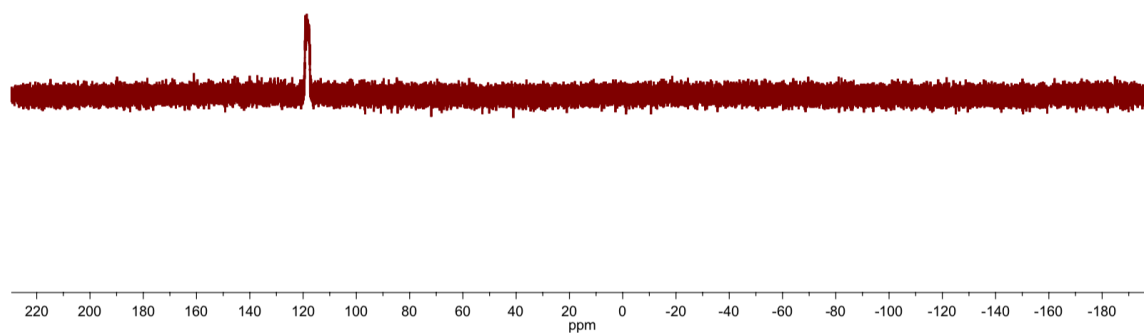


Figure A.3. $^{31}\text{P}\{^1\text{H}\}$ NMR spectrum of $\text{NiFe}(\text{TPAP})(\text{CO})_5$ in C_6D_6 .

A.6. References

1. Lacasse, M. J.; Zamble, D. B., [NiFe]-Hydrogenase Maturation. *Biochemistry* **2016**, *55* (12), 1689-1701.
2. Kaur-Ghumaan, S.; Stein, M., [NiFe] hydrogenases: how close do structural and functional mimics approach the active site? *Dalton Transactions* **2014**, *43* (25), 9392-9405.
3. Shafaat, H. S., Heterobimetallic Models of the [NiFe] Hydrogenases: A Structural and Spectroscopic Comparison AU - Behnke, Shelby L. *Comments on Inorganic Chemistry* **2016**, *36* (3), 123-140.
4. Thammavongsy, Z.; Cunningham, D. W.; Sutthirat, N.; Eisenhart, R. J.; Ziller, J. W.; Yang, J. Y., Adaptable ligand donor strength: tracking transannular bond interactions in tris(2-pyridylmethyl)-azaphosphatane (TPAP). *Dalton Transactions* **2018**, *47* (39), 14101-14110.
5. Matthews, A. D.; Gravalis, G. M.; Schley, N. D.; Johnson, M. W., Synthesis, Structure, and Reactivity of Palladium Proazaphosphatane Complexes Invoked in C–N Cross-Coupling. *Organometallics* **2018**, *37* (18), 3073-3078.
6. Evans, R. M.; Brooke, E. J.; Wehlin, S. A. M.; Nomerotskaia, E.; Sargent, F.; Carr, S. B.; Phillips, S. E. V.; Armstrong, F. A., Mechanism of hydrogen activation by [NiFe] hydrogenases. *Nature Chemical Biology* **2015**, *12*, 46.
7. Addison, A. W.; Rao, T. N.; Reedijk, J.; van Rijn, J.; Verschoor, G. C., Synthesis, structure, and spectroscopic properties of copper(II) compounds containing nitrogen–sulphur donor ligands; the crystal and molecular structure of aqua[1,7-bis(*N*-methylbenzimidazol-2'-yl)-2,6-dithiaheptane]copper(II) perchlorate. *Journal of the Chemical Society, Dalton Transactions* **1984**, (7), 1349-1356.
8. Garcin, E.; Vernede, X.; Hatchikian, E. C.; Volbeda, A.; Frey, M.; Fontecilla-Camps, J. C., The crystal structure of a reduced [NiFeSe] hydrogenase provides an image of the activated catalytic center. *Structure* **1999**, *7* (5), 557-566.
9. Tang, J.; Dopke, J.; Verkade, J. G., Synthesis of new exceedingly strong non-ionic bases: RN:P(MeNCH₂CH₂)₃N. *Journal of the American Chemical Society* **1993**, *115* (12), 5015-5020.
10. Song, L.-C.; Lu, Y.; Zhu, L.; Li, Q.-L., Dithiolato- and Diselenolato-Bridged Nickel–Iron Biomimetics for the Active Site of [NiFe]Hydrogenases. *Organometallics* **2017**, *36* (3), 750-760.
11. Zhu, W.; Marr, A. C.; Wang, Q.; Neese, F.; Spencer, D. J. E.; Blake, A. J.; Cooke, P. A.; Wilson, C.; Schröder, M., Modulation of the electronic structure and the Ni–Fe distance in heterobimetallic models for the active site in [NiFe]hydrogenase. **2005**, *102* (51), 18280-18285.
12. Barton, B. E.; Whaley, C. M.; Rauchfuss, T. B.; Gray, D. L., Nickel–Iron Dithiolato Hydrides Relevant to the [NiFe]-Hydrogenase Active Site. *Journal of the American Chemical Society* **2009**, *131* (20), 6942-6943.
13. Carroll, M. E.; Barton, B. E.; Gray, D. L.; Mack, A. E.; Rauchfuss, T. B., Active-Site Models for the Nickel–Iron Hydrogenases: Effects of Ligands on Reactivity and Catalytic Properties. *Inorganic Chemistry* **2011**, *50* (19), 9554-9563.
14. Manor, B. C.; Rauchfuss, T. B., Hydrogen Activation by Biomimetic [NiFe]-Hydrogenase Model Containing Protected Cyanide Cofactors. *Journal of the American Chemical Society* **2013**, *135* (32), 11895-11900.

15. Walther, D.; Geßler, S.; Sieler, J., Organometallchemie binuclearer 1-Azadien-nickel(0)-Komplexe Bimetallverbindungen mit NiFe-Bindung durch Addition von Pentacarbonyleisen(0) und Nickelalactone durch Ringöffnung cyclischer Anhydride. *Zeitschrift für anorganische und allgemeine Chemie* **1995**, 621 (4), 635-639.
16. Sun, P.; Yang, D.; Li, Y.; Zhang, Y.; Su, L.; Wang, B.; Qu, J., Thiolate-Bridged Nickel–Iron and Nickel–Ruthenium Complexes Relevant to the CO-Inhibited State of [NiFe]-Hydrogenase. *Organometallics* **2016**, 35 (5), 751-757.
17. Tanino, S.; Li, Z.; Ohki, Y.; Tatsumi, K., A Dithiolate-Bridged (CN)₂(CO)Fe–Ni Complex Reproducing the IR Bands of [NiFe] Hydrogenase. *Inorganic Chemistry* **2009**, 48 (6), 2358-2360.
18. Liaw, W.-F.; Chiang, C.-Y.; Lee, G.-H.; Peng, S.-M.; Lai, C.-H.; Darensbourg, M. Y., Heterobimetallics of Nickel–Iron Dinitrosyl: Electronic Control by Chelate and Diatomic Ligands. *Inorganic Chemistry* **2000**, 39 (3), 480-484.

APPENDIX B

Attempted Protonation and pK_a Measurement of Tris(2-pyridylmethyl)azaphosphatranecoxide

Data in this appendix was collected by undergraduate Jessica Mendoza under the guidance and supervision of Zachary Thammavongsy.

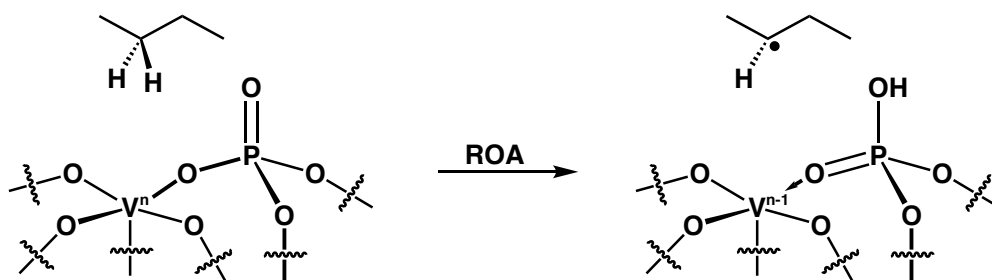
B.1. Motivation and Specific Aims

Vanadium phosphates (VPO) are heterogeneous catalysts used for the oxidation of butane to maleic anhydride, an industrially valuable chemical. A proposed mechanism by Goddard and coworkers suggests the C-H bond activation step occurs at the P=O unit¹, rather than the vanadium center. This appendix describes work towards understanding the basicity of phosphine oxides in acetonitrile, particularly tris(2-pyridylmethyl)azaphosphatranes oxide (TPAPO) and tri(benzyl)-azaphosphatranes oxide (TBAPO).

B.2. Background

Theoretical work by Goddard and coworkers proposed that the terminal P=O linkages in VPO heterogeneous catalysis are responsible for C-H activation at butane (Scheme B.1).¹ Goddard coined the mechanism as “reduction-coupled oxo activation” (ROA) and occurs due to the strong basicity at the P=O bond that is coupled to the neighboring high-valent, oxidative V(V) centers, which undergo reduction.

Scheme B.1. Proposed Reduction-Coupled Oxo Activation (ROA) Mechanism in VPO system.



The role of a strong basic P=O in VPO motivated this work on quantifying the basicity of P=O, particularly in tris(2-pyridylmethyl)azaphosphatranes oxide (TPAPO) and tris(benzyl)azaphosphatranes oxide (TBAPO). Previous pK_a studies on general P=O with alkyl or aryl substituents indicate they are very weak bases.² Proazaphosphatranes-oxides have been shown

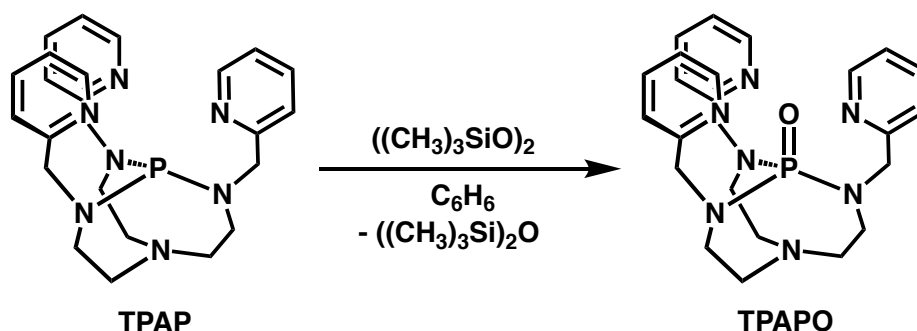
to be good nucleophiles for organic catalysis due to the added stability from the transannular interaction;³ therefore, the P=O in TPAPO and TBAPO could be stronger bases, due to the general correlation between the strength of bases and nucleophiles.

B.3. Results and Discussion

B.3.1. Synthesis and Characterization of tris(2-pyridylmethyl)azaphosphatraneoxide (TPAPO)

The synthesis and characterization of tris(2-pyridylmethyl)azaphosphatraneoxide (TPAPO) was not reported by Verkade and coworkers, despite being used as an organic catalyst in their study.⁴ The synthesis of TPAPO followed a published procedure,⁵ where a slight excess of $((\text{CH}_3)_3\text{SiO})_2$ is added to a solution of tris(2-pyridylmethyl)azaphosphatrane (TPAP) in benzene (Scheme B.2).

Scheme B.2. Synthesis of tris(2-pyridylmethyl)azaphosphatraneoxide (TPAPO).

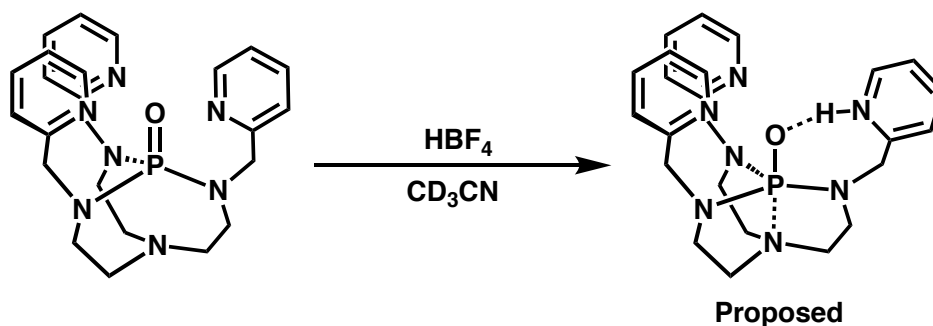


After work up, a white solid is obtained and characterized by ^1H and $^{31}\text{P}\{^1\text{H}\}$ NMR spectroscopy. The $^{31}\text{P}\{^1\text{H}\}$ NMR spectrum displayed a resonance at 23 ppm, closely matching $^{31}\text{P}\{^1\text{H}\}$ NMR spectrum of tris(benzyl)azaphosphatraneoxide (24 ppm).⁵

B.3.2. Protonation study of tris(2-pyridylmethyl)azaphosphatranexoxide (TPAPO)

Verkade and coworkers attempted the protonation of the methyl substituted Verkade's Superbase with HCl ($pK_a = 10.3$ in acetonitrile) but the data and discussion were brief.³ In this study, HBF_4 ($pK_a = 1.8$ in acetonitrile) and *p*-toluenesulfonic acid (TsOH, $pK_a = 8.5$ in acetonitrile) are used to protonate TPAPO. Excess HBF_4 was added to TPAPO in acetonitrile (Scheme B.3) to approximate the pK_a of $[\text{TPAPOH}]^+$.

Scheme B.3. Proposed reactivity of tris(2-pyridylmethyl)azaphosphatranexoxide (TPAPO) with HBF_4 .



After the solvent was removed under reduced pressure, a white solid is obtained. The $^{31}\text{P}\{^1\text{H}\}$ NMR spectrum of the white solid displayed four resonances at 20.0, 16.9, 14.1 and 10.9 ppm (Figure B.1).

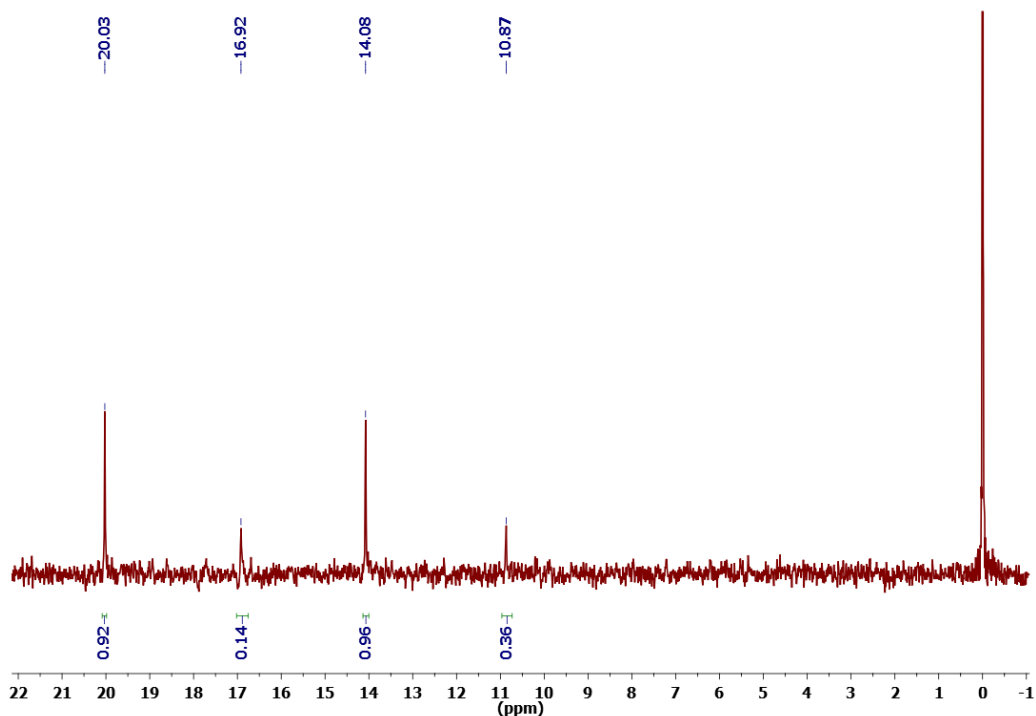
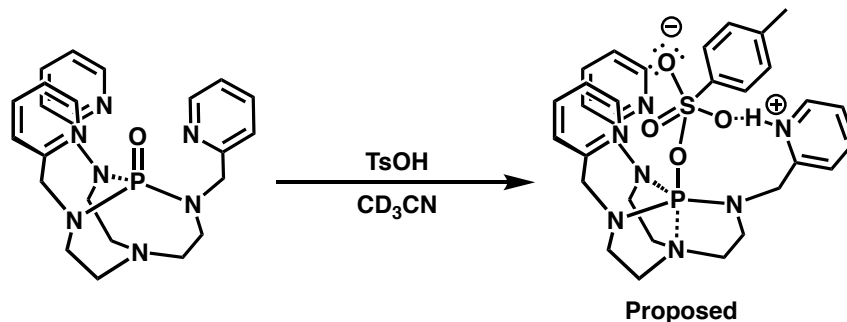


Figure B.1. $^{31}\text{P}\{^1\text{H}\}$ NMR spectrum of tris(2-pyridylmethyl)azaphosphatraneoxide (TPAPO) + HBF_4 in CD_3CN .

The multiple resonances could correspond to protonation at the $\text{P}=\text{O}$ oxygen, the N_{py} and/or the N_{ax} . These are all possible sites of protonation due to the $\text{p}K_{\text{a}}$ of pyridinium ($\text{p}K_{\text{a}} = 12.53$ in acetonitrile) and tertiary amines (Et_3NH , $\text{p}K_{\text{a}} = 18.82$). The $\text{p}K_{\text{a}}$ of the $\text{P}=\text{O}$ oxygen is not measured but is proposed to be the protonation site in tris(methyl)azaphosphatrane)oxide.³ The resonance at 14.1 ppm in the $^{31}\text{P}\{^1\text{H}\}$ NMR spectrum is the largest resonance, and is close to the resonance in the ^{31}P NMR spectrum of Verkade's proposed protonated methyl substituted azaphosphatraneoxide at 14.6 ppm.

Due to the difficulty of accurately measuring 1 equivalent of HBF_4 , TsOH is used. A 1:1 ratio of TPAPO and TsOH is mixed together in acetonitrile (Scheme B.4). After the solvent is removed under reduced pressure, a white solid was obtained.

Scheme B.4. Proposed reactivity of tris(2-pyridylmethyl)azaphosphatraneoxide (TPAPO) with TsOH.



The $^{31}\text{P}\{^1\text{H}\}$ NMR spectrum of the white solid displayed a major resonance at 1.64 ppm in CD_3CN (Figure B.2) and the disappearance of the $\text{P}=\text{O}$ signal at 23 ppm. This data could signify a complete conversion to the protonated form TPAPO; however, $\text{P}=\text{O}$ in proazaphosphatranes are known to be good nucleophiles that could attack electrophilic sites, such as the S in TsOH .³

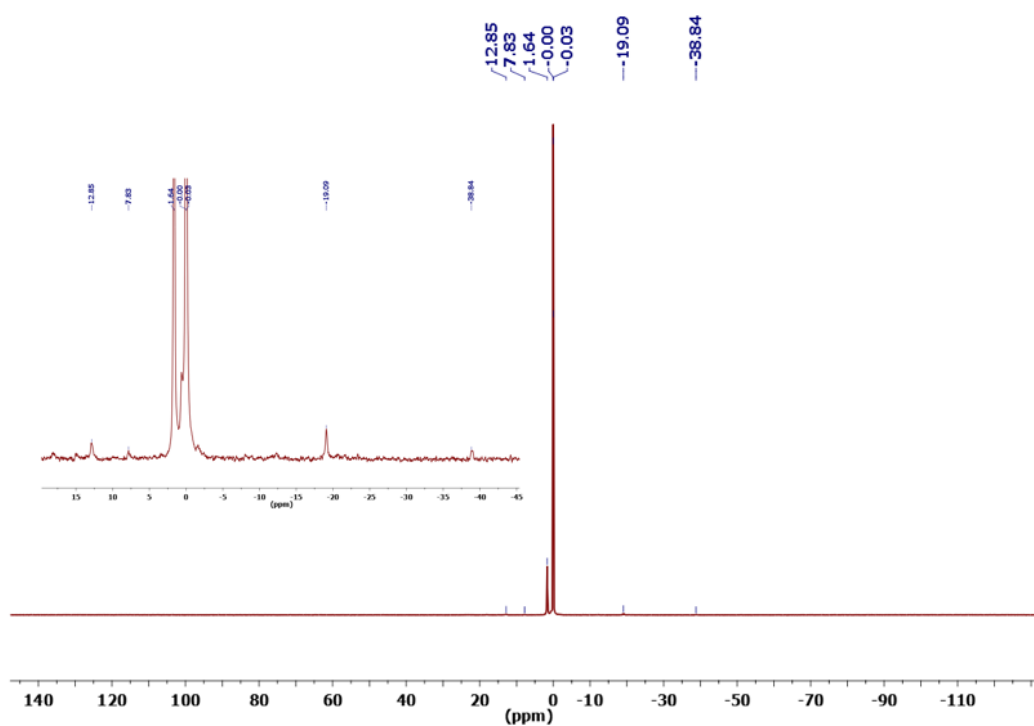
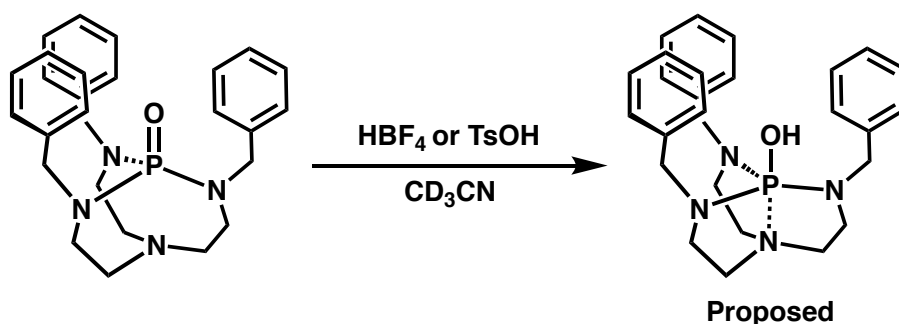


Figure B.2. $^{31}\text{P}\{^1\text{H}\}$ NMR spectrum of tris(2-pyridylmethyl)azaphosphatraneoxide (TPAPO) + TsOH in CD_3CN .

B.3.3. Protonation study of tris(benzyl)azaphosphatranexide (TBAPO)

The benzyl version of azaphosphatrane lacks the basic pyridine N site and limits the possible sites of protonation. The synthesis of tris(benzyl)azaphosphatranexide (TBAPO) is outlined in previous publication from Verkade and coworkers.⁵ The addition of excess HBF₄ to TBAPO in acetonitrile is performed (Scheme B.5). After removal of solvent under reduced pressure, a white solid is obtained.

Scheme B.5. Reactivity of tris(benzyl)azaphosphatranexide (TBAPO) with HBF₄ or TsOH.



The ³¹P{¹H} NMR spectrum of the white solid displayed a single resonance at 14.7 ppm (Figure B.3) This resonance is very close to the ³¹P NMR spectrum reported for Verkade's proposed protonated methyl substituted azaphosphatranexide at 14.6 ppm.³ By switching to the benzyl version of azaphosphatrane, there are now less protonation sites to account for and less resonances in the ³¹P{¹H} NMR spectrum compared to the addition of HBF₄ to TPAPO.

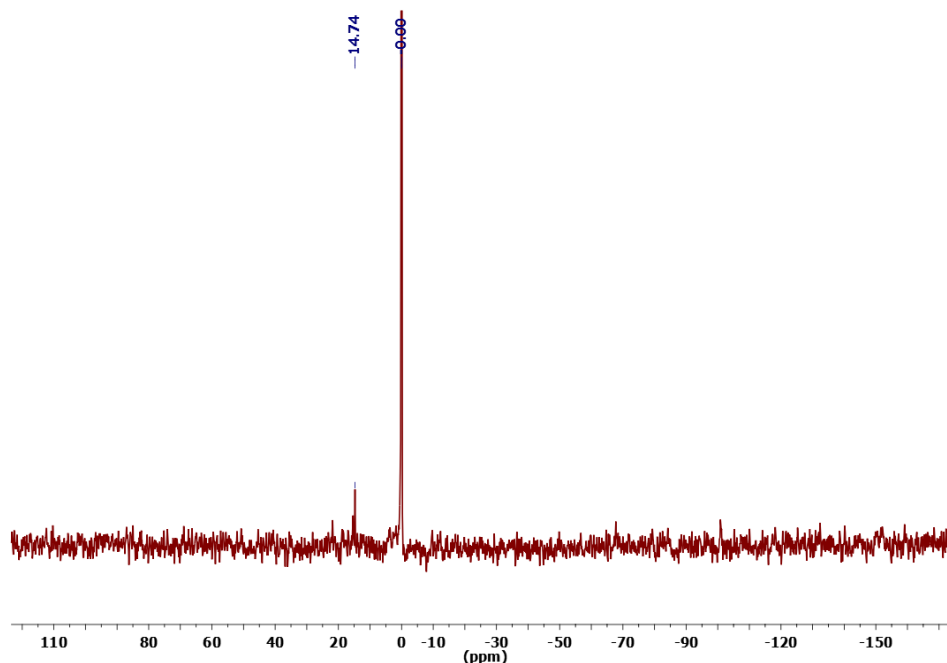


Figure B.3. $^{31}\text{P}\{^1\text{H}\}$ NMR spectrum of tris(benzy)azaphosphatraneoxide (TBAPO) + HBF_4 in CD_3CN .

Once again, due to the difficulty of accurately measuring 1 equivalent of HBF_4 , TsOH was used. A 1:1 ratio of TBAPO and TsOH was mixed in acetonitrile (Scheme B.5). After removal of solvent under reduced pressure, a white solid was obtained. The $^{31}\text{P}\{^1\text{H}\}$ NMR spectrum of the white solid displayed resonances at 21.0 and 15.7 ppm in CD_3CN (Figure B.4). The resonance at 21.0 ppm maybe the original TBAPO (24 ppm), but shifted due to potential hydrogen bonding interaction with nearby protonated TBAPO or TsOH . The appearance of both TBAPO and protonated TBAPO in the $^{31}\text{P}\{^1\text{H}\}$ NMR spectrum would indicate an incomplete reaction, potentially due to similar $\text{p}K_a$ between the protonated TBAPO and TsOH in CD_3CN .

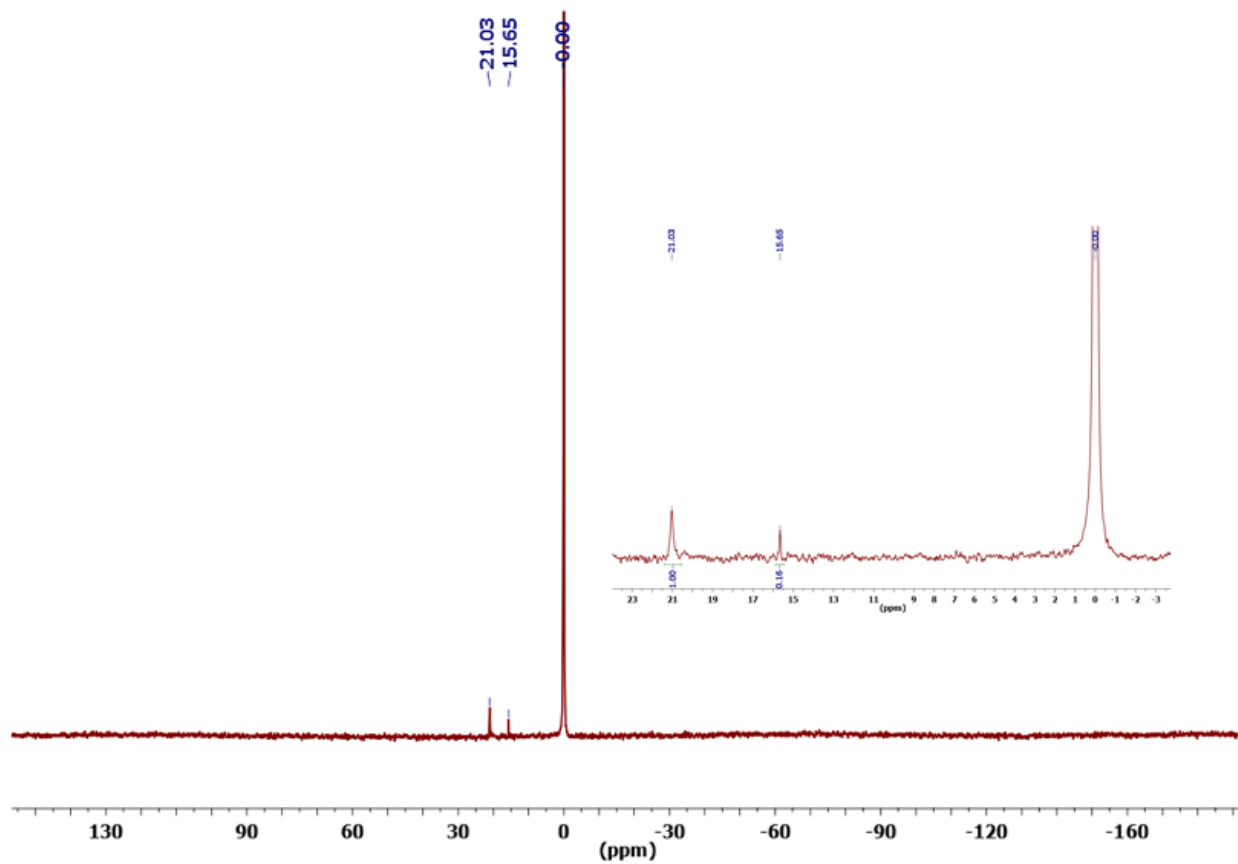


Figure B.4. $^{31}\text{P}\{^1\text{H}\}$ NMR spectrum of tris(benzy)azaphosphatraneoxide (TBAPO) + TsOH in CD_3CN .

B.4. Conclusion

The protonation study of tris(2-pyridylmethyl)azaphosphatraneoxide (TPAPO) and tris(benzy)azaphosphatraneoxide (TBAPO) with HBF_4 and TsOH was performed. The $^{31}\text{P}\{^1\text{H}\}$ NMR spectra displayed shifts consistent with a protonated $\text{P}=\text{O}$ in both azaphosphatraneoxides when HBF_4 was used, however, the addition of TsOH to TPAPO resulted in a $^{31}\text{P}\{^1\text{H}\}$ NMR spectrum that suggests nucleophilic addition to the electrophilic S of TsOH. Furthermore, the $\text{p}K_a$ of the protonated TBAPO may be close to that of TsOH.

B.5. Experimental Details

General Considerations

All manipulations were performed outside the glovebox. All solvents were first purged with argon and dried using a solvent purification system. The compound, $((\text{CH}_3)_3\text{SiO})_2$, was provided by the Borovik group and used without further purification. *p*-toluenesulfonic acid and $\text{HBF}_4 \cdot \text{Et}_2\text{O}$ (48% w/w) were commercially purchased and used without further purification.

Physical Methods

Nuclear Magnetic Resonance (NMR) Spectroscopy: Nuclear magnetic resonance (NMR) spectra were recorded on a Bruker AVANCE 600 MHz (^1H , ^{13}C and ^{31}P) ^1H NMR spectra were referenced to (tetramethylsilane) TMS using the residual proton signal of the solvent and ^{31}P NMR spectra were referenced to an internal H_3PO_4 sample in D_2O .

Tris(2-pyridylmethyl)azaphosphatraneoxide (TPAPO): A solution of $((\text{CH}_3)_3\text{SiO})_2$ (35.0 mg, 0.19 mmol) in 5 mL of benzene was added to a solution of tris(2-pyridylmethyl)azaphosphatrane (79.0 mg, 0.17 mmol) in 6 mL of benzene. After the solution was stirred for 1 day, the solvent was removed under reduced pressure, yielding a white solid. ^1H NMR (CD_3CN , 600 MHz) δ = 2.82 (t, 6H, $\text{NCH}_2\text{CH}_2\text{NP}$), 2.96 (m, 6H, $\text{NCH}_2\text{CH}_2\text{NP}$), 4.33 (d, 6H, PyCH_2N), 7.22 (m, 3H, Py), 7.76 (s, 6H, Py), 8.48 (d, 3H, Py). $^{31}\text{P}\{^1\text{H}\}$ (CD_3CN , 243 MHz) δ = 23.95.

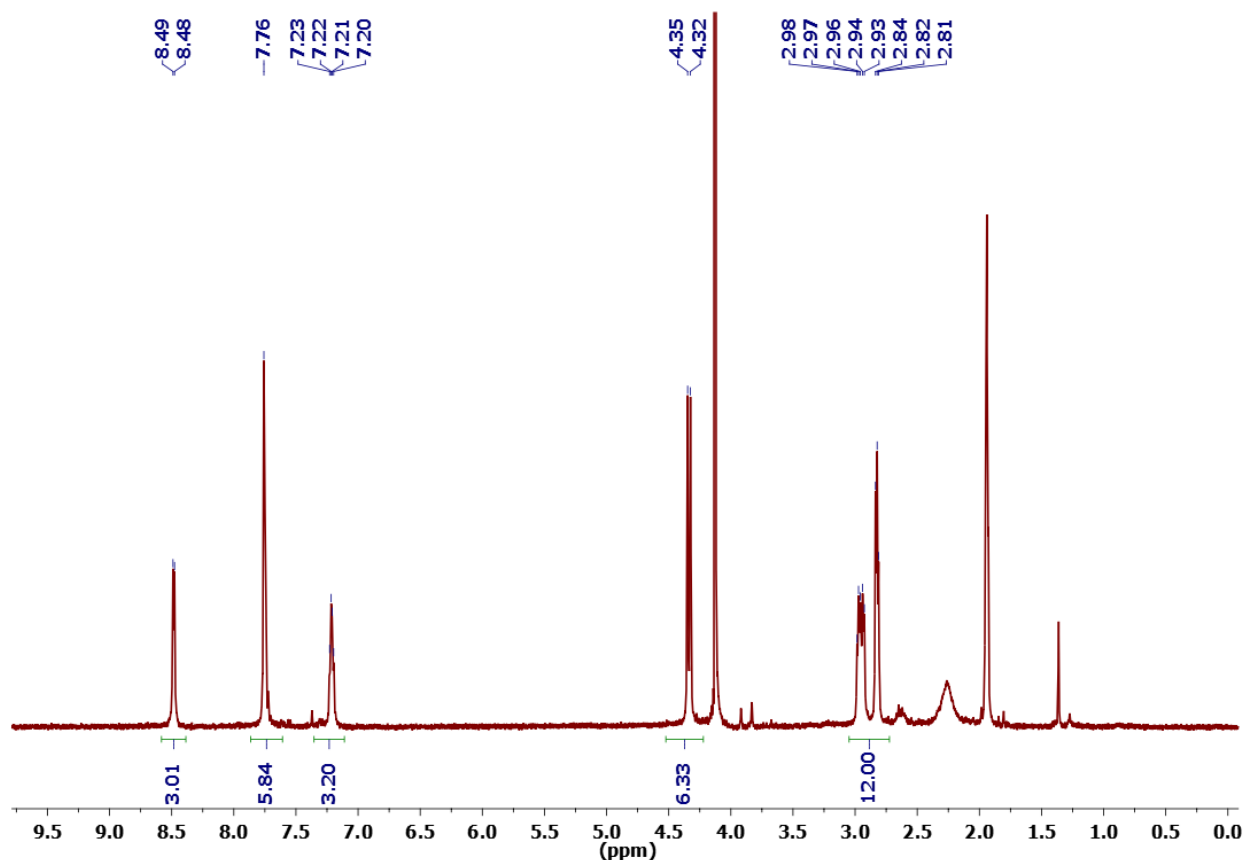


Figure B.5. ^1H NMR spectrum of tris(2-pyridylmethyl)azaphosphatraneoxide (TPAPO) in CD_3CN .

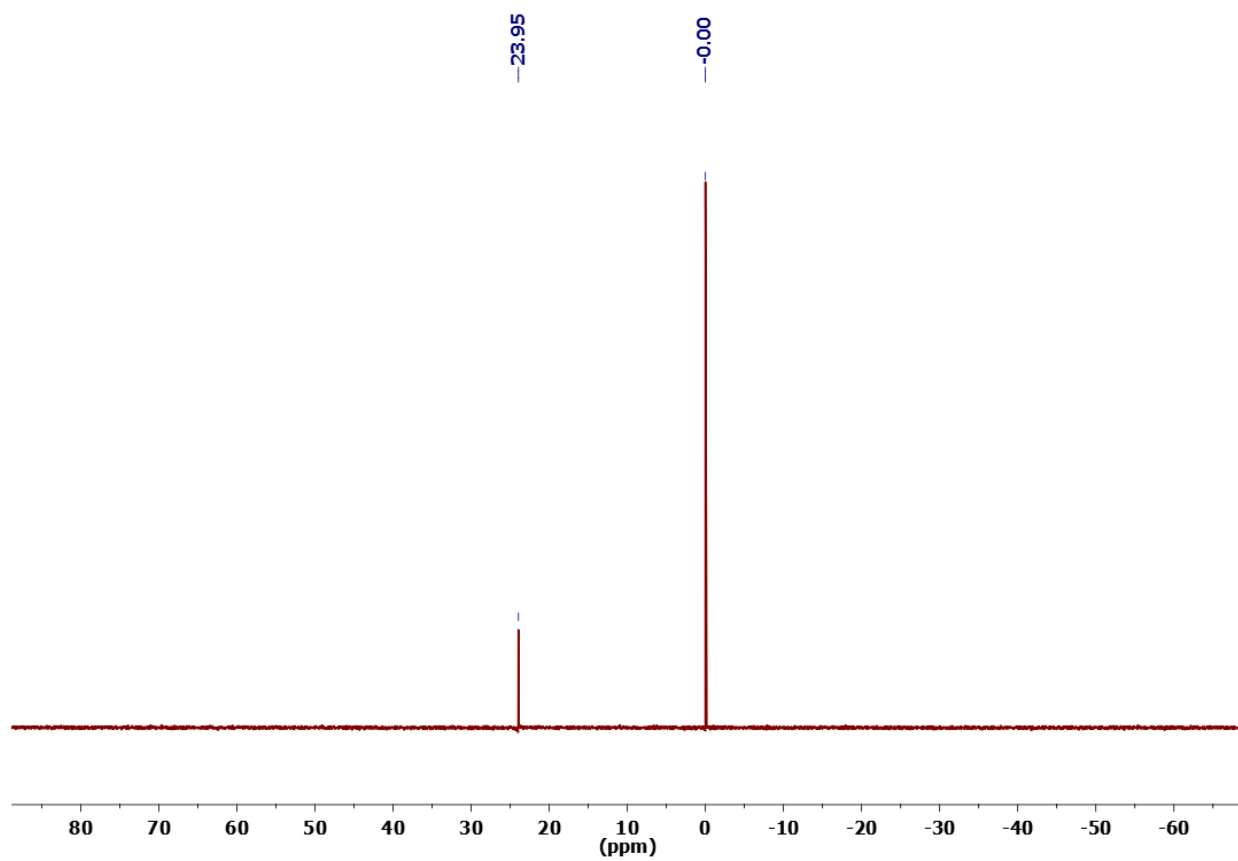


Figure B.6. $^{31}\text{P}\{^1\text{H}\}$ NMR spectrum of tris(2-pyridylmethyl)azaphosphatraneoxide (TPAPO) in CD_3CN .

Tris(2-pyridylmethyl)azaphosphatraneoxide (TPAPO) + HBF₄ : 20 drops of HBF₄ (48% w/w) were added to a solution of tris(2-pyridylmethyl)azaphosphatrane in benzene . After the solution was stirred for 1 day, the solvent was removed under reduced pressure yielding a white solid. ³¹P{¹H} (CD₃CN, 243 MHz) δ = 20.0, 16.9, 14.1 and 10.9.

Tris(2-pyridylmethyl)azaphosphatraneoxide (TPAPO) + TsOH : TsOH (16.1 mg, 0.08 mmol) in acetonitrile was added to a solution of tris(2-pyridylmethyl)azaphosphatrane (37.0 mg, 0.08 mmol) in acetonitrile. After the solution was stirred for 1 day, the solvent was removed under reduced pressure yielding a white solid. ³¹P{¹H} (CD₃CN, 243 MHz) δ = 12.9, 7.8, 1.64, -19.1 and -38.8.

Tris(benzyl)azaphosphatraneoxide (TBAPO) + HBF₄ : 20 drops of HBF₄ (48% w/w) were added to a solution of tris(benzyl)azaphosphatrane in benzene . After the solution was stirred for 1 day, the solvent was removed under reduced pressure yielding a white solid. ³¹P{¹H} (CD₃CN, 243 MHz) δ = 14.7.

Tris(benzyl)azaphosphatraneoxide (TBAPO) + TsOH : TsOH (15.4 mg, 0.08 mmol) in acetonitrile was added to a solution of tris(benzyl)azaphosphatrane (36.8 mg, 0.08 mmol) in acetonitrile. After the solution was stirred for 1 day, the solvent was removed under reduced pressure yielding a white solid. ³¹P{¹H} (CD₃CN, 243 MHz) δ = 21.0 and 15.7.

B.6. References

1. Cheng, M.-J.; Goddard, W. A., The Critical Role of Phosphate in Vanadium Phosphate Oxide for the Catalytic Activation and Functionalization of n-Butane to Maleic Anhydride. *Journal of the American Chemical Society* **2013**, *135* (12), 4600-4603.
2. Haake, P.; Cook, R. D.; Hurst, G. H., Evaluation of the basicity of phosphine oxides and phosphine sulfides by measurements of chemical shift in sulfuric acid solutions. *Journal of the American Chemical Society* **1967**, *89* (11), 2650-2654.
3. Liu, X.-D.; Verkade, J. G., Unusual Phosphoryl Donor Properties of OP(MeNCH₂CH₂)₃N. *Inorganic Chemistry* **1998**, *37* (20), 5189-5197.
4. Liu, X.; Verkade, J. G., Electron-rich O=PR₃ compounds: Catalysts for alcohol silylation. *Heteroatom Chemistry* **2001**, *12* (1), 21-26.
5. Chintareddy, V. R.; Wadhwa, K.; Verkade, J. G., P(PhCH₂NCH₂CH₂)₃N Catalysis of Mukaiyama Aldol Reactions of Aliphatic, Aromatic, and Heterocyclic Aldehydes and Trifluoromethyl Phenyl Ketone. *The Journal of Organic Chemistry* **2009**, *74* (21), 8118-8132.

APPENDIX C

Coordination Complexes of Phosphine Ligands without Transannular Interactions

Portions of this chapter have been published:

Thammavongsy, Z.; Khosrowabadi Kotyk, J. F.; Tsay, C.; Yang, J. Y. *Inorg. Chem.* **2015**, *54*, 11505-11510

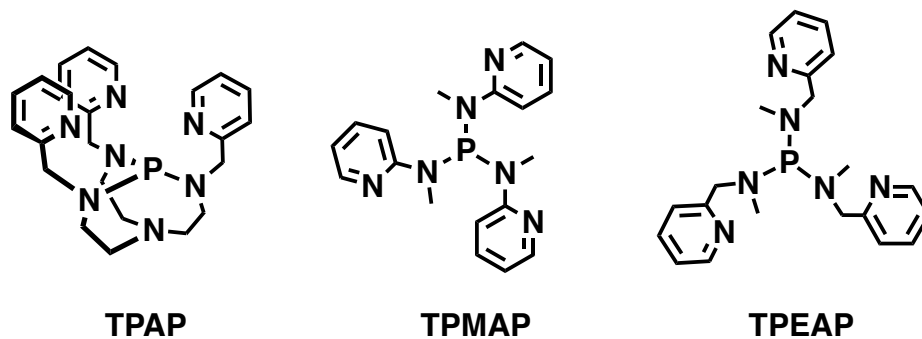
C.1. Motivation and Specific Aims

Ligand scaffold without the bicyclic cage frame in TPAP was designed and coordinated to Co(II) metal ions. These complexes were structurally characterized and compared with [Co(II)(TPAP)(CH₃CN)][BF₄]₂. The ligands without the bicyclic cage frame were designed in order to compare future reactivity studies with transition metal TPAP analogues.

C.2. Background

The role of transannular interactions in transition metal complexes was outlined in the introduction of chapter 3. In this appendix, the transition metal complexes of tris(2-pyridylmethyl)aminophosphine (TPMAP) and tris(2-pyridylethyl)aminophosphine (TPEAP) are described. Both TMAP and TPEAP ligands lack the transannular interaction of the P-N_{ax} bond in comparison to TPAP (Chart C.1).

Chart C.1. Ligand with Bicyclic Caged Framed (TPAP) and without (TPMAP & TPEAP).

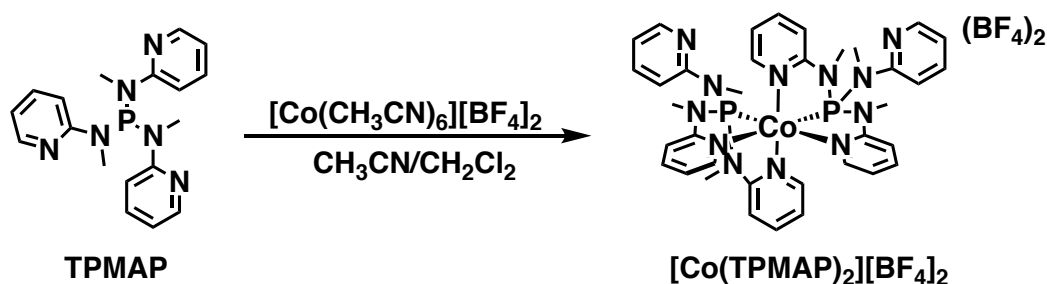


C.3. Results and Discussion

C.3.1. Synthesis of Co(II) Complexes of Tris(2-pyridylmethyl)aminophosphine (TPMAP)

The ligand, TPMAP, was synthesized following a published procedure.¹ One equivalent of TPMAP in dichloromethane was combined with one equivalent of $[\text{Co}(\text{CH}_3\text{CN})_6][\text{BF}_4]_2$ in acetonitrile (Scheme C.1). Electrospray ionization mass spectrum (ESI-MS) of the reaction mixture reveals the presence of the $[\text{Co}(\text{TPMAP})_2]^{2+}$ ion and an absence of the $[\text{Co}(\text{TPMAP})]^{2+}$ ion. The isolated product $[\text{Co}(\text{TPMAP})_2][\text{BF}_4]_2$ was precipitated and washed with diethyl ether to afford a green solid in 32.5% yield.²

Scheme C.1. Coordination of TPMAP with $[\text{Co}(\text{CH}_3\text{CN})_6][\text{BF}_4]_2$.



$[\text{Co}(\text{TPMAP})_2][\text{BF}_4]_2$ was analyzed by single crystal X-ray diffraction (Figure C.1). The crystal structure contains two 6-coordinate $[\text{Co}(\text{TPMAP})_2]^{2+}$ complexes in the asymmetric unit. In each TPMAP ligand, only two pyridines and the central phosphorus donor are coordinated, leaving one pyridine unbound to the Co(II) center. This binding mode is similar to what was previously observed with Cr(III), Fe(II), and Ru(II).¹

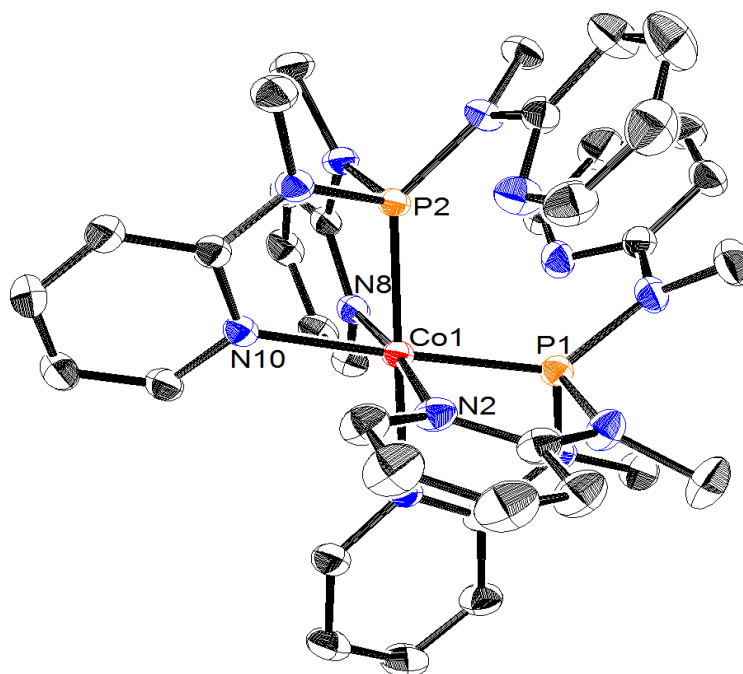
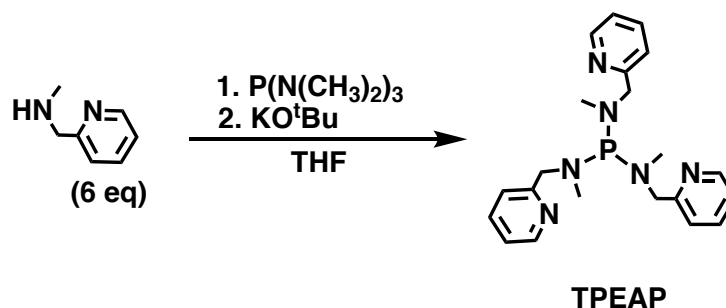


Figure C.1. Crystal structure of $[\text{Co}(\text{TPMAP})_2][\text{BF}_4]_2$. Thermal ellipsoids are drawn at 50% probability. Hydrogen atoms and counter anions are omitted for clarity. Adapted with permission from Thammavongsy, Z.; Khosrowabadi Kotyk, J. F.; Tsay, C.; Yang, J. Y. *Inorg. Chem.* **2015**, 54, 11505-11510. Copyright 2015 American Chemical Society.

C.3.2. Synthesis of Tris(2-pyridylethyl)aminophosphine (TPEAP)

The ligand, TPEAP, which has an additional methylene linker compared to TPMAP, is a closer analogue of TPAP due to the potential 6-membered chelate ring formation. TPEAP was synthesized by mixing 2-pyridinemethanamine and tris(dimethylamino)phosphine in a 6:1 ratio at room temperature followed by the addition of KO^tBu in tetrahydrofuran (Scheme C.2). The $^{31}\text{P}\{^1\text{H}\}$ NMR spectrum of TPEAP displayed one resonance at 125.6 ppm. The ^1H NMR spectrum contained impurities consistent to the starting material 2-pyridinemethaneamine, which can impact potential metallation reactions. Care must be taken with the ratio of the starting materials to regulate the amount of impurities found in the product.

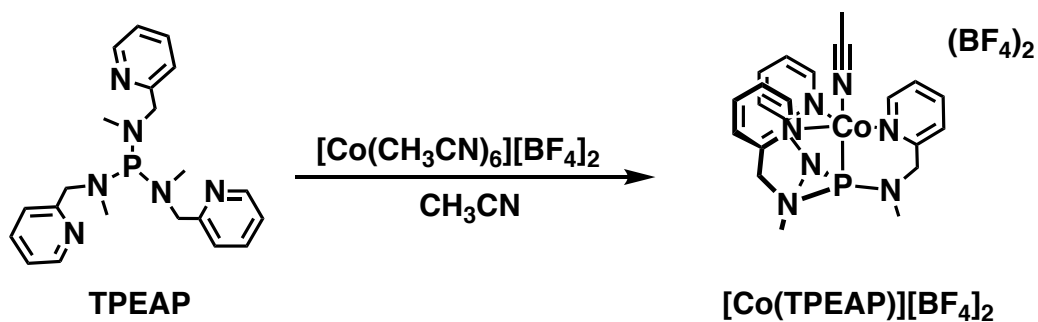
Scheme C.2. Synthesis of tris(2-pyridylethyl)aminophosphine (TPEAP).



C.3.3. Synthesis of Co(II) Complexes of Tris(2-pyridylethyl)aminophosphine (TPEAP)

One equivalent of TPEAP in dichloromethane was combined with one equivalent of $[\text{Co}(\text{CH}_3\text{CN})_6][\text{BF}_4]_2$ in acetonitrile (Scheme C.3). The solution exhibited a color change from light pink to brown. After solvent was removed under reduced pressure, a brown solid was isolated in 61.19% yield. X-ray quality crystals were grown from layering a solution of the brown solid in dichloromethane with diethyl ether.

Scheme C.3. Coordination of TPEAP with $[\text{Co}(\text{CH}_3\text{CN})_6][\text{BF}_4]_2$.



The crystal structure contains two 5-coordinate $[\text{Co}(\text{TPEAP})(\text{CH}_3\text{CN})]^{2+}$ complexes in the asymmetric unit (Figure C.2). Unlike TPAP, the TPEAP version coordinates to the Co(II) ion in a tetradentate fashion. The τ_5 value of $[\text{Co}(\text{TPEAP})(\text{CH}_3\text{CN})][\text{BF}_4]_2$ is 0.274 (average of both complexes in unit cell), where a value of 0 represents an ideal square pyramid, and a value of 1 represents an ideal trigonal bipyramid.³ Comparing the τ_5 value of $[\text{Co}(\text{TPEAP})(\text{CH}_3\text{CN})][\text{BF}_4]_2$ and $[\text{Co}(\text{TPAP})(\text{CH}_3\text{CN})][\text{BF}_4]_2$ ($\tau_5 = 0.418$), the geometry of the $[\text{Co}(\text{TPEAP})(\text{CH}_3\text{CN})][\text{BF}_4]_2$ is more square pyramidal than $[\text{Co}(\text{TPAP})(\text{CH}_3\text{CN})][\text{BF}_4]_2$, potentially due to the non-bicyclic cage frame that would restrict coordination to a more C_3 symmetric complex. The Co–P distance in $[\text{Co}(\text{TPEAP})(\text{CH}_3\text{CN})][\text{BF}_4]_2$ is 2.147 Å (average of both complexes in unit cell) which is similar to that of $[\text{Co}(\text{TPAP})(\text{CH}_3\text{CN})][\text{BF}_4]_2$ (Co–P = 2.1693(7) Å).

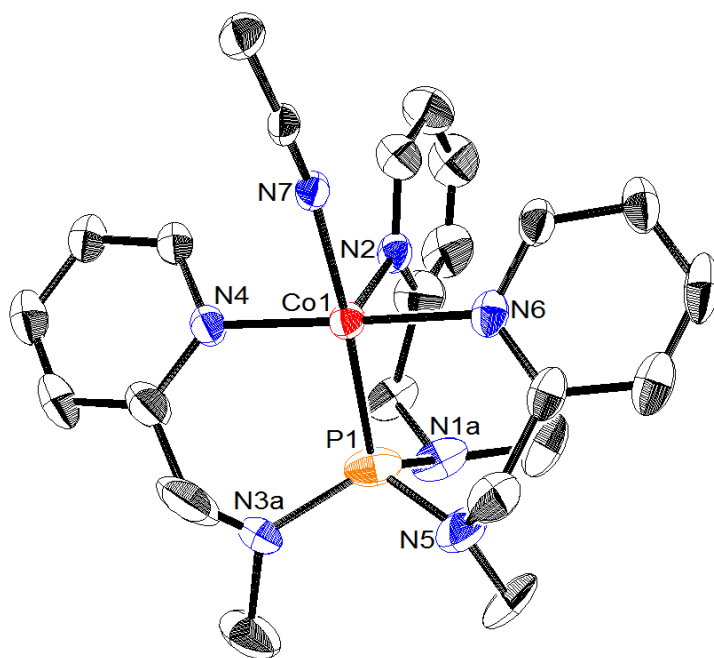


Figure C.2. Crystal structure of $[\text{Co}(\text{TPEAP})(\text{CH}_3\text{CN})][\text{BF}_4]_2$. Thermal ellipsoids are drawn at 50% probability. Hydrogen atoms and counter anions are omitted for clarity.

C.4. Conclusion

Co(II) complexes of TPMPAP and TPEAP (non-bicyclic analogue of TPAP) were synthesized and structurally characterized. The additional methylene linker in TPEAP (compared to TPMPAP) provided flexibility for tetradentate coordination to a Co(II) ion. TPEAP displayed tetradentate chelation in $[\text{Co}(\text{TPEAP})(\text{CH}_3\text{CN})][\text{BF}_4]_2$, just like TPAP in $[\text{Co}(\text{TPAP})(\text{CH}_3\text{CN})][\text{BF}_4]_2$.

C.5. Experimental Details

General Considerations

All manipulations were performed in the glovebox, as all complexes are air- and moisture-sensitive. All solvents were first purged with argon and dried using a solvent purification system. 2-pyridinemethanamine, KO^tBu, tris(dimethylamino)phosphine were commercially purchased and used without further purification. Ni(TPAP)(COD) was synthesized according to an established procedure.⁴ $[\text{Co}(\text{CH}_3\text{CN})_6][\text{BF}_4]_2$ ⁵ and TPMPAP¹ were synthesized according to published procedures.

Physical Methods

Nuclear Magnetic Resonance (NMR) Spectroscopy: Nuclear magnetic resonance (NMR) spectra were recorded on a DRX400 with a switchable QNP probe (¹H and ³¹P) or a Bruker AVANCE 600 MHz (¹H and ³¹P). ¹H NMR spectra were referenced to (tetramethylsilane) TMS using the residual proteo impurities of the solvent; ³¹P{¹H} NMR spectroscopy experiments are referenced to the absolute frequency of 0 ppm in the ¹H dimension according to the Xi scale.⁶

X-ray Crystallography (XRC): X-ray diffraction studies were carried out at the UCI Department of Chemistry X-ray Crystallography Facility on a Bruker SMART APEX II diffractometer. Data

were collected at 88 K using Mo K α radiation ($\lambda = 0.71073 \text{ \AA}$). A full sphere of data was collected for each crystal structure. The APEX2 program suite was used to determine unit-cell parameters and to collect data. The raw frame data were processed and absorption corrected using the SAINT and SADABS programs, respectively, to yield the reflection data files. Structures were solved by direct methods using SHELXS and refined against F2 on all data by full-matrix least-squares with SHELXL-97.

For the structure of $[\text{Co}(\text{TPMAP})_2][\text{BF}_4]_2$, checkCIF reports one level B alert (PLAT214_ALERT_2_B) due to a high ratio of maximum to minimum anisotropic displacement parameters (ADPs) for atom F2B, which can signify a substitutional or positional disorder. As this atom is in the minor part of a disordered BF_4 anion, the identity of which is not in question.

$[\text{Co}(\text{TPMAP})_2][\text{BF}_4]_2$: In the glovebox, $[\text{Co}(\text{CH}_3\text{CN})_6][\text{BF}_4]_2$ (61.3 mg, 0.128 mmol) was added to a solution of TMAP (45.1 mg, 0.128 mmol) in 3 mL of dichloromethane. The solution immediately turned dark green and was stirred for 6 h at room temperature. The solvent was removed under reduced pressure, and the resulting green solid was washed with diethyl ether. The green solid was re-dissolved in acetonitrile and filtered through a glass pipet packed with a glass microfiber filter. Slow vapor diffusion with diethyl ether afforded green crystals. ESI-MS (m/z): $[\text{M} - \text{BF}_4]^+$ Calculation for $\text{C}_{36}\text{H}_{42}\text{BCoF}_4\text{N}_{12}\text{P}_2$, 850.25; Found, 850.17. UV-vis (CH_3CN) λ_{max} , nm (ϵ): 230 (49377), and 290 (18654). Analytical Calculation for $\text{C}_{36}\text{H}_{42}\text{B}_2\text{Cl}_3\text{CoF}_8\text{N}_{12}\text{P}_2 \cdot (\text{CH}_2\text{C}_2)_{1.5}$: C, 42.14; H, 4.13; N, 15.92. Found: C, 42.30; H, 4.26; N, 15.79. μ_{eff} (solution) = 2.11 μB

Tris(2-pyridylethyl)aminophosphine (TPEAP): In a Schlenk flask, 2-pyridinemethanamine (200 mg, 1.64 mmol), tris(dimethylamino)phosphine (44.5 mg, 0.273 mmol) and 15 mL of tetrahydrofuran were added. The reaction was stirred for 4 days at room temperature, under N₂. The reaction mixture was brought into the glove box and was added KO^tBu (0.061 mg, 0.54 mmol). A color change was observed from colorless to pink and stirred for 1 day. The reaction was filtered through a medium fritted funnel. The filtrate was collected, and the solvent was removed under reduced pressure. The solid was redissolved in acetonitrile and refiltered through a medium fritted funnel to remove excess potassium tert-butoxide. The filtrate was collected, the solvent was removed under reduced pressure, and the solid was redissolved in tetrahydrofuran and layered with pentane. After 1 day of standing, the solution was decanted from crystalline potassium tert-butoxide. The solvent from the filtrate was removed under reduced pressure to afford the product as a colorless oil. ¹H NMR (CD₃CN, 400 MHz) δ = 2.51 (d, 9H, NCH₃), 4.18 (d, 6H, PyrCH₂N), 7.18 (m, 3H, Py), 7.40 (d, 3H, Py), 7.68 (m, 3H, Py), 8.49 (d, 3H, Py). ³¹P{¹H}NMR (CD₃CN, 162 MHz) δ = 125.6.

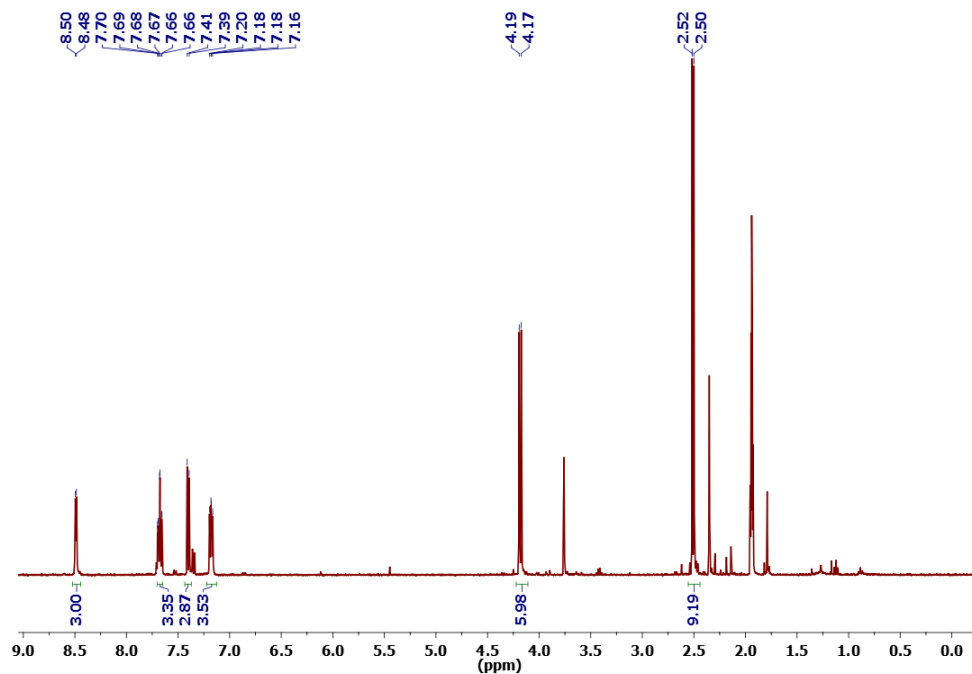


Figure C.3. ^1H NMR spectrum of tris(2-pyridylethyl)aminophosphine (TPEAP) in CD_3CN .

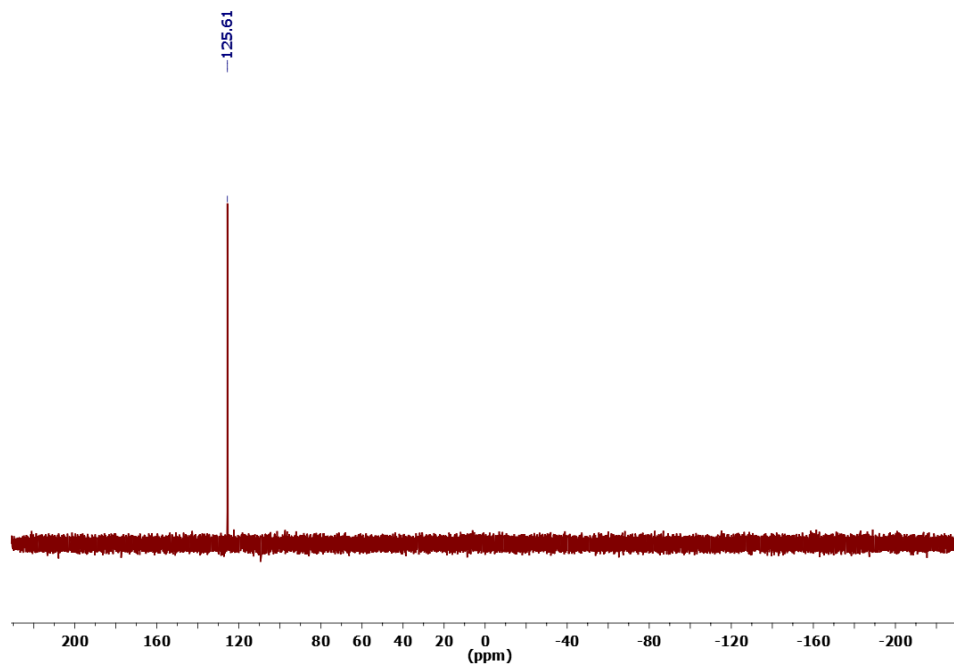


Figure C.4. $^{31}\text{P}\{^1\text{H}\}$ NMR spectrum of tris(2-pyridylethyl)aminophosphine (TPEAP) in CD_3CN .

[Co(TPEAP)(CH₃CN)][BF₄]₂: In the glovebox, a solution of [Co(CH₃CN)₆][BF₄]₂ (42.6 mg, 0.0889 mmol) in 3 mL acetonitrile was added to a solution of TPEAP (35.1 mg, 0.0889 mmol) in 3 mL of dichloromethane. The solution turned brown and was stirred for 1 day at room temperature. The solvent was removed under reduced pressure, and the resulting brown solid was washed with diethyl ether. The green solid was re-dissolved in dichloromethane and filtered through a glass pipet packed with a glass microfiber filter. A layering system of diethyl ether/dichloromethane afforded red crystals.

C.6. References

1. Whiteoak, C. J.; Nobbs, J. D.; Kiryushchenkov, E.; Pagano, S.; White, A. J. P.; Britovsek, G. J. P., Tri(pyridylmethyl)phosphine: The Elusive Congener of TPA Shows Surprisingly Different Coordination Behavior. *Inorganic Chemistry* **2013**, *52* (12), 7000-7009.
2. Thammavongsy, Z.; Khosrowabadi Kotyk, J. F.; Tsay, C.; Yang, J. Y., Flexibility is Key: Synthesis of a Tripyridylamine (TPA) Congener with a Phosphorus Apical Donor and Coordination to Cobalt(II). *Inorganic Chemistry* **2015**, *54* (23), 11505-11510.
3. Addison, A. W.; Rao, T. N.; Reedijk, J.; van Rijn, J.; Verschoor, G. C., Synthesis, structure, and spectroscopic properties of copper(II) compounds containing nitrogen-sulphur donor ligands; the crystal and molecular structure of aqua[1,7-bis(N-methylbenzimidazol-2'-yl)-2,6-dithiaheptane]copper(II) perchlorate. *Journal of the Chemical Society, Dalton Transactions* **1984**, (7), 1349-1356.
4. Thammavongsy, Z.; Cunningham, D. W.; Sutthirat, N.; Eisenhart, R. J.; Ziller, J. W.; Yang, J. Y., Adaptable ligand donor strength: tracking transannular bond interactions in tris(2-pyridylmethyl)-azaphosphatane (TPAP). *Dalton Transactions* **2018**, *47* (39), 14101-14110.
5. Coucouvanis, D., Useful Reagents and Ligands. In *Inorganic Syntheses*, Coucouvanis, D., Ed. John Wiley & Sons, Inc.: 2002; Vol. 33, pp 75-121.
6. Harris Robin, K.; Becker Edwin, D.; Cabral de Menezes Sonia, M.; Goodfellow, R.; Granger, P., NMR nomenclature. Nuclear spin properties and conventions for chemical shifts (IUPAC Recommendations 2001). In *Pure and Applied Chemistry*, 2001; Vol. 73, p 1795.

APPENDIX D

Attempted Synthesis of an Fe-Sulfur-Carbide Cluster

D.1. Motivation and Specific Aims

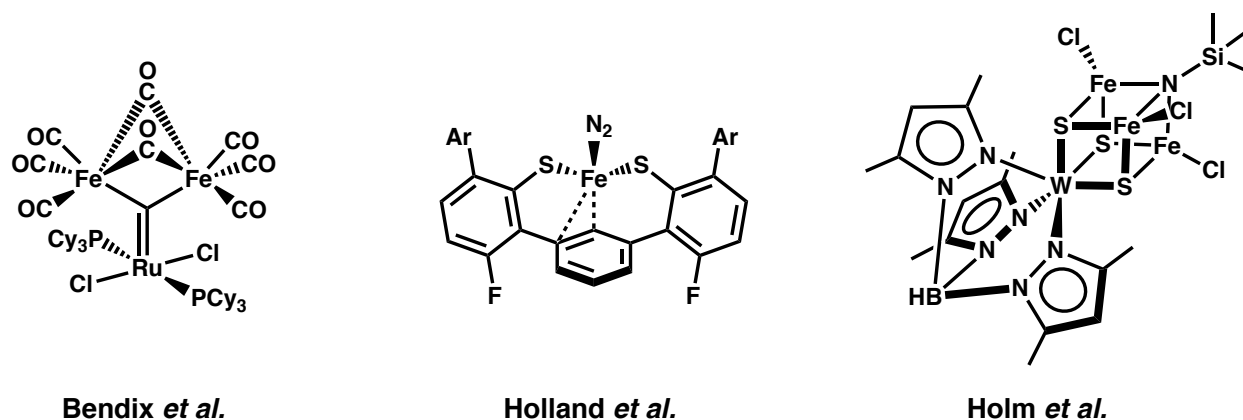
Cluster chemistry is a rich subset of inorganic chemistry since Albert Cotton first used the word “cluster” to describe multimetallic complexes in the 1960s.¹ One of the motivations driving inorganic chemists to pursue these synthetic challenges is the importance cluster complexes play in biology. There is great interest in a synthetic mimic of the FeMocofactor (FeMoco) in the molybdenum nitrogenase enzyme due to the recent identification of the carbide interstitial atom.²³ The work detailed in this appendix describes efforts to synthesize an Fe-carbide cluster containing sulfur ligands.

D.2. Background

In 2011, the mysterious interstitial atom was revealed in the nitrogenase’s FeMocofactor (FeMoco) as a tetraanionic carbon.^{2, 3} Although chemists have not yet synthesized a FeMoco mimic containing all components of the active site (Fe, S, and a carbide), some groups have published related complexes in hopes of shedding light on the role some of these atoms play in the active site.⁴ Holland and coworkers came close to incorporating relevant atoms of FeMoco with their Fe-bis(thiolate)arene ligand system, where the arene system is illustrated as a carbide (Figure D.1).⁵ Their electron rich Fe-bis(thiolate)arene complex binds N₂, where Holland and coworkers found the breaking of an Fe-S bond, from an exogenous sulfur ligand, to be an important step before N₂ binding. Holm synthesized a tris-pyrazolylylborate capping ligand on an Fe₃S₃ cluster group on W (Figure D.1). The Fe₃S₃ cluster contains a light atom, N, presenting a unique synthetic pathway to potentially incorporate other light atoms (i.e. carbon).⁶ Recently, Bendix and coworkers developed a new methodology to incorporate a carbide center in a Fe₂Ru cluster

complex.⁷ Although this system is missing sulfur ligands, the rare presence of a carbide center provides a solid foundation for more synthetic modifications in pursuit of a more structurally complete synthetic model of FeMoco.

Figure D.1. Structurally characterized Fe complexes containing either sulfur or carbide-like components as partial FeMoco synthetic mimics.



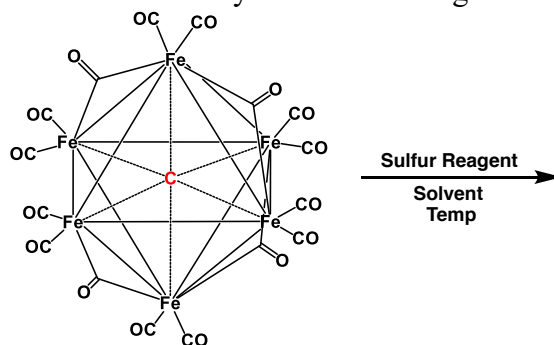
This appendix describes efforts to decorate a well-known Fe-carbide carbonyl cluster with sulfur ligands to generate the first synthetic model that incorporates all three components of FeMoco (Fe, S, and carbide atom).

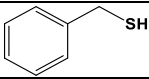
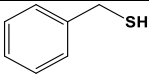
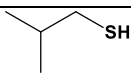
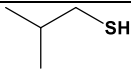
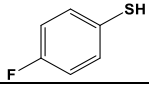
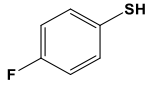
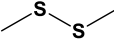
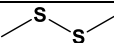
D.3. Results and Discussion

The starting point of this study was the cluster $[\text{Me}_4\text{N}]_2[\text{Fe}_6(\text{CO})_{16}\text{C}^{2-}]$ which was synthesized following a procedure by Churchill.⁸ The composition was confirmed by ^{13}C NMR and IR spectroscopy.⁸ The carbide is located downfield in the ^{13}C NMR spectrum, at 484 ppm and the IR spectrum display two major CO vibrational frequency at 1863 and 1727 cm^{-1} .⁹ Despite the difference in geometry between the $[\text{Me}_4\text{N}]_2[\text{Fe}_6(\text{CO})_{16}\text{C}^{2-}]$ cluster and the FeMoco active site, the closest Fe-C distance measured by X-ray diffraction is quite similar, at 1.9⁹ and 2.0¹⁰ Å, for $[\text{Me}_4\text{N}]_2[\text{Fe}_6(\text{CO})_{16}\text{C}^{2-}]$ and FeMoco, respectively.

The addition of sulfur atoms to $[\text{Me}_4\text{N}]_2[\text{Fe}_6(\text{CO})_{16}\text{C}^{2-}]$ was attempted through the addition of various sulfur compounds to $[\text{Me}_4\text{N}]_2[\text{Fe}_6(\text{CO})_{16}\text{C}^{2-}]$ in acetonitrile or tetrahydrofuran (Table D.1). These reactions were motivated by Holm's Fe_4S_4 cluster work with sulfur ligand exchange.¹¹

Table D.1. Attempted substitution of carbonyl with sulfur reagents in $[\text{Me}_4\text{N}]_2[\text{Fe}_6(\text{CO})_{16}\text{C}^{2-}]$.



Number	Sulfur Reagent	Ratio (Cluster:Sulfur)	Condition	Solvent	Duration (day)
1	S_8	1:4.5	Room Temperature	THF	1 day
2	S_8	1:4.5	UV-Lamp Room Temperature	CH_3CN	1 day
3		1:20	Room Temperature	CH_3CN	2 days
4		1:20	UV-Lamp Room Temperature	CH_3CN	1 day
5		1:18	Room Temperature	CH_3CN	2 days
6		1:22	UV-Lamp Room Temperature	CH_3CN	1 days
7		1:20	Room Temperature	CH_3CN	2 days
8		1:17	UV-Lamp Room Temperature	CH_3CN	1 days
9		1:17	Room Temperature	CH_3CN	2 days
10		1:20	UV-Lamp Room Temperature	CH_3CN	1 days

The reactions under a UV-lamp (365 nm) did produce a color change, resulting in the isolation of a brown or red brown solid. However, all reactions produced IR spectra with CO stretches that matched the vibrational spectra of the starting material. Infrared spectra of the isolated products from all the reactions can be found in the Experimental Details.

Reactions run at room temperature did not display a color change from purple (except with S₈). The reaction of [Me₄N]₂[Fe₆(CO)₁₆C²⁻] with S₈ in tetrahydrofuran (row **1** in Table D.1) produced a brown solid. Washing the brown solid with diethyl ether resulted in an orange yellow solution, in which colorless crystals formed upon slow evaporation of the diethyl ether. IR spectrum of the colorless crystals displayed CO vibrational frequencies at higher wavenumber (2082 and 1998 cm⁻¹) than the starting material (1863 and 1727 cm⁻¹ of [Me₄N]₂[Fe₆(CO)₁₆C²⁻]).

X-ray analysis of the colorless crystals displayed a Fe₅(CO)₁₅C, which is consistent with previous structures of Fe₅(CO)₁₅C (Figure D.2).⁹ It is documented that the [Me₄N]₂[Fe₆(CO)₁₆C²⁻] cluster can undergo chemical oxidation via the oxidative elimination of {Fe₁(CO)_m(X)_n} units.¹² However, the IR stretching frequency of the Fe₅(CO)₁₅C produced in this appendix do not match that of previous published Fe₅(CO)₁₅C (2015, 1975 and 1945 cm⁻¹).⁹

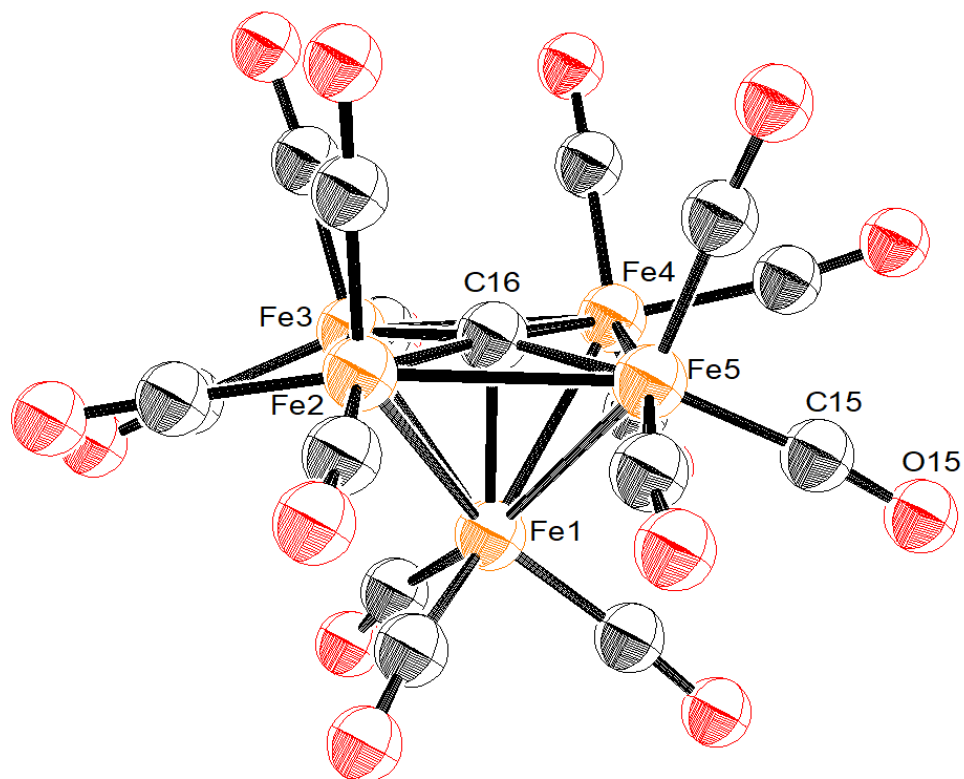


Figure D.2. Crystal structure of Fe₅(CO)₁₅C. Thermal ellipsoids are drawn at 50% probability.

D.4. Conclusion

The cluster, [Me₄N]₂[Fe₆(CO)₁₆C²⁻] was mixed with various sulfur reagents in order to produce a Fe-S-Carbide cluster that would mimic the FeMoco active site of nitrogenase. The reaction of [Me₄N]₂[Fe₆(CO)₁₆C²⁻] with S₈ (row 1 in Table D.1) produced crystal structures that identified as the Fe₅(CO)₁₅C cluster. However, the IR spectrum displayed CO vibrational frequencies that are not consistent with the literature values of a Fe₅(CO)₁₅C cluster.

D.5. Experimental Details

General Considerations

All manipulations were performed in the glovebox, as the clusters can undergo oxidative elimination. All solvents were first purged with argon and dried using a solvent purification system. Methyl disulfide, 4-fluorothiophenol, 2-methyl-1-propanethiol and benzyl mercaptan were provided from the Rychnovsky lab at UCI and used without further purification. Na(Hg), $\text{Mn}_2(\text{CO})_{10}$, $\text{Fe}(\text{CO})_5$ and S_8 were commercially purchased and used without further purification.

Physical Methods

Infrared (IR) Spectroscopy: In a glove box, the IR absorption was taken on a Thermo Scientific Nicolet iS5 spectrophotometer with an iD5 ATR attachment.

UV-Lamp Condition: All experiments with a UV-Lamp were conducted in the Evans' lab. In a hood with aluminum foil covered windows is a Hanovia medium-pressure 450 W (254 nm) mercury vapor lamp (PC451050/ 610741). The 5.5 in. long lamp was clamped to hang inside a 13 in. \times 1.5 in. diameter cavity of a double-walled quartz water cooling jacket. Samples were placed on a stir plate, placed on one side of the lamp.

General Reaction: In the glove box, the neat sulfur reagent was added to a solution of $[\text{Me}_4\text{N}]_2[\text{Fe}_6(\text{CO})_{16}\text{C}^{2-}]$ in 10 mL of THF. The mixture was stirred for either 1 d (UV-Lamp) or 2 d (no UV-Lamp). The solvent was then removed under reduced pressure to obtain a solid. For reactions with UV-light, the reaction vial (20 mL scintillation vial) was sealed with electrical tape and brought outside the box. After the reaction was finished, the solvent was removed under reduced pressure before analyzing the solid by IR spectroscopy in the glovebox.

(1) Solid S₈ (45.0mg) was added to a solution of [Me₄N]₂[Fe₆(CO)₁₆C²⁻] (36.8 mg) in THF. The purple mixture was stirred for 1 day, during which time the color changed from purple to brown. Solvent was removed under reduced pressure to obtain a brown solid. The brown solid was extracted with diethyl ether to give an orange yellow solution. X-ray quality crystals were grown from the slow evaporation of diethyl ether.

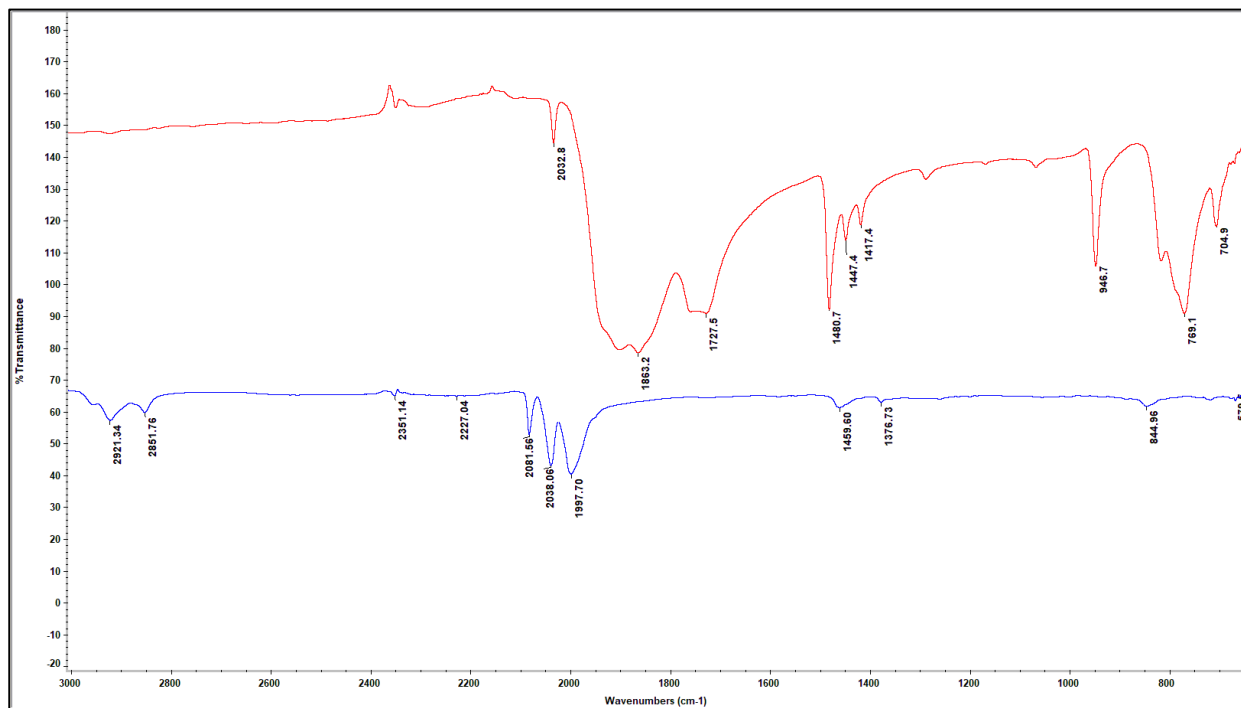


Figure D.3. IR spectra of (red, top) [Me₄N]₂[Fe₆(CO)₁₆C²⁻] and the product of (blue, bottom) [Me₄N]₂[Fe₆(CO)₁₆C²⁻] + S₈.

(2) Solid S₈ (52.9 mg) was added to a solution of [Me₄N]₂[Fe₆(CO)₁₆C²⁻] (43.3 mg) in CH₃CN. The purple mixture was stirred for 1 day under UV light, during which time the color changed from purple to red-brown.

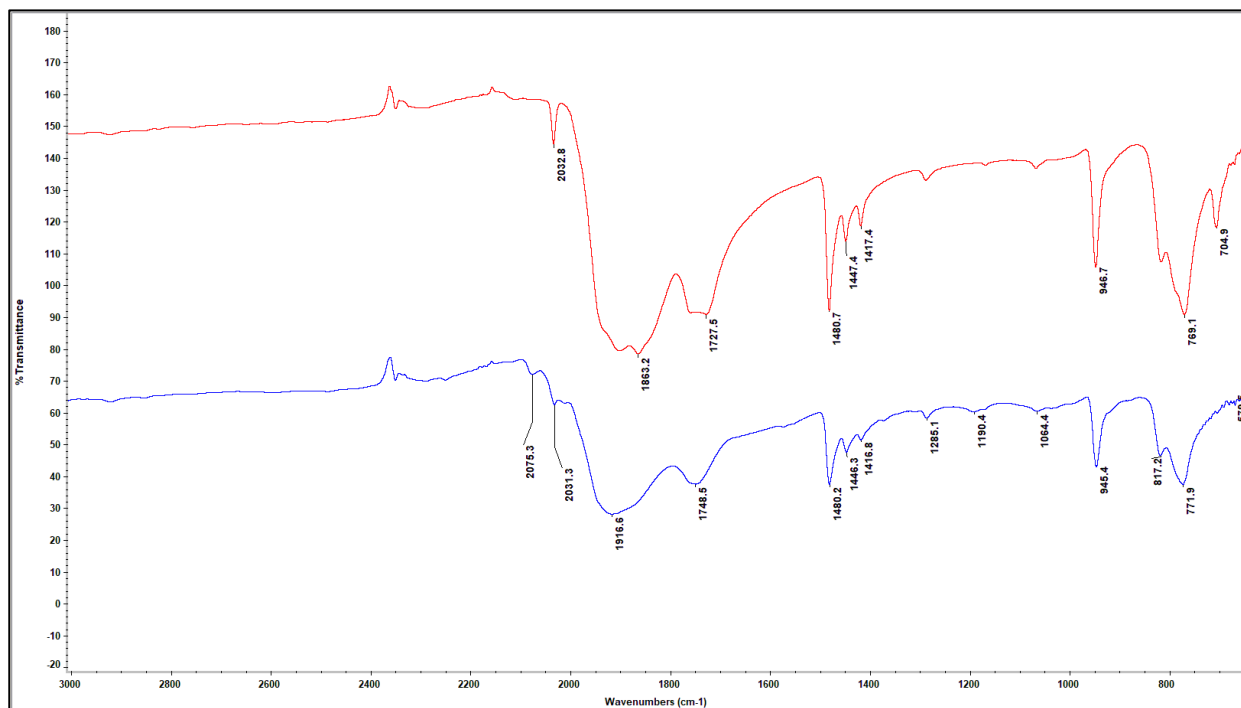


Figure D.4. IR spectra of (red, top) [Me₄N]₂[Fe₆(CO)₁₆C²⁻] and the product of (blue, bottom) [Me₄N]₂[Fe₆(CO)₁₆C²⁻] + S₈ under UV light.

(3) PhCH₂SH (53.7 mg) was added to a solution of [Me₄N]₂[Fe₆(CO)₁₆C²⁻] (25.5 mg) in CH₃CN.

The purple mixture was stirred for 1 day at room temperature. No color changed occurred.

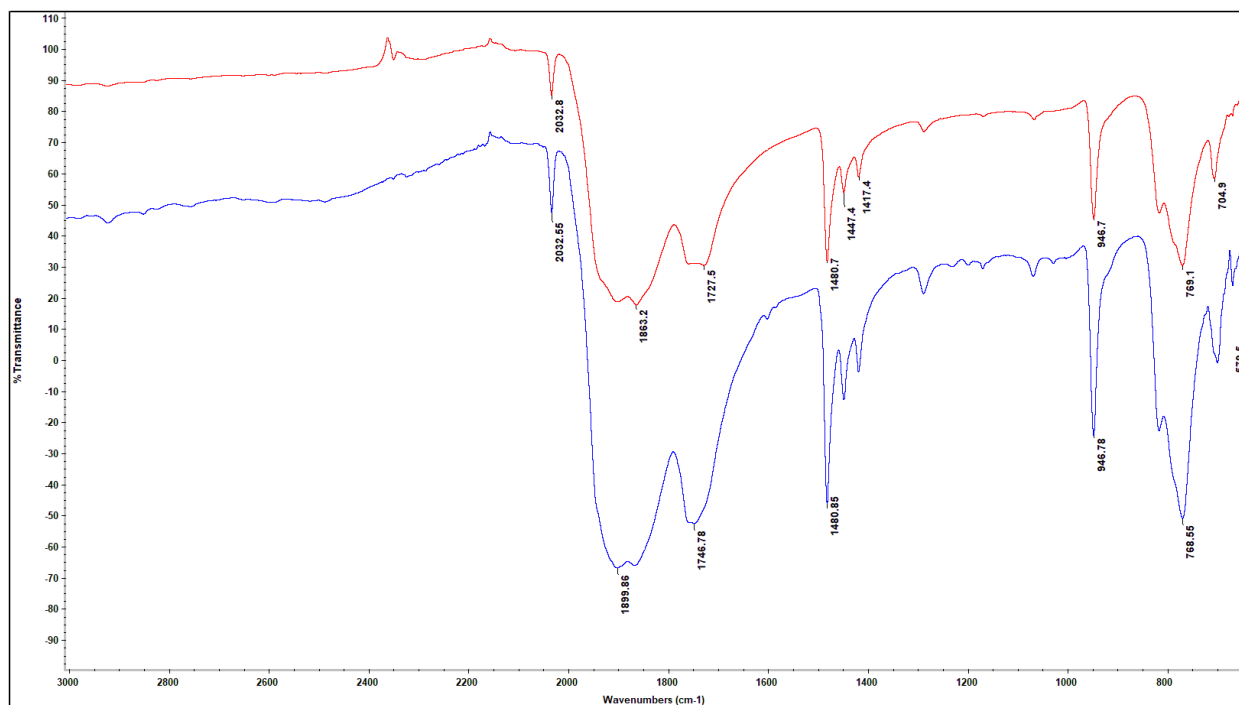


Figure D.5. IR spectra of (red, top) [Me₄N]₂[Fe₆(CO)₁₆C²⁻] and the product of (blue, bottom) [Me₄N]₂[Fe₆(CO)₁₆C²⁻] + PhCH₂SH.

(4) PhCH₂SH (52.9 mg) was added to a solution of Me₄N]₂[Fe₆(CO)₁₆C²⁻] (43.3 mg) in CH₃CN. The purple mixture was stirred for 1 day under UV light, during which time the color changed from purple to red-brown.

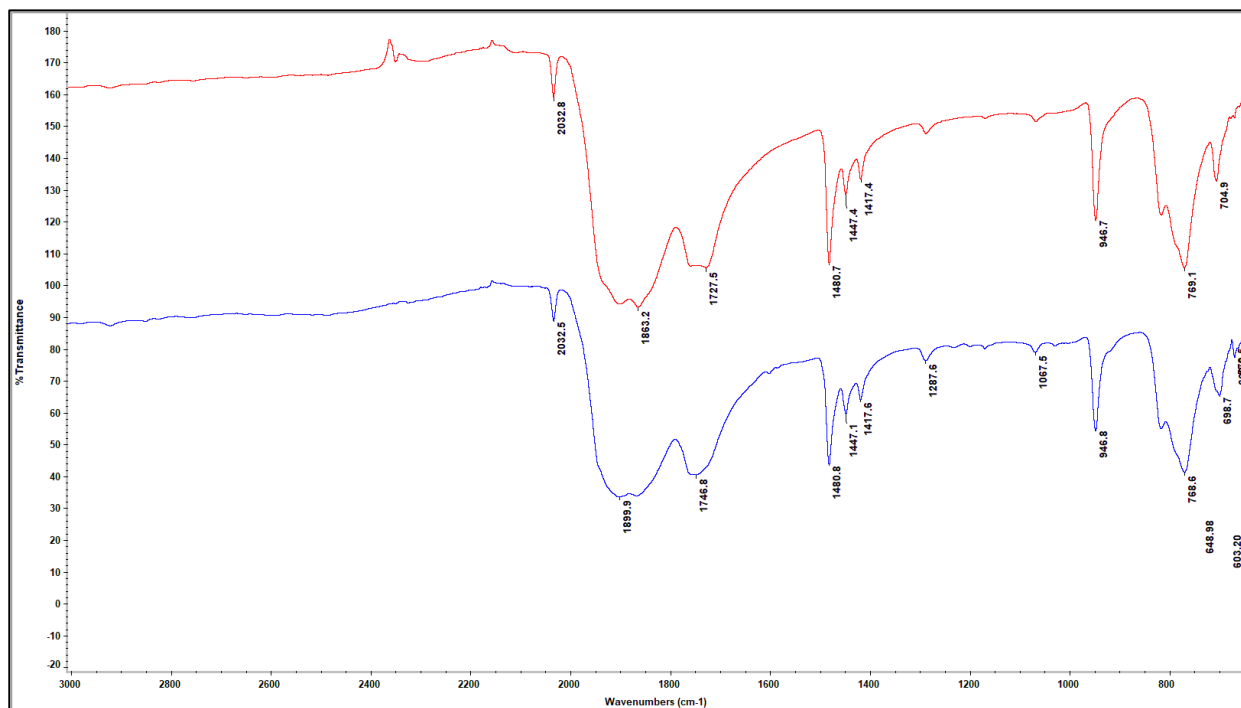


Figure D.6. IR spectra of (red, top) [Me₄N]₂[Fe₆(CO)₁₆C²⁻] and the product of (blue, bottom) [Me₄N]₂[Fe₆(CO)₁₆C²⁻] + PhCH₂SH under UV light.

(5) *i*PrSH (42.2 mg) was added to a solution of $[\text{Me}_4\text{N}]_2[\text{Fe}_6(\text{CO})_{16}\text{C}^{2-}]$ (24.2 mg) in CH_3CN . The purple mixture was stirred for 1 day at room temperature. No color change occurred.

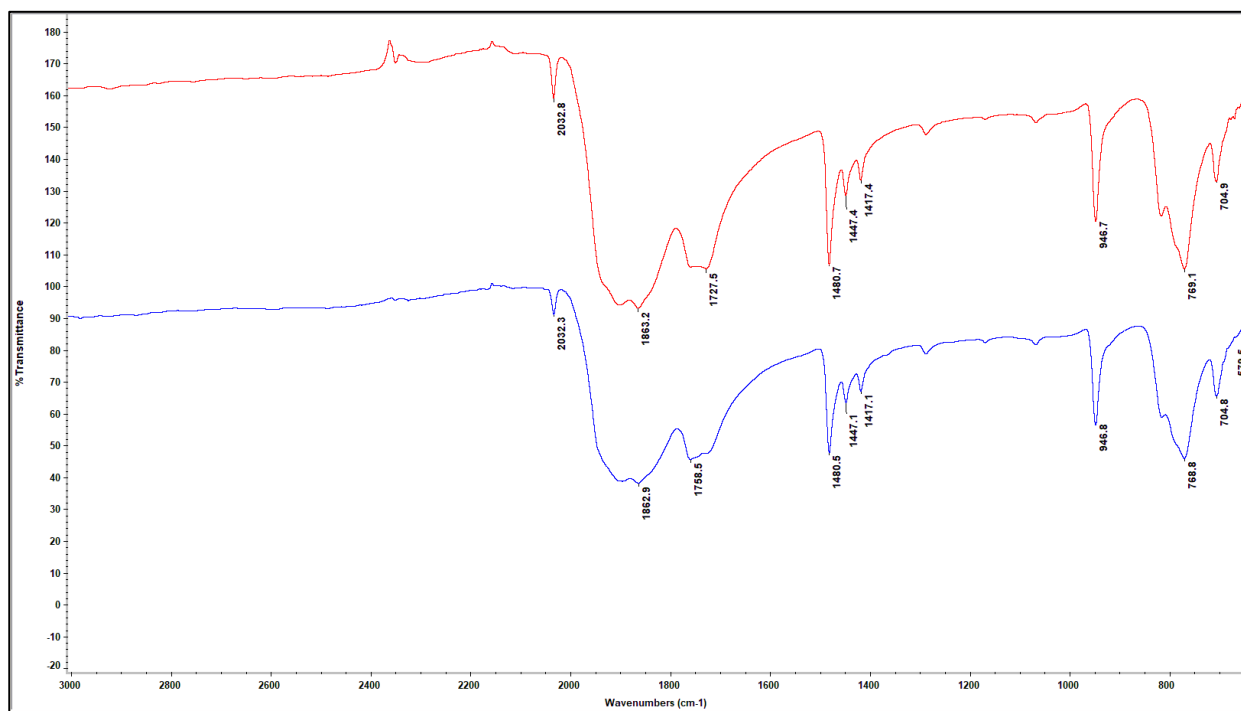


Figure D.7. IR spectra of (red, top) $[\text{Me}_4\text{N}]_2[\text{Fe}_6(\text{CO})_{16}\text{C}^{2-}]$ and the product of (blue, bottom) $[\text{Me}_4\text{N}]_2[\text{Fe}_6(\text{CO})_{16}\text{C}^{2-}] + i\text{PrSH}$.

(6) i PrSH (72.5 mg) was added to a solution of $[\text{Me}_4\text{N}]_2[\text{Fe}_6(\text{CO})_{16}\text{C}^{2-}]$ (34.2 mg) in CH_3CN . The purple mixture was stirred for 1 day under UV light, during which time the color changed from purple to red-brown.

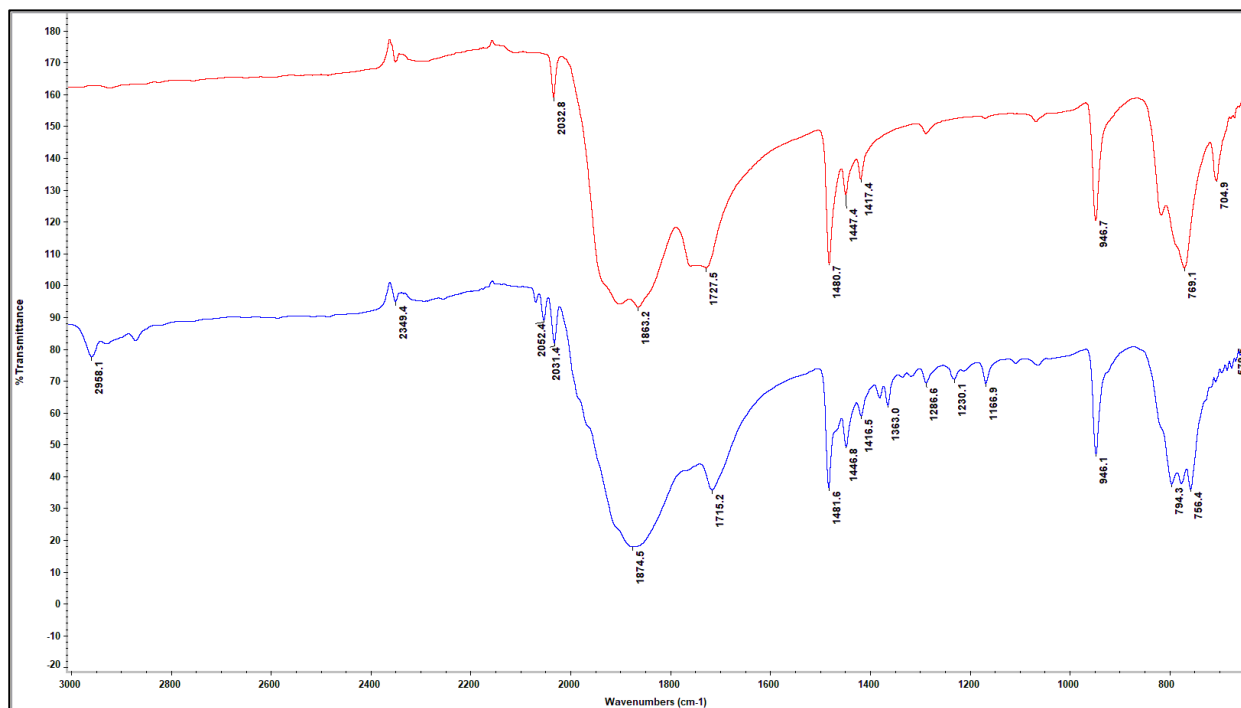


Figure D.8. IR spectra of (red, top) $[\text{Me}_4\text{N}]_2[\text{Fe}_6(\text{CO})_{16}\text{C}^{2-}]$ and the product of (blue, bottom) $[\text{Me}_4\text{N}]_2[\text{Fe}_6(\text{CO})_{16}\text{C}^{2-}] + i$ PrSH under UV light.

(7) *p*-FC₆H₄SH (69.6 mg) was added to the solution of [Me₄N]₂[Fe₆(CO)₁₆C²⁻] (26.0 mg) in CH₃CN. The purple mixture was stirred for 1 day at room temperature. No color changed occurred.

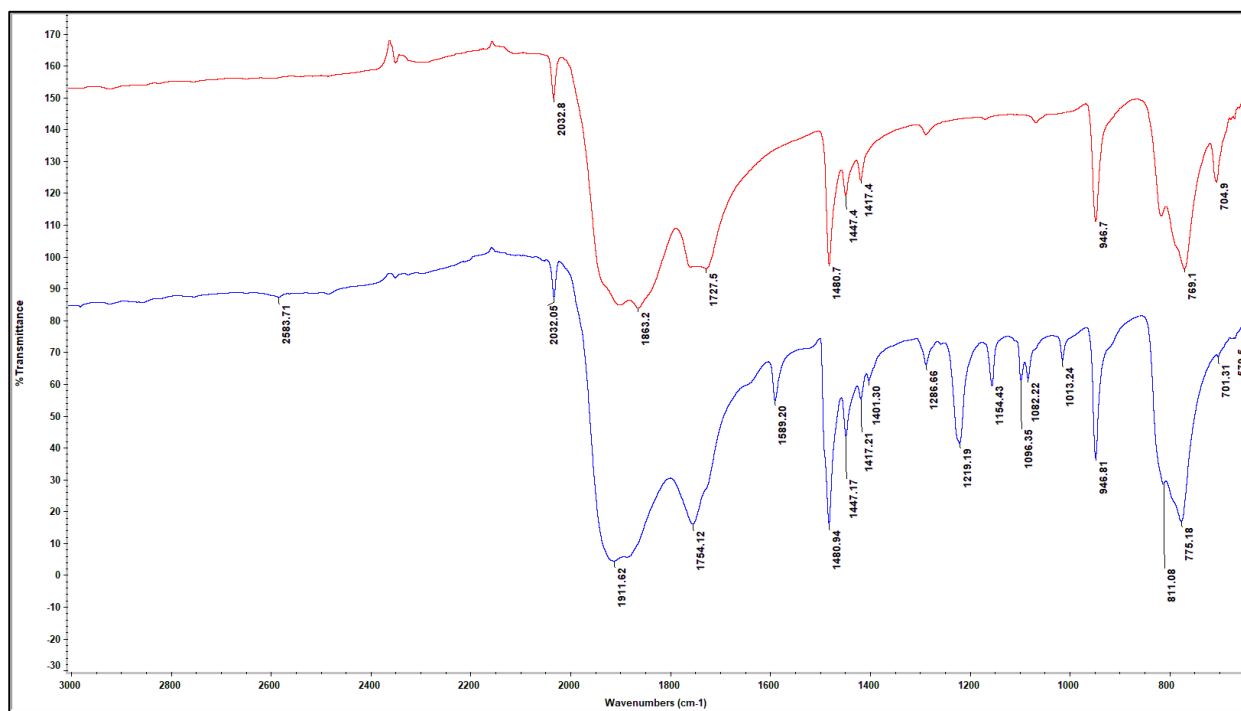


Figure D.9. IR spectra of (red, top) [Me₄N]₂[Fe₆(CO)₁₆C²⁻] and the product of (blue, bottom) [Me₄N]₂[Fe₆(CO)₁₆C²⁻] + *p*-FC₆H₄SH.

(8) *p*-FC₆H₄SH (64.5 mg) was added to a solution of [Me₄N]₂[Fe₆(CO)₁₆C²⁻] (28.4 mg) in CH₃CN.

The purple mixture was stirred for 1 day under UV light, during which time the color changed from purple to red-brown.

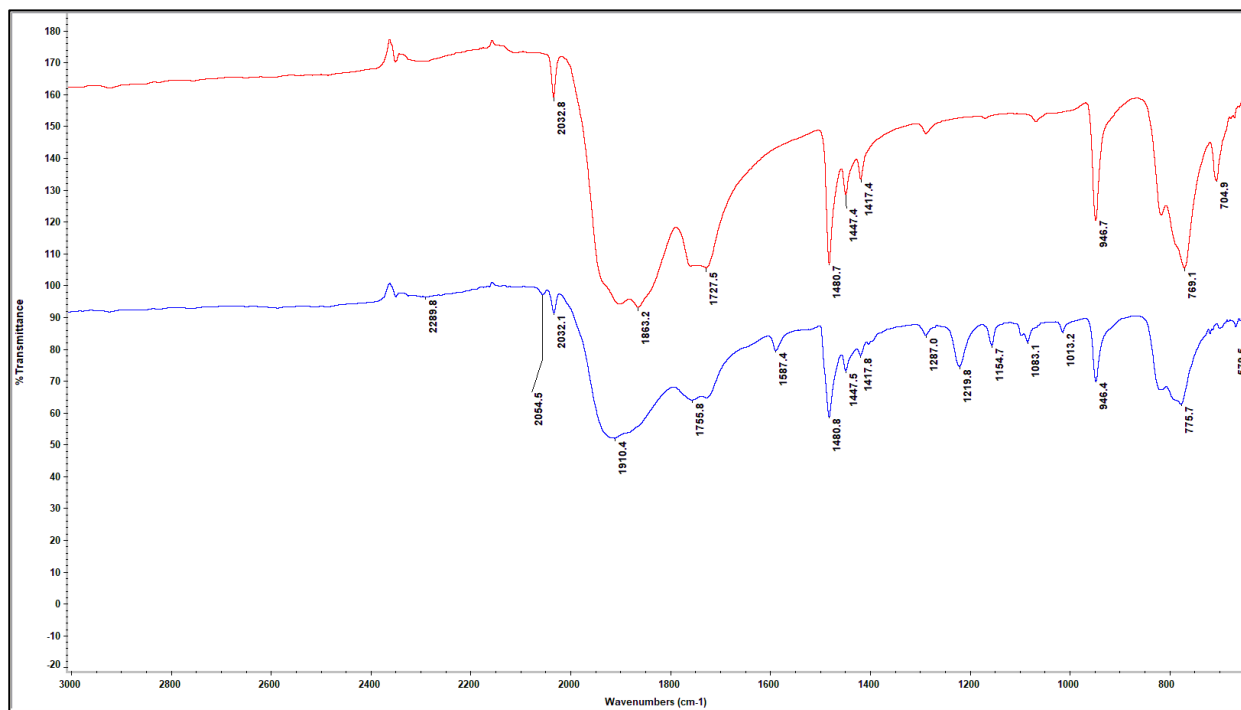


Figure D.10. IR spectra of (red, top) [Me₄N]₂[Fe₆(CO)₁₆C²⁻] and the product of (blue, bottom) [Me₄N]₂[Fe₆(CO)₁₆C²⁻] + *p*-FC₆H₄SH under UV light.

(9) Me_2S_2 (41.9 mg) was added to a solution of $[\text{Me}_4\text{N}]_2[\text{Fe}_6(\text{CO})_{16}\text{C}^{2-}]$ (25.0 mg) in CH_3CN . The purple mixture was stirred for 1 day at room temperature. No color change occurred.

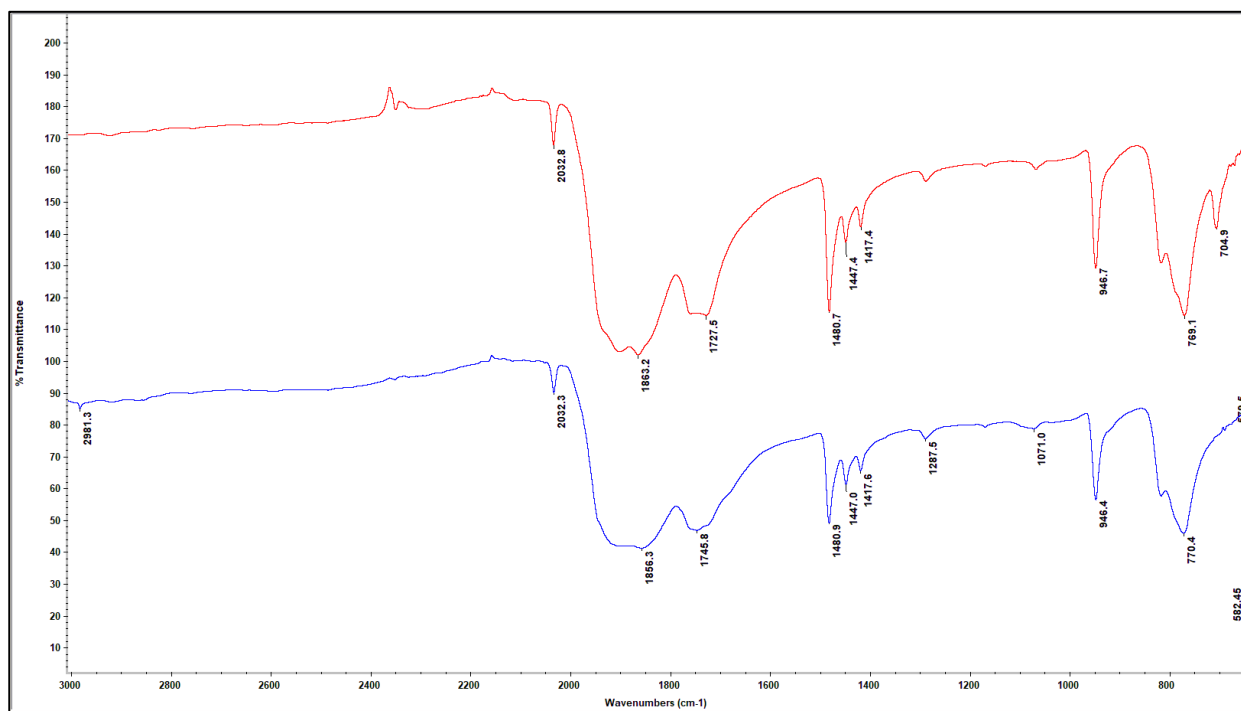


Figure D.11. IR spectra of (red, top) $[\text{Me}_4\text{N}]_2[\text{Fe}_6(\text{CO})_{16}\text{C}^{2-}]$ and the product of (blue, bottom) $[\text{Me}_4\text{N}]_2[\text{Fe}_6(\text{CO})_{16}\text{C}^{2-}] + \text{Me}_2\text{S}_2$.

(10) Me₂S₂ (64.5 mg) was added to a solution of [Me₄N]₂[Fe₆(CO)₁₆C²⁻] (28.4 mg) in CH₃CN. The purple mixture was stirred for 1 day under UV light, during which time the color changed from purple to red-brown.

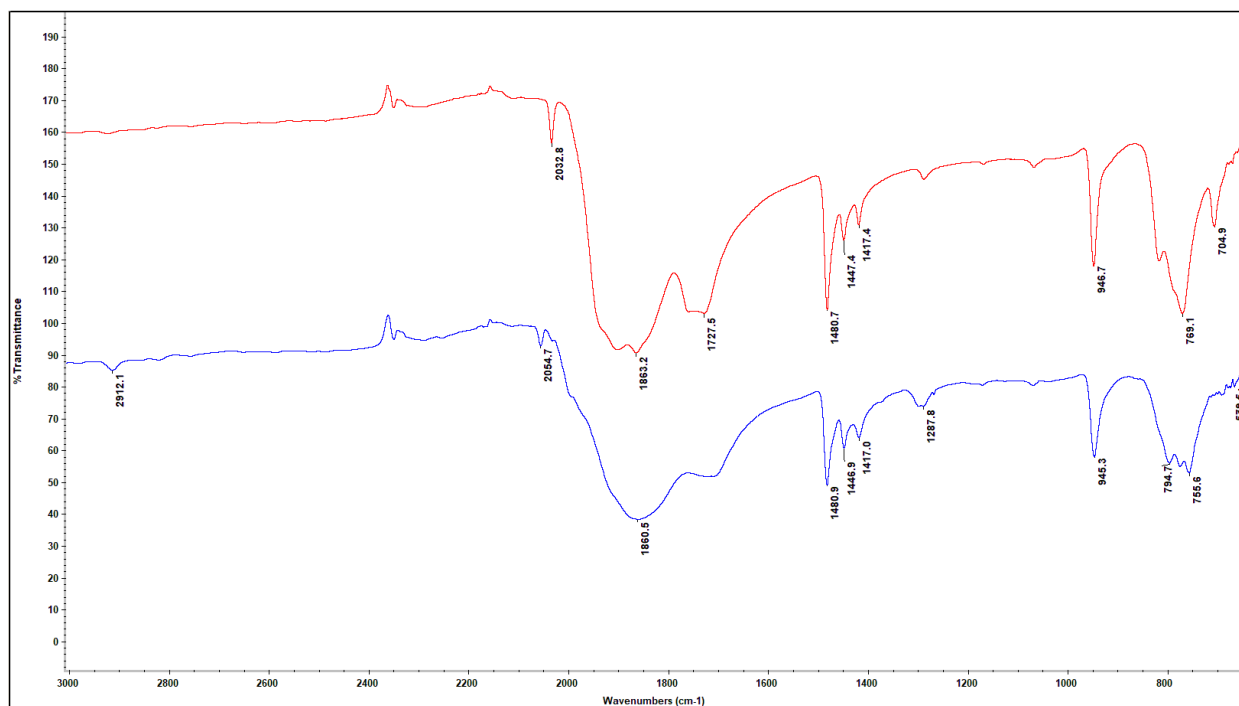


Figure D.12. IR spectra of (red, top) [Me₄N]₂[Fe₆(CO)₁₆C²⁻] and the product of (blue, bottom) [Me₄N]₂[Fe₆(CO)₁₆C²⁻] + Me₂S₂ under UV light.

D.6. References

1. Bertrand, J. A.; Cotton, F. A.; Dollase, W. A., The Crystal Structure of Cesium Dodecachlorotrirhenate-(III), a Compound with a New Type of Metal Atom Cluster. *Inorganic Chemistry* **1963**, *2* (6), 1166-1171.
2. Lancaster, K. M.; Roemelt, M.; Ettenhuber, P.; Hu, Y.; Ribbe, M. W.; Neese, F.; Bergmann, U.; DeBeer, S., X-ray Emission Spectroscopy Evidences a Central Carbon in the Nitrogenase Iron-Molybdenum Cofactor. *Science* **2011**, *334* (6058), 974.
3. Spatzal, T.; Aksoyoglu, M.; Zhang, L.; Andrade, S. L. A.; Schleicher, E.; Weber, S.; Rees, D. C.; Einsle, O., Evidence for Interstitial Carbon in Nitrogenase FeMo Cofactor. *Science* **2011**, *334* (6058), 940.
4. Čorić, I.; Holland, P. L., Insight into the Iron–Molybdenum Cofactor of Nitrogenase from Synthetic Iron Complexes with Sulfur, Carbon, and Hydride Ligands. *Journal of the American Chemical Society* **2016**, *138* (23), 7200-7211.
5. Čorić, I.; Mercado, B. Q.; Bill, E.; Vinyard, D. J.; Holland, P. L., Binding of dinitrogen to an iron–sulfur–carbon site. *Nature* **2015**, *526*, 96.
6. Xu, G.; Wang, Z.; Ling, R.; Zhou, J.; Chen, X.-D.; Holm, R. H., Ligand metathesis as rational strategy for the synthesis of cubane-type heteroleptic iron–sulfur clusters relevant to the FeMo cofactor. *Proceedings of the National Academy of Sciences* **2018**, *115* (20), 5089.
7. Reinholdt, A.; Majer, S. H.; Gelardi, R. M.; MacMillan, S. N.; Hill, A. F.; Wendt, O. F.; Lancaster, K. M.; Bendix, J., An Approach to Carbide-Centered Cluster Complexes. *Inorganic Chemistry* **2019**, *58* (8), 4812-4819.
8. Churchill, M. R.; Wormald, J.; Knight, J.; Mays, M. J., Synthesis and crystallographic characterization of bis(tetramethylammonium) carbidoheptadecacarbonylhexaferrate, a hexanuclear carbido-carbonyl derivative of iron. *Journal of the American Chemical Society* **1971**, *93* (12), 3073-3074.
9. Kuppuswamy, S.; Wofford, J. D.; Joseph, C.; Xie, Z.-L.; Ali, A. K.; Lynch, V. M.; Lindahl, P. A.; Rose, M. J., Structures, Interconversions, and Spectroscopy of Iron Carbonyl Clusters with an Interstitial Carbide: Localized Metal Center Reduction by Overall Cluster Oxidation. *Inorganic Chemistry* **2017**, *56* (10), 5998-6012.
10. Einsle, O.; Tezcan, F. A.; Andrade, S. L. A.; Schmid, B.; Yoshida, M.; Howard, J. B.; Rees, D. C., Nitrogenase MoFe-Protein at 1.16 Å Resolution: A Central Ligand in the FeMo-Cofactor. *Science* **2002**, *297* (5587), 1696.
11. Holm, R. H.; Lo, W., Structural Conversions of Synthetic and Protein-Bound Iron–Sulfur Clusters. *Chemical Reviews* **2016**, *116* (22), 13685-13713.
12. Tachikawa, M.; Geerts, R. L.; Muetterties, E. L., Metal carbide clusters synthesis systematics for heteronuclear species. *Journal of Organometallic Chemistry* **1981**, *213* (1), 11-24.

APPENDIX E

CH₄ Activation Study with Fe(depe)₂ Derivatives

E.1. Motivation and Specific Aims

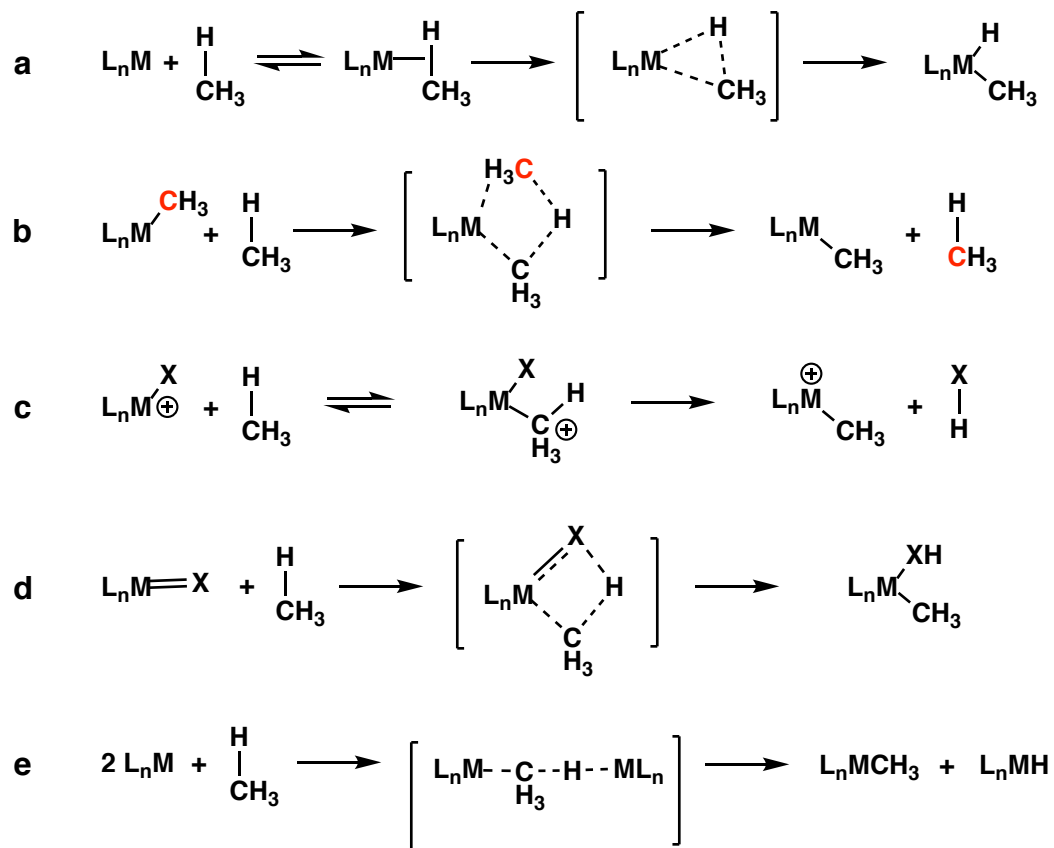
Methane is used as a resource for the production of many important industrialized chemicals such as ammonia, methanol and acetic acid.¹ Unfortunately, this process proceeds through a very energy intensive pathway (700 - 1100 °C) via the steam reforming of methane.¹ Therefore, efforts to directly convert methane to valuable chemicals such as methanol² are highly sought after and is the motivation of this project.

One of the challenges with direct conversion of methane is the activation of the strong C-H bond. There are many approaches possible for C-H bond activation; this appendix describes attempts to activate the C-H bond of methane by heterolysis in a base-assisted pathway.

E.2. Background

Methane is inert due to its strong C-H bond (BDE = 105 kcal/mol⁻¹) and its high lying LUMO and low lying HOMO.³ Although C-H bond cleavage is possible at high temperatures under atmospheric conditions, combustion of methane is not controlled and produces undesirable products. The first step towards functionalization is activating the C-H bond of methane. This can be challenging due to two reasons; the inertness of the C-H bond and competing reactions once the oxidized product is formed.⁴ Examples of C-H bond activation of methane by metal complexes are categorized into 5 classes,⁵ which exclude some approaches that are not directly related to metal-CH₃ bond formation. These classes are detailed below and outlined in Scheme E.1.

Scheme E.1. Categories of C-H activation of methane. a) oxidative addition, b) σ -bond metathesis, c) electrophilic activation, d) 1,2 addition and e) metalloradical.



E.2.1. Oxidative Addition

These complexes feature electron rich, low-valent late transition metal centers with low-coordination numbers. The low-coordination number allows space for the addition of both carbon and hydrogen from methane while the highly electron rich metal center can easily undergo two electron oxidation. Examples can be seen with metals such as Re,⁶ Fe,⁷ Os,⁸ and Ir.⁹ Early examples of oxidative addition of methane involve a Cp*Ir(CO) complex, under 20 atm of methane using light at room temperature.¹⁰ The drawback of this system is the use of expensive precious metals.

E.2.2. Sigma-Bond Metathesis

These complexes feature electron poor, high-valent early transition metal centers. The process goes through a net zero oxidation state change. In all but one case, a reversible reaction occurs in which alkyl fragments interchange with no further methane functionalization.¹¹ Examples include metals in group 3,¹² lanthanides¹³ and actinides.¹⁴ The first example of σ -bond metathesis focuses on the lanthanide complex, $\text{Cp}^*_2\text{LuCH}_3$, which showed a reversible methane activation at 70 °C.¹⁵

E.2.3. 1,2-Addition

Similar to σ -bond metathesis, 1,2-addition features electron-poor, high-valent, and typically early transition metal centers. However, they have a unique feature that incorporates metal-ligand multiple bonds. The addition of methane does not change the oxidation state of the metal and examples can be seen with Zr,¹⁶ V,¹⁷ Ti¹⁸ and W¹⁹ metals. The transient imido complex, $[(\text{tBu}_3\text{SiNH})_2\text{Zr}=\text{NSi}^t\text{Bu}_3]$ incorporates methane and other aliphatic C-H bonds in high yields (99%).¹⁶ However, the resulting product is relatively unreactive and does not undergo subsequent functionalization.

E.2.4. Metalloradicals

These complexes feature two metal centers that can homolytically split the C-H bond in methane. Rh(II) is an example of a metal capable of metalloradicals, which oxidize to Rh(III) upon the addition of the alkyl or hydrogen atom. A porphyrin Rh dimer was shown to slowly activate methane after 15 days at 40 °C with 40% conversion.²⁰

E.2.5. Electrophilic Activation

Electrophilic activation of methane was pioneered by Shilov using square planar Pt(II) complexes²¹ and can now be seen with other late metals such as Pd,²² Co,²³ Hg²⁴ and Tl.²⁵ The reaction conditions for Shilov's chemistry usually involve strong polar mediums (such as water or an anhydrous strong acid) at 100 °C. Additionally, this chemistry suffers from an expensive sacrificial oxidant [Pt(IV)]. However, this system is catalytic, oxidizing methane to methanol or chloroform.²¹

E.2.6. Base Assisted Activation for C-H Activation

Similar to electrophilic activation, this work described in this appendix aims to activate C-H bonds by employing a base and a metal center to facilitate base-assisted heterolytic cleavage of the C-H bond. The base used in this work is 1,8-diazabicyclo[5.4.0]undec-7-ene (DBU, pK_a 24.3 in acetonitrile).²⁶ A few examples of base-assisted C-H activation involve sp^2 and sp^3 carbons, but none involve methane.^{27, 28} Recent work from Darensbourg and colleagues utilizes a pendant base amine to assist in the intramolecular cleavage of an sp^3 C-H bond in an iron complex.²⁸

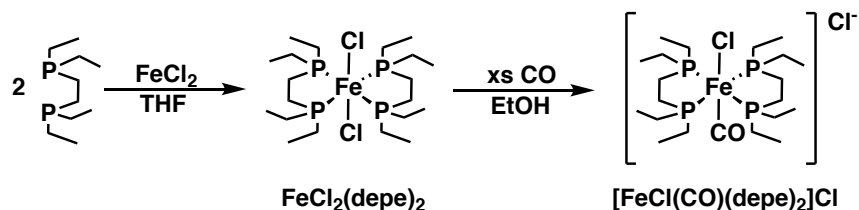
E.3. Results and Discussions

E.3.1. Synthesis of $[\text{FeCl}(\text{CO})(\text{depe})_2]\text{Cl}$

Following a literature procedure,^{29,30} two equivalent of bis(diethylphosphino)ethane (depe) were added to FeCl_2 in THF to isolate the product, $\text{FeCl}_2(\text{depe})_2$ as a green solid. CO gas was then added to the solution of $\text{FeCl}_2(\text{depe})_2$ in ethanol. The color changed from green to orange after dissolution in ethanol and then to orange-yellow when CO gas was added to

generate the complex, $[\text{FeCl}(\text{CO})(\text{depe})_2]\text{Cl}$ (Scheme E.2). $[\text{FeCl}(\text{CO})(\text{depe})_2]\text{Cl}$ displayed a CO vibrational frequency peak in the solution-IR (dichloromethane) at 1915 cm^{-1} , matching the literature value.³¹ The ^{31}P NMR spectrum of $[\text{FeCl}(\text{CO})(\text{depe})_2]\text{Cl}$ had a single resonance at 65.97 ppm, also matching the previously reported value.³¹

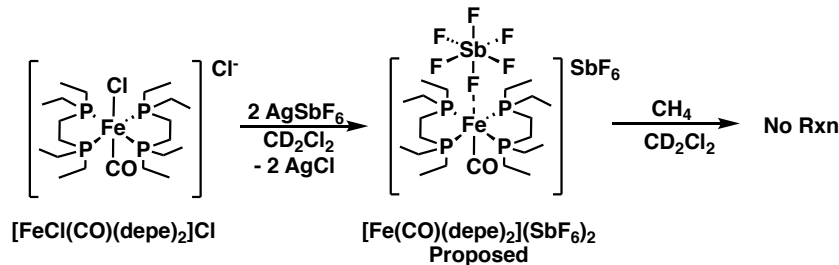
Scheme E.2. Synthesis of $\text{FeCl}_2(\text{depe})_2$ and $[\text{FeCl}(\text{CO})(\text{depe})_2]\text{Cl}$.



E.3.2. Reactivity with CH_4

Following the literature procedure, $[\text{FeCl}(\text{CO})(\text{depe})_2]\text{Cl}$ undergoes a salt metathesis with 2 equivalents of AgSbF_6 in CD_2Cl_2 to obtain a bright orange-yellow solution (Scheme E.3). The proposed structure of $[\text{Fe}(\text{SbF}_6)(\text{CO})(\text{depe})_2](\text{SbF}_6)$ is in line with other structurally characterized $[\text{Fe}(\text{CO})(\text{X})(\text{depe})_2](\text{X})$ complex, where X is BF_4 or OTf . The solution containing $[\text{Fe}(\text{SbF}_6)(\text{CO})(\text{depe})_2](\text{SbF}_6)$ was filtered into a J. Young tube and sealed. A $^{31}\text{P}\{^1\text{H}\}$ NMR spectrum of $[\text{Fe}(\text{SbF}_6)(\text{CO})(\text{depe})_2](\text{SbF}_6)$ displayed three resonances at 64.7, 64.3 and 64.1 ppm. The weak Fe-F bond presented an opportunity for CH_4 binding, as it was demonstrated previously that H_2 can bind to Fe in this system.³¹ CH_4 gas was then added to the J. Young tube but no color change was observed (Scheme E.3). In addition, the $^{31}\text{P}\{^1\text{H}\}$ NMR spectrum was unchanged from $[\text{Fe}(\text{SbF}_6)(\text{CO})(\text{depe})_2](\text{SbF}_6)$

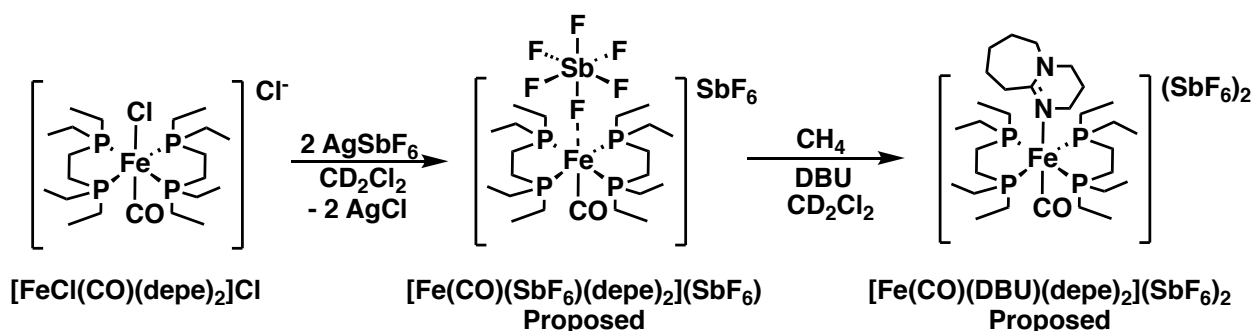
Scheme E.3. Reactivity of $[\text{FeCl}(\text{CO})(\text{depe})_2]\text{Cl}$ with CH_4 .



E.3.3. Reactivity with CH_4 and DBU

The addition of an external base (DBU) was added to achieve the base assisted activation of CH_4 . The goal was to produce the $[\text{Fe}(\text{CH}_3)(\text{depe})_2]$ complex and a $[\text{DBU-H}]$ molecule. The characterization of a Fe-CH_3 complex of the $\text{Fe}(\text{depe})_2$ system was previously published and can help identify if a Fe-CH_3 bond was formed.³² The J. Young tube was filled with $[\text{FeCl}(\text{CO})(\text{depe})_2]\text{Cl}$, 1.5 equiv DBU, 2.5 equiv of AgSbF_6 and CH_4 gas (Scheme E.4). The ^{31}P NMR spectrum of product showed a major resonance at 70.0 ppm, which is consistent with the controlled experiment of DBU addition (without CH_4) to the proposed $[\text{Fe}(\text{SbF}_6)(\text{CO})(\text{depe})_2](\text{SbF}_6)$. Thus, it appears DBU binds directly to the iron complex, inhibiting any direct CH_4 interaction. R. H. Morris has noted the importance of using less nucleophilic bases in these systems to prevent ligation to the Fe center.³¹ One method to circumvent this issue is to use a sterically bulky base, where access to the Fe center would be hindered.

Scheme E.4. Reactivity of $[\text{FeCl}(\text{CO})(\text{depe})_2]\text{Cl}$ with CH_4 and DBU.



E.4. Conclusions

Base assisted C-H bond activation was attempted with $[\text{FeCl}(\text{CO})(\text{depe})_2]\text{Cl}$, DBU, CH_4 and SbF_6 . No reaction was observed for CH_4 activation, potentially due to the formation of an Fe-DBU bond that may prevent CH_4 from accessing the Fe center of $[\text{Fe}(\text{CO})(\text{depe})_2](\text{SbF}_6)_2$. Future work with this system could utilize a bulkier base, such as the tertbutyl functionalized Verkade's Superbase, in order to inhibit coordination.

E.5. Experimental Details

General Considerations

All manipulations were performed in the glovebox or on a Schlenk line, as the complex is moisture-sensitive. All solvents were first purged with argon and dried using a solvent purification system. Bis(diethylphosphino)ethane (depe), FeCl_2 , 1,8-diazabicyclo[5.4.0]undec-7-ene (DBU), and CH_4 were commercially purchased and used without further purification. AgSbF_6 was generously donated from the Pronin Lab from UCI and used without further purification. Complexes $[\text{FeCl}_2(\text{depe})_2]$, $[\text{FeCl}(\text{CO})(\text{depe})_2]\text{Cl}$, and $[\text{Fe}(\text{SbF}_6)(\text{CO})(\text{depe})_2](\text{SbF}_6)$ were synthesized using published procedures.³¹

Physical Methods

Nuclear Magnetic Resonance (NMR) Spectroscopy: Nuclear magnetic resonance (NMR) spectra were recorded on a DRX400 with a switchable QNP probe (^1H and ^{31}P) or a Bruker AVANCE 600 MHz (^1H and ^{31}P). ^1H NMR spectra were referenced to (tetramethylsilane) TMS using the residual proteo impurities of the solvent; $^{31}\text{P}\{^1\text{H}\}$ NMR spectroscopy experiments are referenced to an internal standard (PPh_3 in toluene).

Reactivity with CH_4 : In the glove box a solution of AgSbF_6 (7.3 mg, 21 nmol) in CD_2Cl_2 was added to a solution of $[\text{FeCl}_2(\text{depe})_2]$ (5.0 mg, 8.8 nmol) in CD_2Cl_2 . An immediate white precipitate formed and the color changed from light yellow to bright orange-yellow. The solution was filtered through a pipette packed with filter paper into a J. Young tube with an inner tube filled with PPh_3 in toluene as an internal standard. The J. Young tube was taken out of the glove box and subject to three freeze-pump-thaw cycles before CH_4 was introduced. $^{31}\text{P}\{^1\text{H}\}$ NMR (CD_2Cl_2 , 243 MHz) $\delta = 64.7, 64.4, 64.1,$ and 63.5 ppm.

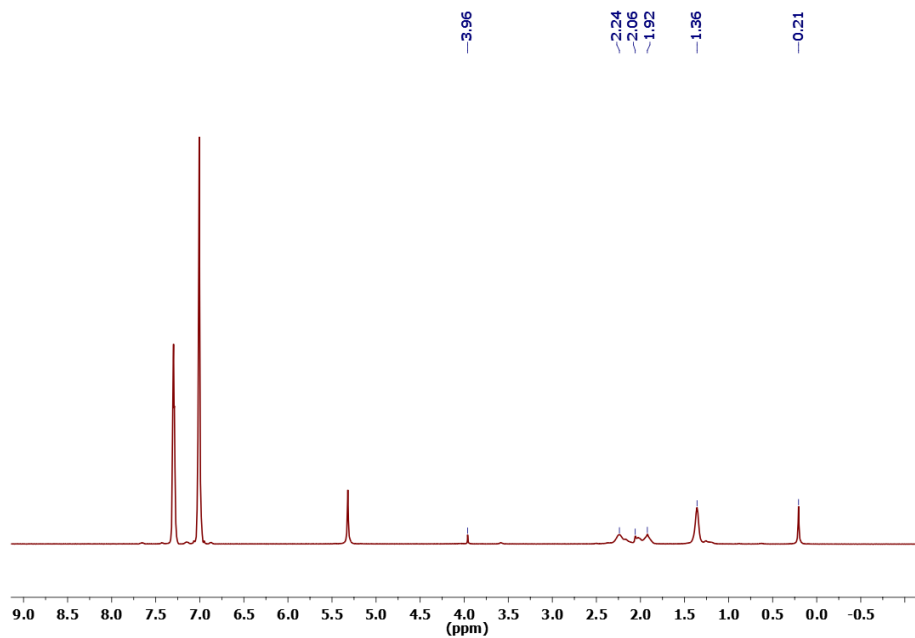


Figure E.1. ^1H NMR spectrum of $[\text{Fe}(\text{CO})(\text{depe})_2]\text{Cl} + \text{AgSbF}_6 + \text{CH}_4$ in CD_2Cl_2 .

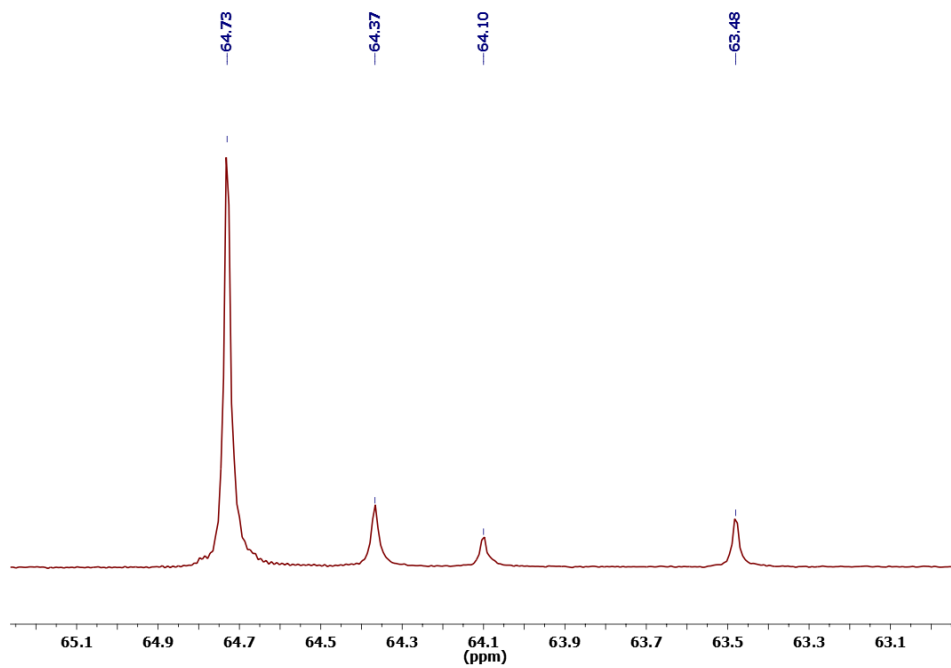


Figure E.2. $^{31}\text{P}\{^1\text{H}\}$ NMR spectrum of $[\text{Fe}(\text{CO})(\text{depe})_2]\text{Cl} + \text{AgSbF}_6 + \text{CH}_4$ in CD_2Cl_2 .

Reactivity with CH₄ and DBU: In the glove box 2 μL of DBU was added via microsyringe to a J. Young tube with [Fe(SbF₆)(CO)(depe)₂](SbF₆) in CD₂Cl₂. The J. Young tube was taken out of the glove box and subject to three freeze-pump-thaw cycles before CH₄ (~1 atm) was introduced. No color change was observed when CH₄ was introduced. ³¹P{¹H}NMR (CD₂Cl₂, 243 MHz) δ = 71.9, 71.81, 70.0, 65.5, 65.2, 64.1, 63.5, 51.8, 51.7, and 49.8 ppm.

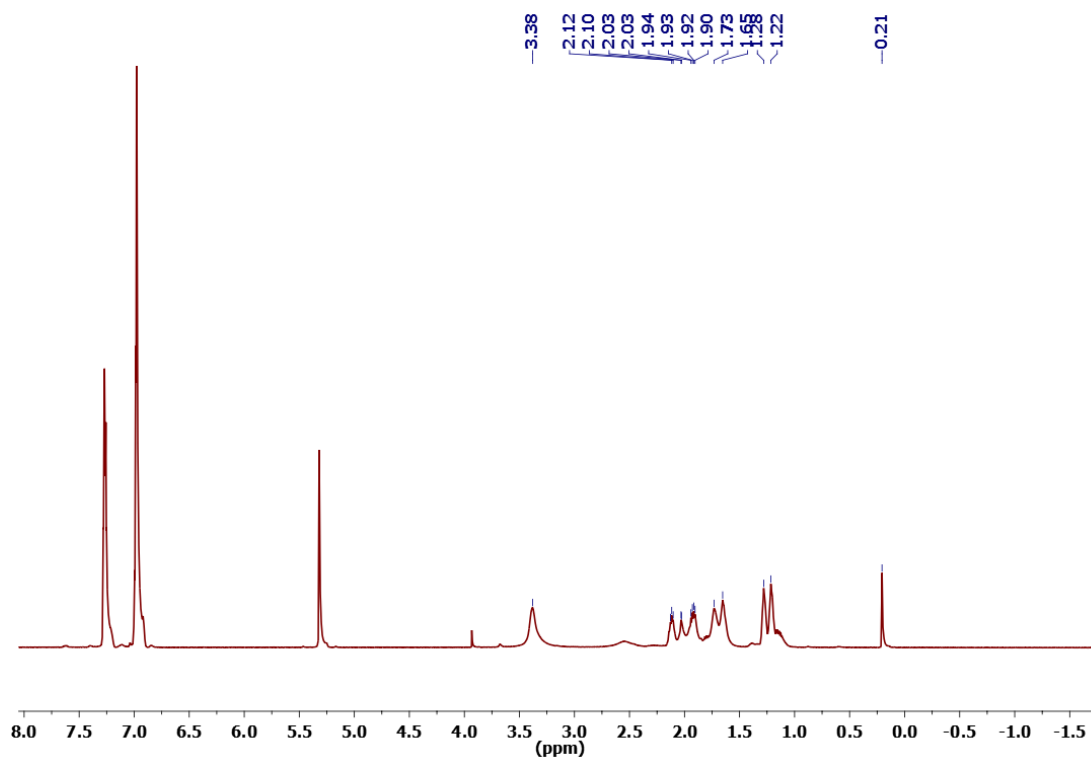


Figure E.3. ¹H NMR spectrum of [Fe(CO)(depe)₂]Cl + AgSbF₆ + CH₄ + DBU in CD₂Cl₂.

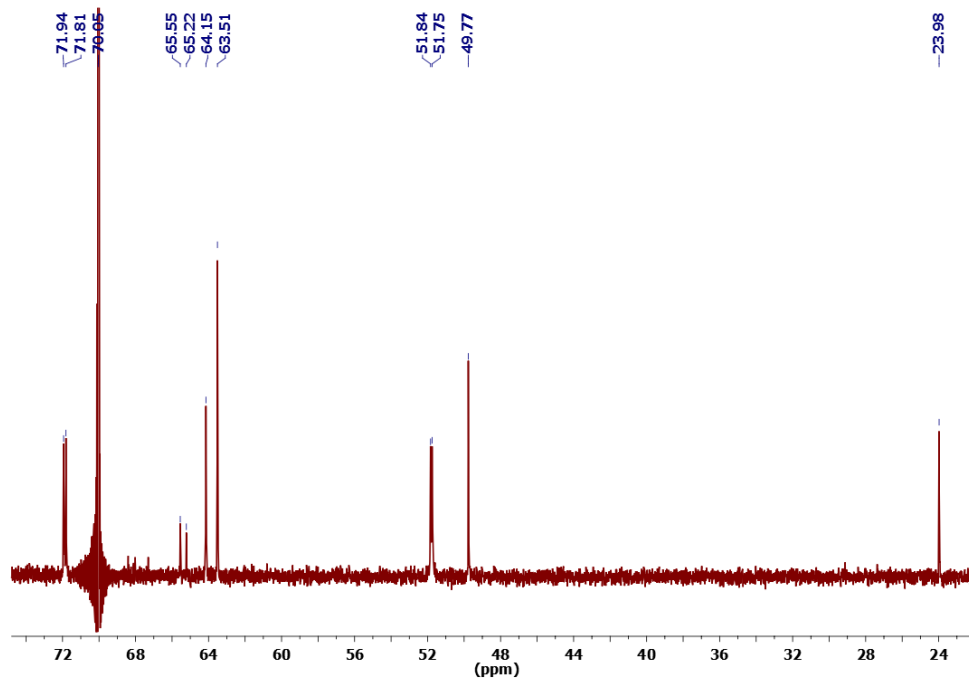


Figure E.4. $^{31}\text{P}\{^1\text{H}\}$ NMR spectrum of $[\text{Fe}(\text{CO})(\text{depe})_2]\text{Cl} + \text{AgSbF}_6 + \text{CH}_4 + \text{DBU}$ in CD_2Cl_2 .

E.6. References

1. Chenier, P. J., Chemicals from Methane. In *Survey of Industrial Chemistry*, Chenier, P. J., Ed. Springer US: Boston, MA, 2002; pp 205-215.
2. Olah, G. A.; Goepfert, A.; Prakash, G. K. S., *Beyond Oil and Gas: The Methanol Economy*. Wiley: 2006.
3. Blanksby, S. J.; Ellison, G. B., Bond Dissociation Energies of Organic Molecules. *Acc. Chem. Res.* **2003**, *36* (4), 255-263.
4. Tang, P.; Zhu, Q.; Wu, Z.; Ma, D., Methane activation: the past and future. *Energ. Environ. Sci.* **2014**, *7* (8), 2580-2591.
5. Cavaliere, V. N.; Mindiola, D. J., Methane: a new frontier in organometallic chemistry. *Chem. Sci.* **2012**, *3* (12), 3356-3365.
6. Jones, W. D.; Maguire, J. A., The activation of methane by rhenium. Catalytic hydrogen/deuterium exchange in alkanes with CpRe(PPh₃)₂H₂. *Organometallics* **1986**, *5* (3), 590-591.
7. Field, L. D.; George, A. V.; Messerle, B. A., Methane activation by an iron phosphine complex in liquid xenon solution. *J. Chem. Soc., Chem. Comm.* **1991**, (19), 1339-1341.
8. Harper, T. G. P.; Shinomoto, R. S.; Deming, M. A.; Flood, T. C., Activation of methane by the reactive intermediate tris(trimethylphosphine)osmium(0). *J. Am. Chem. Soc.* **1988**, *110* (23), 7915-7916.
9. Burger, P.; Bergman, R. G., Facile intermolecular activation of carbon-hydrogen bonds in methane and other hydrocarbons and silicon-hydrogen bonds in silanes with the iridium(III) complex Cp*(PMe₃)Ir(CH₃)(OTf). *J. Am. Chem. Soc.* **1993**, *115* (22), 10462-10463.
10. Hoyano, J. K.; McMaster, A. D.; Graham, W. A. G., Activation of methane by iridium complexes. *J. Am. Chem. Soc.* **1983**, *105* (24), 7190-7191.
11. Sadow, A. D.; Tilley, T. D., Homogeneous Catalysis with Methane. A Strategy for the Hydromethylation of Olefins Based on the Nondegenerate Exchange of Alkyl Groups and σ -Bond Metathesis at Scandium. *J. Am. Chem. Soc.* **2003**, *125* (26), 7971-7977.
12. Fontaine, F.-G.; Tilley, T. D., Control of Selectivity in the Hydromethylation of Olefins via Ligand Modification in Scandocene Catalysts. *Organometallics* **2005**, *24* (18), 4340-4342.
13. Watson, P. L.; Parshall, G. W., Organolanthanides in catalysis. *Acc. Chem. Res.* **1985**, *18* (2), 51-56.
14. Bruno, J. W.; Marks, T. J.; Day, V. W., Intra- and intermolecular organoactinide carbon-hydrogen activation pathways. Formation, properties, and reactions of thoracyclobutanes. *J. Am. Chem. Soc.* **1982**, *104* (25), 7357-7360.
15. Watson, P. L., Methane exchange reactions of lanthanide and early-transition-metal methyl complexes. *J. Am. Chem. Soc.* **1983**, *105* (21), 6491-6493.
16. Cummins, C. C.; Baxter, S. M.; Wolczanski, P. T., Methane and benzene activation via transient (tert-Bu₃SiNH)₂Zr:NSi-tert-Bu₃. *J. Am. Chem. Soc.* **1988**, *110* (26), 8731-8733.
17. de With, J.; Horton, A. D., C-H Bond Addition to a V=NR Bond: Hydrocarbon Activation by a Sterically Crowded Vanadium System. *Angew. Chem. Int. Ed. Eng.* **1993**, *32* (6), 903-905.

18. Bennett, J. L.; Wolczanski, P. T., Energetics of C-H Bond Activation and Ethylene Binding to d⁰ Transient (silox)₂Ti:NSitBu₃. *J. Am. Chem. Soc.* **1994**, *116* (5), 2179-2180.
19. Schafer, D. F.; Wolczanski, P. T., d⁰ Alkane Complexes (tBu₃SiN)₃W(RH) Precede CH Activation and Formation of (tBu₃SiN)₂(tBuSiNH)WR/R'. *J. Am. Chem. Soc.* **1998**, *120* (19), 4881-4882.
20. Cui, W.; Wayland, B. B., Activation of C-H/H-H Bonds by Rhodium(II) Porphyrin Bimetallo-radicals. *J. Am. Chem. Soc.* **2004**, *126* (26), 8266-8274.
21. Shilov, A. E.; Shul'pin, G. B., Activation of C-H Bonds by Metal Complexes. *Chem. Rev.* **1997**, *97* (8), 2879-2932.
22. Ahrens, S.; Zeller, A.; Taige, M.; Strassner, T., Extension of the Alkane Bridge in BisNHC-Palladium-Chloride Complexes. Synthesis, Structure, and Catalytic Activity. *Organometallics* **2006**, *25* (22), 5409-5415.
23. Gol'dshleger, N. F.; Tyabin, M. B.; Shilov, A. E.; Shteinman, A. A., *Russ. J. Phys. Chem.* **1969**, *43*, 1222.
24. Periana, R. A.; Taube, D. J.; Evitt, E. R.; Löffler, D. G.; Wentreck, P. R.; Voss, G.; Masuda, T., A Mercury-Catalyzed, High-Yield System for the Oxidation of Methane to Methanol. *Sci.* **1993**, *259* (5093), 340-343.
25. Hashiguchi, B. G.; Konnick, M. M.; Bischof, S. M.; Gustafson, S. J.; Devarajan, D.; Gunsalus, N.; Ess, D. H.; Periana, R. A., Main-Group Compounds Selectively Oxidize Mixtures of Methane, Ethane, and Propane to Alcohol Esters. *Sci.* **2014**, *343* (6176), 1232-1237.
26. Kovačević, B.; Barić, D.; Maksić, Z. B., Basicity of exceedingly strong non-ionic organic bases in acetonitrile - Verkade's superbases and some related phosphazenes. *New. J. Chem.* **2004**, *28* (2), 284-288.
27. Ryabov, A. D.; Sakodinskaya, I. K.; Yatsimirsky, A. K., Kinetics and mechanism of ortho-palladation of ring-substituted *N,N*-dimethylbenzylamines. *J. Chem. Soc., Dalton. Trans.* **1985**, (12), 2629-2638.
28. Zheng, D.; Wang, N.; Wang, M.; Ding, S.; Ma, C.; Darensbourg, M. Y.; Hall, M. B.; Sun, L., Intramolecular Iron-Mediated C-H Bond Heterolysis with an Assist of Pendant Base in a [FeFe]-Hydrogenase Model. *J. Am. Chem. Soc.* **2014**, *136* (48), 16817-16823.
29. Schwarz, F.; Kastlunger, G.; Lissel, F.; Riel, H.; Venkatesan, K.; Berke, H.; Stadler, R.; Lörtscher, E., High-Conductive Organometallic Molecular Wires with Delocalized Electron Systems Strongly Coupled to Metal Electrodes. *Nano Letters* **2014**, *14* (10), 5932-5940.
30. Bellerby, J. M.; Mays, M. J.; Sears, P. L., Cationic low-spin bis[1,2-bis(dialkylphosphino)ethane]iron(II) complexes. *Journal of the Chemical Society, Dalton Transactions* **1976**, (13), 1232-1236.
31. Landau, S. E.; Morris, R. H.; Lough, A. J., Acidic Dicationic Iron(II) Dihydrogen Complexes and Compounds Related by H₂ Substitution. *Inorganic Chemistry* **1999**, *38* (26), 6060-6068.
32. Allen, O. R.; Dalgarno, S. J.; Field, L. D.; Jensen, P.; Turnbull, A. J.; Willis, A. C., Addition of CO₂ to Alkyl Iron Complexes, Fe(PP)₂Me₂. *Organometallics* **2008**, *27* (9), 2092-2098.